INFORMATION TO USERS

This manuscript has been reproduced from the microfilm master. UMI films the text directly from the original or copy submitted. Thus, some thesis and dissertation copies are in typewriter face, while others may be from any type of computer printer.

The quality of this reproduction is dependent upon the quality of the copy submitted. Broken or indistinct print, colored or poor quality illustrations and photographs, print bleedthrough, substandard margins, and improper alignment can adversely affect reproduction.

In the unlikely event that the author did not send UMI a complete manuscript and there are missing pages, these will be noted. Also, if unauthorized copyright material had to be removed, a note will indicate the deletion.

Oversize materials (e.g., maps, drawings, charts) are reproduced by sectioning the original, beginning at the upper left-hand corner and continuing from left to right in equal sections with small overlaps.

Photographs included in the original manuscript have been reproduced xerographically in this copy. Higher quality 6" x 9" black and white photographic prints are available for any photographs or illustrations appearing in this copy for an additional charge. Contact UMI directly to order.

ProQuest Information and Learning
300 North Zeeb Road, Ann Arbor, MI 48106-1346 USA
800-521-0600

ON SOOT INCEPTION IN NONPREMIXED FLAMES AND THE EFFECTS OF FLAME STRUCTURE

A DISSERTATION SUBMITTED TO THE GRADUATE DIVISION OF THE UNIVERSITY OF HAWAII IN PARTIAL FULFILLMENT OF THE REQUIREMENTS FOR THE DEGREE OF

DOCTOR OF PHILOSOPHY

IN

MECHANICAL ENGINEERING

DECEMBER 2001

by
Shiling Liu

Dissertation Committee:

Beei-Huan Chao, Chairperson
Carlos Coimbra
Bruce E. Liebert
Stephen M. Masutani
Michelle Teng

We certify that we have read this dissertation and that, in our opinion, it is satisfactory in scope and quality as a dissertation for the degree of Doctor of Philosophy in Mechanical Engineering.

DISSERTATION COMMITTEE

Chairperson

To

my parents and the family members
for their encouragement and understanding,

and

all the teachers in my life
who gave so much to the development of my career.

"I hear and I forget. I see and I remember. I do and I understand."

Confucius

ACKNOWLEDGMENTS

The path leading to the completion of a doctoral dissertation research is an arduous and challenging one. It is full of false starts, dead ends, and maddening mazes. Its travel requires a strong heart and stout legs. Yet, once a while one is cheered by the sight of a lily and the chirps of a nightingale as new knowledge are discovered and new understanding revealed. So one keeps on pressing ahead. As I am now within sight of the pot of gold at the end of the rainbow, and as I look back at the journey that I have traveled during the past five years, I feel profoundly fortunate that this journey has been made easier, and indeed possible, by the wisdom, generosity, and kindness of some very special people.

At the top of the list is my dissertation advisor, Professor Beei-Huan Chao, whose guidance, patience, and encouragement have been absolutely essential in my growth as a scholar and as a person. To whom I am most grateful.

The progress of my research has also been greatly benefited by the valuable discussions with Professors Carlos Coimbra, Bruce E. Liebert, Stephen M. Masutani, and Michelle Teng, who served as members of my dissertation committee. Furthermore, it is a pleasure to acknowledge Mr. Oliver Easterday and Mr. Jonathan Iloreta for helpful suggestions.

I am also deeply indebted to Professor Richard L. Axelbaum of Washington University for his many important inputs to my research in his role as a project collaborator, and to Professor Chung K. Law of Princeton University for his wisdom and encouragement.

On a personal level, I humbly offer my utmost gratitude to my parents, whose love and care have instilled in me the drive and confidence necessary to accomplish this task. Last but by no means the least, I must thank my husband, Xiuwen, and my son, James, for their understanding and support that have enabled me to pursue a career of this nature.

This research was supported by the National Aeronautics and Space Administration (NASA), under contract numbers NAG3-1912 and NCC3-696a granted to Professor Beei-Huan Chao, and by a Teaching Assistantship from the Department of Mechanical Engineering.

ABSTRACT

A simplified three-step model that describes the oxidation, soot formation and soot consumption reactions has been employed with high activation energy asymptotics to study soot inception in nonpremixed counterflow and spherical flames. Emphasis has been made on the understanding of the effects of hydrodynamics and transport on the soot inception processes. The resulting scheme yields three distinct reaction regions: (1) a fuel oxidation region wherein the fuel and oxidizer react to form product as well as a radical R, (*e.g.*, H), (2) a soot/precursor formation region where the radical R reacts with fuel to form "soot/precursor" S, and (3) a soot/precursor consumption region where S reacts with the oxidizer to form product. This kinetic scheme, although greatly simplified, allows for the coupling between soot inception and flame structure to be assessed. The analysis yields the solution of flame temperature, flame location, and soot/precursor indices, S_I and S_B, as functions of the Damköhler number of the soot formation reaction, Da_2, and the mass flow rate issued from the burner for the spherical flames. The soot/precursor index S_I indicates the amount of S at the boundary between the reaction region and the inert transport region at the fuel side for the counterflow flame, or the burner side for the spherical flame. The other index S_B indicates the amount of S at the boundary between the reaction region and the inert transport region at the oxidizer side for the counterflow flame, or the ambient side for the spherical flame. The flame temperature indirectly indicates the total amount of soot/precursor production because as soot/precursor is formed less heat is released.

Two limiting cases, the fuel/air flame and diluted-fuel/oxygen flame, were studied for both the counterflow and spherical flame configurations. The effects of flame structure, initial reactant concentrations, Lewis numbers of the radical and the soot/precursor, as well as the rates of soot formation and consumption reactions on the sooting behavior were investigated. Results show that the diluted-fuel/oxygen flame produces much lower soot/precursor than its fuel/air counterpart. In addition, when soot consumption reaction is negligible, the net amount of soot/precursor

produced increases with increasing Da_2 and decreasing radical diffusivity, where it is independent of the diffusivity of soot/precursor. On the other hand, when soot consumption reaction is considered, there exists a critical Da_2 above which soot/precursor production decreases with increasing Da_2 because of the enhanced soot/precursor consumption reaction. In addition, lower soot/precursor diffusion rate yields a lower soot production and a higher flame temperature as a result of the higher soot/precursor concentration in the soot consumption region.

The results also show that for the spherical flame, increasing the mass flow rate increases the flame temperature until the heat loss to the burner becomes negligible, and then decreases the flame temperature because of the enhanced soot formation reaction. The net soot amount increases with the mass flow rate when the soot consumption reaction is weak. It decreases with stronger soot consumption reaction for any given mass flow rate. There is also a critical mass flow rate at which the soot production is the highest for moderate soot consumption rates. Because the production of soot/precursor is more difficult to occur for the diluted-fuel/oxygen flame compared to the fuel/air flame as indicated by the much lower soot/precursor production, soot inception can be reduced or completely suppressed by the redistribution of inert gas from the oxidizer side to the fuel side, even when the flow direction favors soot formation. This suggests that flame structure represented by the stoichiometric mixture fraction plays a more important role on soot inception in diffusion flames than hydrodynamics.

TABLE OF CONTENTS

LIST OF TABLES

LIST OF FIGURES

NOMENCLATURE

$a_{i,j}$	integration constants
B_j	pre-exponential factor of reaction Rj
c_P	specific heat at constant pressure
D_i	mass diffusion coefficient of species i
Da_j	Damköhler number of reaction Rj, defined after Eqs. (2.7) and (3.8)
E_j	activation temperature of reaction Rj
F	fuel
I	function defined in Eq. (2.19)
k	flow velocity gradient, also the strain rate
m	mass flow rate from the spherical porous burner
Le_i	Lewis number of species i, defined as $\lambda / (\rho D_i c_P)$
O	oxidizer
P	combustion products
$q_{F,1}$	heat of combustion per unit mass of fuel consumed in the oxidation reaction
$q_{S,3}$	heat of combustion per unit mass of soot/precursor consumed in the soot/precursor consumption reaction
$\tilde{q}_S$	heat of combustion ratio proportional to $q_{S,3}/q_{F,1}$, defined after Eq. (2.7)
R	radical
S	soot/precursor
S_B	soot/precursor break-through parameter defined in Eqs. (2.138) and (3.136)
S_I	soot/precursor index parameter defined in Eqs. (2.137) and (3.135)
T	temperature
T_f	flame temperature
$\tilde{T}_{f,j}$	j^{th} order expansion of the nondimensional flame temperature $\tilde{T}_f$
W_i	molecular weight of species i
x, r	spatial coordinate
x_f, r_f	flame position
Y_i	mass fraction of species i

Greek Symbols

α activation energy ratio defined as E_3 / E_2

β pre-exponential factor ratio proportional to B_3 / B_2, defined after Eq. (2.7)

δ small parameter defined as $\tilde{T}_{f,0}^2 / \tilde{E}_2$

ε small parameter defined as $\tilde{T}_f^2 / \tilde{E}_1$

ζ stretched coordinate in the soot/precursor formation and consumption regions, defined as $(\tilde{x} - \tilde{x}_f) / \delta$ or $(\tilde{r} - \tilde{r}_f) / \delta$

θ_j j^{th} order expansion of temperature in the oxidation region

Θ_j j^{th} order expansion of temperature in the soot/precursor formation and consumption regions

λ thermal conductivity

Λ_j Reduced Damköhler numbers defined in Eqs. (2.28), (2.60), (3.28) and (3.62)

ν_i stoichiometric coefficient of species i at a specified reaction

$\nu_{i,j}$ stoichiometric coefficient of species i at reaction Rj

$\tilde{\nu}_F$ stoichiometric coefficient ratio defined as $\nu_{F,2} / \nu_{F,1}$

$\tilde{\nu}_O$ stoichiometric coefficient ratio defined as $\nu_{O,3} / \nu_{O,1}$

$\hat{\nu}$ stoichiometric coefficient ratio defined as $\tilde{\nu}_F / \tilde{\nu}_O$

ν^* stoichiometric coefficient ratio defined as $(1 + \tilde{\nu}_O) / (1 + \tilde{\nu}_F)$

ξ stretched coordinate in the oxidation region, defined as $(\tilde{x} - \tilde{x}_f) / \varepsilon$ or $(\tilde{r} - \tilde{r}_f) / \varepsilon$

ρ gas density

$\phi_{i,j}$ j^{th} order expansion of species i in the oxidation region

$\Phi_{i,j}$ j^{th} order expansion of species i in the soot/precursor formation and consumption regions

Subscripts

F fuel

O oxidizer

R radical

S soot/precursor

T	temperature
∞	imposed free boundary conditions of the oxidizer stream
$-\infty$	imposed free boundary conditions of the fuel stream

Superscripts

+	solutions in the oxidizer side of the oxidation region
−	solutions in the fuel side of the oxidation region
~	nondimensional quantities

CHAPTER 1

INTRODUCTION

1.1 Overview

Combustion of hydrocarbon or carbohydrate fuels with air under ideal conditions produces carbon dioxide and water with the amount given by the stoichiometric composition of the reactant mixture. An ideal condition refers to that for which the oxygen supply in the mixture is sufficient to completely oxidize the carbon in the fuel to carbon dioxide and the hydrogen to water. At an ideal condition, the chemical equation that governs the overall reaction of a carbohydrate fuel in air is given by

$$C_xH_yO_z + [x + (y/4) - (z/2)](O_2 + 3.76N_2) \rightarrow xCO_2 + (y/2)H_2O + 3.76[x + (y/4) - (z/2)]N_2 \quad . \qquad (1.1)$$

Equation (1.1) can be reduced to the burning of a hydrocarbon fuel by taking $z = 0$. Reaction under ideal conditions yields the highest heat release, flame temperature and maximum fuel economy.

In practical combustion devices such as internal combustion engines, gas turbines, and industrial furnaces, the burning conditions are usually not ideal. In regions where the mixture is locally rich in fuel, other undesired components such as carbon monoxide, hydrogen, residual hydrocarbons and soot are produced in addition to carbon dioxide and water. For premixed flames, meaning those with the fuel and oxidizer already mixed before entering the reaction region, the generation of undesired products can be minimized to a negligible level by burning at fuel lean conditions. For

nonpremixed flames (diffusion flames), the fuel and oxidizer are originally separated and brought into the reaction region through convection and molecular diffusion. They then are mixed at the molecular level within the reaction region and consumed to produce products and heat. The reaction region for a diffusion flame is located where the supply of fuel and oxidizer are stoichiometrically proportional such that both the fuel and oxidizer are completely consumed in the reaction-sheet limit. Here the reaction-sheet limit is the condition when the reaction rate is infinitely fast compared to the rate of diffusion-convection transport such that the reaction is diffusion limited. There is a fuel rich region at the fuel side of the reaction region, even if the overall supply is fuel lean, in which the production of the above-mentioned undesirable components is favored. Among those components, the presence of soot particles introduces strong impacts on both the fuel economy and our living environment.

Soot is generally referred to as the combustion-generated carbonaceous particulate that are produced from gas-phase processes. The characteristics of soot are well described by Palmer and Cullis (1965). In a soot particle, the carbon group generally contains approximately 1% hydrogen by weight. On an atomic basis this corresponds to an empirical formula of C_8H. Soot particles are very fine particles with diameters less than 2.5 micrometers. They are indicated by the United States Environmental Protection Agency (US-EPA) as a major component of Particulate Matter PM-2.5, the general term for solid particles or liquid droplets with diameters of 2.5 micrometers or less in air, and is identified as one of the six primary pollutants. These fine particles are produced from the combustion of hydrocarbon and carbohydrate

fuels in motor vehicles, power generators, and industrial burners. Thousands of research accomplishments published in reputable journals indicate that particulate matters, especially fine particles such as soot, lead to serious health problems (*c.f.* Abramson, *et al.*, 1991; Abramson, 1991; Green 1995; Barnes, 1994; Meyer, *et al.*, 1999; Lahiri, *et al.*, 2000; Chan-Yeung, 2000; Lewis, *et al.*, 1998; Holt, 1996; Cunningham, *et al.*, 1995). Examples of health issues induced by soot particles include: premature death, respiratory related hospital and emergency room visits, aggravated asthma, acute respiratory symptoms such as aggravated coughing and difficult or painful breathing, weakened lung function that yields shortness of breath, and chronic bronchitis. Realizing the hazard of soot particles on human health, the Federal Air Quality Standards were updated on July 16, 1997, making it the most stringent standards after the 1990 Clean Air Act. Two new standards were added to regulate the PM-2.5 matters which require the content of these matters in the atmosphere be less than $65\,\mu g/m^3$ on 24-hour average and $15\,\mu g/m^3$ on annual average basis. To fulfill these stringent standards, emission of soot from combustion facilities needs to be further reduced and soot particles are required to be oxidized before the combustion product can be released into the atmosphere.

The presence of soot particulate in gas turbines can severely affect the lifetime of the blades; soot particulate in diesel engines absorb carcinogenic materials, thereby posing a healthy hazard (Glassman, 1996). Soot formation within combustion devices also reduces fuel economy and combustion efficiency due to incomplete combustion. Less heat is liberated from combustion processes when soot is produced. Nonetheless, particulate can be

useful. In many industry furnaces, the presence of soot particulate enhances flame radiation and thus increase appreciably the heat transfer rates. Soot also can be a raw material in the chemical industry with a wide variety of applications such as filler in tires and toner for copiers and printers.

Because of the significance of soot particles, understanding of the nucleation process that yields soot particles is of both fundamental and practical importance. It is a formidable challenge to investigate the mechanisms responsible for soot formation, starting from the inception, and to identify means of controlling these mechanisms. The control of soot formation in diffusion flames is of utmost importance because a fuel rich region that favors the formation of soot is part of the flame structure and cannot be avoided. The objective of this study is, therefore, to study the soot formation processes in diffusion flames.

1.2 Literature Review

Significant advances in the understanding of the mechanisms, phenomenology and chemistry on soot formation and destruction in combustion systems have been made over the past few decades. The enthusiastic attention received by researchers and engineers on soot production reflects the great challenges encountered by scientists and combustion system designers and operators. Although tremendous progress has been accomplished in understanding the fundamental chemistry and physics, many questions regarding the details of soot formation, growth and oxidation remain to be addressed. Combustion engineers are challenged to design systems in which soot production is controllable.

Theoretically, there are three classes of model currently available for the prediction of soot production from combustion systems, viz., (i) purely empirical models that employ correlation of experimental data to predict tendency towards soot loading, (ii) semi-empirical formulations that solve the rate equations for soot formation with some input from experimental data, and (iii), models that employ detailed chemistry to solve the rate equations numerically. In (iii) a system of elementary reactions is adopted for the prediction of the concentrations of all major species in a reactive mixture. Subsequent to this is the determination of the reaction paths that marches from fuel to polyaromatic hydrocarbons (PAH), which is the soot precursor, and to soot. Although all these models have demonstrated success in predicting soot concentration, their applications require some degree of correlation in rate constants to match experimental measurements. Whether this manipulation is consistent with the underlying fundamental principles on soot formation and destruction is uncertain. Moreover, the interaction between the flame and its background flow field, which yields the effects of flame structure and diffusion transport on soot formation, has not been studied.

1.2.1 Background to Soot Formation and Oxidation

Soot is composed mostly of carbon; with tracing amounts of other elements such as hydrogen and oxygen. It is produced during the high temperature pyrolysis or combustion of hydrocarbons and/or carbohydrates. The emission of soot from a combustor or more specifically, a flame, is determined by the competition between the soot formation and oxidation reactions. A comprehensive model that studies the soot process must include

both of these reactions.

As hydrocarbons pyrolyze, lower molecular weight hydrocarbons, in particular acetylene, are produced as the primary products. These aliphatic hydrocarbons subsequently combine to form the first aromatic species as the initial step leading to the production of soot. The aromatic species then grow through the addition of other aromatic and smaller alkyl species to produce PAH. Continuous growth of the PAH eventually leads to the smallest identifiable soot particles with diameters of the order of 1 nm and masses of around 1000 amu (atomic mass unit, 1 amu equals to 1.66×10^{-24} gram). The production of soot particles in a flame is inherently determined by chemical kinetics. Low molecular weight gaseous hydrocarbons are converted to essentially solid carbon within just a few milliseconds. Chemical reactions that govern soot formation occur at nearly all phases of soot processes from inception, surface growth, aging, to surface oxidation.

For soot particle inception in aliphatic fuels, the coupling between chemistry and transport can be summarized as follows. The process begins with the essential chemistry of fuel pyrolysis and is then followed by precursor formation. Though there exist various opinions as to the exact reaction path to soot inception (c.f., Frenklach and Wang, 1990; Calcote and Keil, 1990; Colket, 1995), it is generally agreed that hydrogen radicals (H) play a critical role in this process. For nonpremixed flames, the availability of H radicals in the high temperature region where soot is formed is supported by both the chemical and transport processes. As the first step, hydrogen molecules are produced from the fuel pyrolysis reaction. They then are diffused into the oxidation region and converted to H radicals through

reactions with oxygen radicals (O) and hydroxyl radicals (OH) via

$$H_2 + O \rightarrow OH + H \quad , \tag{1.2}$$

$$H_2 + OH \rightarrow H_2O + H \quad . \tag{1.3}$$

These newly formed hydrogen radicals subsequently are diffused back to the fuel pyrolysis region where they are consumed to pyrolyze the fuel and converted back to H_2 through H abstraction reactions. The H radicals are also responsible for the growth of PAH by, for example, the sequential reactions (Frenklach, 1988) of hydrogen-abstraction given by

$$\text{Aryl-H} + H \rightarrow \text{Aryl} + H_2 \quad , \tag{1.4}$$

and addition of acetylene to the aryl radical formed given by

$$\text{Aryl} + C_2H_2 \rightarrow \text{Products} \quad . \tag{1.5}$$

Therefore, the H radicals are active in many aspects of the soot inception process including: fuel pyrolysis, initial ring formation, PAH growth, and ultimate soot particle inception and growth (Frenklach and Wang, 1990).

This understanding suggests that the critical steps leading to the inception of soot particles are the formation of H radicals at the flame front (oxidation region) and their subsequent diffusion into the fuel pyrolysis region. After inception, soot particles may grow by reaction with other PAH or other components produced from fuel pyrolysis. They may also be oxidized through reaction with oxygen molecules or hydroxyl radicals. In a diffusion flame, oxidation of soot can occur only upon the transportation of soot particles into the oxidizer side of the oxidation region, where oxidizer is present in high concentration. Since the transport of radicals and soot particles depends strongly on the flame structure for a diffusion flame, the

flame structure has a strong impact on the soot production.

To understand how the structure of a diffusion flame affects the soot inception process, it is necessary, at the simplest level, to characterize the following: (1) the formation of H radicals in the oxidation region, (2) the transport of the H radicals into the fuel pyrolysis region, and (3) the reaction of H radicals with the fuel or fuel-related species such as the soot precursors. Although the detailed chemistry that describes the production and destruction of H radicals is very complicated, it is less important compared to the effect of flame structure on the soot inception process. It is therefore assumed that the reaction of H radical with the fuel characterizes the essential features of the soot inception process. This simplification is justified by considering the initial pyrolysis from any heavier hydrocarbon/carbohydrate fuel to ethylene, and then to acetylene. Since the hydrogen abstraction reactions are the primary steps for the pyrolysis of C_2H_4, and the production as well as consumption reactions of C_2H_3 can be considered steady state, the rate of C_2H_2 production is given by $d[C_2H_2]/dt \sim [C_2H_4][H]$, where t represents time and $[A]$ the molar concentration of component A. Glassman and co-workers (Gomez *et al.*, 1984; Gomez and Glassman, 1986) have shown that the rate of this C_2H_4 pyrolysis is the primary reaction that controls the tendency of the reaction from fuels to soot. From the hydrogen abstraction-acetylene addition growth mechanism, acetylene is an essential ingredient for initial aromatic ring formation and the subsequent PAH growth. The growth of PAH is proportional to the product of the concentrations of H and C_2H_2, *i.e.*, $d[PAH]/dt \sim [H][C_2H_2]$ (Frenklach, 1988).

Acetylene and PAH can be oxidized through the attack by oxygen

molecules and hydroxyl radicals. Modeling of OH oxidation of soot is less fundamental than that of O_2 oxidation, albeit there exist significant uncertainties surrounding the latter as well. Although the actual soot oxidation reaction in nonpremixed flames involve OH, it is not essential to consider the OH chemistry because the reaction

$$H + O_2 \rightarrow OH + O \tag{1.6}$$

dominates the formation of OH and this reaction forces the OH distribution to follow that of O_2 in the soot oxidation region where the oxidation of acetylene and PAH occurs.

1.2.2 Overview of Existing Soot Models

The success in modeling of soot production requires, in general, an accurate account of both the formation and oxidation reactions. In a diffusion flame, soot production is inextricably linked to the flame structure through its impact on the flame temperature. Predication of soot concentration remains amongst the greatest challenges to researchers involved in combustion science and engineering. Advances are hampered by uncertainties in the fundamental rates of reactions such as O_2 oxidation and surface growth. Nevertheless, some useful predictions regarding soot formation have been obtained from relatively crude models.

As mentioned earlier, there are three classes of models available for the predication of soot production. The first one is based purely on empirical correlation. In a premixed flame, soot begins to form at a critical or threshold equivalence ratio, ϕ_c, where the equivalence ratio is defined as the fuel/oxidizer ratio divided by the stoichiometric fuel/oxidizer ratio

($\phi = (F/O)/(F/O)_{stoi}$). For a diffusion flame, the onset of soot emission is gauged by a sooting height, defined as the flame height at which soot is emitted. Calcote and Manos (1983) proposed the use of a threshold sooting index (TSI) as a means of absorbing all system and burner dependencies from measurements of the sooting tendency of fuels. The TSI is defined by these authors as

$$TSI = a - b\phi_c \quad , \tag{1.7}$$

where the apparatus dependent constants a and b were determined by calibration. The TSI method has later been further developed by other researchers such as Gill and Olson (1984) and Olson *et al.* (1985). Gill and Olson (1984) adopted the TSI definition of Eq. (1.7) to predict soot thresholds for fuel mixtures by using individual TSIs of each component and then combine them to the mixture TSI was obtained through the relation of

$$(1.1)^{TSI_{mix}} = \sum_j X_j (1.1)^{TSI_j} \quad , \tag{1.8}$$

where X_j is the mole fraction of species j. Olson *et al.* (1985) extended the threshold soot index to laminar diffusion flames for a wide variety of fuels. The TSI approach appeared to be useful in assessing the sooting tendencies of various fuels and stoichiometries by being able to account for the variations in the measured smoke point heights to different apparatus and flow configurations. Other researchers, such as Takahashi and Glassman (1984) and Harris *et al.* (1986) used a critical C/O ratio as the defined onset of sooting in premixed flames and found that the sooting tendency of a fuel is a function of its flame temperature, the C/H ratio, and the number of C atoms, but not the structure of the fuel. The critical C/O ratio is defined as the ratio of the

stoichiometric oxygen requirement to the actual experimental value at the sooting limit on the base that the carbon and hydrogen atoms in the fuel are completely converted to carbon monoxide and hydrogen molecular, respectively. These simple analyses yielded excellent correlation to the experimental data.

The second category of soot modeling are the semi-empirical models that attempt to incorporate aspects of the physics and chemistry of soot formation phenomena into the experimental data. This usually leads to the development of rate equations for the reactions yielding the production of soot precursors and soot particles by a simple description of chemistry.

This second approach was first adopted by Tesner and co-workers (Tesner *et al.*, 1971) who presented a model of soot formation that has been widely employed over the years. They interpreted their measurements of soot formation within an acetylene-hydrogen flame in terms of a simple kinetic model, then proposed a two-step mechanism that described the formation rate of soot nuclei and the particle number density. This model was subsequently modified to multiple-step reactions to describe the production of carbon black.

Hiroyasu *et al.* (1983) later proposed another soot model that considered the net soot formation rate to be the difference between the rates of its formation and oxidation, given by

$$dm_S / dt = (dm_{Sf} / dt) - (dm_{Sc} / dt) \quad , \tag{1.9}$$

where m_S is the total mass of soot particles, m_{Sf} is the mass of soot formed, and m_{Sc} is the mass of soot oxidized. The formation of soot is assumed to

follow a first order reaction characterized by the concentration of fuel vapor while the oxidation of soot is controlled by a second order reaction depending on the concentrations of soot and oxygen. Accordingly, the soot formation and oxidation reactions were described by the following rate equations:

$$dm_{Sf}/dt = A_f m_{fg} P^{0.5} \exp(-E_{Sf}/RT) \quad , \tag{1.10}$$

$$dm_{Sc}/dt = A_c m_S (P_{O_2}/P) P^{1.8} \exp(-E_{Sc}/RT) \quad , \tag{1.11}$$

where m_{fg} is the mass of fuel vapor, P is the system pressure, P_{O_2} is the partial pressure of oxygen, R is the universal gas constant, and T is the gas temperature. The values of activation energies were given by the authors as $E_{Sf} = 1.25\times10^4$ kcal/kmol and $E_{Sc} = 1.4\times10^4$ kcal/kmol. A_f and A_c are the pre-exponential constants that can be determined by measuring the soot content in the exhaust.

Delichatsios (1994) also developed a model that included a scaling of soot formation with flame height and pressure. His model focused on the evolution of soot along the axis of a laminar diffusion flame. The transport of soot was described by

$$\rho u (dY_S/dx) = \dot{w}_S \quad , \tag{1.12}$$

where Y_s is the mass fraction of soot, ρ the gas density, u and axial flow velocity, and x the spatial coordinate in the axial direction. The reaction rate $\dot{w}_S$ is a function of the mixture fraction, Z, temperature, T, and the initial fuel mass fraction at its source boundary, $Y_{F,0}$, given by

$$\dot{w}_S = A\rho^2 \left(Y_{F,0} \frac{Z - Z^*}{1 - Z^*} \right) \exp\left(-\frac{E}{RT} \right) \tag{1.13}$$

for $Z > Z^*$, and $\dot{w}_S = 0$ for $Z < Z^*$, where A is the pre-exponential factor. The mixture fraction, Z, is defined as

$$Z = (\beta - \beta_{O,0}) / (\beta_{F,1} - \beta_{O,0}) \quad , \tag{1.14}$$

where the variable β is defined as $\beta = Y_F / (\nu_F W_F) - Y_O / (\nu_O W_O)$, with W the molecular weight and ν the stoichiometric coefficient (Williams, 1985). The subscripts 1 and 0 refer to the boundaries where the fuel and oxidizer are supplied, respectively. At the fuel boundary, $Y_F = Y_{F,1}$ and $Y_O = 0$ such that $\beta = \beta_{F,1}$ and $Z = 1$. Similarly, at the oxidizer boundary, $Y_F = 0$ and $Y_O = Y_{O,0}$ such that $\beta = \beta_{O,0}$ and $Z = 0$. The values of $Y_{F,1}$ and $Y_{O,0}$ are controllable and the boundaries may be infinitely far away from the flame.

The model was built on the assumption that soot growth was solely controlled by the availability of gaseous soot formation species such as acetylene. The maximum soot mass fraction was assumed to locate at the flame tip where $Z = Z_{st}$ in which Z_{st} is the value of the mixture fraction at the stoichiometric condition.

Kennedy *et al.* (1990) attempted to use only a single equation, namely the conservation of soot volume fraction, to predict soot formation in a circular, laminar diffusion flame, and then apply it to model soot production in turbulent diffusion flames. In his model, mixture fraction is the primary quantity that is calculated and other quantities, such as temperature, density and gas composition are determined as functions of the mixture fraction. The soot volume fraction is a function of the rates of nucleation, surface growth, and oxidation reactions that are functions of the mixture fraction. The conservation equation for soot volume fraction, f_V, is thus

$$\rho u\frac{\partial f_V}{\partial x}+\rho(v+V_T)\frac{\partial f_V}{\partial r}=\frac{1}{r}\frac{\partial}{\partial r}\left(r\rho D_S\frac{\partial f_V}{\partial r}\right)+\rho\dot{w}_n+\rho\dot{w}_g-\rho\dot{w}_O \quad , \qquad (1.15)$$

where $\dot{w}_n$ and $\dot{w}_g$ are the rates of soot formation via nucleation and surface growth, $\dot{w}_O$ the rate of soot oxidation, u the axial velocity component, x and r the spatial coordinates along the axial and radial directions, u and v the flow velocity along the x and r directions, and D_S the diffusion coefficient of the soot. In addition, V_T is the thermophoretic velocity in the radial direction with the expression given by Talbot *et al.* (1980) as

$$V_T=-0.55\frac{\nu_k}{T}\frac{\partial T}{\partial r} \quad , \qquad (1.16)$$

where ν_k is the kinematic viscosity of the gas. The soot volume fraction equation is integrated along with the other conservation equations through a detailed numerical procedure to obtain the soot content. Good agreement was obtained between this model and the measurements for two different experimental conditions. The success, however, was limited to ethylene flames.

Said *et al.* (1997) subsequently removed the limitation by postulating the existence of a hypothetical intermediate species between the fuel and soot. In reality, this hypothetical species could be associated with acetylene. A two-equation model that describes the soot formation and oxidation processes was adopted to predict the soot volume fraction in a laminar diffusion flame. The first equation provided the rate of formation and oxidation of the intermediate species, while the other yielded the production rate of soot as a result of the competition between the formation of soot from the intermediate species and the soot oxidation.

Moss *et al.* (1988) also proposed a flamelet approach to model soot formation in diffusion flames. The complete transport equations were considered in this model. Two additional equations that govern the balance of the number density of soot particles, n, and the soot volume fraction, f_V, given by

$$d(n/N_0)/dt = \alpha(Z) - \beta(Z)(n/N_0)^2 \quad , \tag{1.17}$$

$$\rho_S(df_V/dt) = \gamma(Z)n + \delta(Z) \quad , \tag{1.18}$$

were included. In these equations, N_0 is the Avagadro's number and ρ_S is the density of soot taken to be 1800 kg/m^3. The first term in the right-hand side (RHS) of Eq. (1.17) represents the increase in the number of soot particles because of particle inception and the second term accounts for the loss of particles as a result of coagulation. Similarly, the first term in the RHS of Eq. (1.18) represents the increase of soot volume through surface growth, while the second term describes the increase of soot volume caused by nucleation of new particles. The source terms ($\alpha,\beta,\gamma,\delta$) were given as functions of the mixture fraction and temperature. The various constants in these expressions were determined from experimental measurements.

The impact of soot radiation on the flame structure has also been studied by using a semi-empirical soot formation model. Kaplan *et al.* (1994) used a rather complete radiation model in their calculations of a laminar ethylene diffusion flame. Their model accounted for and included the radiative emission of CO_2, H_2O and soot. Experimental data were used to estimate the absorption coefficient of these species. In their formulation, the model of Moss *et al.* (1988) was adopted such that Eqs. (1.17) and (1.18) were used to

describe the soot volume fraction and the soot number density. Oxidation of soot was attributed to the reaction with O_2. A detailed description of the conservation of mass, momentum, energy and species number densities has been formulated.

Kennedy *et al.* (1996) modeled a sooting and a non-sooting circular laminar jet flame with radiation. The governing equations in the boundary layer were solved with the assumption of a flow without axial pressure gradient. The radiative heat loss included in the energy conservation equation is considered to be caused by soot emission in an optically thin flame. Radiation from other species was neglected. The transport equations governing the mass fraction of the $N-2$ species for this study were given by

$$\rho u\frac{\partial Y_n}{\partial x}+\rho v\frac{\partial Y_n}{\partial r}=-\frac{1}{r}\frac{\partial}{\partial r}\{r\rho Y_n V_n\}+M_n\dot{w}_n \quad , \tag{1.19}$$

with the $(N-1)^{\text{th}}$ species being the soot and the N^{th} species being N_2, where V_n is the diffusion velocity, Y_n the mass concentration, M_n the molecular weight and $\dot{w}_n$ the reaction rate, of species n. The explicit expression of the equation for the soot mass fraction, Y_S, is

$$\rho u\frac{\partial Y_S}{\partial x}+\rho v\frac{\partial Y_S}{\partial r}=-\frac{1}{r}\frac{\partial}{\partial r}\{r\rho Y_S V_S\}+\rho S(Y_S,T,Y_{C_2H_2},Y_{O_2},Y_{OH},N) \quad , \tag{1.20}$$

where the main component of V_S is the thermophoretic velocity V_T given by Eq. (1.16), and N is the total number of species. The source term in Eq. (1.20) includes the contributions of soot nucleation ($\dot{w}_{nucl}$), soot surface growth ($\dot{w}_g$) and soot oxidation ($\dot{w}_O$), that is,

$$S(Y_S,T,Y_{C_2H_2},Y_{O_2},Y_{OH},N)=\dot{w}_{nucl}+\dot{w}_g-\dot{w}_O \quad . \tag{1.21}$$

The soot may be oxidized to CO by O_2 or OH . The early soot formation model by Kennedy *et al.* (1990) used an average number density to obtain an estimate of the soot aerosol surface area. This more recent study by Kennedy *et al.* (1996) followed the approach of Fairweather *et al.* (1992) in solving the equation for the number density of particles. The primary difference between the works by Kennedy *et al.* (1996) and Fairweather *et al.* (1992) is that the rate of the soot surface growth used by Kennedy *et al.* (1996) was doubled from that of Fairweather *et al.* (1992) to yield an adequate representation of the measured soot volume fractions in the flame. Kennedy *et al.* (1996) observed from their study that the flame structure could have a significant consequence on the formation of soot in a diffusion flame.

Extensions that include detailed reaction kinetics into a model for soot formation and radiation permits the examination of concerns regarding the impact of the soot processes on flame chemistry that cannot be addressed by experimental investigations alone.

The third category of soot models are the ones that employ detailed chemistry. These models were developed because those that rely on empirical inputs to soot nucleation, growth and oxidation rates are limited to specific conditions and cannot be extended to conditions far from those under which the rates were measured. Such variations include different fuels or different combustion pressures.

Early works on the development of these types of soot models were performed over the last few decades and focused on the description of soot formation in laminar premixed flames (Frenklach and co-workers 1984, 1990,

1994). The chemistry describing the soot formation can be thought as consisting of four major processes: (1) initial PAH formation, which includes the formation of the first aromatic ring in an aliphatic system; (2) PAH growth, comprised of replicating-type growth; (3) particle nucleation, consisting of coalescence of PAH into three-dimensional clusters; and (4) particle growth by coagulation and surface reactions of the forming clusters and particles. Recently, Lindstedt (1994) considered a detailed chemistry that included 242 reaction steps to model the processes leading to soot formation and particle growth in laminar nonpremixed flames. The reaction steps include a detailed gas phase oxidation chemistry as well as some simplified steps for the description of soot nucleation, surface growth and particle agglomeration processes. The soot nucleation and surface growth reactions are connected to the gas phase oxidation reactions by assuming that the location where soot nucleation and growth occurs is characterized by the concentrations of benzene and acetylene. The reaction mechanisms so developed were applied to study a wide range of ethylene and propane counterflow diffusion flames as well as the dependence of soot formation on nucleation and surface growth reactions.

Lindstedt (1994) also compared the predictions of soot production from his model against experimental data reported by Vandaburger *et al.* (1984) from their counterflow diffusion flame measurements. These experiments provided measurements of soot volume fraction, particle size and soot number density across a wide range of conditions. The comparison showed good agreement only for high sooting flames in which particle coagulation is rapid. The application of this model is, therefore, limited as with the other

models.

In addition to modeling, experimental investigations have also been widely undertaken to study the influence of gas additives and pressure on soot formation in diffusion flames (Axelbaum *et al.*, 1988, 1990; Hura and Glassman, 1988; Du and Axelbaum, 1995; Du *et al.*, 1990, 1998). Among the various possible gas additive effects, the following three categories are the most important: (a) dilution effect as a result of the reduction in the concentrations of the reactive species and thereby their collision frequencies; (b) thermal effect caused by the change of flame temperature as a consequence of the addition; and (c) chemical effect induced by the active participation of additives in the chemical reactions leading to soot formation and destruction. It is understood that the dilution and thermal effects also indirectly influence the chemical reactivity.

Results of Du *et al.* (1990) demonstrated that carbon dioxide addition, either to the fuel or oxidizer, can suppress the soot formation chemistry. The effect of oxygen addition, however, is more complicated. When oxygen is added to the fuel side of an ethylene flame, it leads to an abrupt increase in the soot inception, indicating that the inception chemistry has been accelerated. The oxygen addition to propane, on the other hand, is initially suppressive and results in a significant reduction in the soot inception. The addition becomes promoting as the molar fraction of oxygen approaches 40%. The effect of oxygen addition to the oxidizer side is almost totally thermal for both the ethylene and propane flames. Experiments on the inert addition to fuel by Axelbaum and Law (1990) exhibited that the effect of inert addition is a consequence of a reduction in fuel concentration (dilution) and temperature

(thermal), both of which decrease the soot concentration. The relative importance of dilution and temperature depends on the extent of addition. When a moderate amount of inert is added, the temperature reduction is typically very small so that the effect of dilution can be considerably greater than that of temperature. With a large amount of inert addition, temperature effects may dominate over those of dilution although in an absolute scale, dilution effects could still be important because of the low fuel concentration. The influence of pressure on the sooting limit of diluted ethylene counterflow flames was later investigated by Du *et al.* (1998) with pressure varying between 1 to 2.5 atm. Their results showed that the sooting tendency is enhanced with increasing pressure.

1.2.3 Summary of the Modeling

Modeling of soot formation in combustion systems requires approximation at various degrees of simplification. The simplest approach, taken by engineers in the engine community, is the empirical correlation of soot production into a function based on engine operating conditions. This method is useful only for conditions close to those under which the correlation was performed. As to the more sophisticated numerical methods that solve the rate equations governing the formation of soot nuclei, particle growth and oxidation, as well, can only be used for conditions under which the original data were measured. Recently, a surge of advancement on soot models featuring very detailed description of the underlying physics and chemistry was accomplished (Frenklach and Wang, 1994; Yoshihara *et al.*, 1994; Kazakov, *et al.* , 1995; Balthasar, *et al.* ,1996).

It is remarkable to note that all the above mentioned models have demonstrated potential for accurate predication of soot production over a wide range of conditions. As to the effects of flame structure on the sooting behavior, especially for a diffusion flame, and whether soot production can be reduced or eliminated in a diffusion flame, the understanding is still at its infancy. Many experiments have been performed using counterflow and coflow diffusion flames to study the characteristics of soot production and significant advances have been achieved. However, interpretations of the results differ. Du and Axelbaum (1995) experimentally and numerically investigated the effects of flame structure on the inception of soot precursors by varying the stoichiometric mixture fraction Z_{st} through the variation of initial fuel and/or oxidizer concentrations. Their work demonstrated that soot inception for an ethylene/oxygen counterflow flame can be completely suppressed, even at low strain rates, by varying the stoichiometric mixture fraction while maintaining the same, high flame temperature. The strain rate is defined as the gradient of the axial flow velocity. They found that as Z_{st} is increased, the flame shifts towards the fuel side and the soot inception process is retarded, and eventually completely suppressed. In an ethylene/oxygen counterflow flame, no luminous soot is detected for strain rates greater than 60 s^{-1} when Z_{st} is larger than 0.16. Comparing to the ethylene/air flame whose Z_{st} is 0.064 and the critical strain rate above which soot production is terminated is 175 s^{-1}, there is a significant improvement in the reduction of soot from combustion devices. For the laminar coflow ethylene flame, soot free flame was observed for Z_{st} greater than 0.72 regardless of the flame height. For low values of Z_{st}, the effect of Z_{st} upon soot inception is primarily through fuel dilution. For larger values of Z_{st},

where the oxygen concentration is significantly increased, the transport of OH into the fuel side of the flame has a dramatic influence on soot inception.

Lin and Faeth (1996) later studied the effects of hydrodynamics on soot formation using the similar conditions of Du and Axelbaum (1995), and obtained similar results. They attributed the diminishment of soot inception to the change of flow properties, especially the velocity component normal to the reaction regions. Their results suggested that soot formation in nonpremixed flames could be controlled by varying the flow velocity normal to the flame. When the normal component of the flow velocity near the flame is directed toward the oxidizer side of the flame, the residence time of the reactants in the fuel-rich region where soot is produced is reduced such that a lesser amount of soot particles is produced. When these precursors and particles are transported into the fuel-lean region, they are more readily to be oxidized and the soot production is reduced. In contrast, when the normal component of the flow is directed toward the fuel side of the flame, the motion of soot precursors and particles toward the oxidation region can only be through diffusion against convection and is primarily blocked, yielding a longer residence time for soot formation within the fuel-rich region, and a higher soot production that results in greater soot emission. This conclusion emphasized the importance of convection upon the sooting processes within diffusion flames. Lin and Faeth (1996) also extended their experiments by testing a number of other hydrocarbon fuels including acetylene and the results were qualitatively similar.

Up to the present, all the models developed have been supported by experimental or numerical investigations. However, the primary

mechanism responsible for soot inception and suppression has not been identified. Suppression of soot and PAH may be accomplished by adding inert gas to the fuel and oxidizer such that the flame temperature is reduced and consequently, the soot chemistry is retarded. Temperature reduction is one means of suppressing soot, but the reduction in temperature that is necessary to completely suppress soot formation weakens the flames to the extent that they become unstable. The recognition by Du and Axelbaum (1995) and Lin and Faeth (1996) that there exist conditions in which soot inception can be completely suppressed at very high flame temperatures and low strain rates introduces a promising method for the control of soot inception processes without sacrificing the burning intensity. Identification of the effects that hydrodynamics, transport and flame structure have on soot formation in nonpremixed flames is essential in understanding how soot production can be suppressed through variation of the mixture fraction. This task can be achieved by theoretical investigations employing simplified reaction chemistry.

1.3 Objectives

Recognizing the significance of combustion generated soot on energy utilization and environmental protection, as well as the importance of hydrodynamics and transport on the formation of soot particles within nonpremixed flames, the objective of this study is to identify and characterize the parameters that affect the soot production process in such flames. Theoretical approaches that employ activation energy asymptotics will be adopted to study the effect of various controlling mechanisms on the soot inception process.

To facilitate the analysis, the reaction kinetics needs to be sufficiently simplified, yet still includes important steps that describe the inception and oxidation of soot precursors such that the coupling between soot inception and flame structure can be assessed. Following the understanding gained from the literature discussed earlier, a simplified three-step model given by

$$\nu_{F,1} F + \nu_{O,1} O \rightarrow \nu_{P,1} P + \nu_R R \quad , \tag{R1}$$

$$\nu_{F,2} F + \nu_R R \rightarrow \nu_S S \quad , \tag{R2}$$

$$\nu_S S + \nu_{O,3} O \rightarrow \nu_{P,3} P \quad , \tag{R3}$$

is adopted. These reaction steps respectively represent the oxidation, soot precursor formation, and soot precursor consumption reactions. This scheme yields three distinct reaction zones. For the oxidation reaction (reaction R1), fuel (F) and oxidizer (O) are consumed in an oxidation region to produce final products P and radical R (e.g., H). Part of the radical produced is transported toward the fuel side and reacts with the fuel (reaction R2) to produce the soot/precursor S in a formation region adjacent to the oxidation region. Part

of the soot precursor subsequently penetrates through the oxidation region, and reacts with the oxidizer (reaction R3) in a consumption region adjacent to the primary oxidation region, to produce more final products. Recognizing that the production of soot is dependent on the presence of soot precursors, S will hereforth be the representation of soot without considering the soot growth reaction.

The study will include the following tasks for two flame geometries, the counterflow diffusion flame and the spherical diffusion flame stabilized by a spherical porous burner.

1. Formulate the conservation equations that describe the oxidation, soot formation and soot consumption reactions following the reaction kinetics described above.

2. Solve the conservation equations by high activation energy asymptotics to yield analytical solutions of flame temperature, flame standoff distance and soot concentration.

3. Develop a FORTRAN code to perform numerical calculations to obtain values for the variables solved in 2, and other flame responses as functions of the controlling parameters. Detailed information on the flame responses and controlling parameters will be identified later.

4. Investigate the effect of hydrodynamics, transport and flame structure on the soot inception and consumption processes.

5. Identify approaches to suppress soot production for diffusion flames.

CHAPTER 2

COUNTERFLOW DIFFUSION FLAMES

A counterflow diffusion flame is generated by impinging a fuel stream supplied from $x \to -\infty$, where x is the axial spatial coordinate, with a temperature $T_{-\infty}$ into an oxidizer stream supplied from $x \to \infty$ with a temperature T_{∞}, similar to that of Liñán (1974). This flame configuration has been widely employed in combustion experiments because of its geometric simplicity. It allows the isolation of many controlling parameters such that the effect of each parameter can be assessed individually. In theoretical studies, the problem can be formulated based on conservation laws and analyzed both analytically and numerically. Comparison between theoretical and experimental results can also be made to characterize the flame behavior under specified conditions.

2.1 Formulation

The three-step, simplified reaction scheme introduced in Chapter 1 and expressed in Eqs. (R1) – (R3) is adopted to describe the chemistry with the rate of each of these reactions following second-order Arrhenius kinetics. To facilitate the analysis, the properties of the gas including the gas density ρ, thermal conductivity λ and the mass diffusion coefficient of all the components, D_i, are considered to be constants so that the flow field is an irrotational potential flow. This simplification allows for decoupling of the continuity and momentum equations from the energy and species equations so that only the latter need be solved. The result agrees qualitatively with that obtained from the analysis when properties vary with temperature.

Since only qualitative behavior is interested, the more involved variable-property approach does not possess additional scientific value and is avoided. Because the soot formation reaction (reaction R2) is only slightly endothermic, it is assumed that this reaction is thermally neutral. Moreover, since the effects of mass diffusion of the fuel and oxidizer are already well-known, they will not be considered in this study. Thus the Lewis numbers of the fuel and oxidizer, where the Lewis number is defined as the ratio between the thermal and the mass diffusivities, are taken to be unity for simplicity in the analysis.

With the above assumptions, the conservation equations are given by

$$\rho u c_p \frac{dT}{dx} - \frac{d}{dx}\left(\lambda \frac{dT}{dx}\right) = \nu_{F,1} W_F q_{F,1} B_1 \left(\frac{\rho Y_F}{W_F}\right)\left(\frac{\rho Y_O}{W_O}\right)\exp(-E_1/T) + \nu_S W_S q_{S,3} B_3 \left(\frac{\rho Y_S}{W_S}\right)\left(\frac{\rho Y_O}{W_O}\right)\exp(-E_3/T) \quad , \tag{2.1}$$

$$\rho u \frac{dY_F}{dx} - \frac{d}{dx}\left(\rho D_F \frac{dY_F}{dx}\right) = -\nu_{F,1} W_F B_1 \left(\frac{\rho Y_F}{W_F}\right)\left(\frac{\rho Y_O}{W_O}\right)\exp(-E_1/T) - \nu_{F,2} W_F B_2 \left(\frac{\rho Y_F}{W_F}\right)\left(\frac{\rho Y_R}{W_R}\right)\exp(-E_2/T) \quad , \tag{2.2}$$

$$\rho u \frac{dY_O}{dx} - \frac{d}{dx}\left(\rho D_O \frac{dY_O}{dx}\right) = -\nu_{O,1} W_O B_1 \left(\frac{\rho Y_F}{W_F}\right)\left(\frac{\rho Y_O}{W_O}\right)\exp(-E_1/T) - \nu_{O,3} W_O B_3 \left(\frac{\rho Y_S}{W_S}\right)\left(\frac{\rho Y_O}{W_O}\right)\exp(-E_3/T) \quad , \tag{2.3}$$

$$\rho u \frac{dY_R}{dx} - \frac{d}{dx}\left(\rho D_R \frac{dY_R}{dx}\right) = \nu_R W_R B_1 \left(\frac{\rho Y_F}{W_F}\right)\left(\frac{\rho Y_O}{W_O}\right)\exp(-E_1/T) - \nu_R W_R B_2 \left(\frac{\rho Y_F}{W_F}\right)\left(\frac{\rho Y_R}{W_R}\right)\exp(-E_2/T) \quad , \tag{2.4}$$

$$\rho u\frac{dY_S}{dx}-\frac{d}{dx}\left(\rho D_S\frac{dY_S}{dx}\right)=\nu_S W_S B_2\left(\frac{\rho Y_F}{W_F}\right)\left(\frac{\rho Y_R}{W_R}\right)\exp(-E_2/T)$$

$$-\nu_S W_S B_3\left(\frac{\rho Y_S}{W_S}\right)\left(\frac{\rho Y_O}{W_O}\right)\exp(-E_3/T) \quad , \tag{2.5}$$

which will be solved subject to the boundary conditions:

$$x\to-\infty \quad : \quad T\to T_{-\infty} \quad , \quad Y_F\to Y_{F,-\infty} \quad ,$$

$$Y_O\to 0 \quad , \quad Y_R\to 0 \quad , \quad Y_S\to 0 \quad ; \tag{2.6}$$

$$\tilde{x}\to\infty \quad : \quad T\to T_{\infty} \quad , \quad Y_F\to 0 \quad ,$$

$$Y_O\to Y_{O,\infty} \quad , \quad Y_R\to 0 \quad , \quad Y_S\to 0 \quad . \tag{2.7}$$

In Eqs. (2.1)–(2.5), the axial flow velocity is given by $u=-kx$, where k is the flow velocity gradient which is also the strain rate. In the above equations T is the temperature, Y_i is the mass fraction of species i, $q_{F,1}$ is the heat of combustion per unit mass of fuel consumed in the oxidation reaction, $q_{S,3}$ is the heat of combustion per unit mass of soot/precursor consumed in the soot consumption reaction, ρ is the gas density, c_p is the specific heat at constant pressure, λ is the thermal conductivity, D_i and W_i are the mass diffusivity and molecular weight of species i, B_j and E_j are the pre-exponential factor and activation temperature of reaction R_j, respectively, ν_i is the stoichiometric coefficient of species i and $\nu_{i,j}$ is the stoichiometric coefficient of species i at reaction R_j.

The nondimensional quantities are defined as

$$\tilde{Y}_F=Y_F \quad , \quad \tilde{Y}_O=Y_O/\left(\frac{\nu_{O,1}W_O}{\nu_{F,1}W_F}\right) \quad , \quad \tilde{Y}_R=Y_R/\left(\frac{\nu_R W_R}{\nu_{F,1}W_F}\right) \quad ,$$

$$\tilde{Y}_S = Y_S / (\frac{\nu_S W_S}{\nu_{F,2} W_F}) \quad , \quad \tilde{\nu}_O = \frac{\nu_{O,3}}{\nu_{O,1}} \quad , \quad \tilde{x} = \frac{x}{\sqrt{\lambda / (\rho k c_p)}} \quad ,$$

$$\tilde{T} = \frac{T}{q_{F,1} / c_p} \quad , \quad \tilde{E}_i = \frac{E_i}{q_{F,1} / c_p} \quad , \quad \tilde{\nu}_F = \frac{\nu_{F,2}}{\nu_{F,1}} \quad , \quad Le_i = \frac{\lambda}{\rho D_i c_p} \quad ,$$

$$Da_1 = \frac{\rho \nu_{O,1} B_1}{k W_F} \quad , \quad Da_2 = \frac{\rho \tilde{\nu}_F \nu_R B_2}{k W_F} \quad , \quad \alpha = \frac{E_3}{E_2} \quad , \quad \hat{\nu} = \frac{\tilde{\nu}_F}{\tilde{\nu}_O} \quad ,$$

$$\tilde{q}_S = \frac{\nu_S W_S q_{S,3}}{\nu_{F,2} W_F q_{F,1}} \quad , \quad \beta = \frac{\nu_{O,1} \nu_S B_3}{\nu_{F,2} \nu_R B_2} \quad , \quad \nu^* = \frac{1 + \tilde{\nu}_O}{1 + \tilde{\nu}_F} \quad ,$$

where Le_i is the Lewis number of species i, Da_j the Damköhler number of reaction R_j, α and β the activation energy ratio and Damköhler number ratio between the soot/precursor consumption and soot/precursor formation reactions, respectively, and $\hat{\nu}$, ν^* some stoichiometric coefficient ratios. Applying these quantities to the conservation equations and the boundary conditions, we obtain the following nondimentional equations :

$$\tilde{x}\frac{d\tilde{T}}{d\tilde{x}} + \frac{d^2\tilde{T}}{d\tilde{x}^2} = -Da_1 \tilde{Y}_F \tilde{Y}_O \exp(-\tilde{E}_1 / \tilde{T}) - \tilde{q}_S \beta Da_2 \tilde{Y}_S \tilde{Y}_O \exp(-\alpha \tilde{E}_2 / \tilde{T}) \quad , \tag{2.8}$$

$$\tilde{x}\frac{d\tilde{Y}_F}{d\tilde{x}} + \frac{d^2\tilde{Y}_F}{d\tilde{x}^2} = Da_1 \tilde{Y}_F \tilde{Y}_O \exp(-\tilde{E}_1 / \tilde{T}) + Da_2 \tilde{Y}_F \tilde{Y}_R \exp(-\tilde{E}_2 / \tilde{T}) \quad , \tag{2.9}$$

$$\tilde{x}\frac{d\tilde{Y}_O}{d\tilde{x}} + \frac{d^2\tilde{Y}_O}{d\tilde{x}^2} = Da_1 \tilde{Y}_F \tilde{Y}_O \exp(-\tilde{E}_1 / \tilde{T}) + (\beta / \hat{\nu}) Da_2 \tilde{Y}_S \tilde{Y}_O \exp(-\alpha \tilde{E}_2 / \tilde{T}) \quad , \tag{2.10}$$

$$\tilde{x}\frac{d\tilde{Y}_R}{d\tilde{x}} + \frac{1}{Le_R}\frac{d^2\tilde{Y}_R}{d\tilde{x}^2} = -Da_1 \tilde{Y}_F \tilde{Y}_O \exp(-\tilde{E}_1 / \tilde{T}) + (Da_2 / \tilde{\nu}_F) \tilde{Y}_F \tilde{Y}_R \exp(-\tilde{E}_2 / \tilde{T}) \quad , \tag{2.11}$$

$$\tilde{x}\frac{d\tilde{Y}_S}{d\tilde{x}}+\frac{1}{Le_S}\frac{d^2\tilde{Y}_S}{d\tilde{x}^2}=-Da_2\tilde{Y}_F\tilde{Y}_R\exp(-\tilde{E}_2/\tilde{T})$$

$$+\beta Da_2\tilde{Y}_S\tilde{Y}_O\exp(-\alpha\tilde{E}_2/\tilde{T})\ , \qquad (2.12)$$

and boundary conditions:

$$\tilde{x}\to-\infty \ : \ \tilde{T}\to\tilde{T}_{-\infty}\ , \ \tilde{Y}_F\to\tilde{Y}_{F,-\infty}\ ,$$

$$\tilde{Y}_O\to 0\ , \ \tilde{Y}_R\to 0\ , \ \tilde{Y}_S\to 0\ ; \qquad (2.13)$$

$$\tilde{x}\to\infty \ : \ \tilde{T}\to\tilde{T}_{\infty}\ , \ \tilde{Y}_F\to 0\ ,$$

$$\tilde{Y}_O\to\tilde{Y}_{O,\infty}\ , \ \tilde{Y}_R\to 0\ , \ \tilde{Y}_S\to 0\ . \qquad (2.14)$$

2.2 Asymptotic Analysis

In the present analysis, high activation energy reactions are considered so that all the three reactions are confined to regions much thinner than the characteristic transport regions. Moreover, the activation energies of the soot/precursor formation and consumption reactions are assumed to be of the same order and much smaller than that of the oxidation reaction. As a result the soot/precursor formation and consumption regions are much thicker in extent than the oxidation region. The reaction regions are located near where the maximum temperature is initially attained. Designating the small parameters ε and δ to be the ratio of the characteristic oxidation region to diffusion region, and soot/precursor formation region to diffusion region length scales, respectively, the solutions are expanded using ε and δ as small parameters with $1 \gg \delta \gg \varepsilon$ since $E_1 \gg E_2$ is considered as a condition.

2.2.1 Outer Solutions

In the chemically inert diffusion regions that are regulated by the balance between the convection and diffusion transport, solving the source free form of Eqs. (2.8)–(2.12) subject to the boundary conditions in Eqs. (2.13) and (2.14) yields the outer solutions

$$\tilde{T}^{-} = \tilde{T}_{-\infty} + \{[a^{-}_{T,0} + \delta a^{-}_{T,1} + O(\delta^2)] + O(\varepsilon)\} I(\tilde{x}) \quad , \tag{2.15a}$$

$$\tilde{T}^{+} = \tilde{T}_{\infty} + \{[a^{+}_{T,0} + \delta a^{+}_{T,1} + O(\delta^2)] + O(\varepsilon)\} [\sqrt{2\pi} - I(\tilde{x})] \quad , \tag{2.15b}$$

$$\tilde{Y}^{-}_{F} = \tilde{Y}_{F,-\infty} - \{[a^{-}_{F,0} + \delta a^{-}_{F,1} + O(\delta^2)] + O(\varepsilon)\} I(\tilde{x}) \quad , \tag{2.16a}$$

$$\tilde{Y}^{+}_{F} = \{[a^{+}_{F,0} + \delta a^{+}_{F,1} + O(\delta^2)] + O(\varepsilon)\} [\sqrt{2\pi} - I(\tilde{x})] \quad , \tag{2.16b}$$

$$\tilde{Y}^{-}_{O} = \{[a^{-}_{O,0} + \delta a^{-}_{O,1} + O(\delta^2)] + O(\varepsilon)\} I(\tilde{x}) \quad , \tag{2.17a}$$

$$\tilde{Y}^{+}_{O} = \tilde{Y}_{O,\infty} - \{[a^{+}_{O,0} + \delta a^{+}_{O,1} + O(\delta^2)] + O(\varepsilon)\} [\sqrt{2\pi} - I(\tilde{x})] \quad , \tag{2.17b}$$

$$\tilde{Y}^{-}_{i} = \{[a^{-}_{i,0} + \delta a^{-}_{i,1} + O(\delta^2)] + O(\varepsilon)\} I(\sqrt{Le_i}\,\tilde{x}) \quad , \quad i = R, S \quad , \tag{2.18a}$$

$$\tilde{Y}^{+}_{i} = \{[a^{+}_{i,0} + \delta a^{+}_{i,1} + O(\delta^2)] + O(\varepsilon)\} [\sqrt{2\pi} - I(\sqrt{Le_i}\,\tilde{x})] \quad , \quad i = R, S \quad , \tag{2.18b}$$

where $a^{\pm}_{i,j}$ are integration constants to be determined. The superscripts "–" and "+" denote, respectively, solutions within the fuel and oxidizer sides of the reaction regions, and

$$I(\sqrt{Le_i}\,\tilde{x}) = \int_{-\infty}^{\sqrt{Le_i}\,\tilde{x}} \exp(-t^2/2)\, dt \quad . \tag{2.19}$$

2.2.2 Structure Equations in the Soot Formation Region

In the $O(\delta)$ soot/precursor formation region that is located in the fuel side of and adjacent to the oxidation region, only the soot/precursor formation reaction (R2) is significant and only $O(\delta)$ variation on all the quantities is possible. Defining the stretched coordinate as $\zeta = (\tilde{x} - \tilde{x}_f)/\delta$, where $\delta = \tilde{T}_{f,0}^{2} / \tilde{E}_2$ and $\zeta < 0$, and expanding the various quantities as:

$$\tilde{T}^{-} = [\tilde{T}_{f,0}^{\cdot} - \delta \Theta_1^{-} - \delta^2 \Theta_2^{-} + O(\delta^3)] + O(\varepsilon) \quad , \tag{2.20}$$

$$\tilde{Y}_i^{-} = \delta[\Phi_{i,1}^{-} + \delta \Phi_{i,2}^{-} + O(\delta^2)] + O(\varepsilon) \quad , \quad i = F, O, R \quad , \tag{2.21}$$

$$\tilde{Y}_S^{-} = \Phi_{S,0}^{-} + \delta[\Phi_{S,1}^{-} + \delta \Phi_{S,2}^{-} + O(\delta^2)] + O(\varepsilon) \quad , \tag{2.22}$$

Eqs. (2.8)–(2.12) can be expanded and rearranged. Collecting terms of the same order based on δ, we obtain the following structure equations:

$$d^2\Phi_{F,1}^{-} / d\zeta^2 = \Lambda_2 \Phi_{F,1}^{-} \Phi_{R,1}^{-} \exp(-\Theta_1^{-}) \quad , \tag{2.23}$$

$$\frac{d^2\Theta_1^{-}}{d\zeta^2} = \frac{d^2\Phi_{S,0}^{-}}{d\zeta^2} = \frac{d^2\Phi_{F,1}^{-}}{d\zeta^2} - \frac{\tilde{\nu}_F}{Le_R}\frac{d^2\Phi_{R,1}^{-}}{d\zeta^2}$$

$$= \frac{\tilde{\nu}_F}{Le_R}\frac{d^2\Phi_{R,1}^{-}}{d\zeta^2} + \frac{1}{Le_S}\frac{d^2\Phi_{S,1}^{-}}{d\zeta^2} + \tilde{x}_f \frac{d\Phi_{S,0}^{-}}{d\zeta} = 0 \quad , \tag{2.24}$$

$$\hat{\nu}\tilde{q}_S \frac{d^2\Phi_{O,2}^{-}}{d\zeta^2} - \left(\frac{d^2\Theta_2^{-}}{d\zeta^2} + \tilde{x}_f \frac{d\Theta_1^{-}}{d\zeta}\right) = 0 \quad , \tag{2.25}$$

$$\left(\frac{d^2\Phi_{F,2}^{-}}{d\zeta^2} + \tilde{x}_f \frac{d\Phi_{F,1}^{-}}{d\zeta}\right) - \tilde{\nu}_F\left(\frac{1}{Le_R}\frac{d^2\Phi_{R,2}^{-}}{d\zeta^2} + \tilde{x}_f \frac{d\Phi_{R,1}^{-}}{d\zeta}\right) = 0 \quad , \tag{2.26}$$

$$\left(\frac{d^2\Phi_{F,2}^{-}}{d\zeta^2}+\tilde{x}_f\frac{d\Phi_{F,1}^{-}}{d\zeta}\right)-\hat{\nu}\frac{d^2\Phi_{O,2}^{-}}{d\zeta^2}$$

$$+\left(\frac{1}{Le_S}\frac{d^2\Phi_{S,2}^{-}}{d\zeta^2}+\tilde{x}_f\frac{d\Phi_{S,1}^{-}}{d\zeta}+\zeta\frac{d\Phi_{S,0}^{-}}{d\zeta}\right)=0 \quad . \tag{2.27}$$

In the above equations, $\tilde{T}_{f,0}$ is the leading order flame temperature and

$$\Lambda_2=\delta^3 Da_2\exp(-\tilde{E}_2/\tilde{T}_{f,0}) \tag{2.28}$$

is the reduced Damköhler number of the soot/precursor formation reaction. The soot/precursor concentration in the soot/precursor formation region is considered an $O(1)$ quantity since the soot/precursor consumption reaction is considered to be slower than the soot/precursor formation reaction. Because oxidizer leaks only in $O(\varepsilon)$ amounts through the oxidation region into this region, $\Phi_{O,1}^{-}\equiv 0$ is a required condition.

2.2.3 Matching of Solutions in the Outer and Soot Formation Regions

The required boundary conditions to solve the structure equations in the soot formation region can be obtained from matching the solutions in the soot formation region with the outer solutions from the fuel side in the common region between these regions.

Matching can be performed by first substituting the stretched variable $\tilde{x}=\tilde{x}_f+\delta\zeta$ into the outer solutions, expanding the resulting equation in terms of δ, collecting the terms of the same ordering, and then equating the transformed outer solutions with the solutions in the soot formation region in the limit of $\zeta\to-\infty$ and $\tilde{x}\to\tilde{x}_f$. The procedure will be illustrated by the matching of the temperature solutions in the following. Applying the

stretched variable, Eq. (2.19) is first expanded to

$$I(\sqrt{Le_i}\,\tilde{x}) = I(\sqrt{Le_i}\,\tilde{x}_f) + \delta\sqrt{Le_i}\exp(-Le_i\tilde{x}_f^2/2)\zeta$$
$$-\delta^2[const + Le_i^{3/2}\tilde{x}_f\exp(-Le_i\tilde{x}_f^2/2)\zeta^2/2] + O(\delta^3) \quad . \qquad (2.29)$$

Next, substituting Eq. (2.29) into Eq. (2.15a), rearranging in terms of δ and equating the resulting expression with Eq. (2.20) as $\zeta \to -\infty$, we have

$$\tilde{T}^- = [\tilde{T}_{-\infty} + a_{T,0}^- I(\tilde{x}_f)] + \delta[a_{T,1}^- I(\tilde{x}_f) + a_{T,0}^- \exp(-\tilde{x}_f^2/2)\zeta]$$
$$+\delta^2[const + a_{T,1}^- \exp(-\tilde{x}_f^2/2)\zeta - a_{T,0}^- \tilde{x}_f \exp(-\tilde{x}_f^2/2)\zeta^2/2] + O(\delta^3)$$
$$= \{[\tilde{T}_{f,0} - \delta\Theta_1^- - \delta^2\Theta_2^- + O(\delta^3)] + O(\varepsilon)\}_{\zeta\to-\infty} \quad . \qquad (2.30)$$

By comparing terms of the same order in δ, the following results are obtained:

$$\tilde{T}_{f,0} = \tilde{T}_{-\infty} + a_{T,0}^- I(\tilde{x}_f) \quad \text{or} \quad a_{T,0}^- = (\tilde{T}_{f,0} - \tilde{T}_{-\infty})/I(\tilde{x}_f) \quad , \qquad (2.31)$$

$$\Theta_1^-(\zeta \to -\infty) = -a_{T,1}^- I(\tilde{x}_f) - a_{T,0}^- \exp(-\tilde{x}_f^2/2)\zeta \quad , \qquad (2.32)$$

$$(d\Theta_2^-/d\zeta)_{(\zeta\to-\infty)} = \exp(-\tilde{x}_f^2/2)(-a_{T,1}^- + a_{T,0}^-\tilde{x}_f\zeta) \quad . \qquad (2.33)$$

Other matching conditions can be derived through the same process, yielding

$$a_{F,0}^- = \tilde{Y}_{F,-\infty}/I(\tilde{x}_f) \quad , \qquad (2.34)$$

$$a_{O,0}^- = a_{O,1}^- = a_{R,0}^- = 0 \quad , \qquad (2.35)$$

$$\Phi_{F,1}^-(\zeta \to -\infty) = -a_{F,1}^- I(\tilde{x}_f) - a_{F,0}^- \exp(-\tilde{x}_f^2/2)\,\zeta \quad , \qquad (2.36a)$$

$$(d\Phi_{F,2}^-/d\zeta)_{\zeta\to-\infty} = \exp(-\tilde{x}_f^2/2)(-a_{F,1}^- + a_{F,0}^-\,\tilde{x}_f\zeta) \quad , \qquad (2.37)$$

$$(d\Phi_{O,2}^-/d\zeta)_{\zeta\to-\infty} = 0 \quad , \qquad (2.38)$$

$$\Phi_{R,1}^{-}(\zeta \to -\infty) = a_{R,1}^{-} I(\sqrt{Le_R}\,\tilde{x}_f) \quad , \tag{2.39}$$

$$(d\Phi_{R,2}^{-} / d\zeta)_{\zeta \to -\infty} = a_{R,1}^{-} \sqrt{Le_R} \exp(-Le_R \tilde{x}_f^2 / 2) \quad , \tag{2.40}$$

$$\Phi_{S,0}^{-}(\zeta \to -\infty) = a_{S,0}^{-} I(\sqrt{Le_S}\,\tilde{x}_f) \quad , \tag{2.41}$$

$$\Phi_{S,1}^{-}(\zeta \to -\infty) = a_{S,1}^{-} I(\sqrt{Le_S}\,\tilde{x}_f) + a_{S,0}^{-} \sqrt{Le_S} \exp(-Le_S \tilde{x}_f^2 / 2)\zeta \quad , \tag{2.42}$$

$$(d\Phi_{S,2}^{-} / d\zeta)_{\zeta \to -\infty} = \sqrt{Le_S} \exp(-Le_S \tilde{x}_f^2 / 2)(a_{S,1}^{-} - a_{S,0}^{-} Le_S \tilde{x}_f \zeta) \quad . \tag{2.43}$$

Equation (2.36a) also implies

$$(d\Phi_{F,1}^{-} / d\zeta)_{\zeta \to -\infty} = -a_{F,0}^{-} \exp(-\tilde{x}_f^2 / 2) \quad . \tag{2.36b}$$

Integrating the four expressions in Eq. (2.24) twice and Eqs. (2.25)–(2.27) once subject to the matching conditions in Eqs. (2.32)–(2.33), and (2.36)–(2.43), we obtain

$$\Phi_{S,0}^{-} = a_{S,0}^{-} I(\sqrt{Le_S}\,\tilde{x}_f) \quad , \tag{2.44}$$

$$\Theta_1^{-} = -a_{T,1}^{-} I(\tilde{x}_f) - a_{T,0}^{-} \exp(-\tilde{x}_f^{\,2} / 2)\,\zeta \quad , \tag{2.45}$$

$$\Phi_{F,1}^{-} - \frac{\tilde{\nu}_F}{Le_R} \Phi_{R,1}^{-} = -a_{F,1}^{-} I(\tilde{x}_f) - \frac{\tilde{\nu}_F}{Le_R} a_{R,1}^{-} I(\sqrt{Le_R}\,\tilde{x}_f) - a_{F,0}^{-} \exp(-\tilde{x}_f^{\,2} / 2)\,\zeta \quad , \tag{2.46}$$

$$\frac{\tilde{\nu}_F}{Le_R} \Phi_{R,1}^{-} + \frac{1}{Le_S} \Phi_{S,1}^{-} = \frac{\tilde{\nu}_F}{Le_R} a_{R,1}^{-} I(\sqrt{Le_R}\,\tilde{x}_f) + \frac{1}{Le_S} a_{S,1}^{-} I(\sqrt{Le_S}\,\tilde{x}_f) + a_{S,0}^{-} \frac{\exp(-Le_S \tilde{x}_f^2 / 2)}{\sqrt{Le_S}} \zeta \quad , \tag{2.47}$$

$$\hat{\nu} \tilde{q}_S \frac{d\Phi_{O,2}^{-}}{d\zeta} - \left(\frac{d\Theta_2^{-}}{d\zeta} + \tilde{x}_f \Theta_1^{-} \right) = a_{T,1}^{-} \Gamma^{-}(1) \quad , \tag{2.48}$$

$$\left(\frac{d\Phi_{F,2}^{-}}{d\zeta}+\tilde{x}_f\Phi_{F,1}^{-}\right)-\tilde{\nu}_F\left(\frac{1}{Le_R}\frac{d\Phi_{R,2}^{-}}{d\zeta}+\tilde{x}_f\Phi_{R,1}^{-}\right)$$

$$=-a_{F,1}^{-}\Gamma^{-}(1)-\tilde{\nu}_F a_{R,1}^{-}\Gamma^{-}(Le_R) \quad , \tag{2.49}$$

$$\left(\frac{d\Phi_{F,2}^{-}}{d\zeta}+\tilde{x}_f\Phi_{F,1}^{-}\right)+\left(\frac{1}{Le_S}\frac{d\Phi_{S,2}^{-}}{d\zeta}+\tilde{x}_f\Phi_{S,1}^{-}\right)-\hat{\nu}\frac{d\Phi_{O,2}^{-}}{d\zeta}$$

$$=a_{S,1}^{-}\Gamma^{-}(Le_S)-a_{F,1}^{-}\Gamma^{-}(1) \ , \tag{2.50}$$

where

$$\Gamma^{-}(Le)=[\exp(-Le\tilde{x}_f^2/2)/\sqrt{Le}]+\tilde{x}_f I(\sqrt{Le}\,\tilde{x}_f) \quad . \tag{2.51}$$

2.2.4 Structure Equations in the Soot Consumption Region

In the $O(\delta)$ soot/precursor consumption region located adjacent to the oxidizer side of the oxidation region, only the soot/precursor consumption reaction (R3) is important. Because E_2 and E_3 are of the same order, the same stretched coordinate $\zeta=(\tilde{x}-\tilde{x}_f)/\delta$ is used except that $\zeta>0$ in this region. The expansions of the various variables are:

$$\tilde{T}^{+}=[\tilde{T}_{f,0}-\delta\Theta_1^{+}-\delta^2\Theta_2^{+}+O(\delta^3)]+O(\varepsilon) \quad , \tag{2.52}$$

$$\tilde{Y}_i^{+}=\delta[\Phi_{i,1}^{+}+\delta\Phi_{i,2}^{+}+O(\delta^2)]+O(\varepsilon) \quad , \quad i=F,O,R \quad , \tag{2.53}$$

$$\tilde{Y}_S^{+}=\Phi_{S,0}^{+}+\delta[\Phi_{S,1}^{+}+\delta\Phi_{S,2}^{+}+O(\delta^2)]+O(\varepsilon) \quad , \tag{2.54}$$

which are similar to Eqs. (2.20)–(2.22). Because only an $O(\varepsilon)$ amount of the fuel leaks through the oxidation region, $\Phi_{F,1}^{+}\equiv 0$ is a required condition. Substituting Eqs. (2.52)–(2.54) into Eqs. (2.8)–(2.12), expanding and collecting the terms of the same order in δ, we obtain the structure equations:

$$d^2\Phi^+_{O,1}/d\zeta^2 = \Lambda_3 \Phi^+_{S,0}\Phi^+_{O,1}\exp(-\alpha\Theta^+_1) \quad , \tag{2.55}$$

$$\frac{d^2\Phi^+_{S,0}}{d\zeta^2} = \frac{d^2\Phi^+_{R,1}}{d\zeta^2} = \hat{\nu}\tilde{q}_S\frac{d^2\Phi^+_{O,1}}{d\zeta^2} - \frac{d^2\Theta^+_1}{d\zeta^2}$$

$$= \left(\frac{1}{Le_S}\frac{d^2\Phi^+_{S,1}}{d\zeta^2} + \tilde{x}_f\frac{d\Phi^+_{S,0}}{d\zeta}\right) - \hat{\nu}\frac{d^2\Phi^+_{O,1}}{d\zeta^2} = 0 \quad , \tag{2.56}$$

$$\frac{d^2\Phi^+_{F,2}}{d\zeta^2} - \tilde{\nu}_F\left(\frac{1}{Le_R}\frac{d^2\Phi^+_{R,2}}{d\zeta^2} + \tilde{x}_f\frac{d\Phi^+_{R,1}}{d\zeta}\right) = 0 \quad , \tag{2.57}$$

$$\hat{\nu}\tilde{q}_S\left(\frac{d^2\Phi^+_{O,2}}{d\zeta^2} + \tilde{x}_f\frac{d\Phi^+_{O,1}}{d\zeta}\right) - \left(\frac{d^2\Theta^+_2}{d\zeta^2} + \tilde{x}_f\frac{d\Theta^+_1}{d\zeta}\right) = 0 \quad , \tag{2.58}$$

$$\frac{d^2\Phi^+_{F,2}}{d\zeta^2} + \left(\frac{1}{Le_S}\frac{d^2\Phi^+_{S,2}}{d\zeta^2} + \tilde{x}_f\frac{d\Phi^+_{S,1}}{d\zeta} + \zeta\frac{d\Phi^+_{S,0}}{d\zeta}\right)$$

$$- \hat{\nu}\left(\frac{d^2\Phi^+_{O,2}}{d\zeta^2} + \tilde{x}_f\frac{d\Phi^+_{O,1}}{d\zeta}\right) = 0 \quad , \tag{2.59}$$

where

$$\Lambda_3 = (\delta^2/\hat{\nu})\beta Da_2\exp(-\alpha\tilde{E}_2/\tilde{T}_{f,0}) \tag{2.60}$$

is the reduced Damköhler number of the soot/precursor consumption reaction.

2.2.5 Matching of Solutions in the Outer and Soot Consumption Regions

Boundary conditions required to solve the structure equations in soot consumption region can be obtained by matching the solutions in the soot consumption region with the outer solutions in the oxidizer side. The procedure is similar to that described in section 2.2.3 and illustrated in Eqs.

(2.29) and (2.30) except that $\zeta \to \infty$ in this region. Upon matching, we obtain

$$\tilde{T}_{f,0} = \tilde{T}_\infty + a^+_{T,0} I_C(1) \quad \text{or} \quad a^+_{T,0} = (\tilde{T}_{f,0} - \tilde{T}_\infty) / I_C(1) \quad , \tag{2.61}$$

$$\Theta^+_1(\zeta \to \infty) = -a^+_{T,1} I_C(1) - a^+_{T,0} \exp(-\tilde{x}_f^2 / 2)\zeta \quad , \tag{2.62}$$

$$(d\Theta^+_2 / d\zeta)_{\zeta\to\infty} = \exp(-\tilde{x}_f^2 / 2)(a^+_{T,1} - a^+_{T,0} \tilde{x}_f \zeta) \quad , \tag{2.63}$$

$$a^+_{O,0} = \bar{Y}_{O,\infty} / I_C(1) \quad , \tag{2.64}$$

$$a^+_{F,0} = a^+_{F,1} = a^+_{R,0} = 0 \quad , \tag{2.65}$$

$$\Phi^+_{O,1}(\zeta \to \infty) = -a^+_{O,1} I_C(1) + a^+_{O,0} \exp(-\tilde{x}_f^2 / 2)\zeta \quad , \tag{2.66a}$$

$$(d\Phi^+_{O,2} / d\zeta)_{\zeta\to\infty} = \exp(-\tilde{x}_f^2 / 2)(a^+_{O,1} - a^+_{O,0} \tilde{x}_f \zeta) \quad , \tag{2.67}$$

$$(d\Phi^+_{F,2} / d\zeta)_{\zeta\to\infty} = 0 \quad , \tag{2.68}$$

$$\Phi^+_{R,1}(\zeta \to \infty) = a^+_{R,1} I_C(Le_R) \quad , \tag{2.69}$$

$$(d\Phi^+_{R,2} / d\zeta)_{\zeta\to\infty} = -a^+_{R,1}\sqrt{Le_R} \exp(-Le_R \tilde{x}_f^2 / 2) \quad , \tag{2.70}$$

$$\Phi^+_{S,0}(\zeta \to \infty) = a^+_{S,0} I_C(Le_S) \quad , \tag{2.71}$$

$$\Phi^+_{S,1}(\zeta \to \infty) = a^+_{S,1} I_C(Le_S) - a^+_{S,0}\sqrt{Le_S} \exp(-Le_S \tilde{x}_f^2 / 2)\zeta \quad , \tag{2.72}$$

$$(d\Phi^+_{S,2} / d\zeta)_{\zeta\to\infty} = \sqrt{Le_S} \exp(-Le_S \tilde{x}_f^2 / 2)(-a^+_{S,1} + a^+_{S,0} Le_S \tilde{x}_f \zeta) \quad . \tag{2.73}$$

Equation (2.66a) also implies

$$(d\Phi^+_{O,1} / d\zeta)_{\zeta\to\infty} = a^+_{O,0} \exp(-\tilde{x}_f^2 / 2) \quad . \tag{2.66b}$$

Integrating the four expressions in Eq. (2.56) twice and Eqs. (2.57)–(2.59) once subject to the matching conditions in Eqs. (2.62)–(2.63) and (2.66)–(2.73) yields

$$\Phi^{+}_{S,0} = a^{+}_{S,0}\, I_C(Le_S) \quad , \tag{2.74}$$

$$\Phi^{+}_{R,1} = a^{+}_{R,1}\, I_C(Le_R) \quad , \tag{2.75}$$

$$\hat{v}\tilde{q}_S\, \Phi^{+}_{O,1} - \Theta^{+}_1 = (a^{+}_{T,1} - \hat{v}\tilde{q}_S\, a^{+}_{O,1})\, I_C(1) + (\hat{v}\tilde{q}_S\, a^{+}_{O,0} - a^{+}_{T,0}) \exp(-\tilde{x}_f^2/2)\, \zeta \quad , \tag{2.76}$$

$$\frac{\Phi^{+}_{S,1}}{Le_S} - \hat{v}\,\Phi^{+}_{O,1} = \frac{a^{+}_{S,1}}{Le_S} I_C(Le_S) + \hat{v}\, a^{+}_{O,1}\, I_C(1) - \left[a^{+}_{S,0} \exp(-Le_S\, \tilde{x}_f^2/2)/\sqrt{Le_S} + \hat{v}\, a^{+}_{O,0} \exp(-\tilde{x}_f^2/2)\right] \zeta \quad , \tag{2.77}$$

$$\frac{d\Phi^{+}_{F,2}}{d\zeta} - \tilde{v}_F \left(\frac{1}{Le_R} \frac{d\Phi^{+}_{R,2}}{d\zeta} + \tilde{x}_f\, \Phi^{+}_{R,1} \right) = \tilde{v}_F\, a^{+}_{R,1} \Gamma^{+}(Le_R) \quad , \tag{2.78}$$

$$\hat{v}\tilde{q}_S \left(\frac{d\Phi^{+}_{O,2}}{d\zeta} + \tilde{x}_f\, \Phi^{+}_{O,1} \right) - \left(\frac{d\Theta^{+}_2}{d\zeta} + \tilde{x}_f\, \Theta^{+}_1 \right) = (\hat{v}\tilde{q}_S\, a^{+}_{O,1} - a^{+}_{T,1})\, \Gamma^{+}(1) \quad , \tag{2.79}$$

$$\frac{d\Phi^{+}_{F,2}}{d\zeta} + \left(\frac{1}{Le_S} \frac{d\Phi^{+}_{S,2}}{d\zeta} + \tilde{x}_f\, \Phi^{+}_{S,1} \right) - \hat{v} \left(\frac{d\Phi^{+}_{O,2}}{d\zeta} + \tilde{x}_f\, \Phi^{+}_{O,1} \right) = -a^{+}_{S,1}\, \Gamma^{+}(Le_S) - \hat{v}\, a^{+}_{O,1}\, \Gamma^{+}(1) \quad , \tag{2.80}$$

where

$$I_C(Le) = \sqrt{2\pi} - I(\sqrt{Le}\, \tilde{x}_f) \quad , \tag{2.81}$$

$$\Gamma^{+}(Le) = \exp(-Le\, \tilde{x}_f^2/2)/\sqrt{Le} - \tilde{x}_f\, I_C(Le) \quad . \tag{2.82}$$

2.2.6 Structure Equations in the Oxidation Region

In the $O(\varepsilon)$ oxidation region, only the oxidation reaction (R1) is significant. The proper stretched coordinate is defined as $\xi = (\tilde{x} - \tilde{x}_f)/\varepsilon$

where $\varepsilon = \tilde{T}_f^2 / \tilde{E}_1$, and the expansions of the variables are

$$\tilde{T} = \tilde{T}_f - \varepsilon[\theta_1 + \delta\theta_2 + O(\delta^2)] + O(\varepsilon^2) \quad , \tag{2.83}$$

$$\tilde{Y}_i = \varepsilon[\phi_{i,1} + \delta\phi_{i,2} + O(\delta^2)] + O(\varepsilon^2) \quad , \quad i = F, O \quad , \tag{2.84}$$

$$\tilde{Y}_R = [\delta\phi_{R,0} + O(\delta^2)] + \varepsilon[\phi_{R,1} + \delta\phi_{R,2} + O(\delta^2)] + O(\varepsilon^2) \quad , \tag{2.85}$$

$$\tilde{Y}_S = [\tilde{Y}_{S,0} + \delta\phi_{S,0} + O(\delta^2)] + \varepsilon[\phi_{S,1} + \delta\phi_{S,2} + O(\delta^2)] + O(\varepsilon^2) \quad , \tag{2.86}$$

where

$$\tilde{T}_f = \tilde{T}_{f,0} - \delta\tilde{T}_{f,1} + O(\delta^2) \quad . \tag{2.87}$$

Substituting Eqs. (2.83)–(2.86) into Eqs. (2.8)–(2.12), expanding and collecting terms of the same order in ε, we obtain

$$d^2\tilde{Y}_{S,0}/d\xi^2 = d^2\phi_{R,0}/d\xi^2 = d^2\phi_{S,0}/d\xi^2 = 0 \quad , \tag{2.88}$$

$$\frac{d^2(\phi_{F,1} - \theta_1)}{d\xi^2} = \frac{d^2(\phi_{F,1} - \phi_{O,1})}{d\xi^2} = \frac{d^2}{d\xi^2}\left(\phi_{F,1} + \frac{\phi_{R,1}}{Le_R}\right)$$

$$= \frac{d^2\phi_{S,1}}{d\xi^2} + Le_S\tilde{x}_f\frac{d\tilde{Y}_{S,0}}{d\xi} = 0 \quad , \tag{2.89}$$

$$\frac{d^2(\phi_{F,2} - \theta_2)}{d\xi^2} = \frac{d^2(\phi_{F,2} - \phi_{O,2})}{d\xi^2} = \frac{d^2}{d\xi^2}\left(\phi_{F,2} + \frac{\phi_{R,2}}{Le_R}\right) + x_f\frac{d\phi_{R,0}}{d\xi}$$

$$= \frac{d^2\phi_{S,2}}{d\xi^2} + Le_S x_f\frac{d\phi_{S,0}}{d\xi} = 0 \quad . \tag{2.90}$$

A structure equation similar to that of Liñán (1974) can also be derived, but it will not be presented because it is not of direct relevance to this study.

2.2.7 Matching of Solutions in the Oxidation, Soot Formation, and Consumption Regions

The required boundary conditions to solve Eqs. (2.88)–(2.90) are derived from matching the solutions in the oxidation region with those in the soot/precursor formation and consumption regions as $\xi \to \pm\infty$ and $\zeta \to 0$. Matching can be performed by first letting $\zeta = (\varepsilon / \delta)\xi$, substituting into the solutions in the soot/precursor formation and consumption regions, expanding the resulting expressions for proper ordering, and equating with the solutions in the oxidation region. Following this procedure, any variable, $\Delta(\zeta)$, in the soot/precursor formation or consumption region can be expended as

$$\begin{aligned}
\Delta(\zeta) &= [\Delta_0(\zeta) + \delta\Delta_1(\zeta) + \delta^2\Delta_2(\zeta) + O(\delta^3)] + O(\varepsilon) \\
&= \{[\Delta_0(\zeta = 0) + O(\varepsilon / \delta)] + \delta[\Delta_1(\zeta = 0) + (d\Delta_1 / d\zeta)_{\zeta=0}(\varepsilon\xi / \delta) + O(\varepsilon / \delta)^2] \\
&\quad + \delta^2[\Delta_2(\zeta = 0) + (d\Delta_2 / d\zeta)_{\zeta=0}(\varepsilon\xi / \delta) + O(\varepsilon / \delta)^2] + O(\delta^3)\} + O(\varepsilon) \\
&= [\Delta_0(\zeta = 0) + \delta\Delta_1(\zeta = 0) + O(\delta^2)] \\
&\quad + \varepsilon\{const + [(d\Delta_1 / d\zeta)_{\zeta=0} + \delta(d\Delta_2 / d\zeta)_{\zeta=0} + O(\delta^2)]\xi\} + O(\varepsilon^2) \quad .
\end{aligned} \tag{2.91}$$

Taking the matching of the temperature solution as an example, by substituting Eq. (2.91) into Eqs. (2.20) and (2.52), we have

$$\begin{aligned}
\tilde{T}^{\pm} &= [\tilde{T}_{f,0} - \delta\Theta_1^{\pm} - \delta^2\Theta_2^{\pm} + O(\delta^3)] + O(\varepsilon) \\
&= [\tilde{T}_{f,0} - \delta\Theta_1^{\pm}(\zeta = 0) + O(\delta^2)] \\
&\quad + \varepsilon\{const - [(d\Theta_1^{\pm} / d\zeta)_{\zeta=0} + \delta(d\Theta_2^{\pm} / d\zeta)_{\zeta=0} + O(\delta^2)]\xi\} + O(\varepsilon^2) \\
&= \{[\tilde{T}_{f,0} - \delta\tilde{T}_{f,1} + O(\delta^2)] - \varepsilon[\theta_1 + \delta\theta_2 + O(\delta^2)] + O(\varepsilon^2)\}_{\xi \to \pm\infty} \quad .
\end{aligned} \tag{2.92}$$

Subsequent substitution of Eq. (2.45) with $\zeta = 0$ into Eq. (2.92) yields,

$$\tilde{T}_{f,1} = \Theta_1^-(\zeta = 0) = \Theta_1^+(\zeta = 0) = -a_{T,1}^- I(\tilde{x}_f) \quad , \tag{2.93}$$

$$(d\theta_j / d\xi)_{\xi \to \pm\infty} = (d\Theta_j^{\pm} / d\zeta)_{\zeta=0} \quad , \quad j = 1, 2 \quad . \tag{2.94}$$

Application of the same matching procedure to other variables then gives

$$\Phi_{F,1}^-(\zeta = 0) = 0 \quad , \tag{2.95}$$

$$\Phi_{O,1}^+(\zeta = 0) = 0 \quad , \tag{2.96}$$

$$a_{T,1}^- I(\tilde{x}_f) = (a_{T,1}^+ - \hat{v}\tilde{q}_S a_{O,1}^+) I_C(1) \quad , \tag{2.97}$$

$$\tilde{Y}_{S,0}(\xi \to -\infty) = a_{S,0}^- I(\sqrt{Le_S}\,\tilde{x}_f) \quad , \tag{2.98a}$$

$$\tilde{Y}_{S,0}(\xi \to \infty) = a_{S,0}^+ I_C(Le_S) \quad , \tag{2.98b}$$

$$\phi_{R,0}(\xi \to -\infty) = a_{R,1}^- I(\sqrt{Le_R}\,\tilde{x}_f) + a_{F,1}^- (Le_R / \tilde{v}_F) I(\tilde{x}_f) \quad , \tag{2.99a}$$

$$\phi_{R,0}(\xi \to \infty) = a_{R,1}^+ I_C(Le_R) \quad , \tag{2.99b}$$

$$\phi_{S,0}(\xi \to -\infty) = a_{S,1}^- I(\sqrt{Le_S}\,\tilde{x}_f) - Le_S\, a_{F,1}^- I(\tilde{x}_f) \quad , \tag{2.100a}$$

$$\phi_{S,0}(\xi \to \infty) = a_{S,1}^+ I_C(Le_S) + \hat{v} Le_S\, a_{O,1}^+ I_C(1) \quad , \tag{2.100b}$$

$$(d\phi_{i,j} / d\xi)_{\xi \to \pm\infty} = (d\Phi_{i,j}^{\pm} / d\zeta)_{\zeta=0} \quad , \quad i = F, O, R, S \quad , \quad j = 1, 2 \quad . \tag{2.101}$$

Equations (2.44), (2.46), (2.47) and (2.74)–(2.77) have been used in the derivation of Eqs. (2.97)–(2.100).

Integrating the three expressions in Eq. (2.88) twice and the four expressions in each of Eqs. (2.89) and (2.90) once subject to Eqs. (2.94), (2.98)–(2.101) we obtain

$$\tilde{Y}_{S,0} = \Phi^{-}_{S,0} = \Phi^{+}_{S,0} \quad , \tag{2.102}$$

$$\tilde{v}_F\left[a^{+}_{R,1} I_C(Le_R) - a^{-}_{R,1} I(\sqrt{Le_R}\,\tilde{x}_f)\right] = a^{-}_{F,1} Le_R\, I(\tilde{x}_f) \quad , \tag{2.103}$$

$$Le_S\left[a^{-}_{F,1} I(\tilde{x}_f) + \hat{v} a^{+}_{O,1} I_C(1)\right] = a^{-}_{S,1} I(\sqrt{Le_S}\,\tilde{x}_f) - a^{+}_{S,1} I_C(Le_S) \quad , \tag{2.104}$$

$$(d\Phi^{-}_{S,1}/d\zeta)_{\zeta=0} = (d\Phi^{+}_{S,1}/d\zeta)_{\zeta=0} \quad , \tag{2.105}$$

$$(d\Phi^{-}_{F,1}/d\zeta)_{\zeta=0} + (d\Theta^{+}_{1}/d\zeta)_{\zeta=0} + a^{-}_{T,0}\exp(-\tilde{x}_f^2/2) = 0 \quad , \tag{2.106}$$

$$(d\Phi^{-}_{F,1}/d\zeta)_{\zeta=0} + (d\Phi^{+}_{O,1}/d\zeta)_{\zeta=0} = 0 \quad , \tag{2.107}$$

$$Le_R(d\Phi^{-}_{F,1}/d\zeta)_{\zeta=0} + (d\Phi^{-}_{R,1}/d\zeta)_{\zeta=0} = 0 \quad , \tag{2.108}$$

$$(d\Phi^{-}_{F,2}/d\zeta)_{\zeta=0} - (d\Phi^{+}_{F,2}/d\zeta)_{\zeta=0} = (d\Theta^{-}_{2}/d\zeta)_{\zeta=0} - (d\Theta^{+}_{2}/d\zeta)_{\zeta=0} \quad , \tag{2.109}$$

$$(d\Phi^{-}_{F,2}/d\zeta)_{\zeta=0} - (d\Phi^{+}_{F,2}/d\zeta)_{\zeta=0} = (d\Phi^{-}_{O,2}/d\zeta)_{\zeta=0} - (d\Phi^{+}_{O,2}/d\zeta)_{\zeta=0} \quad , \tag{2.110}$$

$$Le_R\left[(d\Phi^{-}_{F,2}/d\zeta)_{\zeta=0} - (d\Phi^{+}_{F,2}/d\zeta)_{\zeta=0}\right] = (d\Phi^{+}_{R,2}/d\zeta)_{\zeta=0} - (d\Phi^{-}_{R,2}/d\zeta)_{\zeta=0} \quad , \tag{2.111}$$

$$(d\Phi^{-}_{S,2}/d\zeta)_{\zeta=0} = (d\Phi^{+}_{S,2}/d\zeta)_{\zeta=0} \quad . \tag{2.112}$$

2.2.8 Completion of the Analysis

To complete the analysis, Eqs. (2.46), (2.47), (2.76) and (2.77) are differentiated with respect to ζ to yield

$$\frac{d}{d\zeta}\left(\Phi^{-}_{F,1} - \frac{\tilde{v}_F}{Le_R}\Phi^{-}_{R,1}\right) = -a^{-}_{F,0}\exp(-\tilde{x}_f^2/2) \quad , \tag{2.113}$$

$$\frac{\tilde{\nu}_F}{Le_R}\frac{d\Phi^-_{R,1}}{d\zeta}+\frac{1}{Le_S}\frac{d\Phi^-_{S,1}}{d\zeta}=a^-_{S,0}\frac{\exp(-Le_S\tilde{x}_f^2/2)}{\sqrt{Le_S}} \quad , \tag{2.114}$$

$$\hat{\nu}\tilde{q}_S\frac{d\Phi^+_{O,1}}{d\zeta}-\frac{d\Theta^+_1}{d\zeta}=(\hat{\nu}\tilde{q}_S a^+_{O,0}-a^+_{T,0})\exp(-\tilde{x}_f^2/2) \quad , \tag{2.115}$$

$$\frac{1}{Le_S}\frac{d\Phi^+_{S,1}}{d\zeta}-\hat{\nu}\frac{d\Phi^+_{O,1}}{d\zeta}=-\left[a^+_{S,0}\exp(-Le_S\tilde{x}_f^2/2)/\sqrt{Le_S}+\hat{\nu}a^+_{O,0}\exp(-\tilde{x}_f^2/2)\right] . \tag{2.116}$$

Application of Eqs (2.34), (2.107), (2.108) to Eq. (2.113) then gives

$$(d\Phi^-_{F,1}/d\zeta)_{\zeta=0}=-\tilde{Y}_{F,-\infty}\exp(-\tilde{x}_f^2/2)/[(1+\tilde{\nu}_F)I(\tilde{x}_f)] \quad , \tag{2.117}$$

$$(d\Phi^+_{O,1}/d\zeta)_{\zeta=0}=\tilde{Y}_{F,-\infty}\exp(-\tilde{x}_f^{\,2}/2)/[(1+\tilde{\nu}_F)I(\tilde{x}_f)] \quad . \tag{2.118}$$

Next, substitution of the Eqs (2.31), (2.61), (2.64), (2.106), (2.117) and (2.118) into Eq. (2.115) and rearranging terms, one obtains

$$\frac{\tilde{T}_{f,0}-\tilde{T}_{-\infty}}{I(\tilde{x}_f)}+\frac{\tilde{T}_{f,0}-\tilde{T}_{\infty}}{I_C(1)}=\frac{1-\hat{\nu}\tilde{q}_S}{1+\tilde{\nu}_F}\frac{\tilde{Y}_{F,-\infty}}{I(\tilde{x}_f)}+\hat{\nu}\tilde{q}_S\frac{\tilde{Y}_{O,\infty}}{I_C(1)} \quad . \tag{2.119}$$

Moreover, by combining Eqs. (2.44), (2.74), (2.102), (2.105), (2.114), (2.116)–(2.118), we further have

$$a^+_{S,0}=\hat{\nu}\sqrt{\frac{Le_S}{2\pi}}I(\sqrt{Le_S}\,\tilde{x}_f)\left[\frac{\nu^*\tilde{Y}_{F,-\infty}}{I(\tilde{x}_f)}-\frac{\tilde{Y}_{O,\infty}}{I_C(1)}\right]\exp[(Le_S-1)\tilde{x}_f^2/2] \quad , \tag{2.120}$$

$$\tilde{Y}_{S,0}=\hat{\nu}\sqrt{\frac{Le_S}{2\pi}}I(\sqrt{Le_S}\,\tilde{x}_f)I_C(Le_S)\left[\frac{\nu^*\tilde{Y}_{F,-\infty}}{I(\tilde{x}_f)}-\frac{\tilde{Y}_{O,\infty}}{I_C(1)}\right]\exp[(Le_S-1)\tilde{x}_f^2/2] \quad . \tag{2.121}$$

Equations (2.119) and (2.121) determine the leading order flame temperature,

$\tilde{T}_{f,0}$, and soot/precursor concentration in the oxidation region, $\tilde{Y}_{S,0}$, in terms of the flame sheet location, $\tilde{x}_f$, respectively. Finally, substitution of Eqs. (2.48)–(2.50) and (2.78)–(2.80) into Eqs. (2.109)–(2.112) and rearrange provide two additional relations

$$\left[a_{T,1}^{-}+\frac{\hat{\nu}\tilde{q}_S-1}{1+\tilde{\nu}_F}a_{F,1}^{-}\right]\Gamma^{-}(1)=-(a_{T,1}^{+}-\hat{\nu}\tilde{q}_S a_{O,1}^{+})\Gamma^{+}(1)$$

$$-\tilde{\nu}_F\frac{\hat{\nu}\tilde{q}_S-1}{1+\tilde{\nu}_F}[a_{R,1}^{-}\Gamma^{-}(Le_R)+a_{R,1}^{+}\Gamma^{+}(Le_R)] \quad , \qquad (2.122)$$

$$\hat{\nu}\left[\nu^* a_{F,1}^{-}\Gamma^{-}(1)-a_{O,1}^{+}\Gamma^{+}(1)\right]=\left[a_{S,1}^{-}\Gamma^{-}(Le_S)+a_{S,1}^{+}\Gamma^{+}(Le_S)\right]$$

$$-\hat{\nu}(1-\nu^*)\left[a_{R,1}^{-}\Gamma^{-}(Le_R)+a_{R,1}^{+}\Gamma^{+}(Le_R)\right] \quad . \qquad (2.123)$$

2.2.9 Rescale of the Structure Equations for Numerical Computations

The two structure equations, Eq. (2.23) in the soot formation region and Eq. (2.55) in the soot consumption region, need to be solved numerically. Equation (2.23) with Θ_1^{-} and $\Phi_{R,1}^{-}$ given respectively by Eqs. (2.45) and (2.46) is to be integrated subject to the four boundary conditions specified in Eqs. (2.36a, b), (2.95) and (2.117). Similarly, Eq. (2.55) with Θ_1^{+} given by Eq. (2.76) and $\Phi_{S,0}^{+}$ given by Eq. (2.74) and (2.120) can be solved subject to the four boundary conditions in Eqs. (2.66a, b), Eq. (2.96) and Eq. (2.118).

The numerical procedure can be simplified by a transformation of variables. The transformation of Eq. (2.23) is performed by defining the rescaled variable and parameter as:

$$\eta=[\tilde{Y}_{F,-\infty}/I(\tilde{x}_f)]\exp(-\tilde{x}_f^2/2)\zeta \quad , \qquad (2.124)$$

$$\tilde{\Lambda}_2 = Da_2\, Le_R \left(\frac{\tilde{T}_{f,0}^{\,2}}{\tilde{E}_2}\right)^3 \left(\frac{I(\tilde{x}_f)}{\tilde{Y}_{F,-\infty}}\right)^2 \exp\left\{a_{T,1}^{-} I(\tilde{x}_f) + \tilde{x}_f^2 - \frac{\tilde{E}_2}{\tilde{T}_{f,0}}\right\} \quad . \tag{2.125}$$

Substitution of Eqs. (2.124) and (2.125) into Eqs. (2.45) and (2.46) gives

$$\Theta_1^{-} = -a_{T,1}^{-} I(\tilde{x}_f) - [(\tilde{T}_{f,0} - \tilde{T}_{-\infty}) / \tilde{Y}_{F,-\infty}]\eta \quad , \tag{2.126}$$

$$\Phi_{R,1}^{-} = a_{R,1}^{+}[\sqrt{2\pi} - I(\sqrt{Le_R}\,\tilde{x}_f)] + (Le_R / \tilde{\nu}_F)(\Phi_{F,1}^{-} + \eta) \quad . \tag{2.127}$$

Subsequent substitution of Eqs. (2.124)–(2.127) into Eqs. (2.23), (2.36a, b), (2.95) and (2.117) then yields the transformed equation and boundary conditions, given by

$$d^2\Phi_{F,1}^{-} / d\eta^2 = \tilde{\Lambda}_2\, \Phi_{F,1}^{-}\{a_{R,1}^{+}[\sqrt{2\pi} - I(\sqrt{Le_R}\,\tilde{x}_f)] / Le_R + (\Phi_{F,1}^{-} + \eta) / \tilde{\nu}_F\}$$
$$\times \exp\{[(\tilde{T}_{f,0} - \tilde{T}_{-\infty}) / \tilde{Y}_{F,-\infty}]\eta\} \quad , \tag{2.128}$$

$$\Phi_{F,1}^{-}(\eta = 0) = 0 \quad , \tag{2.129a}$$

$$(d\Phi_{F,1}^{-} / d\eta)_{\eta=0} = -1/(1 + \tilde{\nu}_F) \quad , \tag{2.129b}$$

$$\Phi_{F,1}^{-}(\eta \to -\infty) = \tilde{\nu}_F\{a_{R,1}^{-} I(\sqrt{Le_R}\,\tilde{x}_f) - a_{R,1}^{+}[\sqrt{2\pi} - I(\sqrt{Le_R}\,\tilde{x}_f)]\} / Le_R - \eta \quad , \tag{2.130a}$$

$$(d\Phi_{F,1}^{-} / d\eta)_{\eta\to-\infty} = -1 \quad . \tag{2.130b}$$

Similarly, Eq. (2.55) can be transformed by defining

$$\eta = \{\tilde{Y}_{O,\infty} / [\sqrt{2\pi} - I(\tilde{x}_f)]\} \exp(-\tilde{x}_f^2 / 2)\, \zeta \quad , \tag{2.131}$$

$$\tilde{\Lambda}_3 = \beta\, Da_2 (\tilde{T}_{f,0}^{\,2} / \tilde{E}_2)^2 \sqrt{Le_S / 2\pi}\; I(\sqrt{Le_S}\,\tilde{x}_f)[\sqrt{2\pi} - I(\sqrt{Le_S}\,\tilde{x}_f)]$$
$$\times \{\nu^* \tilde{Y}_{F,-\infty} / I(\tilde{x}_f) - \tilde{Y}_{O,\infty} / [\sqrt{2\pi} - I(\tilde{x}_f)]\}$$
$$\times \exp\left\{\alpha\left[a_{T,1}^{-} I(\tilde{x}_f) - \tilde{E}_2 / \tilde{T}_{f,0}\right] + (Le_S - 1)\tilde{x}_f^2 / 2\right\} \quad , \tag{2.132}$$

which can first be substituted into Eq. (2.76) to give

$$\Theta_1^+ = \tilde{q}_S\,\hat{v}(\Phi_{O,1}^+ - \eta) - a_{T,1}^- I(\tilde{x}_f) + [(\tilde{T}_{f,0} - \tilde{T}_\infty)/\tilde{Y}_{O,\infty}]\eta \quad , \tag{2.133}$$

and then substituted into Eq. (2.55), (2.68a, b), (2.96), and (2.118) along with Eqs. (2.74), (2.120) and (2.133) to yield

$$\frac{d^2\Phi_{O,1}^+}{d\eta^2} = \tilde{A}_3\,\Phi_{O,1}^+ \exp\left\{-\alpha\left[\tilde{q}_S\,\hat{v}\,\Phi_{O,1}^+ + \left(\frac{\tilde{T}_{f,0} - \tilde{T}_\infty}{\tilde{Y}_{O,\infty}} - \tilde{q}_S\,\hat{v}\right)\eta\right]\right\} \quad , \tag{2.134}$$

$$\Phi_{O,1}^+(\eta = 0) = 0 \quad , \tag{2.135a}$$

$$(d\Phi_{O,1}^+/d\eta)_{\eta=0} = \{\tilde{Y}_{F,-\infty}[\sqrt{2\pi} - I(\tilde{x}_f)]/[\tilde{Y}_{O,\infty}(1+\tilde{v}_F)I(\tilde{x}_f)]\} \quad , \tag{2.135b}$$

$$\Phi_{O,1}^+(\eta \to \infty) = -a_{O,1}^+[\sqrt{2\pi} - I(\tilde{x}_f)] + \eta \quad , \tag{2.136a}$$

$$(d\Phi_{O,1}^+/d\eta)_{\eta\to\infty} = 1 \quad . \tag{2.136b}$$

2.2.10 Summary of the Analytical Results

The analysis is now complete and the main result is summarized in the following text. First, Eq. (2.134) is numerically integrated subject to four boundary conditions in Eqs. (2.135a, b) and (2.136a, b). Next, Eq. (2.128) is numerically integrated subject to four boundary conditions in Eqs. (2.129a, b) and (2.130a, b). Since there are four boundary conditions for both of these second order differential equations, four additional boundary conditions can be used to determine four other unknowns. These four conditions, along with Eqs. (2.97), (2.103), (2.104), (2.122) and (2.123) are used to determine the flame sheet location, $\tilde{x}_f$, and the eight undetermined constants $a_{T,1}^{\pm}$, $a_{F,1}^-$, $a_{O,1}^+$, $a_{R,1}^{\pm}$ and $a_{S,1}^{\pm}$. With the determination of $\tilde{x}_f$, $a_{S,0}^{\pm}$ can be determined

from Eqs. (2.44), (2.102) and (2.120) while the flame temperature $\bar{T}_f$ can be determined from Eqs. (2.87), (2.93) and (2.119).

The maximum soot/precursor concentration, which is located at the boundary between the soot/precursor formation region and the inert region at the fuel side of the reaction regions, can be obtained from Eq. (2.18a) as

$$\tilde{Y}_S^-(\tilde{x}_f) = (a_{S,0}^- + \delta a_{S,1}^-) I(\sqrt{Le_S}\tilde{x}_f) + \ldots \quad . \tag{2.137}$$

A soot/precursor indicator S_I will be used to express this quantity. Similarly, the soot/precursor concentration at the boundary between the soot/precursor consumption region and the inert region at the oxidizer side of the reaction regions is given by Eq. (2.18b) as

$$\tilde{Y}_S^+(\tilde{x}_f) = (a_{S,0}^+ + \delta a_{S,1}^+) I_C(Le_S) + \ldots \quad , \tag{2.138}$$

which represents the amount of soot/precursor that breaks through the reaction zones into the oxidizer side. The amount of soot/precursor breakthrough will be expressed by a soot break-through parameter S_B .

In the limit of extremely slow soot/precursor consumption reaction, its rate is considered an order of magnitude slower than the soot/precursor formation reaction so that $\beta = O(\delta)$. For this case Eq. (2.134) can be integrated subject to Eqs. (2.135a, b) to yield

$$\Phi_{O,1}^+ = \left\{ \tilde{Y}_{F,-\infty} \left[\sqrt{2\pi} - I(\tilde{x}_f) \right] / \left[\tilde{Y}_{O,\infty} \left(1 + \tilde{\nu}_F \right) I(\tilde{x}_f) \right] \right\} \eta \quad . \tag{2.139}$$

Subsequent application of Eqs. (2.136a, b) into Eq. (2.139) results in $a_{O,1}^+ = 0$ and

$$I(\tilde{x}_f) = \sqrt{2\pi}\, \tilde{Y}_{F,-\infty} / \left[\tilde{Y}_{F,-\infty} + (1 + \tilde{\nu}_F) \tilde{Y}_{O,\infty} \right] \tag{2.140}$$

for the determination of the flame sheet location. This in turn can be

substituted into Eq. (2.119) to provide the solution of $\tilde{T}_{f,0}$, given by

$$\tilde{T}_{f,0} = \tilde{T}_{-\infty} + \tilde{Y}_{F,-\infty}(\tilde{T}_{\infty} - \tilde{T}_{-\infty} + \tilde{Y}_{O,\infty}) / [\tilde{Y}_{F,-\infty} + (1+\tilde{\nu}_F)\tilde{Y}_{O,\infty}] \quad . \quad (2.141)$$

Equation (2.128) still needs to be numerically integrated subject to the four boundary conditions in Eqs. (2.129a, b) and (2.130a, b), with two additional conditions applied to determine $a^{\pm}_{\tilde{T},1}$, $a^{-}_{\tilde{F},1}$, $a^{\pm}_{\tilde{R},1}$ and $a^{\pm}_{\tilde{S},1}$ along with Eqs. (2.97), (2.103), (2.104), (2.122) and (2.123).

It should be mentioned that although the present analysis can be completed without requiring knowledge of flame extinction state, the analysis is based on the existence of a diffusion flame. Thus the result of this analysis is applicable only to a counterflow diffusion flame in Liñán's (1974) diffusion flame regime and for conditions sufficiently far away from the extinction limit. Experiments have shown that soot and PAH fluorescence are completely suppressed at strain rates far less than corresponding extinction strain rates (Du *et al.*, 1988).

2.3 Results and Discussions

To explore the characteristics of flame response, numerical calculations were performed using $T_{-\infty} = T_{\infty} = 300$ K, $q_{F,1} = 10140$ cal/gm, $q_{S,3} = 13500$ cal/gm, $c_p = 0.273$ cal/gm.K, $W_F = 28$ gm/mol, $W_O = 32$ gm/mol, $W_R = 1$ gm/mol, $W_S = 36$ gm/mol, $\nu_{F,1} = 1$, $\nu_{F,2} = 0.05$, $\nu_{O,1} = 2.9$, $\nu_{O,3} = 0.25$, $\nu_R = 0.4$, $\nu_S = 0.05$, and $E_2 = 12590$K, corresponding to an activation energy of 25 kcal/mol. These values approximate the burning of ethylene/oxygen flames. Two limiting cases using air as the oxidizer flow will be studied as shown schematically in Fig 2.1. The first case considers a pure fuel/air flame so that $Y_{F,-\infty} = 1$ and $Y_{O,\infty} = 0.233$ (Fig. 2.1(a)) while for the second case, all the inert gas in the air is extracted and diverted to the fuel stream (Fig. 2.1(b)). For the diluted-fuel/oxygen case, $Y_{O,\infty} = 1$ and the value of $Y_{F,-\infty}$ varies between 0.08143 and 0.08784 depending on the rate of the soot/precursor consumption reaction. This is because when the rate of the soot/precursor consumption reaction varies, the oxygen used to consume the soot/precursor is different, which results in a different amount of inert gas to be diverted to the fuel stream. The solution contains four parameters α, β, Le_R and Le_S, which will be studied systematically.

In this study, the oxidation reaction is considered sufficiently fast so that it belongs to Liñán's diffusion flame regime (1974). By taking the radical R to be an $O(\delta)$ quantity, the soot/precursor formation reaction is sufficiently fast and is also in Liñán's diffusion flame regime. Thus the Damköhler number of the soot/precursor formation reaction, Da_2, cannot be very small. In addition, the flame sheet location, $\tilde{x}_f$, is independent of the rates of these two reactions. However, it varies with the rate of the soot/precursor

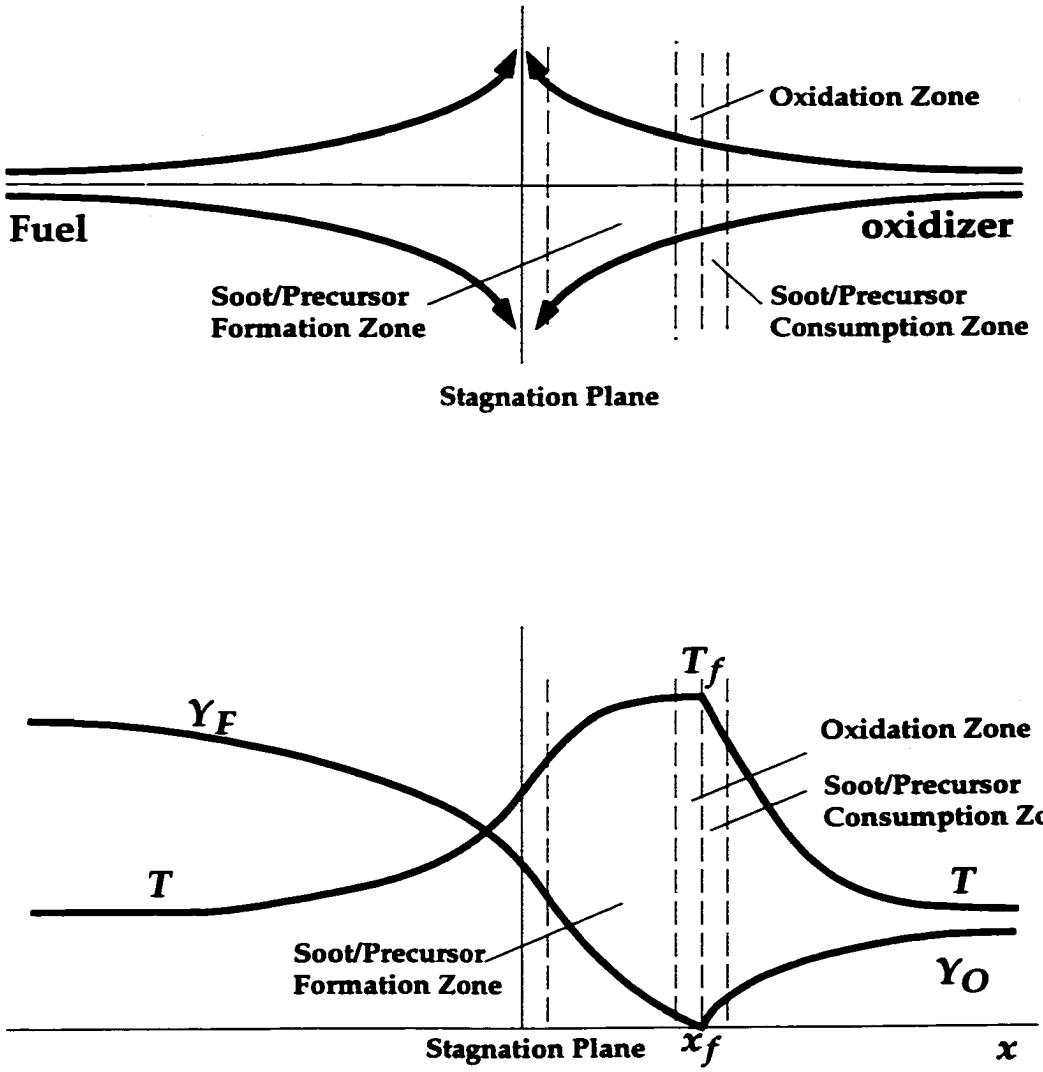

Figure 2.1(a) Schematic diagram of the flame structure for fuel/air flame in the counterflow diffusion flame configuration

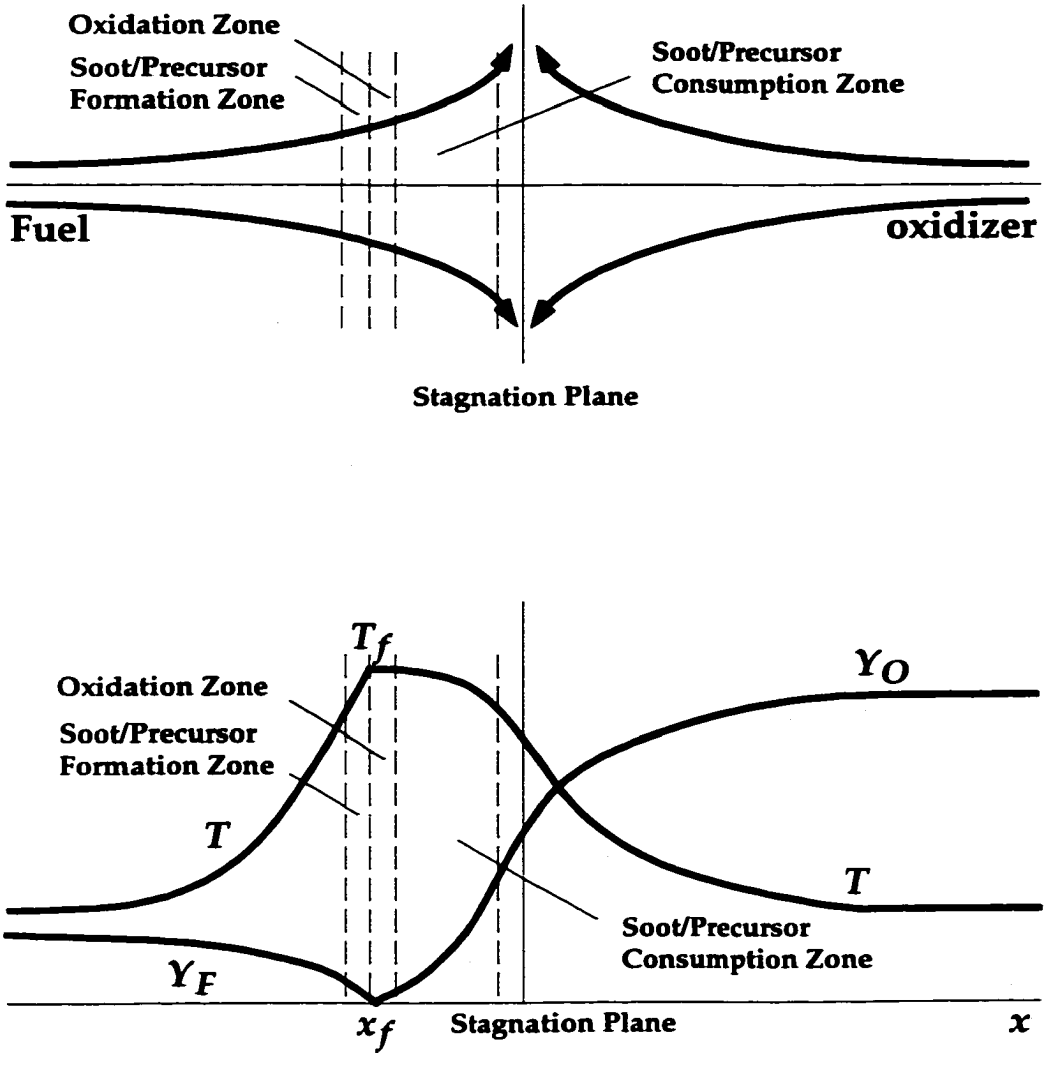

Figure 2.1(b) Schematic diagram of the flame structure for diluted-fuel/oxygen flame in the counterflow diffusion flame configuration

consumption reaction, which will be discussed later. The soot/precursor consumption reaction belongs to Liñán's premixed flame regime.

For the fuel/air flame, all three reaction regions are located on the oxidizer side of the stagnation plane due to the low initial oxidizer mass fraction compared to that of the fuel. Thus, as seen in Fig. 2.1(a), the temperature gradient at the fuel/oxidizer side of the oxidation region is smaller/steeper and hence the soot/precursor formation region is thicker than the consumption region due to a broader high temperature region. Consequently, the soot/precursor formation reaction is favored over consumption reaction because of the larger residence time.

The soot/precursor indicator S_I, which is the maximum mass fraction of the soot/precursor, is shown in Fig. 2.2 versus the Damköhler number of soot/precursor formation, Da_2, for selected values of β and $\alpha = Le_R = Le_S = 1$. Unity Lewis numbers are used as reference values for comparison in our discussion, although they may not be physically realistic. The corresponding flame temperature, $\tilde{T}_f$, and flame sheet location, $\tilde{x}_f$, are plotted in Figs. 2.3 and 2.4. The curve for $\beta = O(\delta)$ in these figures represents the limiting case of extremely slow soot/precursor oxidation reaction. Although Da_2 can be varied by changing the pre-exponential factor B and the strain rate k, it more naturally expresses the effect of k, because B is a property and thus is prescribed with the specification of reactants. The numerical computations show that for realistic values of β, the results are indistinguishable from the case where $\beta = O(\delta)$, which shows that the soot/precursor consumption reaction is relatively weak for fuel/air flames. This is consistent with the

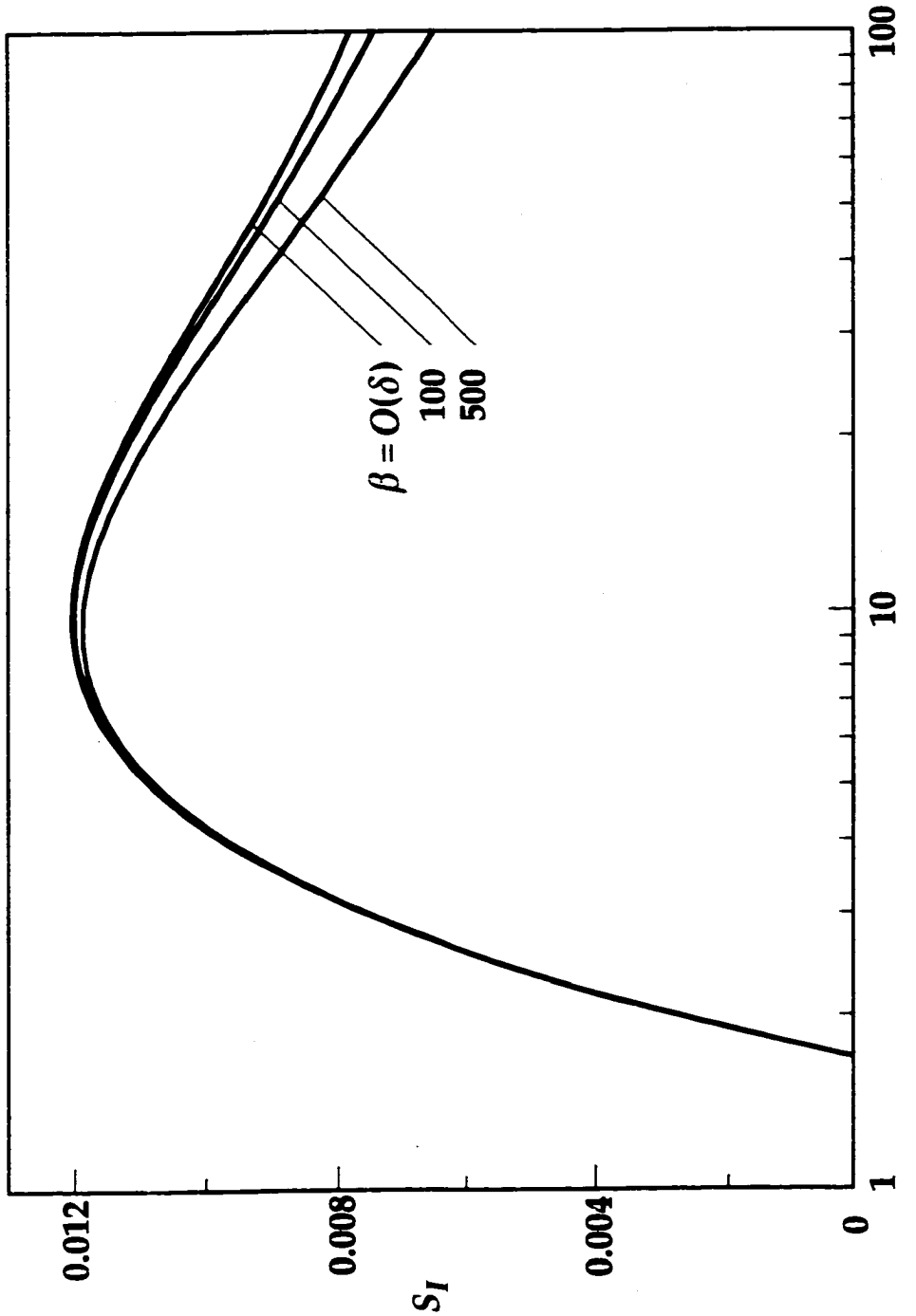

Figure 2.2 Variation of S_I with Da_2 for the fuel/air flame with $\alpha = Le_R = Le_S = 1$ and selected values of β

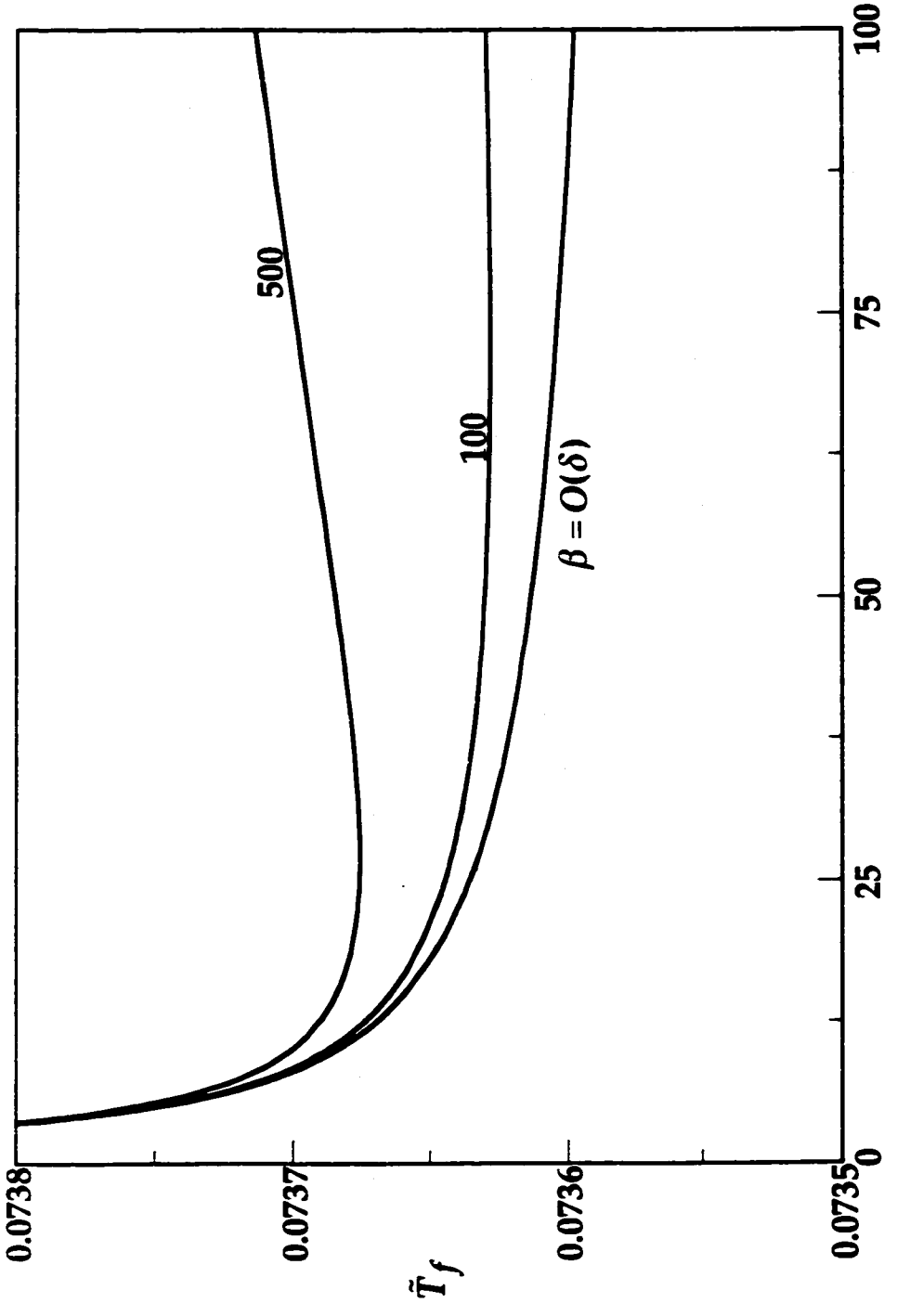

Figure 2.3 The flame temperature $\tilde{T}_f$ corresponding to Fig. 2.2

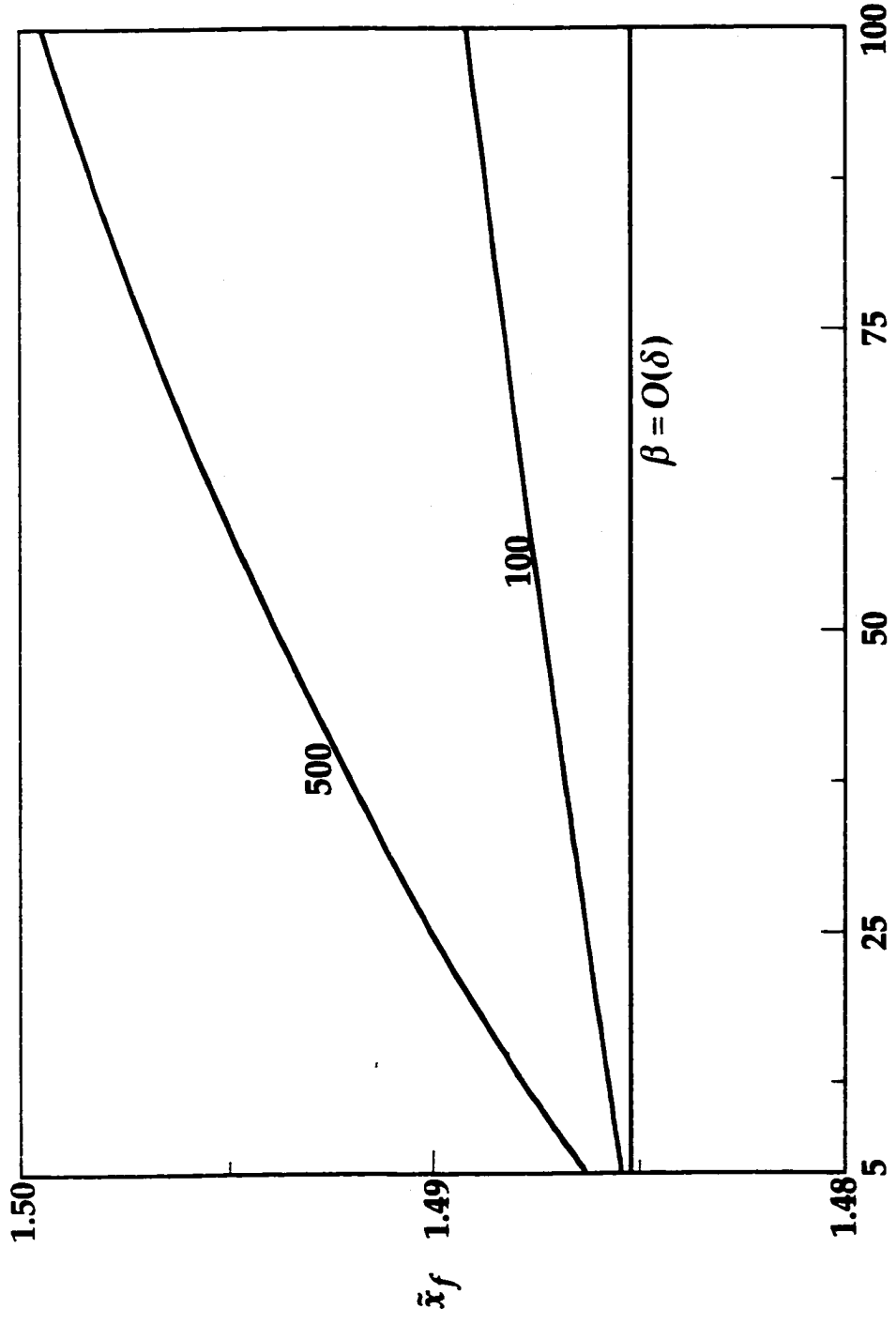

Figure 2.4 The flame sheet location $\tilde{x}_f$ corresponding to Fig. 2.2

analysis and discussion indicating that the soot/precursor formation reaction is favored.

When Da_2 is increased from a relatively small value, the rate of both the soot/precursor formation and consumption reactions is increased because of the increased residence time. This leads to a higher amount of soot/precursor within the system since the formation reaction is faster than the consumption reaction. However, a higher amount of soot/precursor yields a lower flame temperature because the chemical energy stored in the soot/precursor is not released as thermal energy. The decrease in flame temperature then slows down the formation and consumption reactions so that the rate of increase in soot/precursor with increasing Da_2 actually decreases. The above discussion is supported by Fig. 2.3, which shows that the flame temperature decreases with increasing Da_2 (indicating a higher amount of soot/precursor with larger Da_2) and the temperature decrease is slower for higher Da_2 (indicating a slower soot/precursor increase rate). For extremely small values of Da_2, the value of S_I becomes negative, which is physically unrealistic and hence the analysis is not applicable. This is consistent with our earlier statement on the limitation of Da_2.

It is shown in Fig. 2.2 that when Da_2 is increased, S_I increases, attains a maximum, and then decreases. This behavior seems to violate our expectation that the amount of soot/precursor should increase with increasing Da_2 because the soot/precursor consumption reaction is slower than the formation reaction. However, recognizing that the quantity plotted in Fig. 2.2 is the maximum soot/precursor fraction and not the total amount, the observed behavior can be understood in the following way. When Da_2 is

increased, i.e., the strain rate k is decreased, temperature gradient on both sides of the reaction region is smaller and the high temperature region is extended such that the soot/precursor formation and consumption regions are broadened in extent. The increase in the size of these reaction regions yields a larger residence time for both the soot/precursor formation and the consumption reactions so that the amount of soot/precursor increases, as described in the previous paragraph, and the maximum soot/precursor fraction, S_I, also increases. In addition, the broader reaction regions and weaker gradients provide a wider region to contain the soot/precursor, which tends to decrease the maximum soot/precursor fraction. For values of Da_2 lower than the critical value that yields the maximum S_I, the rate of increase in soot/precursor is high, as exhibited by the high temperature gradient shown in Fig. 2.3, so the effect of the increase in soot/precursor mass dominates over the effect of reaction region broadening, and S_I increases with increasing Da_2. After the maximum S_I is passed, the rate of increase in soot/precursor is relatively slow (see Fig. 2.3), and the reaction region broadening effect becomes dominating and leads to the decrease of S_I with increasing Da_2.

Indeed, by letting $Le_S = 1$ and forming an appropriate coupling function, it can be shown that the integration of the soot/precursor mass fraction over the soot/precursor formation region decreases monotonically with decreasing Da_2. This suggests that $\tilde{T}_f$ is a more appropriate indicator of soot/precursor formation and that the increase in $\tilde{T}_f$ with decreasing Da_2 is an indicator of soot/precursor suppression.

As noted previously, the effect of β on the system is negligible for

realistic values of β. Nonetheless, results for two extremely large values, $\beta = 100$ and 500, are shown in Figs. 2.2–2.4 to demonstrate trends when there is a stronger soot/precursor consumption reaction. For large values of β, S_I decreases while the flame temperature, $\tilde{T}_f$, increases compared with small β. Thus, by increasing β, more soot/precursor is oxidized and more heat is generated through the consumption reaction. Consequently, the amount of soot/precursor is decreased and the flame temperature is increased. From Fig. 2.3 it is seen that for $\beta = 500$, there exists a critical value of Da_2 at which $\tilde{T}_f$ attains its minimum value. For values of Da_2 higher than this critical value, the flame temperature increases with increasing Da_2, which indicates that the soot/precursor consumption reaction is faster than the soot/precursor formation reaction so that the total amount of soot/precursor decreases with increasing Da_2. For the same reason a turning point exists for $\beta = 100$, but at a much larger Da_2. These results obviously violate our original assumption and should be discarded. This effect exists only because the values of β employed to reveal this are unrealistically high.

Figure 2.4 shows that the flame sheet location, $\tilde{x}_f$, is positive, meaning that the flame is located on the oxidizer side of the stagnation plane, which is consistent with our earlier discussion. Since $\tilde{x}_f$ does not change with the rates of either oxidation or soot/precursor formation reactions, it is a constant when $\beta = O(\delta)$, i.e., when the soot/precursor consumption reaction is slow. For *non-zero* values of β, the consumption reaction is faster with increasing Da_2. This yields a higher oxidizer consumption rate in the soot/precursor consumption region and hence $\tilde{x}_f$ moves toward the oxidizer side for a new stoichiometric position, so that $\tilde{x}_f$ increases with Da_2. For a larger value of β,

the soot/precursor consumption reaction is stronger, leading to a greater oxidizer consumption rate in the soot/precursor consumption region and a larger $\bar{x}_f$.

The effect of diffusion transport of the radical, R, on the soot/precursor concentration is shown in Figs. 2.5 and 2.6 by plotting, respectively, the soot/precursor index, S_I, and flame temperature, $\tilde{T}_f$, versus Da_2 for selected values of Le_R with $Le_S = 1$, and $\beta = O(\delta)$. Recognizing that the flame behavior is qualitatively similar to that with *non-zero* β, the special case of $\beta = O(\delta)$ is selected for simplicity in numerical computations. Since the radical R (e.g., H) is generally light in weight, its diffusion rate is higher than that of the background gas and hence $Le_R < 1$. Figure 2.5 shows that for $Le_R < 1$, the value of S_I is lower for smaller values of Da_2, indicating that the amount of soot/precursor is lower. This result, however, is not conclusive since the trend reverses itself for larger values of Da_2. Nonetheless, Fig. 2.6 shows that $\tilde{T}_f$ increases monotonically with decreasing Le_R, which indicates that the total amount of soot/precursor decreases with decreasing Le_R for all values of Da_2. This is because the radical diffuses faster for a smaller Le_R, which renders a shorter residence time for the soot/precursor formation reaction and hence less soot/precursor production. Although the radical concentration is higher for a lower Le_R, which enhances soot/precursor production, the suppression of soot/precursor formation caused by the reduced residence time outweighed the promotion induced by the higher concentration.

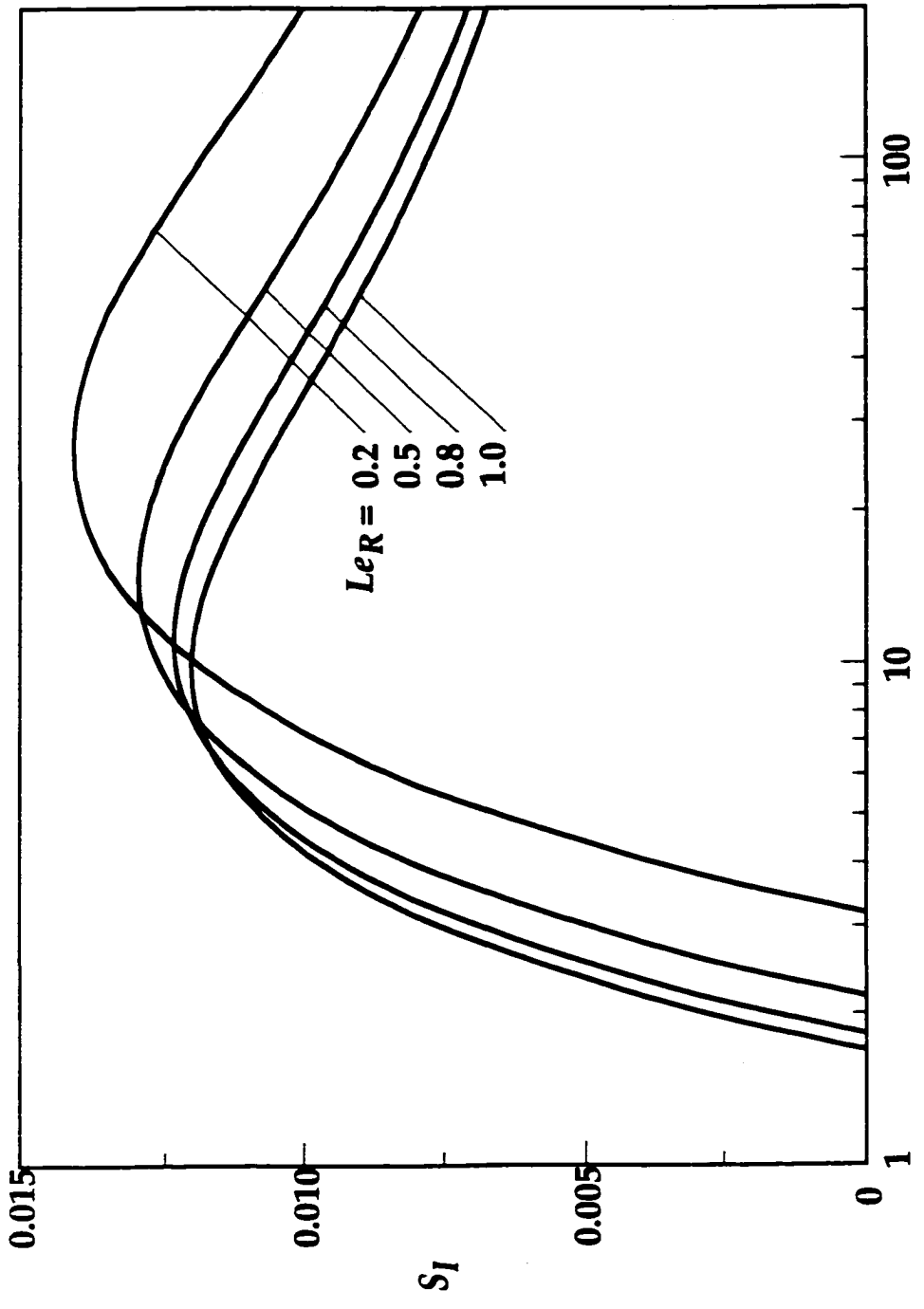

Figure 2.5 Variation of S_I with Da_2 for the fuel/air flame with $\alpha = Le_S = 1, \beta = O(\delta)$, and selected values of Le_R

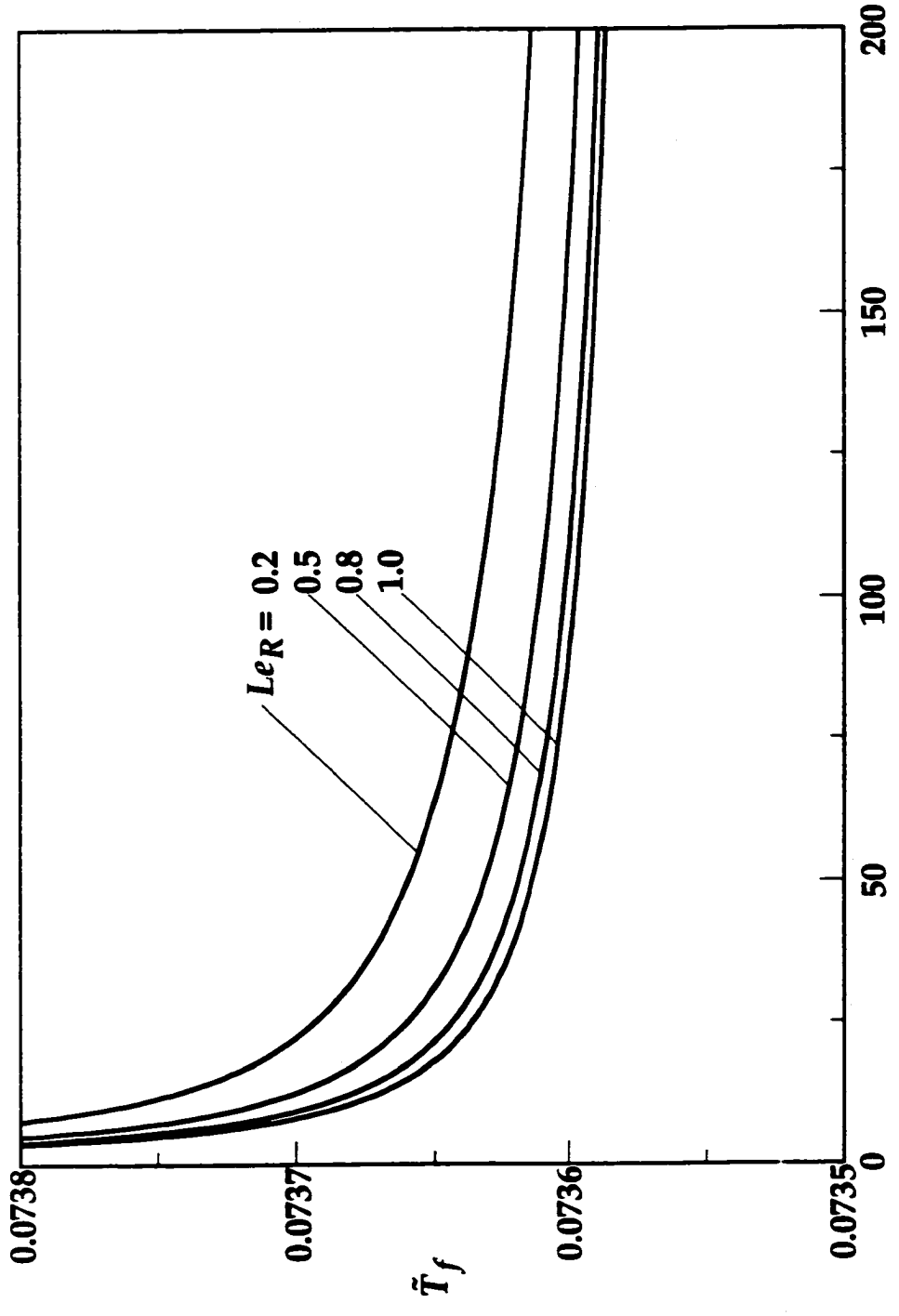

Figure 2.6 The flame temperature $\tilde{T}_f$ corresponding to Fig. 2.5

Figure 2.7 shows the diffusion effect of the soot/precursor by plotting S_I versus Da_2 for selected values of Le_S when $Le_R = 1$, and $\beta = O(\delta)$. The values of Le_S are taken to be greater than unity because the soot/precursor is heavier than the background gas and as a result its diffusion velocity is smaller. The maximum value of Le_S is chosen to be 10 because this is sufficient to exhibit the full impact of Le_S. The value of S_I increases with increasing Le_S, which is expected because the diffusive transport of soot/precursor is slower for higher Le_S. As a result more soot/precursor accumulates within the formation region. Consequently, the soot/precursor concentration is lower in the consumption region. Since the consumption reaction is very weak for realistic values of β, and the formation reaction does not depend on the transport of soot/precursor, the flame temperature and total amount of soot/precursor are independent of Le_S. However, it is expected that for sufficiently large values of β, a larger Le_S will yield a larger amount of soot/precursor and a lower flame temperature because the consumption reaction is weaker due to a lower soot/precursor concentration.

The effect of the activation energy ratio, α, is expected to yield a higher amount of soot/precursor and a lower flame temperature for higher α values because the soot/precursor consumption reaction is less likely to occur. This case will not be discussed further.

For the fuel/air flame considered thus far, the flame is situated on the oxidizer side of the stagnation plane, and the direction of convection is from the oxidizer side to the fuel side. The soot/precursor produced in the formation region will be convected toward the fuel side and appear among the combustion products. Thus, it has been relevant to discuss the

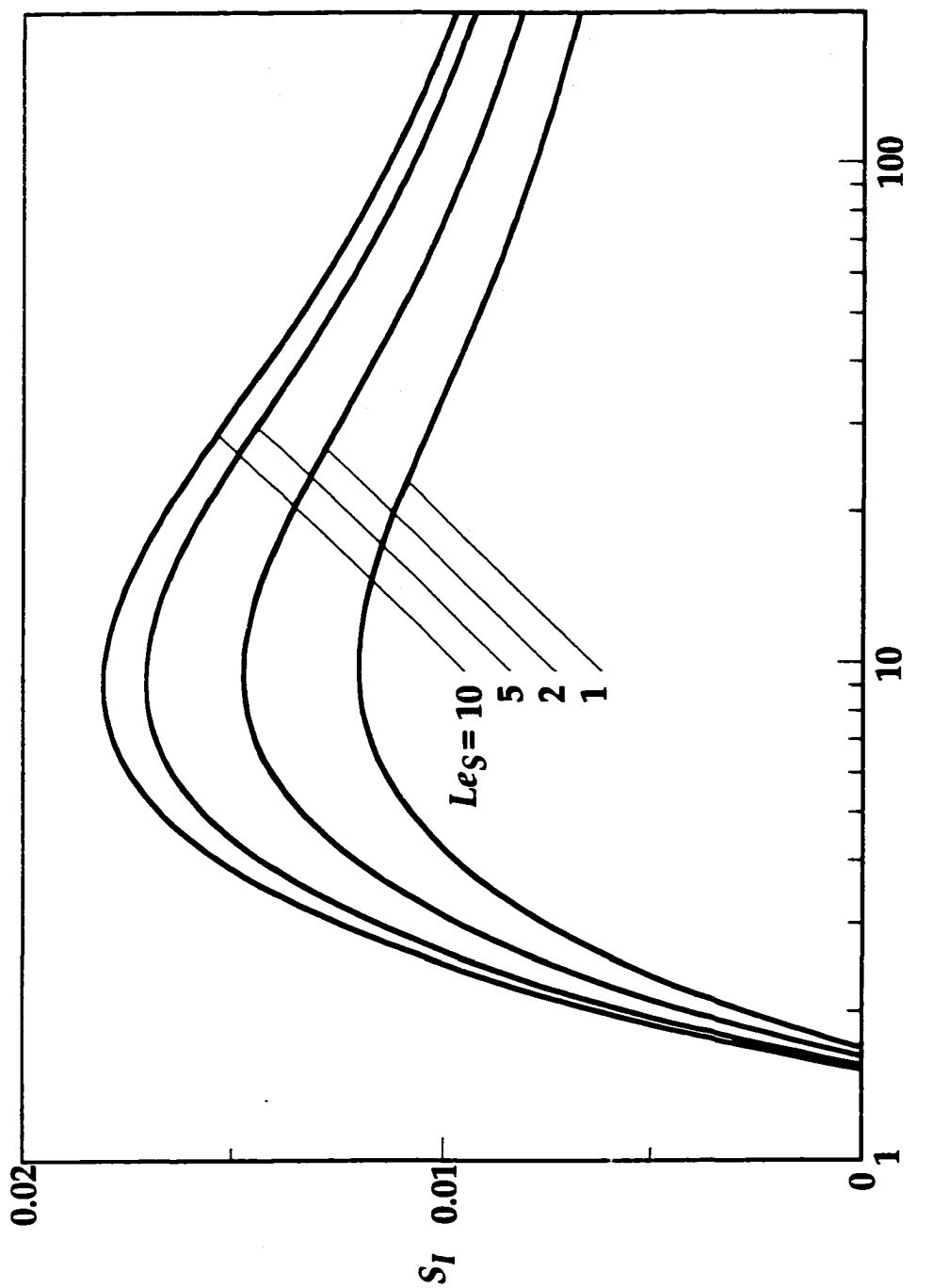

Figure 2.7 Variation of S_I with Da_2 for the fuel/air flame with $\alpha = Le_R = 1, \beta = O(\delta)$, and selected values of Le_S

soot/precursor content in terms of S_I. The quantity, S_B, which represents the amount of soot/precursor that enters the chemically inert transport region of the oxidizer side by breaking through both the oxidation and soot/precursor consumption regions, has not been considered.

The effect of stoichiometric mixture fraction on the soot/precursor content is now evaluated by redistributing the inert gas without changing the total enthalpy. Considering the extreme limit that all inert gas in the air flow is diverted into the fuel stream so that $Y_{O,\infty} = 1$, the flame migrates to the fuel side of the stagnation plane because of the low initial fuel mass fraction as compared to the initial oxidizer mass fraction (Fig 2.1(b)). In Figs. 2.8 and 2.9 the soot/precursor index, S_I, and flame temperature, $\tilde{T}_f$, are plotted versus Da_2 for selected values of β with the conditions that $\alpha = Le_R = Le_S = 1$. The variation of the flame sheet location with β is qualitatively similar to that in Fig. 2.4 for the fuel/air flame so this result will not be shown. Just as in Figs. 2.2 and 2.3, Figs. 2.8 and 2.9 show an initial increase in S_I with Da_2, the existence of an S_I maximum, a lower amount of soot/precursor and higher flame temperature for a higher β, as well as the existence of a $\tilde{T}_f$ minimum for *non-zero* values of β when Da_2 is sufficiently large. However, the values of Da_2 are much larger, S_I much smaller, and β much smaller than those for the fuel/air flame. Also, S_I is quite sensitive to β variations. These observations indicate that the soot/precursor formation reaction is significantly slower while the soot/precursor consumption reaction is much faster for this case. While soot/precursor consumption reactions have virtually no effect on soot/precursor formation in the fuel/air flame, they play a significant role in this diluted-fuel/oxygen flame.

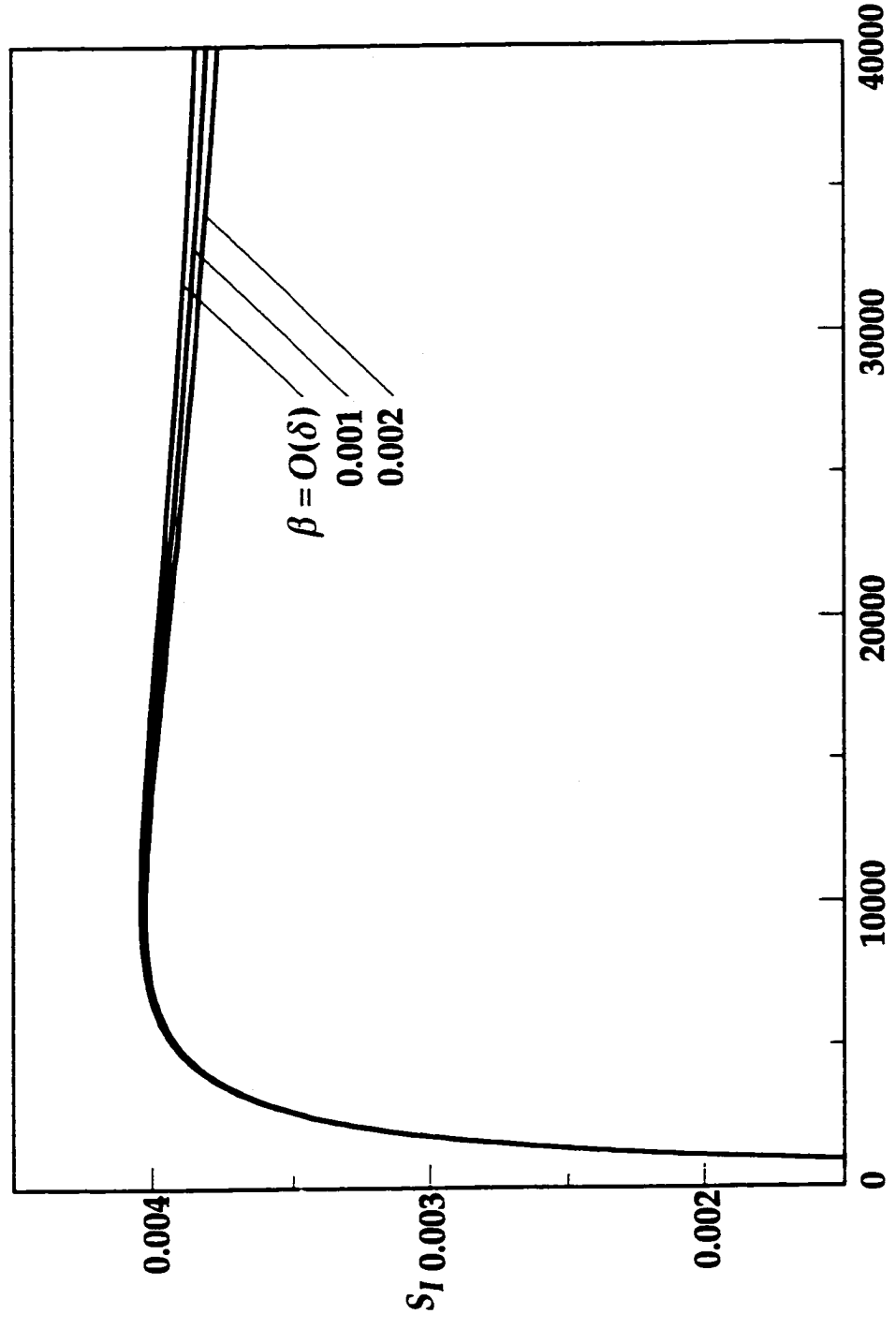

Figure 2.8 Variation of S_I with Da_2 for the diluted-fuel/oxygen flame with $\alpha = Le_R = Le_S = 1$ and selected values of β

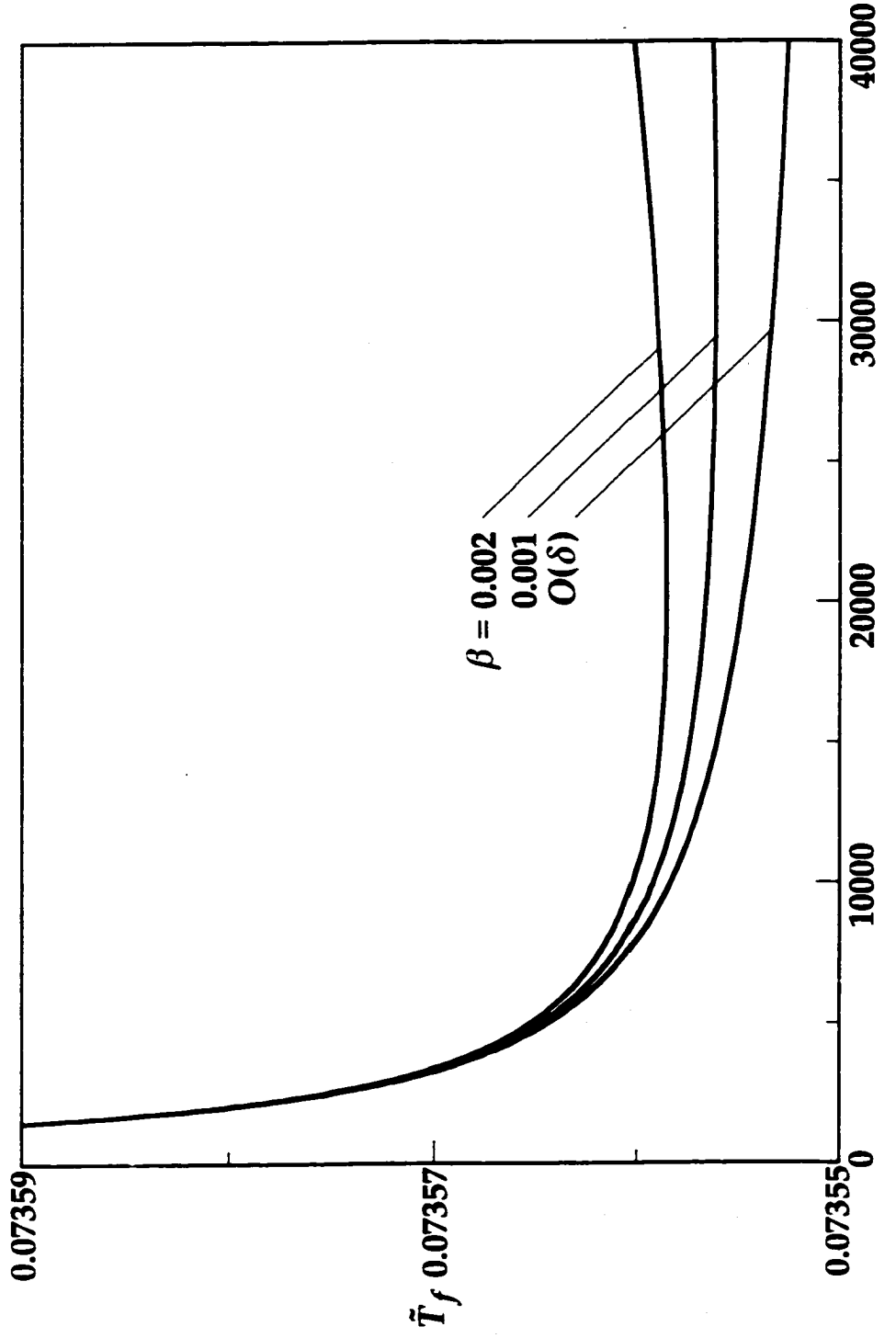

Figure 2.9 The flame temperature $\tilde{T}_f$ corresponding to Fig. 2.8

Thus, for a given fuel and a given strain rate the amount of soot/precursor produced can be substantially less for low initial fuel concentrations, which is in agreement with the experiments of Du and Axelbaum (1995). Furthermore, recognizing that the consumption reaction for the soot/precursor is not dependent on the parent fuel, it is seen that for a given strain rate, a much higher rate for the formation reaction is needed to produce soot/precursor at smaller initial fuel concentration.

Since, for this case, the flame is located at the fuel side of the stagnation plane, convection drives the fluid from the soot/precursor formation region toward the oxidizer side. This means that the soot/precursor produced must first pass through the consumption region before entering the inert region at the oxidizer side to appear as part of the final products. Thus the soot/precursor breakthrough, S_B, is appropriate to describe the soot/precursor content in the products and this is plotted in Fig. 2.10. Comparing Figs. 2.8 and 2.10, the value of S_B is seen to be lower than S_I. This is because part of the soot/precursor is oxidized when passing through the consumption region. Nonetheless, the conclusions drawn above, are the same as to the effect of initial fuel concentration.

The above results may be explained by the following. Since the flame is located at the fuel side of the stagnation plane, the temperature gradient in the fuel side of the oxidation region is much steeper than that of the oxidizer side (See Fig. 2.1(b)). The soot/precursor formation region, which is located on the fuel side of the oxidation region, is then much narrower than the soot/precursor consumption region located on the oxidizer side of the oxidation region. Therefore, the residence time for soot/precursor formation

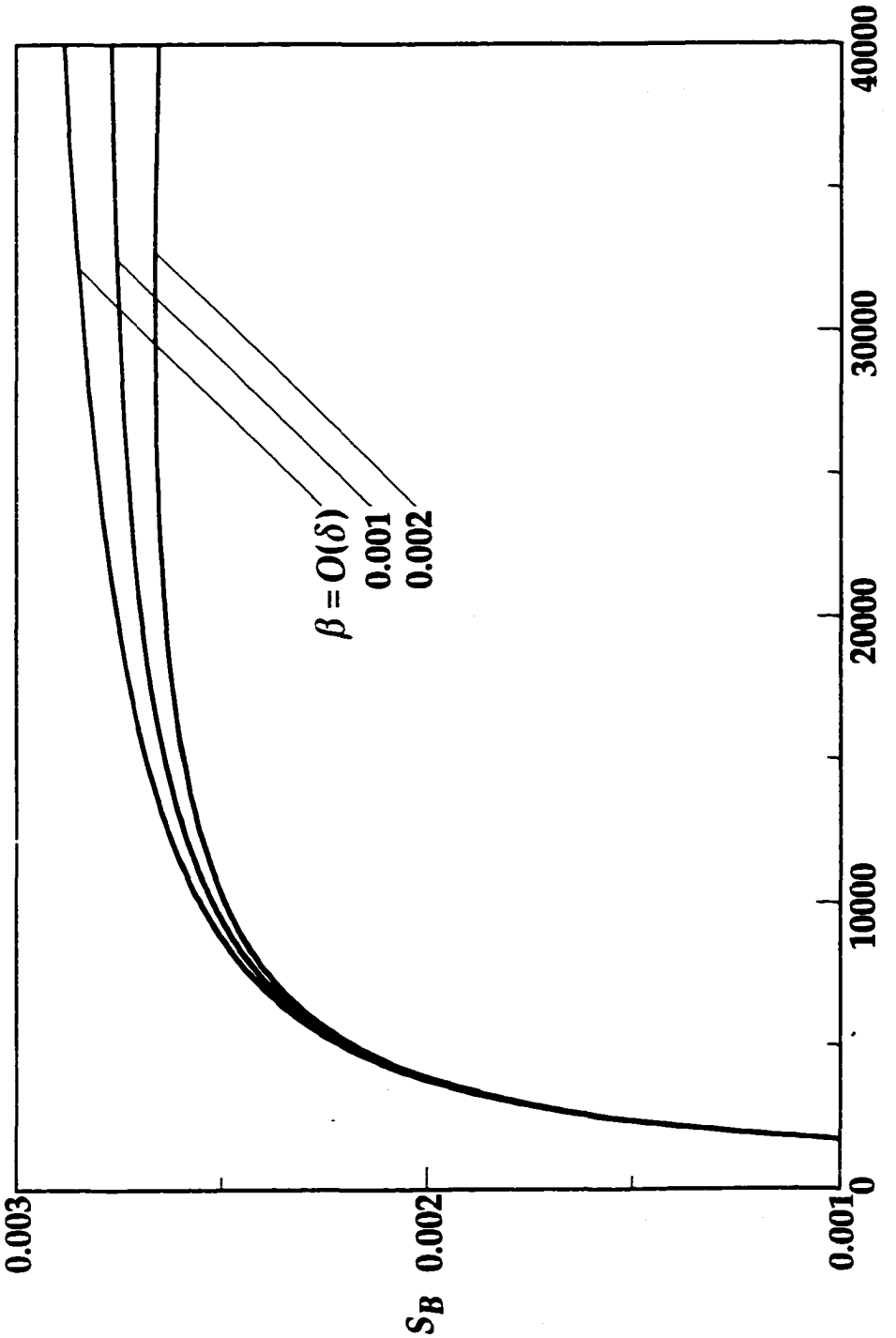

Figure 2.10 Variation of S_B corresponding to Fig. 2.8

is much shorter than that for soot/precursor consumption. The end result is that much higher values of Da_2 are needed to activate the soot/precursor formation reaction, and the soot/precursor concentration is much lower.

CHAPTER 3

SPHERICAL DIFFUSION FLAMES SUPPORTED BY A POROUS BURNER WITH FUEL SUPPLIED FROM THE BURNER

It is recognized from Chapter 2 that for the counterflow flame, the flow direction in the reaction regions is reversed when the inert gas is diverted from the oxidizer side to the fuel side. For this flame, the effect of hydrodynamics cannot be separated from diffusion and flame structure, and the relative importance among these mechanisms is not clear. To gain a better understanding of the impact of each individual process, it is necessary that each of these processes can be independently varied. A flame configuration that maintains the same flow direction before and after the inert gas redistribution so that the effect of hydrodynamics can be isolated is then sought for.

3.1 Formulation

The problem of interest in this chapter is therefore a diffusion flame burning at steady state and stabilized by a spherical porous burner. A stream of gaseous fuel with a specified temperature T_b is injected from the burner into a quiescent oxidizing environment at a temperature of T_∞. A flame is established between the fuel and oxidizer regions. The porous burner is assumed to be ideal in nature so that a uniform flow is supplied at its outer surface. The reaction is considered in a microgravity environment so that the flow field and the flame configuration are spherical symmetric. The same three-step reaction scheme, Eqs. (R1)–(R3), introduced in Chapter 1 and considered in Chapter 2, is adopted for this analysis.

With the above assumptions, the conservation equations are given by

$$d(r^2\rho u)/dr = 0 \quad , \tag{3.1}$$

$$\rho u c_p \frac{dT}{dr} - \frac{1}{r^2}\frac{d}{dr}\left(r^2 \lambda \frac{dT}{dr}\right) = \nu_{F,1} W_F q_{F,1} B_1 \left(\frac{\rho Y_F}{W_F}\right)\left(\frac{\rho Y_O}{W_O}\right)\exp\left(-\frac{E_1}{T}\right)$$
$$+ \nu_S W_S q_{S,3} B_3 \left(\frac{\rho Y_S}{W_S}\right)\left(\frac{\rho Y_O}{W_O}\right)\exp\left(-\frac{E_3}{T}\right) \quad , \tag{3.2}$$

$$\rho u \frac{dY_F}{dr} - \frac{1}{r^2}\frac{d}{dr}\left(r^2 \rho D_F \frac{dY_F}{dr}\right) = -\nu_{F,1} W_F B_1 \left(\frac{\rho Y_F}{W_F}\right)\left(\frac{\rho Y_O}{W_O}\right)\exp\left(-\frac{E_1}{T}\right)$$
$$- \nu_{F,2} W_F B_2 \left(\frac{\rho Y_F}{W_F}\right)\left(\frac{\rho Y_R}{W_R}\right)\exp\left(-\frac{E_2}{T}\right) \quad , \tag{3.3}$$

$$\rho u \frac{dY_O}{dr} - \frac{1}{r^2}\frac{d}{dr}\left(r^2 \rho D_O \frac{dY_O}{dr}\right) = -\nu_{O,1} W_O B_1 \left(\frac{\rho Y_F}{W_F}\right)\left(\frac{\rho Y_O}{W_O}\right)\exp\left(-\frac{E_1}{T}\right)$$
$$- \nu_{O,3} W_O B_3 \left(\frac{\rho Y_S}{W_S}\right)\left(\frac{\rho Y_O}{W_O}\right)\exp\left(-\frac{E_3}{T}\right) \quad , \tag{3.4}$$

$$\rho u \frac{dY_R}{dr} - \frac{1}{r^2}\frac{d}{dr}\left(r^2 \rho D_R \frac{dY_R}{dr}\right) = \nu_R W_R B_1 \left(\frac{\rho Y_F}{W_F}\right)\left(\frac{\rho Y_O}{W_O}\right)\exp\left(-\frac{E_1}{T}\right)$$
$$- \nu_R W_R B_2 \left(\frac{\rho Y_F}{W_F}\right)\left(\frac{\rho Y_R}{W_R}\right)\exp\left(-\frac{E_2}{T}\right) \quad , \tag{3.5}$$

$$\rho u \frac{dY_S}{dr} - \frac{1}{r^2}\frac{d}{dr}\left(r^2 \rho D_S \frac{dY_S}{dr}\right) = \nu_S W_S B_2 \left(\frac{\rho Y_F}{W_F}\right)\left(\frac{\rho Y_R}{W_R}\right)\exp\left(-\frac{E_2}{T}\right)$$
$$- \nu_S W_S B_3 \left(\frac{\rho Y_S}{W_S}\right)\left(\frac{\rho Y_O}{W_O}\right)\exp\left(-\frac{E_3}{T}\right) \quad . \tag{3.6}$$

Integrating Eq. (3.1) yields $r^2\rho u = const$, where u is the flow velocity in the radial direction, and r is the spatial coordinate in the radial direction. The

mass flow rate, $m = 4\pi r^2 \rho u$, which is controllable, is then a constant. Eqs. (3.2)–(3.6) will be solved subject to the following boundary conditions:

$$r = r_b : \quad T = T_b \quad , \quad mY_F - 4\pi r_b^2 \rho D_F (dY_F / dr) = m_F \quad ,$$

$$mY_i - 4\pi r_b^2 \rho D_i (dY_i / dr) = 0 \quad , \quad i = O, R, S \quad ; \tag{3.7}$$

$$r \to \infty : \quad T \to T_\infty \quad , \quad Y_O \to Y_{O,\infty} \quad ,$$

$$Y_i \to 0 \quad , \quad i = F, R, S \quad , \tag{3.8}$$

where r_b is the outer radius of the burner and m_F is the fuel flow rate from the burner. Other notations used have already been defined in Chapter 2 and will not be repeated.

Defining the additional nondimensional quantities for this system as

$$\tilde{r} = \frac{r}{r_b} \quad , \quad \tilde{m} = \frac{c_p m}{4\pi r_b \lambda} \quad , \quad \overline{m}_F = \frac{m_F}{m} \quad , \quad Da_1 = \frac{\rho_f^2 r_b^2 c_p \nu_{O,1} B_1}{\lambda W_F} \quad ,$$

$$Da_2 = \frac{\rho_f^2 r_b^2 c_p \tilde{\nu}_F \nu_R B_2}{\lambda W_F} \quad ,$$

and applying the nondimensional quantities as defined in Chapter 2 except for $\tilde{x}$, Da_1, Da_2 to Eqs. (3.2)–(3.8), we have the following nondimensional conservation equations:

$$\frac{1}{\tilde{r}^2}\left[\tilde{m}\frac{d\tilde{T}}{d\tilde{r}} - \frac{d}{d\tilde{r}}\left(\tilde{r}^2 \frac{d\tilde{T}}{d\tilde{r}}\right)\right] = Da_1 \tilde{Y}_F \tilde{Y}_O \exp\left(-\frac{\tilde{E}_1}{\tilde{T}}\right)$$

$$+ \beta \tilde{q}_S Da_2 \tilde{Y}_S \tilde{Y}_O \exp\left(-\alpha \frac{\tilde{E}_2}{\tilde{T}}\right) \quad , \tag{3.9}$$

$$\frac{1}{\tilde{r}^2}\left[\tilde{m}\frac{d\tilde{Y}_F}{d\tilde{r}}-\frac{1}{Le_F}\frac{d}{d\tilde{r}}\left(\tilde{r}^2\frac{d\tilde{Y}_F}{d\tilde{r}}\right)\right]=-Da_1\tilde{Y}_F\tilde{Y}_O\exp\left(-\frac{\tilde{E}_1}{\tilde{T}}\right)$$

$$-Da_2\tilde{Y}_F\tilde{Y}_R\exp\left(-\frac{\tilde{E}_2}{\tilde{T}}\right) \quad , \tag{3.10}$$

$$\frac{1}{\tilde{r}^2}\left[\tilde{m}\frac{d\tilde{Y}_O}{d\tilde{r}}-\frac{1}{Le_O}\frac{d}{d\tilde{r}}\left(\tilde{r}^2\frac{\tilde{Y}_O}{d\tilde{r}}\right)\right]=-Da_1\tilde{Y}_F\tilde{Y}_O\exp\left(-\frac{\tilde{E}_1}{\tilde{T}}\right)$$

$$-\frac{\beta}{\hat{\nu}}Da_2\tilde{Y}_S\tilde{Y}_O\exp\left(-\alpha\frac{\tilde{E}_2}{\tilde{T}}\right) \quad , \tag{3.11}$$

$$\frac{1}{\tilde{r}^2}\left[\tilde{m}\frac{d\tilde{Y}_R}{d\tilde{r}}-\frac{1}{Le_R}\frac{d}{d\tilde{r}}\left(\tilde{r}^2\frac{d\tilde{Y}_R}{d\tilde{r}}\right)\right]=Da_1\tilde{Y}_F\tilde{Y}_O\exp\left(-\frac{\tilde{E}_1}{\tilde{T}}\right)$$

$$-\frac{1}{\tilde{\nu}_F}Da_2\tilde{Y}_F\tilde{Y}_R\exp\left(-\frac{\tilde{E}_2}{\tilde{T}}\right) \quad , \tag{3.12}$$

$$\frac{1}{\tilde{r}^2}\left[\tilde{m}\frac{d\tilde{Y}_S}{d\tilde{r}}-\frac{1}{Le_S}\frac{d}{d\tilde{r}}\left(\tilde{r}^2\frac{d\tilde{Y}_S}{d\tilde{r}}\right)\right]=Da_2\tilde{Y}_F\tilde{Y}_R\exp\left(-\frac{\tilde{E}_2}{\tilde{T}}\right)$$

$$-\beta Da_2\tilde{Y}_S\tilde{Y}_O\exp\left(-\alpha\frac{\tilde{E}_2}{\tilde{T}}\right) \quad , \tag{3.13}$$

with the boundary conditions:

$$\tilde{r}=1 : \quad \tilde{T}=\tilde{T}_b \quad , \quad \tilde{m}\tilde{Y}_F-\frac{1}{Le_F}\frac{d\tilde{Y}_F}{d\tilde{r}}=\tilde{m}_F \quad ,$$

$$\tilde{m}\tilde{Y}_i-\frac{1}{Le_i}\frac{d\tilde{Y}_i}{d\tilde{r}}=0 \quad , \quad i=O,R,S \quad ; \tag{3.14}$$

$$\tilde{r}\to\infty : \tilde{T}\to\tilde{T}_\infty \quad , \quad \tilde{Y}_O\to\tilde{Y}_{O,\infty} \quad , \quad \tilde{Y}_i\to 0 \quad , \quad i=F,R,S \quad . \tag{3.15}$$

3.2 Asymptotic Analysis

The analysis follows the same high activation energy reactions and their relations as those in Chapter 2. The solution, however, assumes a different functional expression because of the difference in the flow geometry.

3.2.1 Outer Solutions

In the chemically inert outer regions, the process is controlled by the balance between the diffusion and convection transport. Designating the solutions in the fuel and oxidizer sides of the reaction region by superscripts "–" and "+", respectively, and solving the source free form of Eqs. (3.9)–(3.13) subject to the boundary conditions in Eqs. (3.14) and (3.15), we obtain the outer solutions:

$$\tilde{T}^{-} = \tilde{T}_b + \{[a^{-}_{T,0} + \delta a^{-}_{T,1} + O(\delta^2)] + O(\varepsilon)\}[\exp(-\tilde{m}/\tilde{r}) - \exp(-\tilde{m})] \quad , \tag{3.16a}$$

$$\tilde{T}^{+} = \tilde{T}_\infty + \{[a^{+}_{T,0} + \delta a^{+}_{T,1} + O(\delta^2)] + O(\varepsilon)\}[1 - \exp(-\tilde{m}/\tilde{r})] \quad , \tag{3.16b}$$

$$\tilde{Y}^{-}_F = \overline{m}_F - \{[a^{-}_{F,0} + \delta a^{-}_{F,1} + O(\delta^2)] + O(\varepsilon)\}\exp(-Le_F \tilde{m}/\tilde{r}) \quad , \tag{3.17a}$$

$$\tilde{Y}^{+}_F = \{[a^{+}_{F,0} + \delta a^{+}_{F,1} + O(\delta^2)] + O(\varepsilon)\}[1 - \exp(-Le_F \tilde{m}/\tilde{r})] \quad , \tag{3.17b}$$

$$\tilde{Y}^{-}_O = \{[a^{-}_{O,0} + \delta a^{-}_{O,1} + O(\delta^2)] + O(\varepsilon)\}\exp(-Le_O \tilde{m}/\tilde{r}) \quad , \tag{3.18a}$$

$$\tilde{Y}^{+}_O = \tilde{Y}_{O,\infty} - \{[a^{+}_{O,0} + \delta a^{+}_{O,1} + O(\delta^2)] + O(\varepsilon)\}[1 - \exp(-Le_O \tilde{m}/\tilde{r})] \quad , \tag{3.18b}$$

$$\tilde{Y}^{-}_i = \{[a^{-}_{i,0} + \delta a^{-}_{i,1} + O(\delta^2)] + O(\varepsilon)\}\exp(-Le_i \tilde{m}/\tilde{r}) \quad , \quad i = S, R \quad , \tag{3.19a}$$

$$\tilde{Y}^{+}_i = \{[a^{+}_{i,0} + \delta a^{+}_{i,1} + O(\delta^2)] + O(\varepsilon)\}[1 - \exp(-Le_i \tilde{m}/\tilde{r})] \quad , \quad i = S, R \quad , \tag{3.19b}$$

where $a_{i,j}^{\pm}$ are integration constants to be determined later.

3.2.2 Structure Equations in the Soot Formation Region

In the $O(\delta)$ soot/precursor formation region located in the fuel side of, and adjacent to, the oxidation region, only the soot/precursor formation reaction (R2) is significant and only $O(\delta)$ variations on all the quantities are possible. In this region, the stretched coordinate is defined as $\zeta = (\tilde{r} - \tilde{r}_f)/\delta$ with $\zeta < 0$, where the small parameter is given by $\delta = \tilde{T}_{f,0}^2 / \tilde{E}_2$. Moreover, the variables are expanded in terms of δ as

$$\tilde{T}^- = [\tilde{T}_{f,0} - \delta\Theta_1^- - \delta^2\Theta_2^- + O(\delta^3)] + O(\varepsilon) \quad , \tag{3.20}$$

$$\tilde{Y}_i^- = [\delta\Phi_{i,1}^- + \delta^2\Phi_{i,2}^- + O(\delta^3)] + O(\varepsilon) \quad , \quad i = F, O, R \quad , \tag{3.21}$$

$$\tilde{Y}_S^- = [\Phi_{S,0}^- + \delta\Phi_{S,1}^- + \delta^2\Phi_{S,2}^- + O(\delta^3)] + O(\varepsilon) \quad . \tag{3.22}$$

Substituting Eqs. (3.20)–(3.22) into Eqs. (3.9)–(3.13), expanding, then collecting terms of the same order in δ, we obtain the following structure equations:

$$\frac{d^2\Phi_{F,1}^-}{d\zeta^2} = \Lambda_2 \Phi_{F,1}^- \Phi_{R,1}^- \exp(-\Theta_1^-) \quad , \tag{3.23}$$

$$\begin{aligned} \frac{d^2\Phi_{S,0}^-}{d\zeta^2} = \frac{d^2\Theta_1^-}{d\zeta^2} &= \frac{1}{Le_F}\frac{d^2\Phi_{F,1}^-}{d\zeta^2} - \frac{\tilde{\nu}_F}{Le_R}\frac{d^2\Phi_{R,1}^-}{d\zeta^2} \\ &= \left(\tilde{m} - \frac{2\tilde{r}_f}{Le_S}\right)\frac{d\Phi_{S,0}^-}{d\zeta} - \tilde{r}_f^2\left(\frac{\tilde{\nu}_F}{Le_R}\frac{d^2\Phi_{R,1}^-}{d\zeta^2} + \frac{1}{Le_S}\frac{d^2\Phi_{S,1}^-}{d\zeta^2}\right) = 0 \quad , \end{aligned} \tag{3.24}$$

$$\tilde{r}_f^2\left(\frac{d^2\Theta_2^-}{d\zeta^2} - \frac{\tilde{q}_S\hat{\nu}}{Le_O}\frac{d^2\Phi_{O,2}^-}{d\zeta^2}\right) - \left(\tilde{m} - 2\tilde{r}_f\right)\frac{d\Theta_1^-}{d\zeta} = 0 \quad , \tag{3.25}$$

$$\tilde{m}\left(\frac{d\Phi_{F,1}^{-}}{d\zeta}-\tilde{\nu}_F\frac{d\Phi_{R,1}^{-}}{d\zeta}\right)-\tilde{r}_f^2\left(\frac{1}{Le_F}\frac{d^2\Phi_{F,2}^{-}}{d\zeta^2}-\frac{\tilde{\nu}_F}{Le_R}\frac{d^2\Phi_{R,2}^{-}}{d\zeta^2}\right)$$

$$-2\tilde{r}_f\left(\frac{1}{Le_F}\frac{d\Phi_{F,1}^{-}}{d\zeta}-\frac{\tilde{\nu}_F}{Le_R}\frac{d\Phi_{R,1}^{-}}{d\zeta}\right)=0 \quad , \tag{3.26}$$

$$\tilde{m}\left[\frac{d\Phi_{F,1}^{-}}{d\zeta}+\frac{d\Phi_{S,1}^{-}}{d\zeta}\right]-\tilde{r}_f^2\left[\frac{1}{Le_F}\frac{d^2\Phi_{F,2}^{-}}{d\zeta^2}+\frac{1}{Le_S}\frac{d^2\Phi_{S,2}^{-}}{d\zeta^2}-\frac{\hat{\nu}}{Le_O}\frac{d^2\Phi_{O,2}^{-}}{d\zeta^2}\right]$$

$$-2\tilde{r}_f\left[\frac{1}{Le_F}\frac{d\Phi_{F,1}^{-}}{d\zeta}+\frac{1}{Le_S}\frac{d\Phi_{S,1}^{-}}{d\zeta}\right]-2\zeta\left[\frac{\tilde{m}}{\tilde{r}_f}-\frac{1}{Le_S}\right]\frac{d\Phi_{S,0}^{-}}{d\zeta}=0 \quad . \tag{3.27}$$

In the above $\tilde{T}_{f,0}$ is the leading order flame temperature to be determined, and

$$\Lambda_2=\delta^3 Le_F Da_2 \exp(-\tilde{E}_2/\tilde{T}_{f,0}) \tag{3.28}$$

is the reduced Damköhler number for the soot/precursor formation reaction. The soot/precursor concentration is considered an $O(1)$ quantity since the soot/precursor formation and consumption reactions can have different rates. Because only an $O(\varepsilon)$ oxidizer leaks through the oxidation region into this region, the condition of $\Phi_{O,1}^{-}\equiv 0$ is required.

3.2.3 Matching of Solutions in the Outer and Soot Formation Regions

The required boundary conditions to solve Eqs. (3.23)–(3.27) can be obtained from matching the solutions of the soot formation region with the outer solutions of the fuel side region. Matching can be performed by first substituting the stretched variable, $\tilde{r}=\tilde{r}_f+\delta\zeta$, into the outer solution, expanding the resulting equation in terms of δ, collecting the terms of the same order in δ, and then equating the resulting expression with the solution

in the soot formation region in the limit of $\zeta \to -\infty$ and $\tilde{r} \to \tilde{r}_f$. This procedure can be illustrated by matching of the fuel concentration solution. Applying the stretched variable, $(1/\tilde{r})$ and $\exp(-Le\tilde{m}/\tilde{r})$ are first expanded to

$$\frac{1}{\tilde{r}} = \frac{1}{\tilde{r}_f\left(1+\delta\zeta/\tilde{r}_f\right)} = \frac{1}{\tilde{r}_f}\left[1-\delta\frac{\zeta}{\tilde{r}_f}+\delta^2\left(\frac{\zeta}{\tilde{r}_f}\right)^2+O(\delta^3)\right] \quad , \tag{3.29}$$

$$\begin{aligned}
\exp\left(-\frac{Le\tilde{m}}{\tilde{r}}\right) &= \exp\left\{-\frac{Le\tilde{m}}{\tilde{r}_f}\left[1-\delta\frac{\zeta}{\tilde{r}_f}+\delta^2\left(\frac{\zeta}{\tilde{r}_f}\right)^2+O(\delta^3)\right]\right\} \\
&= \exp\left\{-\frac{Le\tilde{m}}{\tilde{r}_f}+\delta\frac{Le\tilde{m}\zeta}{\tilde{r}_f^2}\left[1-\delta\frac{\zeta}{\tilde{r}_f}++O(\delta^2)\right]\right\} \\
&= \exp\left(-\frac{Le\tilde{m}}{\tilde{r}_f}\right)\exp\left\{\delta\frac{Le\tilde{m}\zeta}{\tilde{r}_f^2}\left[1-\delta\frac{\zeta}{\tilde{r}_f}+O(\delta^2)\right]\right\} \\
&= \exp\left(-\frac{Le\tilde{m}}{\tilde{r}_f}\right)\left\{1+\delta\frac{Le\tilde{m}\zeta}{\tilde{r}_f^2}-\delta^2\frac{Le\tilde{m}}{\tilde{r}_f^3}\left(2-\frac{Le\tilde{m}}{\tilde{r}_f}\right)\frac{\zeta^2}{2}+O(\delta^3)\right\} \quad .
\end{aligned} \tag{3.30}$$

Substituting Eq. (3.30) into Eq. (3.17a), rearranging in terms of δ, and equating the resulting equation with Eq. (3.21) for $i = F$ yield

$$\begin{aligned}
\tilde{Y}_{\bar{F}} &= \bar{m}_F - \{[a_{\bar{F},0}^- + \delta a_{\bar{F},1}^- + O(\delta^2)] + O(\varepsilon)\}\exp(-Le_F\tilde{m}/\tilde{r}) \\
&= \bar{m}_F - \{[a_{\bar{F},0}^- + \delta a_{\bar{F},1}^- + O(\delta^2)] + O(\varepsilon)\} \\
&\quad \times \exp\left(-\frac{Le\tilde{m}}{\tilde{r}_f}\right)\left\{1+\delta\frac{Le\tilde{m}\zeta}{\tilde{r}_f^2}-\delta^2\frac{Le\tilde{m}}{\tilde{r}_f^3}\left(2-\frac{Le\tilde{m}}{\tilde{r}_f}\right)\frac{\zeta^2}{2}+O(\delta^3)\right\}
\end{aligned}$$

$$= \bar{m}_F - a_{F,0}^{-} \exp\left(-\frac{Le_F \tilde{m}}{\tilde{r}_f}\right) - \delta\left[a_{F,1}^{-} + a_{F,0}^{-} \frac{Le_F \tilde{m}}{\tilde{r}_f^2}\zeta\right] \exp\left(-\frac{Le_F \tilde{m}}{\tilde{r}_f}\right)$$

$$-\delta^2\left\{a_{F,1}^{-}\zeta - \frac{a_{F,0}^{-}}{\tilde{r}_f}\left(2 - \frac{Le_F \tilde{m}}{\tilde{r}_f}\right)\frac{\zeta^2}{2} + const\right\}\frac{Le_F \tilde{m}}{\tilde{r}_f^2}\exp\left(-\frac{Le_F \tilde{m}}{\tilde{r}_f}\right)$$

$$+O(\delta^3)+O(\varepsilon)$$

$$= \{[\delta \Phi_{F,1}^{-} + \delta^2 \Phi_{F,2}^{-} + O(\delta^3)] + O(\varepsilon)\}_{\zeta \to -\infty} \quad . \tag{3.31}$$

By comparing terms of the same order in δ , the following matching conditions are obtained:

$$\bar{m}_F - a_{F,0}^{-} \exp(-Le_F \tilde{m} / \tilde{r}_f) = 0 \quad \text{or} \quad a_{F,0}^{-} = \bar{m}_F \exp(Le_F \tilde{m} / \tilde{r}_f) \quad , \tag{3.32}$$

$$\Phi_{F,1}^{-}(\zeta \to -\infty) = -a_{F,1}^{-} \exp(-Le_F \tilde{m} / \tilde{r}_f) - \bar{m}_F (Le_F \tilde{m} / \tilde{r}_f^2)\zeta \quad , \tag{3.33a}$$

$$(d\Phi_{F,2}^{-} / d\zeta)_{\zeta \to -\infty} = -\left\{a_{F,1}^{-} \exp\left(-\frac{Le_F \tilde{m}}{\tilde{r}_f}\right) - \frac{\bar{m}_F}{\tilde{r}_f}\left(2 - \frac{Le_F \tilde{m}}{\tilde{r}_f}\right)\zeta\right\}\frac{Le_F \tilde{m}}{\tilde{r}_f^2} \quad . \tag{3.34}$$

Equation (3.33a) also implies

$$(d\Phi_{F,1}^{-} / d\zeta)_{\zeta \to -\infty} = -\bar{m}_F (Le_F \tilde{m} / \tilde{r}_f^2) \quad . \tag{3.33b}$$

Other conditions can be derived following the same process, given by

$$a_{T,0}^{-} = (\tilde{T}_{f,0} - \tilde{T}_b) / [\exp(-\tilde{m} / \tilde{r}_f) - \exp(-\tilde{m})] \quad , \tag{3.35}$$

$$a_{O,0}^{-} = a_{O,1}^{-} = a_{R,0}^{-} = 0 \quad , \tag{3.36}$$

$$\Theta_1^{-}(\zeta \to -\infty) = -a_{T,1}^{-}\left[\exp\left(-\frac{\tilde{m}}{\tilde{r}_f}\right) - \exp(-\tilde{m})\right] - a_{T,0}^{-}\frac{\tilde{m}}{\tilde{r}_f^2}\exp\left(-\frac{\tilde{m}}{\tilde{r}_f}\right)\zeta \quad , \tag{3.37}$$

$$\left(\frac{d\Theta_2^-}{d\zeta}\right)_{\zeta\to-\infty} = -\left\{a_{T,1}^- - \frac{a_{T,0}^-}{\tilde{r}_f}\left(2-\frac{\tilde{m}}{\tilde{r}_f}\right)\zeta\right\}\frac{\tilde{m}}{\tilde{r}_f^2}\exp\left(-\frac{\tilde{m}}{\tilde{r}_f}\right) \quad , \tag{3.38}$$

$$(d\Phi_{O,2}^-/d\zeta)_{\zeta\to-\infty} = 0 \quad , \tag{3.39}$$

$$\Phi_{R,1}^-(\zeta\to-\infty) = a_{R,1}^-\exp(-Le_R\tilde{m}/\tilde{r}_f) \quad , \tag{3.40}$$

$$(d\Phi_{R,2}^-/d\zeta)_{\zeta\to-\infty} = a_{R,1}^-(Le_R\tilde{m}/\tilde{r}_f^2)\exp(-Le_R\tilde{m}/\tilde{r}_f) \quad , \tag{3.41}$$

$$\Phi_{S,0}^-(\zeta\to-\infty) = a_{S,0}^-\exp(-Le_S\tilde{m}/\tilde{r}_f) \quad , \tag{3.42}$$

$$\Phi_{S,1}^-(\zeta\to-\infty) = [a_{S,1}^- + a_{S,0}^-(Le_S\tilde{m}/\tilde{r}_f^2)\zeta]\exp(-Le_S\tilde{m}/\tilde{r}_f) \quad , \tag{3.43}$$

$$\left(\frac{d\Phi_{S,2}^-}{d\zeta}\right)_{\zeta\to-\infty} = \left\{a_{S,1}^- - \frac{a_{S,0}^-}{\tilde{r}_f}\left(2-\frac{Le_S\tilde{m}}{\tilde{r}_f}\right)\zeta\right\}\frac{Le_S\tilde{m}}{\tilde{r}_f^2}\exp\left(-\frac{Le_S\tilde{m}}{\tilde{r}_f}\right) \quad . \tag{3.44}$$

Integrating the four expressions in Eq. (3.24) twice and Eqs. (3.25)–(3.27) once subject to the matching conditions given by Eqs. (3.33), (3.34) and (3.37)–(3.44), we obtain

$$\Phi_{S,0}^- = a_{S,0}^-\exp(-Le_S\tilde{m}/\tilde{r}_f) \quad , \tag{3.45}$$

$$\Theta_1^- = -a_{T,1}^-\left[\exp\left(-\frac{\tilde{m}}{\tilde{r}_f}\right)-\exp(-\tilde{m})\right] - \left[\frac{\tilde{T}_{f,0}-\tilde{T}_b}{\tilde{r}_f^2/\tilde{m}}\frac{\exp(-\tilde{m}/\tilde{r}_f)}{\exp(-\tilde{m}/\tilde{r}_f)-\exp(-\tilde{m})}\right]\zeta \quad , \tag{3.46}$$

$$\frac{\Phi_{F,1}^-}{Le_F} - \tilde{\nu}_F\frac{\Phi_{R,1}^-}{Le_R} = -\frac{a_{F,1}^-}{Le_F}\exp\left(-\frac{Le_F\tilde{m}}{\tilde{r}_f}\right) - \tilde{\nu}_F\frac{a_{R,1}^-}{Le_R}\exp\left(-\frac{Le_R\tilde{m}}{\tilde{r}_f}\right) - \frac{\overline{m}_F\tilde{m}}{\tilde{r}_f^2}\zeta \quad , \tag{3.47}$$

$$\tilde{\nu}_F \frac{\bar{\Phi}_{R,1}}{Le_R} + \frac{\bar{\Phi}_{S,1}}{Le_S} = \tilde{\nu}_F \frac{\bar{a}_{R,1}}{Le_R} \exp\left(-\frac{Le_R \tilde{m}}{\tilde{r}_f}\right) + \frac{\bar{a}_{S,1}}{Le_S} \exp\left(-\frac{Le_S \tilde{m}}{\tilde{r}_f}\right)$$

$$+ \frac{\bar{a}_{S,0} \tilde{m}}{\tilde{r}_f^2} \exp\left(-\frac{Le_S \tilde{m}}{\tilde{r}_f}\right) \zeta \quad , \tag{3.48}$$

$$\left(\frac{d\bar{\Theta}_2}{d\zeta}\right) - \frac{\tilde{q}_S \hat{\nu}}{Le_O}\left(\frac{d\bar{\Phi}_{O,2}}{d\zeta}\right) = \frac{\tilde{m}}{\tilde{r}_f^2}\left[-\bar{a}_{T,1} + \frac{\bar{a}_{T,0}}{\tilde{r}_f}\left(2 - \frac{\tilde{m}}{\tilde{r}_f}\right)\zeta\right] \exp\left(-\frac{\tilde{m}}{\tilde{r}_f}\right) \quad , \tag{3.49}$$

$$\frac{1}{Le_F}\frac{d\bar{\Phi}_{F,1}}{d\zeta} - \frac{\tilde{\nu}_F}{Le_R}\frac{d\bar{\Phi}_{R,1}}{d\zeta} = -\frac{\bar{m}_F \tilde{m}}{\tilde{r}_f^2} = -\frac{\tilde{m}_F}{\tilde{r}_f^2} \quad , \tag{3.50}$$

$$\frac{\tilde{\nu}_F}{Le_R}\frac{d\bar{\Phi}_{R,1}}{d\zeta} + \frac{1}{Le_S}\frac{d\bar{\Phi}_{S,1}}{d\zeta} = \frac{\bar{a}_{S,0}\tilde{m}}{\tilde{r}_f^2} \exp\left(-\frac{Le_S \tilde{m}}{\tilde{r}_f}\right) \quad , \tag{3.51}$$

$$\frac{\tilde{m}}{\tilde{r}_f^2}\tilde{m}(\bar{\Phi}_{F,1} - \tilde{\nu}_F \bar{\Phi}_{R,1}) - \tilde{r}_f^2\left(\frac{1}{Le_F}\frac{d\bar{\Phi}_{F,2}}{d\zeta} - \frac{\tilde{\nu}_F}{Le_R}\frac{d\bar{\Phi}_{R,2}}{d\zeta}\right) = 2\frac{\bar{m}_F \tilde{m}}{\tilde{r}_f}\zeta \quad , \tag{3.52}$$

$$\tilde{m}(\tilde{\nu}_F \bar{\Phi}_{R,1} + \bar{\Phi}_{S,1}) - \tilde{r}_f^2\left(\frac{\tilde{\nu}_F}{Le_R}\frac{d\bar{\Phi}_{R,2}}{d\zeta} + \frac{1}{Le_S}\frac{d\bar{\Phi}_{S,2}}{d\zeta} - \frac{\hat{\nu}}{Le_O}\frac{d\bar{\Phi}_{O,2}}{d\zeta}\right)$$

$$= \bar{a}_{S,0}(2\tilde{m}/\tilde{r}_f)\exp(-Le_S\tilde{m}/\tilde{r}_f)\zeta \quad . \tag{3.53}$$

In the above, Eqs. (3.50) and (3.51) are obtained by differentiating Eqs. (3.47) and (3.48) with respect to ζ.

3.2.4 Structure Equations in the Soot Consumption Region

In the $O(\delta)$ soot/precursor consumption region located in the oxidizer side of, and adjacent to, the oxidation region, only the soot/precursor consumption reaction (R3) is important. Because E_2 and E_3 are of the same order, the same stretched coordinate, $\zeta = (\tilde{r} - \tilde{r}_f)/\delta$, is used, but with $\zeta > 0$.

As in Chapter 2, the expansions of the various variables are:

$$\tilde{T}^{+} = [\tilde{T}_{f,0} - \delta\,\Theta_1^{+} - \delta^2\,\Theta_2^{+} + O(\delta^3)] + O(\varepsilon) \quad , \tag{3.54}$$

$$\tilde{Y}_i^{+} = [\delta\,\Phi_{i,1}^{+} + \delta^2\,\Phi_{i,2}^{+} + O(\delta^3)] + O(\varepsilon) \quad , \quad i = F, O, R \quad , \tag{3.55}$$

$$\tilde{Y}_S^{+} = [\Phi_{S,0}^{+} + \delta\,\Phi_{S,1}^{+} + \delta^2\,\Phi_{S,2}^{+} + O(\delta^3)] + O(\varepsilon) \quad . \tag{3.56}$$

Since only an $O(\varepsilon)$ fuel leakage through the oxidation region is allowed, $\Phi_{F,1}^{+} \equiv 0$ is a required condition. Substituting Eqs. (3.54)–(3.56) into Eqs. (3.9)–(3.13), expanding and collecting terms of the same order in δ, we obtain the following structure equations:

$$d^2\,\Phi_{O,1}^{+} / d\zeta^2 = \Lambda_3\,\Phi_{S,0}^{+}\,\Phi_{O,1}^{+} \exp(-\alpha\,\Theta_1^{+}) \quad , \tag{3.57}$$

$$\frac{d^2\,\Phi_{S,0}^{+}}{d\zeta^2} = \frac{d^2\,\Phi_{R,1}^{+}}{d\zeta^2} = \frac{d^2\,\Theta_1^{+}}{d\zeta^2} - \frac{\tilde{q}_S\,\hat{\nu}}{Le_O}\frac{d^2\,\Phi_{O,1}^{+}}{d\zeta^2}$$

$$= \left(\frac{\hat{\nu}}{Le_O}\frac{d^2\,\Phi_{O,1}^{+}}{d\zeta^2} - \frac{1}{Le_S}\frac{d^2\,\Phi_{S,1}^{+}}{d\zeta^2}\right) + \left(\frac{\tilde{m}}{\tilde{r}_f^2} - \frac{2}{\tilde{r}_f\,Le_S}\right)\frac{d\,\Phi_{S,0}^{+}}{d\zeta} = 0 \quad , \tag{3.58}$$

$$\left(\frac{1}{Le_F}\frac{d^2\,\Phi_{F,2}^{+}}{d\zeta^2} - \frac{\tilde{\nu}_F}{Le_R}\frac{d^2\,\Phi_{R,2}^{+}}{d\zeta^2}\right) + \tilde{\nu}_F\left(\frac{\tilde{m}}{\tilde{r}_f^2} - \frac{2}{\tilde{r}_f\,Le_R}\right)\frac{d\,\Phi_{R,1}^{+}}{d\zeta} = 0 \quad , \tag{3.59}$$

$$\tilde{r}_f^2\left(\frac{d^2\,\Theta_2^{+}}{d\zeta^2} - \frac{\tilde{q}_S\,\hat{\nu}}{Le_O}\frac{d^2\,\Phi_{O,2}^{+}}{d\zeta^2}\right) - \tilde{m}\left(\frac{d\,\Theta_1^{+}}{d\zeta} - \tilde{q}_S\,\hat{\nu}\frac{d\,\Phi_{O,1}^{+}}{d\zeta}\right)$$

$$+ 2\tilde{r}_f\left(\frac{d\,\Theta_1^{+}}{d\zeta} - \frac{\tilde{q}_S\,\hat{\nu}}{Le_O}\frac{d\,\Phi_{O,1}^{+}}{d\zeta}\right) = 0 \quad , \tag{3.60}$$

$$\tilde{r}_f^2\left[\frac{\hat{\nu}}{Le_O}\frac{d^2\Phi_{O,2}^+}{d\zeta^2}-\frac{1}{Le_S}\frac{d^2\Phi_{S,2}^+}{d\zeta^2}-\frac{1}{Le_F}\frac{d^2\Phi_{F,2}^+}{d\zeta^2}\right]+\tilde{m}\left[\frac{d\Phi_{S,1}^+}{d\zeta}-\hat{\nu}\frac{d\Phi_{O,1}^+}{d\zeta}\right]$$

$$+2\tilde{r}_f\left[\frac{\hat{\nu}}{Le_O}\frac{d\Phi_{O,1}^+}{d\zeta}-\frac{1}{Le_S}\frac{d\Phi_{S,1}^+}{d\zeta}\right]-2\zeta\left[\frac{\tilde{m}}{\tilde{r}_f}-\frac{1}{Le_S}\right]\frac{d\Phi_{S,0}^+}{d\zeta}=0 \quad , \tag{3.61}$$

where

$$\Lambda_3=\delta^2 Le_O(\beta/\hat{\nu})Da_2\exp(-\alpha\tilde{E}_2/\tilde{T}_{f,0}) \tag{3.62}$$

is the reduced Damköhler number of the soot/precursor consumption reaction.

3.2.5 Matching of Solutions in the Outer and Soot Consumption Regions

Matching of the solutions in the soot consumption region with the outer solutions in the oxidizer side is performed by an approach similar to that described in Section 3.2.3 and illustrated in Eqs. (3.29)–(3.31) except that $\zeta\to\infty$. The process yields the solutions of leading order constants,

$$a_{T,0}^+=(\tilde{T}_{f,0}-\tilde{T}_\infty)/[1-\exp(-\tilde{m}/\tilde{r}_f)] \quad , \tag{3.63}$$

$$a_{O,0}^+=\tilde{Y}_{O,\infty}/[1-\exp(-Le_O\tilde{m}/\tilde{r}_f)] \quad , \tag{3.64}$$

$$a_{F,0}^+=a_{F,1}^+=a_{R,0}^+=0 \quad , \tag{3.65}$$

and the boundary conditions required to solve Eqs. (3.57)–(3.61),

$$\Phi_{O,1}^+(\zeta\to\infty)=-a_{O,1}^+\left[1-\exp\left(-\frac{Le_O\tilde{m}}{\tilde{r}_f}\right)\right]+a_{O,0}^+\frac{Le_O\tilde{m}}{\tilde{r}_f^2}\exp\left(-\frac{Le_O\tilde{m}}{\tilde{r}_f}\right)\zeta \quad , \tag{3.66a}$$

$$\Theta_1^+(\zeta\to\infty)=-a_{T,1}^+[1-\exp(-\tilde{m}/\tilde{r}_f)]+[a_{T,0}^+(\tilde{m}/\tilde{r}_f^2)\exp(-\tilde{m}/\tilde{r}_f)]\zeta \quad , \tag{3.67}$$

$$(d\Theta_2^+/d\zeta)_{\zeta\to\infty}=\{a_{T,1}^+-(a_{T,0}^+/\tilde{r}_f)[2-(\tilde{m}/\tilde{r}_f)]\zeta\}(\tilde{m}/\tilde{r}_f^2)\exp(-\tilde{m}/\tilde{r}_f) \quad , \tag{3.68}$$

$$(d\Phi_{F,2}^+/d\zeta)_{\zeta\to\infty}=0 \quad , \tag{3.69}$$

$$\left(\frac{d\Phi_{O,2}^+}{d\zeta}\right)_{\zeta\to\infty}=\left[a_{O,1}^+-\frac{a_{O,0}^+}{\tilde{r}_f}\left(2-\frac{Le_O\tilde{m}}{\tilde{r}_f}\right)\zeta\right]\frac{Le_O\tilde{m}}{\tilde{r}_f^2}\exp\left(-\frac{Le_O\tilde{m}}{\tilde{r}_f}\right) \quad , \tag{3.70}$$

$$\Phi_{R,1}^+(\zeta\to\infty)=a_{R,1}^+[1-\exp(-Le_R\tilde{m}/\tilde{r}_f)] \quad , \tag{3.71}$$

$$(d\Phi_{R,2}^+/d\zeta)_{\zeta\to\infty}=-a_{R,1}^+(Le_R\tilde{m}/\tilde{r}_f^2)\exp(-Le_R\tilde{m}/\tilde{r}_f) \quad , \tag{3.72}$$

$$\Phi_{S,0}^+(\zeta\to\infty)=a_{S,0}^+[1-\exp(-Le_S\tilde{m}/\tilde{r}_f)] \quad , \tag{3.73}$$

$$\Phi_{S,1}^+(\zeta\to\infty)=a_{S,1}^+[1-\exp(-Le_S\tilde{m}/\tilde{r}_f)] - a_{S,0}^+(Le_S\tilde{m}/\tilde{r}_f^2)\exp(-Le_S\tilde{m}/\tilde{r}_f)\zeta \quad , \tag{3.74}$$

$$\left(\frac{d\Phi_{S,2}^+}{d\zeta}\right)_{\zeta\to\infty}=-\left[a_{S,1}^+-\frac{a_{S,0}^+}{\tilde{r}_f}\left(2-\frac{Le_S\tilde{m}}{\tilde{r}_f}\right)\zeta\right]\frac{Le_S\tilde{m}}{\tilde{r}_f^2}\exp\left(-\frac{Le_S\tilde{m}}{\tilde{r}_f}\right) \quad . \tag{3.75}$$

Equation (3.66a) also implies

$$(d\Phi_{O,1}^+/d\zeta)_{\zeta\to\infty}=a_{O,0}^+(Le_O\tilde{m}/\tilde{r}_f^2)\exp(-Le_O\tilde{m}/\tilde{r}_f) \quad . \tag{3.66b}$$

Integrating the four expressions in Eq. (3.58) twice and Eqs. (3.59)–(3.61) once subject to the above matching conditions, Eqs. (3.66)–(3.75), we have

$$\Phi_{S,0}^+=a_{S,0}^+[1-\exp(-Le_S\tilde{m}/\tilde{r}_f)] \quad , \tag{3.76}$$

$$\Phi_{R,1}^+=a_{R,1}^+[1-\exp(-Le_R\tilde{m}/\tilde{r}_f)] \quad , \tag{3.77}$$

$$\Theta_1^+ - \tilde{q}_S\,\hat{v}\frac{\Phi_{O,1}^+}{Le_O} = a_{O,1}^+\frac{\tilde{q}_S\,\hat{v}}{Le_O}\left[1-\exp\left(-\frac{Le_O\,\tilde{m}}{\tilde{r}_f}\right)\right] - a_{T,1}^+\left[1-\exp\left(-\frac{\tilde{m}}{\tilde{r}_f}\right)\right]$$
$$+\frac{\tilde{m}}{\tilde{r}_f^2}\left[\frac{\tilde{T}_{f,0}-\tilde{T}_\infty}{\exp(\tilde{m}/\tilde{r}_f)-1} - \frac{\tilde{q}_S\,\hat{v}\tilde{Y}_{O,\infty}}{\exp(Le_O\,\tilde{m}/\tilde{r}_f)-1}\right]\zeta \quad , \tag{3.78}$$

$$\hat{v}\frac{\Phi_{O,1}^+}{Le_O} - \frac{\Phi_{S,1}^+}{Le_S} = -\frac{a_{O,1}^+\,\hat{v}}{Le_O}\left[1-\exp\left(-\frac{Le_O\,\tilde{m}}{\tilde{r}_f}\right)\right] - \frac{a_{S,1}^+}{Le_S}\left[1-\exp\left(-\frac{Le_S\,\tilde{m}}{\tilde{r}_f}\right)\right]$$
$$+\frac{\tilde{m}}{\tilde{r}_f^2}\left[\frac{\hat{v}\tilde{Y}_{O,\infty}}{\exp(Le_O\,\tilde{m}/\tilde{r}_f)-1} + a_{S,0}^+\exp\left(-\frac{Le_S\,\tilde{m}}{\tilde{r}_f}\right)\right]\zeta \quad , \tag{3.79}$$

$$\frac{1}{Le_F}\frac{d\Phi_{F,2}^+}{d\zeta} - \frac{\tilde{\nu}_F}{Le_R}\frac{d\Phi_{R,2}^+}{d\zeta} = a_{R,1}^+\,\tilde{\nu}_F\frac{\tilde{m}}{\tilde{r}_f^2}\exp\left(-\frac{Le_R\,\tilde{m}}{\tilde{r}_f}\right) \quad , \tag{3.80}$$

$$\frac{d\Theta_1^+}{d\zeta} - \frac{\tilde{q}_S\,\hat{v}}{Le_O}\frac{d\Phi_{O,1}^+}{d\zeta} = \frac{\tilde{m}}{\tilde{r}_f^2}\left[\frac{\tilde{T}_{f,0}-\tilde{T}_\infty}{\exp(\tilde{m}/\tilde{r}_f)-1} - \frac{\tilde{q}_S\,\hat{v}\tilde{Y}_{O,\infty}}{\exp(Le_O\,\tilde{m}/\tilde{r}_f)-1}\right] \quad , \tag{3.81}$$

$$\frac{\hat{v}}{Le_O}\frac{d\Phi_{O,1}^+}{d\zeta} - \frac{1}{Le_S}\frac{d\Phi_{S,1}^+}{d\zeta} = \frac{\tilde{m}}{\tilde{r}_f^2}\left[\frac{\hat{v}\tilde{Y}_{O,\infty}}{\exp(Le_O\,\tilde{m}/\tilde{r}_f)-1} + a_{S,0}^+\exp\left(-\frac{Le_S\,\tilde{m}}{\tilde{r}_f}\right)\right] \quad , \tag{3.82}$$

$$\tilde{r}_f^2[(d\Theta_2^+/d\zeta) - (\tilde{q}_S\,\hat{v}/Le_O)(d\Phi_{O,2}^+/d\zeta)] - \tilde{m}(\Theta_1^+ - \tilde{q}_S\,\hat{v}\Phi_{O,1}^+)$$
$$+(2\tilde{m}/\tilde{r}_f)[a_{T,0}^+\exp(-\tilde{m}/\tilde{r}_f) - a_{O,0}^+\tilde{q}_S\,\hat{v}\exp(-Le_O\tilde{m}/\tilde{r}_f)]\zeta$$
$$= \tilde{m}(a_{T,1}^+ - a_{O,1}^+\tilde{q}_S\,\hat{v}) \quad , \tag{3.83}$$

$$\tilde{r}_f^2[(\hat{v}/Le_O)(d\Phi_{O,2}^+/d\zeta) - (1/Le_S)(d\Phi_{S,2}^+/d\zeta) - (1/Le_F)(d\Phi_{F,2}^+/d\zeta)]$$
$$+(2\tilde{m}/\tilde{r}_f)[a_{S,0}^+\exp(-Le_S\tilde{m}/\tilde{r}_f) + a_{O,0}^+\hat{v}\exp(-Le_O\tilde{m}/\tilde{r}_f)]\zeta$$
$$= \tilde{m}[(a_{S,1}^+ + a_{O,1}^+\hat{v}) - (\Phi_{S,1}^+ - \hat{v}\Phi_{O,1}^+)] \quad . \tag{3.84}$$

In the above, Eqs. (3.81) and (3.82) are obtained by differentiating Eqs. (3.78)

and (3.79) with respect to ζ. These equations will be used later in the analysis.

3.2.6 Expansions in the Oxidation Region

In the $O(\varepsilon)$ oxidation region, the dominating reaction is the oxidation reaction (R1). The proper stretched coordinate in this region is $\tilde{r} = \tilde{r}_f + \varepsilon\xi$, where $\varepsilon = \tilde{T}_f^2 / \tilde{E}_1$, and the variables are expanded as:

$$\tilde{T} = \tilde{T}_f - \varepsilon\{[\theta_1 + \delta\theta_2 + O(\delta^2)] + O(\varepsilon/\delta)\} + O(\varepsilon^2) \quad , \tag{3.85}$$

$$\tilde{Y}_i = \varepsilon\{[\phi_{i,1} + \delta\phi_{i,2} + O(\delta^2)] + O(\varepsilon/\delta)\} + O(\varepsilon^2) \quad , \quad i = F, O \quad , \tag{3.86}$$

$$\tilde{Y}_R = [\delta\phi_{R,0} + O(\delta^2) + O(\varepsilon/\delta)] + \varepsilon[\phi_{R,1} + \delta\phi_{R,2} + O(\delta^2) + O(\varepsilon/\delta)] + O(\varepsilon^2) \quad , \tag{3.87}$$

$$\tilde{Y}_S = [\tilde{Y}_{S,0} + \delta\phi_{S,0} + O(\delta^2) + O(\varepsilon/\delta)] + \varepsilon[\phi_{S,1} + \delta\phi_{S,2} + O(\delta^2) + O(\varepsilon/\delta)] + O(\varepsilon^2) \quad , \tag{3.88}$$

where

$$\tilde{T}_f = \tilde{T}_{f,0} - \delta\tilde{T}_{f,1} + O(\delta^2) \quad . \tag{3.89}$$

Substituting Eqs. (3.85)–(3.88) into Eqs. (3.9)–(3.13), expanding and collecting terms of the same order in ε, we obtain

$$\frac{d^2\tilde{Y}_{S,0}}{d\zeta^2} = \frac{d^2\phi_{S,0}}{d\zeta^2} = \frac{d^2\phi_{R,0}}{d\zeta^2} = 0 \quad , \tag{3.90}$$

$$\frac{d^2\theta_1}{d\xi^2} - \frac{1}{Le_F}\frac{d^2\phi_{F,1}}{d\xi^2} = \frac{1}{Le_F}\frac{d^2\phi_{F,1}}{d\xi^2} - \frac{1}{Le_O}\frac{d^2\phi_{O,1}}{d\xi^2} = \frac{1}{Le_F}\frac{d^2\phi_{F,1}}{d\xi^2} + \frac{1}{Le_R}\frac{d^2\phi_{R,1}}{d\xi^2} = \frac{\tilde{r}_f^2}{Le_S}\frac{d^2\phi_{S,1}}{d\xi^2} - \left(\tilde{m} - \frac{2\tilde{r}_f}{Le_S}\right)\frac{d\tilde{Y}_{S,0}}{d\xi} = 0 \quad , \tag{3.91}$$

$$\frac{d^2\theta_2}{d\xi^2}-\frac{1}{Le_F}\frac{d^2\phi_{F,2}}{d\xi^2}=\frac{1}{Le_F}\frac{d^2\phi_{F,2}}{d\xi^2}+\frac{1}{Le_R}\frac{d^2\phi_{R,2}}{d\xi^2}+\frac{1}{\bar{r}_f}\left(\frac{2}{Le_R}-\frac{\bar{m}}{\bar{r}_f}\right)\frac{d\phi_{R,0}}{d\xi}$$

$$=\frac{1}{Le_F}\frac{d^2\phi_{F,2}}{d\xi^2}-\frac{1}{Le_O}\frac{d^2\phi_{O,2}}{d\xi^2}=\frac{1}{Le_S}\frac{d^2\phi_{S,2}}{d\xi^2}+\frac{1}{\bar{r}_f}\left(\frac{2}{Le_S}-\frac{\bar{m}}{\bar{r}_f}\right)\frac{d\phi_{S,0}}{d\xi}=0 \quad . \tag{3.92}$$

An additional equation that carries the reaction term can also be derived, but it will not be presented because it is not of interest to this study.

3.2.7 Matching of Solutions in the Oxidation, Soot Formation and Soot Consumption Regions

The required boundary conditions to solve Eqs. (3.90)–(3.92) are derived from matching the solutions in the oxidation region with those in the soot/precursor formation and consumption regions as $\xi \to \pm\infty$ and $\zeta \to 0$. Matching can be performed following the same procedure introduced in Section 2.2.7 so the details will not be repeated. Taking the fuel concentration as an example, by substituting Eq. (2.91) into Eqs. (3.21) and (3.55) with $i = F$, we have:

$$\begin{aligned}
\tilde{Y}_F^- &= [\delta\Phi_{F,1}^- + \delta^2\Phi_{F,2}^- + O(\delta^3)] + O(\varepsilon) \\
&= [\delta\Phi_{F,1}^-(\zeta=0) + O(\delta^2)] \\
&\quad + \varepsilon\{const + [(d\Phi_{F,1}^-/d\zeta)_{\zeta=0} + \delta(d\Phi_{F,2}^-/d\zeta)_{\zeta=0} + O(\delta^2)]\xi\} \\
&\quad + O(\varepsilon^2) + O(\varepsilon/\delta) \\
&= \varepsilon\{[\phi_{F,1} + \delta\phi_{F,2} + O(\delta^2)] + O(\varepsilon/\delta)\} + O(\varepsilon^2)\Big|_{\xi\to-\infty} \quad ,
\end{aligned} \tag{3.93}$$

$$\tilde{Y}_F^+ = [\delta^2 \Phi_{F,2}^+ + O(\delta^3)] + O(\varepsilon)$$

$$= O(\delta^2) + \varepsilon[const + \delta(d\Phi_{F,2}^+ / d\zeta)_{\zeta=0}\xi + O(\delta^2) + O(\varepsilon/\delta)] + O(\varepsilon^2)$$

$$= \varepsilon\{[\phi_{F,1} + \delta\phi_{F,2} + O(\delta^2)] + O(\varepsilon/\delta)\} + O(\varepsilon^2)\Big|_{\xi\to\infty} \quad . \tag{3.94}$$

Comparing terms of the same order in ε, Eqs. (3.93) and (3.94) provide

$$\Phi_{F,1}^-(\zeta = 0) = 0 \quad , \tag{3.95}$$

$$(d\phi_{F,j} / d\xi)_{\xi\to\pm\infty} = (d\Phi_{F,j}^{\pm} / d\zeta)_{\zeta=0} \quad , \quad j = 1, 2 \quad . \tag{3.96}$$

Application of the same matching procedure to other variables then gives:

$$\Phi_{O,1}^+(\zeta = 0) = 0 \quad , \tag{3.97}$$

$$\tilde{T}_{f,1} = \Theta_1^-(\zeta = 0) = \Theta_1^+(\zeta = 0) = -a_{T,1}^-[\exp(-\tilde{m}/\tilde{r}_f) - \exp(-\tilde{m})] \quad , \tag{3.98}$$

$$a_{T,1}^+\left[1 - \exp\left(-\frac{\tilde{m}}{\tilde{r}_f}\right)\right] - a_{O,1}^+\frac{\tilde{q}_S\,\hat{v}}{Le_O}\left[1 - \exp\left(-\frac{Le_O\tilde{m}}{\tilde{r}_f}\right)\right]$$

$$= a_{T,1}^-[\exp(-\tilde{m}/\tilde{r}_f) - \exp(-\tilde{m})] \quad , \tag{3.99}$$

$$\tilde{Y}_{S,0}(\xi \to -\infty) = a_{S,0}^-\exp(-Le_S\,\tilde{m}/\tilde{r}_f) \quad , \tag{3.100a}$$

$$\tilde{Y}_{S,0}(\xi \to \infty) = a_{S,0}^+\left[1 - \exp(-Le_S\,\tilde{m}/\tilde{r}_f)\right] \quad , \tag{3.100b}$$

$$\phi_{R,0}(\xi \to -\infty) = a_{R,1}^-\exp\left(-\frac{Le_R\,\tilde{m}}{\tilde{r}_f}\right) + \frac{a_{F,1}^-Le_R}{\tilde{v}_F Le_F}\exp\left(-\frac{Le_F\,\tilde{m}}{\tilde{r}_f}\right) \quad , \tag{3.101a}$$

$$\phi_{R,0}(\xi \to \infty) = a_{R,1}^+[1 - \exp(-Le_R\,\tilde{m}/\tilde{r}_f)] \quad , \tag{3.101b}$$

$$\phi_{S,0}(\xi \to -\infty) = a_{S,1}^-\exp\left(-\frac{Le_S\,\tilde{m}}{\tilde{r}_f}\right) - a_{F,1}^-\frac{Le_S}{Le_F}\exp\left(-\frac{Le_F\,\tilde{m}}{\tilde{r}_f}\right) \quad , \tag{3.102a}$$

$$\phi_{S,0}(\xi \to \infty) = a^{+}_{S,1}\left[1-\exp\left(-\frac{Le_S\,\tilde{m}}{\tilde{r}_f}\right)\right]+\frac{a^{+}_{O,1}\,\hat{\nu}Le_S}{Le_O}\left[1-\exp\left(-\frac{Le_O\,\tilde{m}}{\tilde{r}_f}\right)\right] \quad , \tag{3.102b}$$

$$(d\theta_j / d\xi)_{\xi\to\pm\infty} = (d\Theta^{\pm}_j / d\zeta)_{\zeta=0} \quad , \quad j=1,2 \quad , \tag{3.103}$$

$$(d\phi_{i,j} / d\xi)_{\xi\to\pm\infty} = (d\Phi^{\pm}_{i,j} / d\zeta)_{\zeta=0} \quad , \quad i=O,R,S; \quad j=1,2 \quad . \tag{3.104}$$

Equations (3.45)–(3.48) and (3.76)–(3.79) have been used in the derivation of Eqs. (3.98)–(3.102).

Integrating the three expressions in Eq. (3.90) twice and the four expressions in each of Eqs. (3.91) and (3.92) once subject to Eqs. (3.96), (3.100)–(3.104) yields

$$\tilde{Y}_{S,0} = \Phi^{-}_{S,0} = \Phi^{+}_{S,0} \quad , \tag{3.105}$$

$$\frac{a^{-}_{F,1}Le_R}{\tilde{\nu}_F Le_F}\exp\left(-\frac{Le_F\,\tilde{m}}{\tilde{r}_f}\right) = a^{+}_{R,1}\left[1-\exp\left(-\frac{Le_R\,\tilde{m}}{\tilde{r}_f}\right)\right]-a^{-}_{R,1}\exp\left(-\frac{Le_R\,\tilde{m}}{\tilde{r}_f}\right) \quad , \tag{3.106}$$

$$\frac{a^{-}_{F,1}Le_S}{Le_F}\exp\left(-\frac{Le_F\,\tilde{m}}{\tilde{r}_f}\right)+\frac{a^{+}_{O,1}\hat{\nu}Le_S}{Le_O}\left[1-\exp\left(-\frac{Le_O\,\tilde{m}}{\tilde{r}_f}\right)\right]$$
$$= a^{-}_{S,1}\exp\left(-\frac{Le_S\,\tilde{m}}{\tilde{r}_f}\right)-a^{+}_{S,1}\left[1-\exp\left(-\frac{Le_S\,\tilde{m}}{\tilde{r}_f}\right)\right] \quad , \tag{3.107}$$

$$(d\Phi^{-}_{S,1} / d\zeta)_{\zeta=0} = (d\Phi^{+}_{S,1} / d\zeta)_{\zeta=0} \quad , \tag{3.108}$$

$$(d\Theta^{+}_1 / d\zeta)_{\zeta=0} + Le_F^{-1}(d\Phi^{-}_{F,1} / d\zeta)_{\zeta=0} = -a^{-}_{T,0}(\tilde{m} / \tilde{r}_f^2)\exp(-\tilde{m} / \tilde{r}_f) \quad , \tag{3.109}$$

$$Le_F^{-1}(d\Phi^{-}_{F,1} / d\zeta)_{\zeta=0} + Le_O^{-1}(d\Phi^{+}_{O,1} / d\zeta)_{\zeta=0} = 0 \quad , \tag{3.110}$$

$$Le_F^{-1}(d\Phi_{F,1}^{-}/d\zeta)_{\zeta=0}+Le_R^{-1}(d\Phi_{R,1}^{-}/d\zeta)_{\zeta=0}=0 \quad , \tag{3.111}$$

$$(d\Theta_2^{-}/d\zeta)_{\zeta=0}-(d\Theta_2^{+}/d\zeta)_{\zeta=0}$$

$$=Le_F^{-1}[(d\Phi_{F,2}^{-}/d\zeta)_{\zeta=0}-(d\Phi_{F,2}^{+}/d\zeta)_{\zeta=0}] \quad , \tag{3.112}$$

$$Le_F^{-1}[(d\Phi_{F,2}^{-}/d\zeta)_{\zeta=0}-(d\Phi_{F,2}^{+}/d\zeta)_{\zeta=0}]$$

$$=Le_O^{-1}[(d\Phi_{O,2}^{-}/d\zeta)_{\zeta=0}-(d\Phi_{O,2}^{+}/d\zeta)_{\zeta=0}] \quad , \tag{3.113}$$

$$Le_F^{-1}[(d\Phi_{F,2}^{-}/d\zeta)_{\zeta=0}-(d\Phi_{F,2}^{+}/d\zeta)_{\zeta=0}]$$

$$=-Le_R^{-1}[(d\Phi_{R,2}^{-}/d\zeta)_{\zeta=0}-(d\Phi_{R,2}^{+}/d\zeta)_{\zeta=0}] \quad , \tag{3.114}$$

$$(d\Phi_{S,2}^{-}/d\zeta)_{\zeta=0}=(d\Phi_{S,2}^{+}/d\zeta)_{\zeta=0} \quad . \tag{3.115}$$

3.2.8 Completion of the Analysis

Finally, substituting Eqs. (3.35), (3.50), (3.51), (3.81), and (3.82) into Eqs. (3.108)–(3.111) and rearranging, we obtain

$$\frac{\tilde{T}_{f,0}-\tilde{T}_b}{1-\exp[\tilde{m}(\tilde{r}_f^{-1}-1)]}+\frac{\tilde{T}_{f,0}-\tilde{T}_\infty}{\exp(\tilde{m}/\tilde{r}_f)-1}=\frac{(1-\tilde{q}_S\,\hat{\nu})\overline{m}_F}{1+\tilde{\nu}_F}+\frac{\tilde{q}_S\,\hat{\nu}\tilde{Y}_{O,\infty}}{\exp(Le_O\,\tilde{m}/\tilde{r}_f)-1} \quad , \tag{3.116}$$

$$\tilde{Y}_{S,0}=\hat{\nu}\left[\nu^*\overline{m}_F-\frac{\tilde{Y}_{O,\infty}}{\exp(Le_O\,\tilde{m}/\tilde{r}_f)-1}\right]\left[1-\exp\left(-\frac{Le_S\,\tilde{m}}{\tilde{r}_f}\right)\right] \quad , \tag{3.117}$$

$$Le_F^{-1}(d\Phi_{F,1}^{-}/d\zeta)_{\zeta=0}=-\tilde{m}\,\overline{m}_F/[\tilde{r}_f^2(1+\tilde{\nu}_F)] \quad , \tag{3.118}$$

$$Le_O^{-1}(d\Phi_{O,1}^{+}/d\zeta)_{\zeta=0}=\tilde{m}\,\overline{m}_F/[\tilde{r}_f^2(1+\tilde{\nu}_F)] \quad . \tag{3.119}$$

Equations (3.116) and (3.117) are the ones that determine the leading order flame temperature, $\tilde{T}_{f,0}$, and soot/precursor concentration in the oxidation

region, $\tilde{Y}_{S,0}$, in terms of flame sheet location, $\tilde{r}_f$. The solution of $\tilde{Y}_{S,0}$ in turn can be applied to determine $a^{\pm}_{S,0}$ through Eqs. (3.45), (3.76) and (3.105). In addition, substitution of Eqs. (3.49), (3.52)–(3.53) and (3.80), (3.83)–(3.84) into Eqs. (3.112)–(3.115) and rearranging render

$$(1+\tilde{\nu}_F)[a^{-}_{T,1}\exp(-\tilde{m})+a^{+}_{T,1}-\tilde{q}_S\,\hat{\nu}a^{+}_{O,1}]=\tilde{\nu}_F(1-\tilde{q}_S\,\hat{\nu})a^{+}_{R,1} \quad , \tag{3.120}$$

$$\hat{\nu}a^{+}_{O,1}+a^{+}_{S,1}+(\nu^*-1)\hat{\nu}a^{+}_{R,1}=0 \quad . \tag{3.121}$$

3.2.9 Rescale of the Structure Equations for Numerical Computations

The two structure equations, Eq. (3.23) in the soot formation region and Eq. (3.57) in the soot consumption region, need to be solved numerically. Equation (3.23) with Θ^{-}_1 and $\Phi^{-}_{R,1}$ respectively given by Eqs. (3.46) and (3.47) is to be integrated subject to the four boundary conditions specified in Eqs. (3.33a, b), (3.95) and (3.118). Similarly, Eq. (3.57) with Θ^{+}_1 given by Eq. (3.78), and $\Phi^{+}_{S,0}$ given by Eqs. (3.105) and (3.117) can be solved subject to the four boundary conditions in Eqs. (3.66a, b), Eq. (3.97) and Eq. (3.119).

The numerical procedure can be simplified by a transformation of variables. The transformation of Eq. (3.23) is performed by defining the rescaled variable and parameter

$$\eta=(Le_F\,\overline{m}_F\,\tilde{m}/\tilde{r}_f^2)\zeta \quad , \tag{3.122}$$

$$\tilde{A}_2=(Da_2\,Le_R/\tilde{\nu}_F)(\tilde{T}_{f,0}^{\,2}/\tilde{E}_2)^3[\tilde{r}_f^2/(Le_F\,\overline{m}_F\,\tilde{m})]^2$$
$$\times\exp\{a^{-}_{T,1}[\exp(-\tilde{m}/\tilde{r}_f)-\exp(-\tilde{m})]-\tilde{E}_2/\tilde{T}_{f,0}\} \quad . \tag{3.123}$$

Substituting Eqs. (3.122) and (3.123) into Eqs. (3.46) and (3.47), we obtain

$$\Theta_1^- = -a_{T,1}^-[\exp(-\tilde{m}/\tilde{r}_f) - \exp(-\tilde{m})]$$

$$-\left[\frac{\tilde{T}_{f,0} - \tilde{T}_b}{Le_F \tilde{m}_F} \frac{\exp(-\tilde{m}/\tilde{r}_f)}{\exp(-\tilde{m}/\tilde{r}_f) - \exp(-\tilde{m})}\right]\eta \quad , \tag{3.124}$$

$$\Phi_{R,1}^- = a_{R,1}^+ [1 - \exp(-Le_R \tilde{m}/\tilde{r}_f)] + [Le_R/(\tilde{\nu}_F Le_F)](\Phi_{F,1}^- + \eta) \quad . \tag{3.125}$$

Subsequent substitution of Eqs. (3.122)–(3.125) into Eqs. (3.23), (3.33a, b), (3.95) and (3.118) then yields the transformed equation and boundary conditions, given by

$$\frac{d^2 \Phi_{F,1}^-}{d\eta^2} = \tilde{\Lambda}_2 \Phi_{F,1}^- \left\{ \frac{\tilde{\nu}_F Le_F}{Le_R} a_{R,1}^+ \left[1 - \exp\left(-\frac{Le_R \tilde{m}}{\tilde{r}_f} \right) \right] + \Phi_{F,1}^- + \eta \right\}$$

$$\times \exp\left\{ \frac{\tilde{T}_{f,0} - \tilde{T}_b}{Le_F \tilde{m}_F} \frac{\exp(-\tilde{m}/\tilde{r}_f)}{\exp(-\tilde{m}/\tilde{r}_f) - \exp(-\tilde{m})} \eta \right\} \quad , \tag{3.126}$$

$$\Phi_{F,1}^-(\eta = 0) = 0 \quad , \tag{3.127a}$$

$$(d\Phi_{F,1}^-/d\eta)_{\eta=0} = -1/(1 + \tilde{\nu}_F) \quad , \tag{3.127b}$$

$$\Phi_{F,1}^-(\eta \to -\infty) = \frac{\tilde{\nu}_F Le_F}{Le_R} \left\{ a_{R,1}^- \exp\left(-\frac{Le_R \tilde{m}}{\tilde{r}_f} \right) - a_{R,1}^+ \left[1 - \exp\left(-\frac{Le_R \tilde{m}}{\tilde{r}_f} \right) \right] \right\} - \eta \quad , \tag{3.128a}$$

$$(d\Phi_{F,1}^-/d\eta)_{\eta \to -\infty} = -1 \quad . \tag{3.128b}$$

Similarly, Eq. (3.57) can be transformed by defining

$$\eta = \{\tilde{Y}_{O,\infty} Le_O (\tilde{m}/\tilde{r}_f^2)/[\exp(Le_O \tilde{m}/\tilde{r}_f) - 1]\}\zeta \quad , \tag{3.129}$$

$$\tilde{\Lambda}_3 = \frac{\beta\, Da_2}{Le_O\, \hat{\nu}}\, a^+_{S,0}\left[1-\exp\left(-\frac{Le_S\,\tilde{m}}{\tilde{r}_f}\right)\right]\left[\frac{\exp(Le_O\,\tilde{m}/\tilde{r}_f)-1}{\tilde{Y}_{O,\infty}\,\tilde{m}/\tilde{r}_f^2}\,\frac{\tilde{T}_{f,0}^{\,2}}{\tilde{E}_2}\right]^2$$

$$\times\exp\left\{a_{\tilde{T},1}^{-}\,\alpha\left[\exp\left(-\frac{\tilde{m}}{\tilde{r}_f}\right)-\exp(-\tilde{m})\right]-\alpha\frac{\tilde{E}_2}{\tilde{T}_{f,0}}\right\} \quad , \tag{3.130}$$

and substituting into Eqs. (3.78) and (3.99) to yield

$$\Theta_1^+ = -a_{\tilde{T},1}^{-}\left[\exp\left(-\frac{\tilde{m}}{\tilde{r}_f}\right)-\exp(-\tilde{m})\right]+\tilde{q}_S\,\hat{\nu}\frac{\Phi_{O,1}^+}{Le_O}$$

$$+\left[\frac{\tilde{T}_{f,0}-\tilde{T}_\infty}{\tilde{Y}_{O,\infty}\,Le_O}\,\frac{\exp(Le_O\,\tilde{m}/\tilde{r}_f)-1}{\exp(\tilde{m}/\tilde{r}_f)-1}-\frac{\tilde{q}_S\,\hat{\nu}}{Le_O}\right]\eta \quad . \tag{3.131}$$

As the last step, Eq. (3.105), (3.117), (3.129)–(3.131) are substituted into Eqs. (3.57), (3.66a, b), (3.97), and (3.119), which results in

$$(d^2\,\Phi_{O,1}^+/d\,\eta^2) = \tilde{\Lambda}_3\,\Phi_{O,1}^+\exp(-\alpha\tilde{q}_S\,\hat{\nu}\,\Phi_{O,1}^+/Le_O)$$

$$\times\exp\left\{-\alpha\left[\frac{\tilde{T}_{f,0}-\tilde{T}_\infty}{\tilde{Y}_{O,\infty}\,Le_O}\,\frac{\exp(Le_O\,\tilde{m}/\tilde{r}_f)-1}{\exp(\tilde{m}/\tilde{r}_f)-1}-\frac{\tilde{q}_S\,\hat{\nu}}{Le_O}\right]\eta\right\} \quad , \tag{3.132}$$

$$\Phi_{O,1}^+(\eta=0)=0 \quad , \tag{3.133a}$$

$$(d\,\Phi_{O,1}^+/d\,\eta)_{\eta=0} = \{\,\bar{m}_F/[\tilde{Y}_{O,\infty}(1+\bar{\nu}_F)]\,\}[\exp(Le_O\,\tilde{m}/\tilde{r}_f)-1] \quad , \tag{3.133b}$$

$$\Phi_{O,1}^+(\eta\to\infty) = -a_{O,1}^+\,[1-\exp(-Le_O\,\tilde{m}/\tilde{r}_f)]+\eta \quad , \tag{3.134a}$$

$$(d\,\Phi_{O,1}^+/d\,\eta)_{\eta\to\infty}=1 \quad . \tag{3.134b}$$

3.2.10 Summary of the Analytical Results

The analysis is now completed and the primary result is summarized as follows. For any specified state, Eq. (3.132) can first be integrated numerically subject to the four boundary conditions given by (3.133a, b) and (3.134a, b). It is then followed by the numerical integration of Eq. (3.126) subject to the four boundary conditions given by Eqs. (3.127a, b) and (3.128a, b). Since only two boundary conditions are required to solve each of these two second order differential equations, there are four extra conditions. These four conditions, along with Eqs. (3.99), (3.106), (3.107), (3.120) and (3.121) are applied to determine the flame sheet location, $\tilde{r}_f$, and the eight undetermined constants, $a^{\pm}_{\tilde{T},1}$, $a^{-}_{F,1}$, $a^{+}_{O,1}$, $a^{\pm}_{R,1}$ and $a^{\pm}_{S,1}$. By applying these results, $a^{\pm}_{S,0}$ can be determined from Eqs. (3.45), (3.76), (3.105) and (3.117) while the flame temperature, $\tilde{T}_f$, can be determined from Eqs. (3.89), (3.98) and (3.116).

The soot/precursor concentration at the boundary between the soot/precursor formation region and the inert region at the fuel side of the reaction regions can be obtained from Eq. (3.19a) as

$$\tilde{Y}^{-}_{S}(\tilde{r}_f) = (a^{-}_{S,0} + \delta a^{-}_{S,1})\exp(-Le_S \tilde{m} / \tilde{r}_f) + \ldots \quad . \tag{3.135}$$

This quantity is represented by a soot/precursor indicator, S_I. Similarly, the soot/precursor concentration at the boundary between the soot/precursor consumption region and the inert region at the oxidizer side of the reaction regions, which represents the amount of soot/precursor that breaks through the reaction zones into the oxidizer side, is given by Eq. (3.19b) as

$$\tilde{Y}^{+}_{S}(\tilde{r}_f) = (a^{+}_{S,0} + \delta a^{+}_{S,1})[1 - \exp(-Le_S \tilde{m} / \tilde{r}_f)] + \ldots \quad . \tag{3.136}$$

This quantity is expressed by a soot/precursor break-through parameter, S_B.

In the limiting case of extremely slow soot/precursor consumption reaction, the rate of the consumption reaction is considered an order of magnitude slower than that of the soot/precursor formation reaction so that $\beta = O(\delta)$. For this case Eq. (3.132) can be integrated subject to Eqs. (3.133a, b) to yield

$$\Phi^{+}_{O,1} = \{\overline{m}_F / [\tilde{Y}_{O,\infty}(1+\tilde{\nu}_F)]\}[\exp(Le_O \tilde{m} / \tilde{r}_f) - 1]\eta \quad . \tag{3.137}$$

Subsequent application of Eqs. (3.134a, b) into Eq. (3.137) results in $a^{+}_{O,1} = 0$ and

$$\tilde{r}_f = Le_O \tilde{m} / \ln\left[1 + \tilde{Y}_{O,\infty}(1+\tilde{\nu}_F) / \overline{m}_F\right] \tag{3.138}$$

such that the flame location is explicitly determined. This in turn can be substituted into Eq. (3.116) to provide the solution of $\tilde{T}_{f,0}$. Equation (3.126) still need to be solved numerically subject to the four boundary conditions in Eqs. (3.127a, b) and (3.128a, b), with two of which applied to determine $a^{\pm}_{T,1}$, $a^{-}_{F,1}$, $a^{\pm}_{R,1}$ and $a^{\pm}_{S,1}$ together with Eqs. (3.99), (3.106), (3.107), (3.120) and (3.121).

Similar to the discussion in Chapter 2, it is noted that although the present analysis can be completed without requiring knowledge of flame extinction, the analysis is based on the assumed existence of a diffusion flame. The analysis is applicable only for a diffusion flame in Liñán's (1974) diffusion flame regime and sufficiently far away from the extinction limit.

3.3 Results and Discussions

To exhibit the characteristics of various flame responses, numerical calculations are performed by adopting the same physically based thermo-chemical data used in Chapter 2, so that the results obtained in these chapters can be compared with one another. An additional property required in the study of the spherical diffusion flame, namely the thermal conductivity of the gas, is given by $\lambda = 6.28 \times 10^{-5}$ cal/cm·K·s. The spherical porous burner is considered to be a 1/4 inch burner such that $r_b = 3.175$ mm. This is the size used in the experiments performed and to be performed by our collaborators at Washington University, St. Louis and NASA Glenn Center. The fuel flow rate is taken to be 1.51 mg/s, which is also the value used in the experiments, except when the effect of mass flow rate is discussed. The study will cover the two limiting cases discussed in Chapter 2 and the effects of the same parameters will be addressed. The differences between the two limiting cases are shown schematically in Fig. 3.1.

For the fuel/air flame shown in Fig. 3.1 (a), pure fuel is supplied from the burner and issued into the air. The reaction regions for this flame, including the oxidation region, the soot formation region and the soot consumption region, are located relatively far away from the burner due to the relatively low initial oxidizer concentration compared to that of the fuel. As to the diluted-fuel/oxygen flame shown in Fig. 3.1 (b), the inert gas in the air is extracted and diverted into the fuel stream while maintaining the same fuel flow rate so that the mass flow rate issued from the burner is significantly increased. This inert gas redistribution yields a reduction of the initial fuel concentration and an increase in the initial oxidizer concentration.

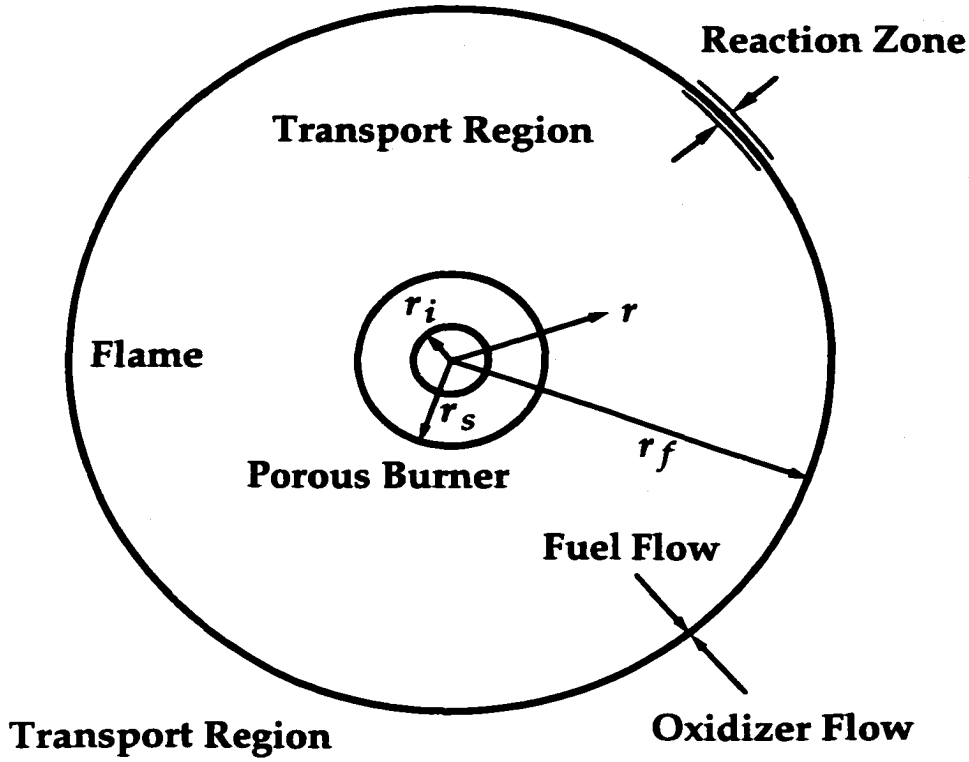

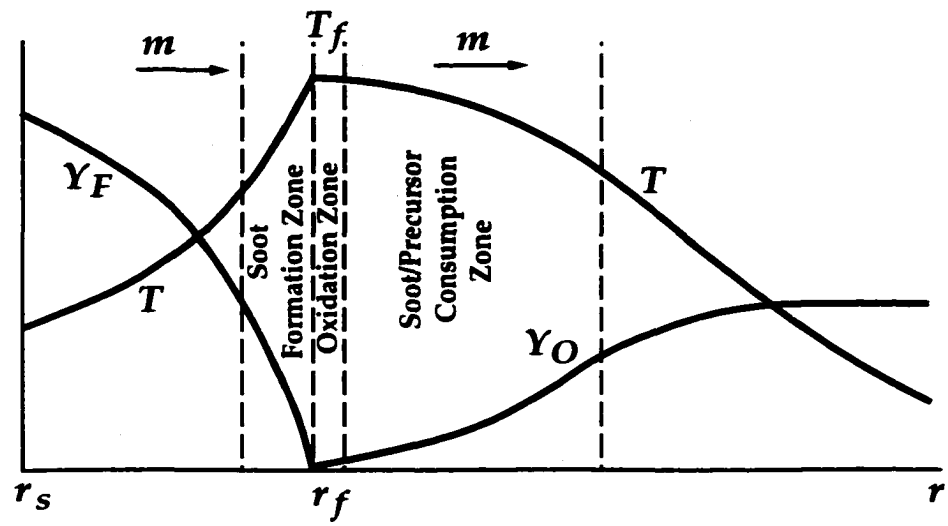

Figure 3.1(a) Schematic diagram of the flame structure for fuel/air flame in the spherical diffusion flame stabilized by a spherical porous burner with the fuel supplied from the burner

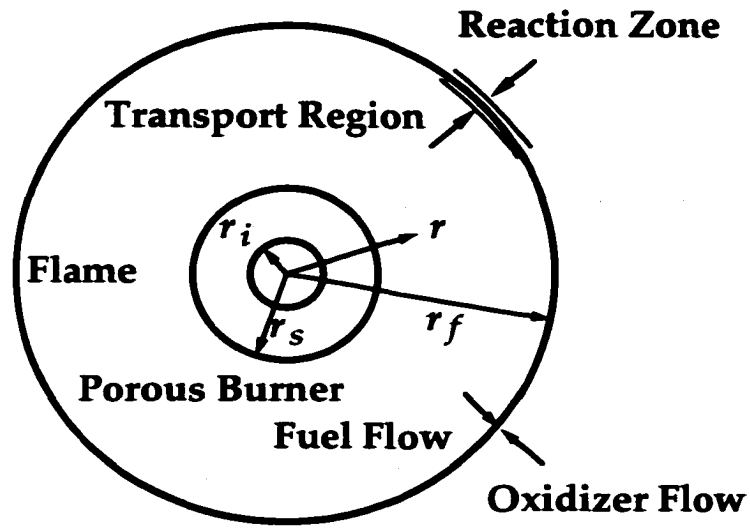

Transport Region

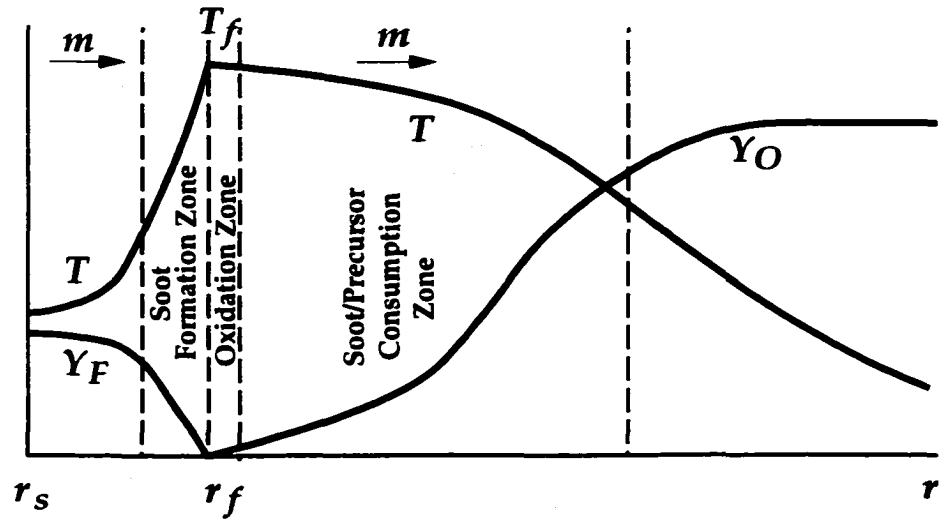

Figure 3.1(b) Schematic diagram of the flame structure for diluted-fuel/oxygen flame in the spherical diffusion flame stabilized by a spherical porous burner with the fuel supplied from the burner

Consequently the reaction regions are much closer to the burner due to the low initial fuel concentration as compared to that of the oxidizer. The variation in the mass flow rate results in a higher temperature gradient for the fuel/air flame near the burner exit so that the resulting heat transfer from the flame to the burner is higher. Since the burner is considered to be cooled, its temperature is a constant and all the heat transferred to the burner is removed by the coolant. It is then expected that the fuel/air flame possesses a lower flame temperature. Moreover, the temperature gradient for the diluted-fuel/oxygen flame is much steeper near the boundary between the reaction regions and the transport region at the fuel side, and meanwhile is flatter near the boundary between the reaction regions and the transport region at the oxidizer side, as shown in Fig. 3.1.

Because both the soot formation and consumption reactions are high activation energy reactions, they occur only at high temperatures. The temperature distribution discussed in the previous paragraph yields a thicker soot/precursor formation region and a thinner soot/precursor consumption region for the fuel/air flame. As a result the production of soot/precursor is favored. On the other hand, the lower flame temperature for this flame yields a slower soot/precursor production. Since there are two opposing mechanisms, namely the residence time (thickness of the reaction regions) and the reaction rate (flame temperature), compete for dominance, it is not clear how the inert redistribution affects soot/precursor production *a priori*.

For the fuel/air flame, we have $Y_{F,0} = 1$, $Y_{O,\infty} = 0.233$, and $\tilde{m} = 1.6485$. Figure 3.2 presents the variation of soot/precursor indicator, S_I, as a function of the Damköhler number of the soot/precursor formation reaction, Da_2,

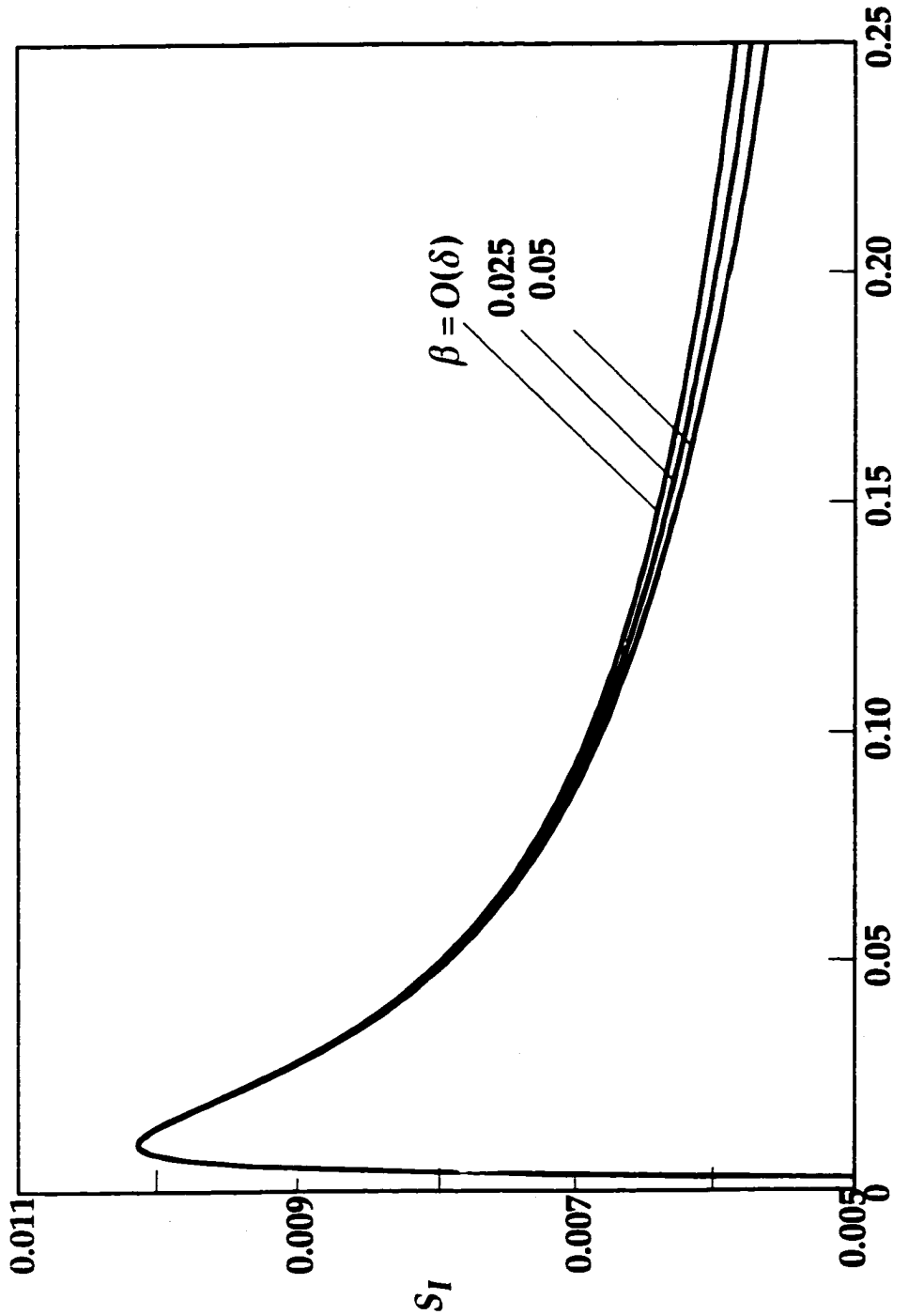

Figure 3.2 Variation of S_I with Da_2 for the fuel/air flame with $\alpha = Le_R = Le_S = 1$ and selected values of β

for selected values of β and $\alpha = Le_R = Le_S = 1$. As in Chapter 2, unity Lewis numbers are used as reference values to facilitate the discussion of results. The corresponding flame temperature, $\tilde{T}_f$, and the flame sheet location, $\tilde{r}_f$, are presented in Figs. 3.3 and 3.4, respectively. The curve for $\beta = O(\delta)$ in these figures represents the limiting case of an extremely slow soot/precursor oxidation reaction. For the problem analyzed in this chapter, the variation of Da_2 is caused solely by the variation of the pre-exponential factor B, or the reaction rate.

It is shown in Fig. 3.2 that by increasing Da_2 from an initial small value, S_I first increases, attains a maximum value, and then decreases. Although this behavior is similar to that of the counterflow flame, the interpretation is different because the variation of Da_2 is caused by the change of reaction rate, not strain rate. There are two opposing processes responsible for the value of S_I when the rate of the soot formation reaction increases. First, it is natural to expect that more soot/precursor is produced when Da_2 is increased, thus S_I is higher since the production rate is increased. However, such an increase leads to a higher consumption of the radical in the soot formation region and a reduction in the radical concentration at the boundary between the soot formation region and the fuel side transport region. This leads to a reduction in the soot/precursor production at this location. For values of Da_2 lower than the critical value that yields the maximum S_I, the radical concentration is so high that the reduction of reactant concentration is less important. The soot/precursor production is then dominated by the reaction rate, and S_I increases with increasing Da_2. After the maximum S_I is reached, the reaction rate is sufficiently high so that the rate of soot/precursor formation is

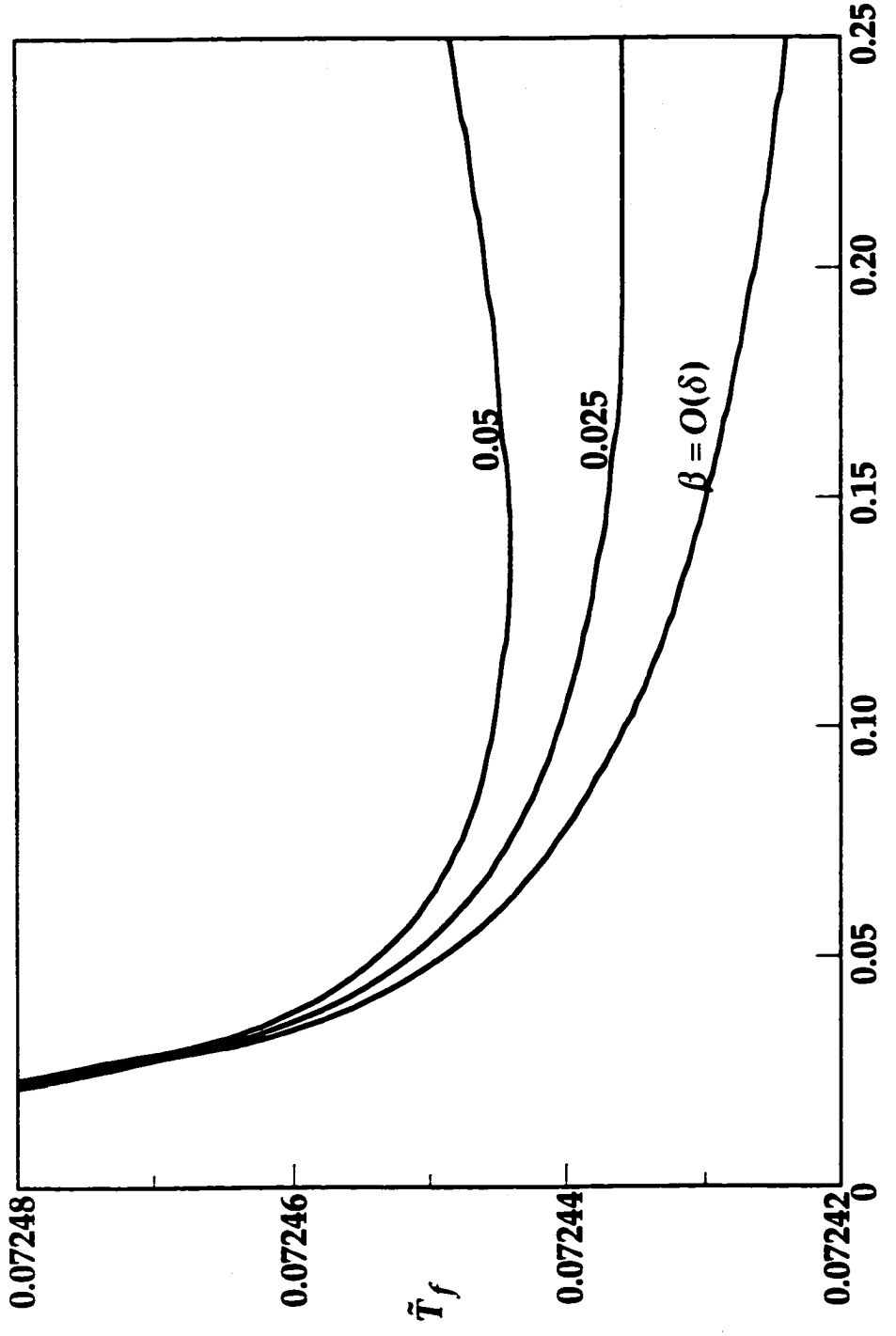

Figure 3.3 The flame temperature $\tilde{T}_f$ corresponding to Fig. 3.2

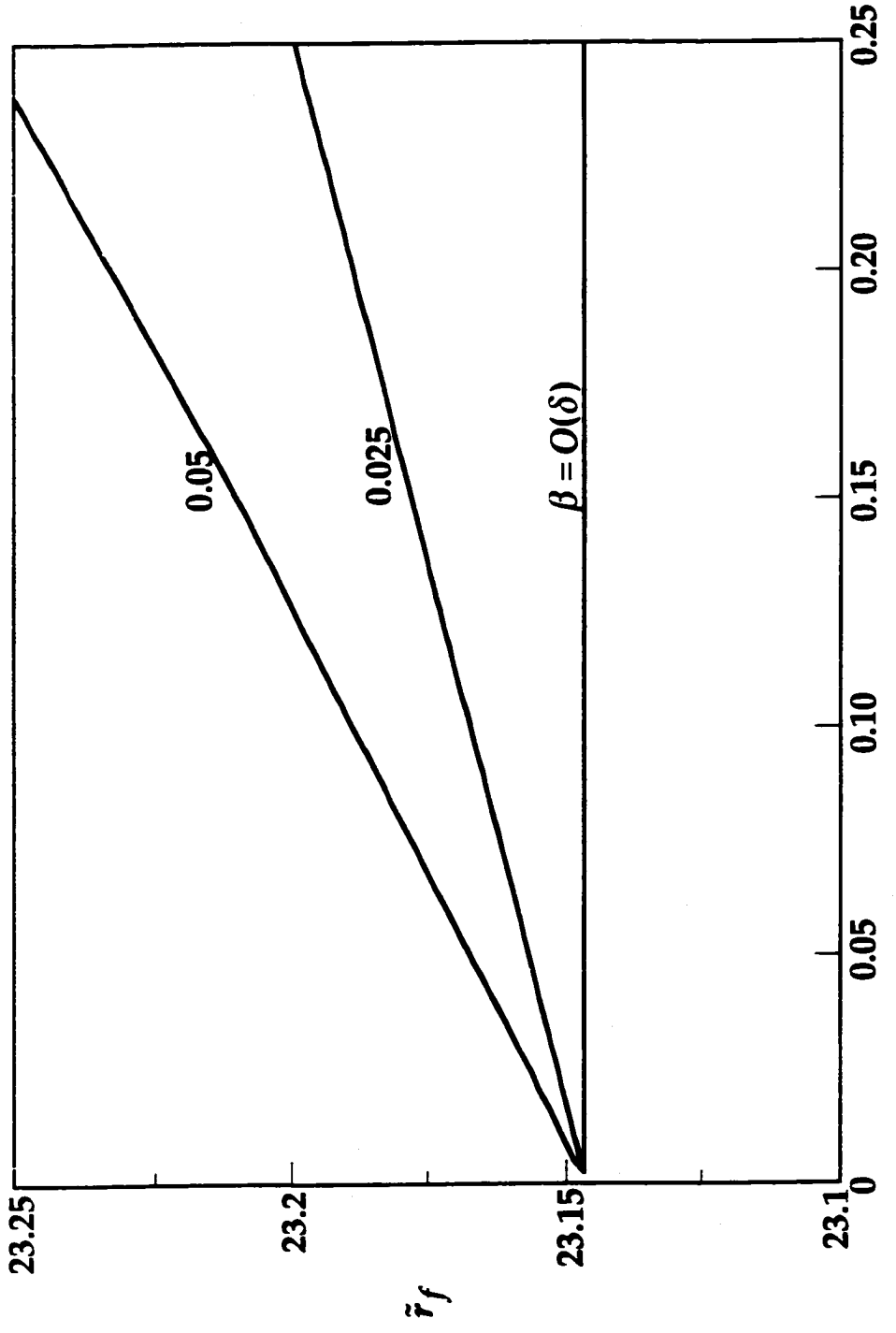

Figure 3.4 The flame sheet location $\tilde{r}_f$ corresponding to Fig. 3.2

controlled by the availability of the radical, and S_I decreases with increasing Da_2. This explanation is also applicable to the counterflow flame when the variation of Da_2 is due to the change of reaction rate instead of the strain rate. With the increase of β, the soot consumption reaction occurs at an accelerated rate such that S_I decreases. For extremely small values of Da_2, the value of S_I becomes negative, which is physically unrealistic and hence the analysis is not applicable. This is consistent with our earlier statement on the limitation of Da_2.

Because S_I only represents the concentration of soot/precursor at the boundary between the soot formation region and the fuel side transport region, it is misleading to consider it as the indicator to quantify the total soot/precursor produced from the flame. As discussed in Chapter 2, a more instrumental parameter to represent the total amount of soot/precursor produced is the flame temperature. When Da_2 is increased, the rate of both the soot/precursor formation and consumption reactions are increased. For the limiting case of $\beta = O(\delta)$, the consumption reaction is extremely weak so that a higher amount of soot/precursor is produced. Existence of a larger amount of soot/precursor then yields a lower flame temperature because a higher portion of chemical energy stored in the soot/precursor is not released to thermal energy. The decrease in flame temperature then slows down the soot/precursor formation reaction so that the rate of increase in the formation of soot/precursor with Da_2 is reduced. This result is supported by Fig. 3.3, which shows that the flame temperature decreases with increasing Da_2, indicating a higher soot/precursor production with a larger Da_2, and the rate of temperature decrease is slower for higher Da_2, indicating a slower

increase in the soot/precursor production.

Figures 3.2 and 3.3 also show the effect of β, which represents the rate of the soot/precursor consumption reaction, on the overall production of soot/precursor. For small values of Da_2, the effect of β is insignificant because of the low reaction rates. For higher values of Da_2, a larger amount of soot/precursor is produced and the effect of soot/precursor consumption rate emerges. That is, by increasing β for a fixed Da_2, more soot/precursor is oxidized and more heat is generated through this consumption reaction. Consequently the concentration of soot/precursor is decreased as shown in Fig. 3.2, meanwhile the flame temperature is increased as shown in Fig. 3.3. When Da_2 is sufficiently high, the soot/precursor formation reaction rate increases only slightly with Da_2 as shown in the $\beta = O(\delta)$ curve and discussed in the previous paragraph. For this case, an increase of Da_2 results in a higher increase in the rate of soot/precursor consumption than that of the formation such that the total soot/precursor production actually decreases and the flame temperature increases. Indeed Fig. 3.3 demonstrates that for $\beta = 0.05$, there exists a critical value of Da_2 above which $\tilde{T}_f$ increases with Da_2. For $\beta = 0.025$, such a turning point also exists, but at a much larger Da_2 value beyond the region plotted in this figure.

Figure 3.4 displays the flame sheet location $\tilde{r}_f$ as a function of Da_2. This figure shows that $\tilde{r}_f$ is independent of Da_2 when β is O(δ), and increases with Da_2 for *non-zero* values of β. $\tilde{r}_f$ also increases with β for a given Da_2. Because the radical is considered an O(δ) quantity, the soot/precursor formation reaction consumes only an O(δ) amount of the fuel and causes a negligible shift in $\tilde{r}_f$. For *non-zero* values of β, the soot/precursor

consumption reaction yields an O(1) oxidation of soot/precursor and accompanies this with an O(1) consumption of the oxidizer. The loss of oxidizer supply in the primary oxidation region through the soot/precursor oxidation reaction then forces the flame to move towards the oxidizer side to seek a new stoichiometric balance. For larger values of β or Da_2, the soot/precursor consumption reaction is stronger and more oxidizer is consumed so that $\tilde{r}_f$ is larger.

For the flame studies in this chapter, the flow direction is from the burner to the ambient such that the convection is from the fuel side to the oxidizer side. Thus the soot/precursor produced in the formation region is driven by the bulk flow to the soot consumption region before entering the ambient and appearing as part of the combustion products. This suggests that the soot/precursor break-through parameter, S_B, which represents the amount of soot/precursor that breaks through the oxidation and soot consumption regions and enters the transport region at the oxidizer side, is more appropriate in describing the soot/precursor concentration in the products, or the bulk soot/precursor production. The variation of S_B corresponding to Figs. 3.2–3.4 is then plotted versus Da_2 in Fig. 3.5.

It is observed from Fig. 3.5 that for the case of an extremely slow soot consumption reaction, $\beta = O(\delta)$, S_B increases with increasing Da_2 and the rate of S_B growth decreases with Da_2. This agrees with the earlier observation on the total amount of soot production, the flame temperature reduction and the application of the flame temperature to quantify the soot/precursor production. When the rate of the soot/precursor consumption reaction is higher, S_B decreases with increasing β. For $\beta = 0.05$, there exists a critical Da_2

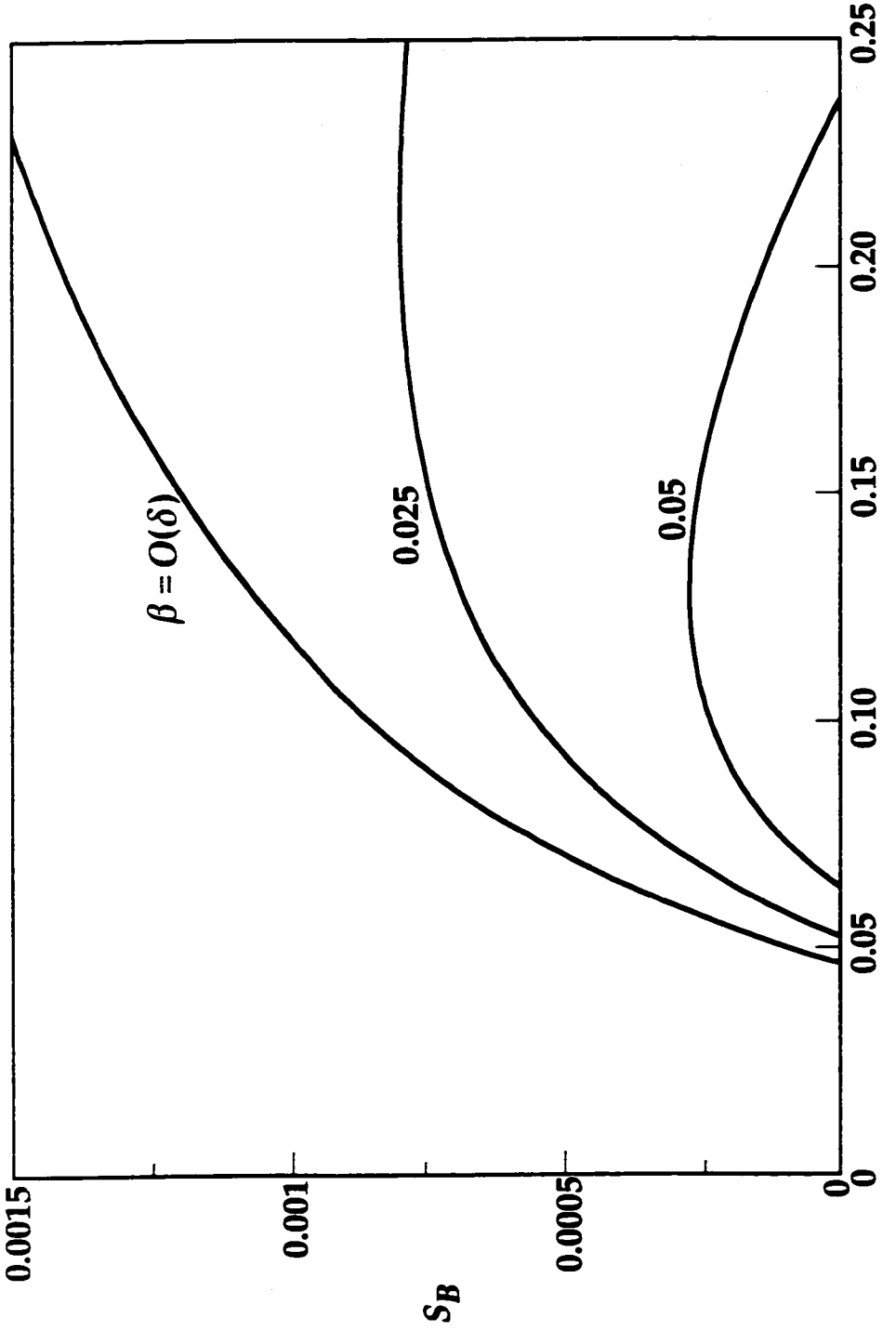

Figure 3.5 Variation of S_B corresponding to Fig. 3.2

at which S_B attains its maximum. These results also are in agreement with our earlier discussion on Fig. 3.3. When Da_2 or β is sufficiently large, S_B is reduced to zero so that the production of soot/precursor is completely suppressed because of the strong soot/precursor consumption reaction, as shown in Fig. 3.5 for $\beta = 0.05$.

The effect of diffusion transport on soot/precursor production will be discussed by varying the Lewis number of either the radical or the soot/precursor while keeping the other unity. The flame response corresponding to the change in radical diffusion, Le_R, is first presented in Figs. 3.6–3.8 by plotting S_I, S_B and $\tilde{T}_f$ versus Da_2 with $\alpha = Le_S = 1$, $\beta = O(\delta)$. Recognizing that the impact of Le_R on the flame behavior is qualitatively similar for all values of β since the radical does not participate in the soot/precursor consumption reaction, the special case of $\beta = O(\delta)$ is selected for simplicity in numerical computations. Since the radical (*e.g.*, H) is generally light in weight, its diffusion rate is higher than that of the background gas so that only the $Le_R < 1$ case is considered. These figures show that the sooting behavior responding to the variation of Le_R is qualitatively similar to that of the counterflow flame. That is, the total amount of soot produced decreases with decreasing Le_R because the radical passes through the soot formation region into the inert region at a faster rate and this reduces the residence time that needed for the soot/precursor formation reaction to occur. A more detailed discussion has already been presented in Chapter 2 and will not be repeated.

This discussion is followed by the effect of soot/precursor diffusion, Le_S. The results are presented in Figs. 3.9–3.11 following the same sequence as

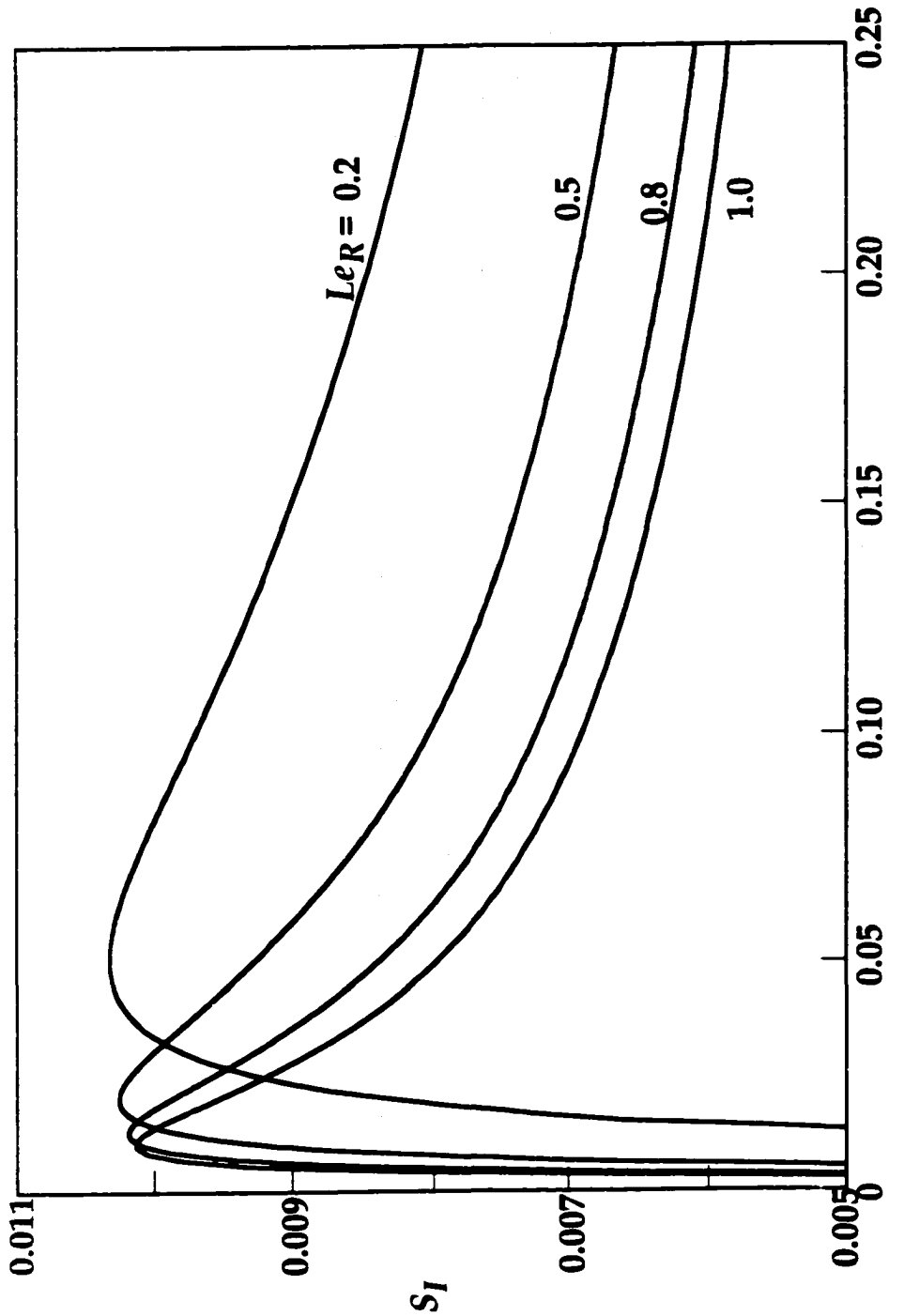

Figure 3.6 Variation of S_I with Da_2 for the fuel/air flame with $\alpha = Le_S = 1, \beta = O(\delta)$, and selected values of Le_R

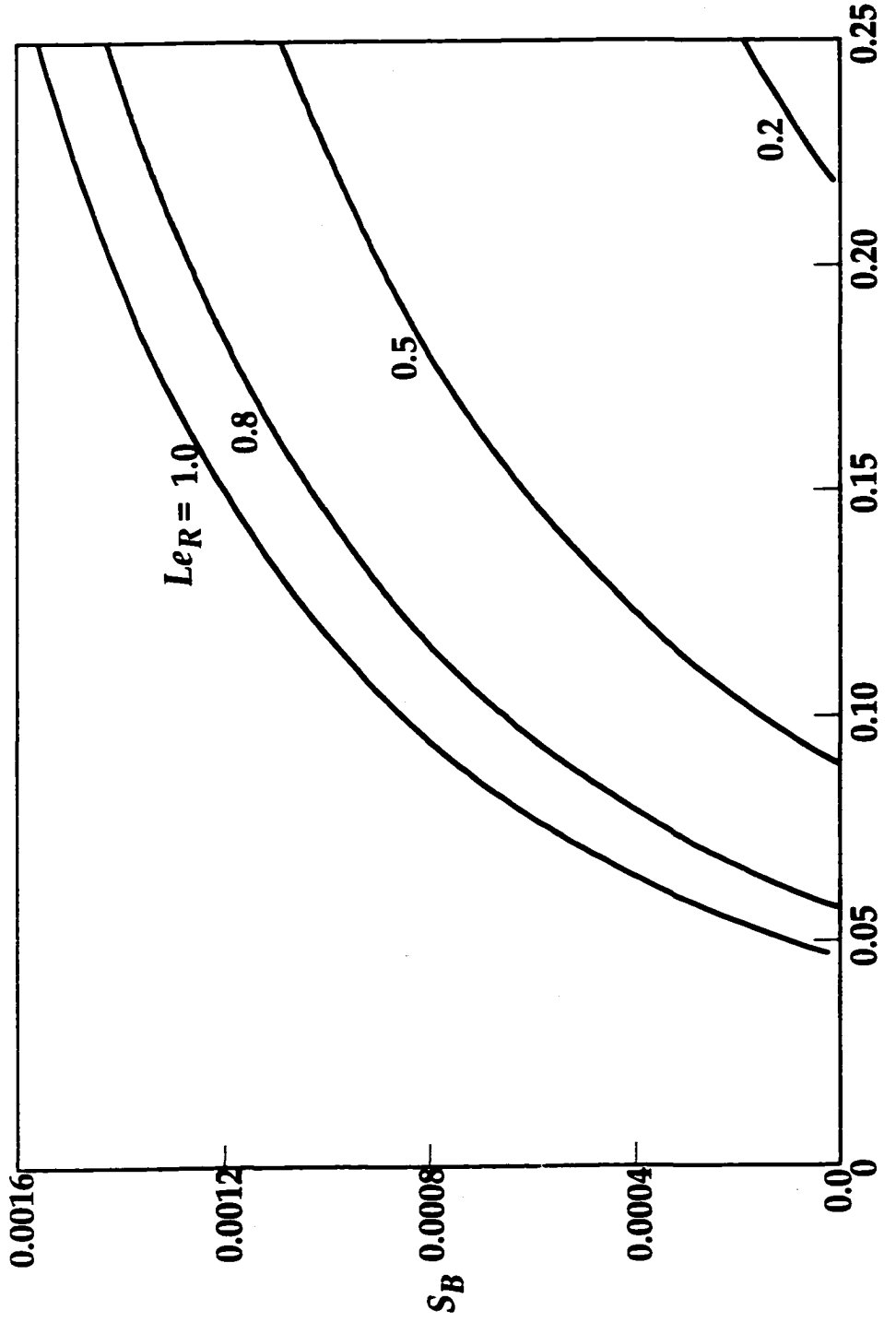

Figure 3.7 Variation of S_B corresponding to Fig. 3.6

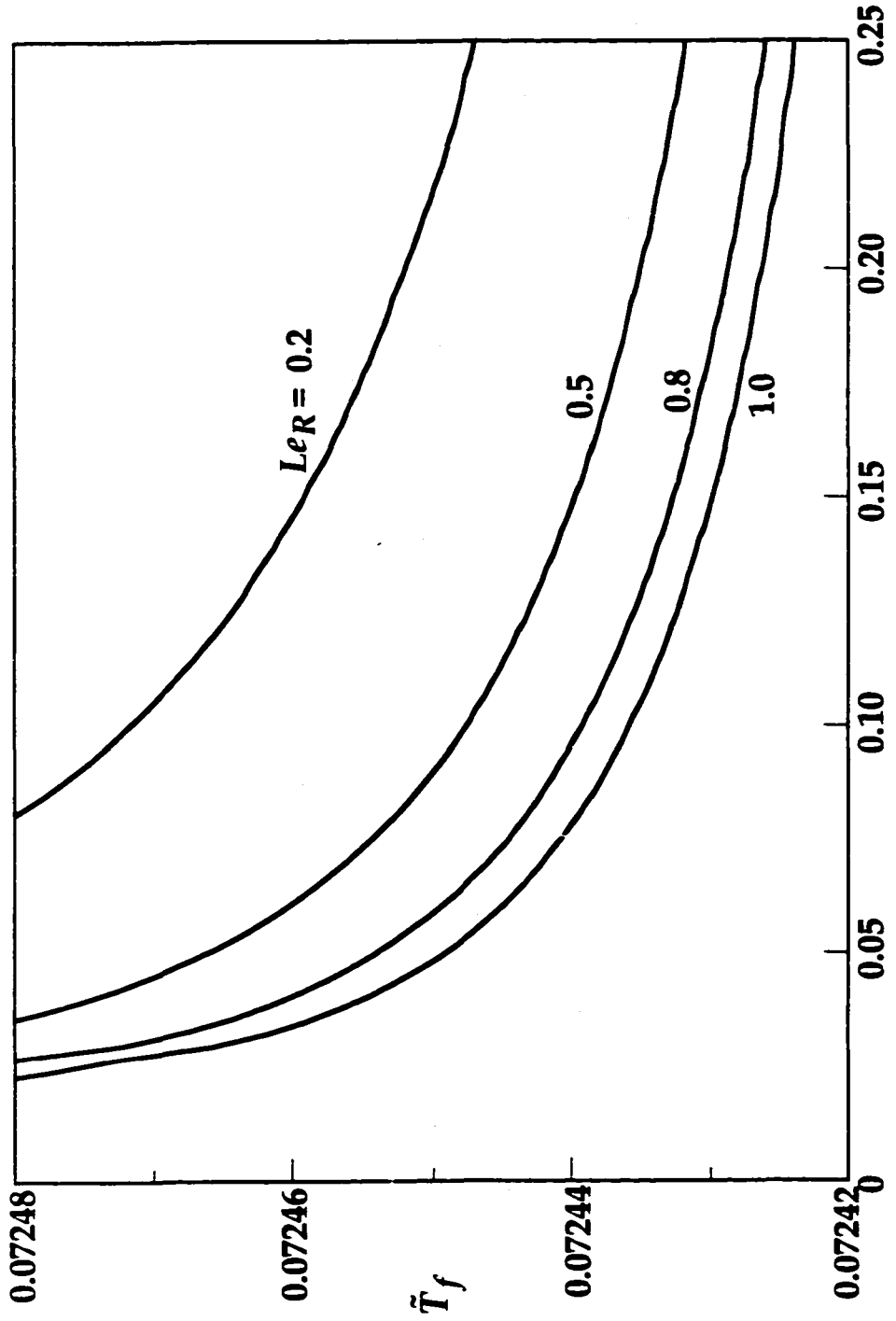

Figure 3.8 The flame temperature $\tilde{T}_f$ corresponding to Fig. 3.6

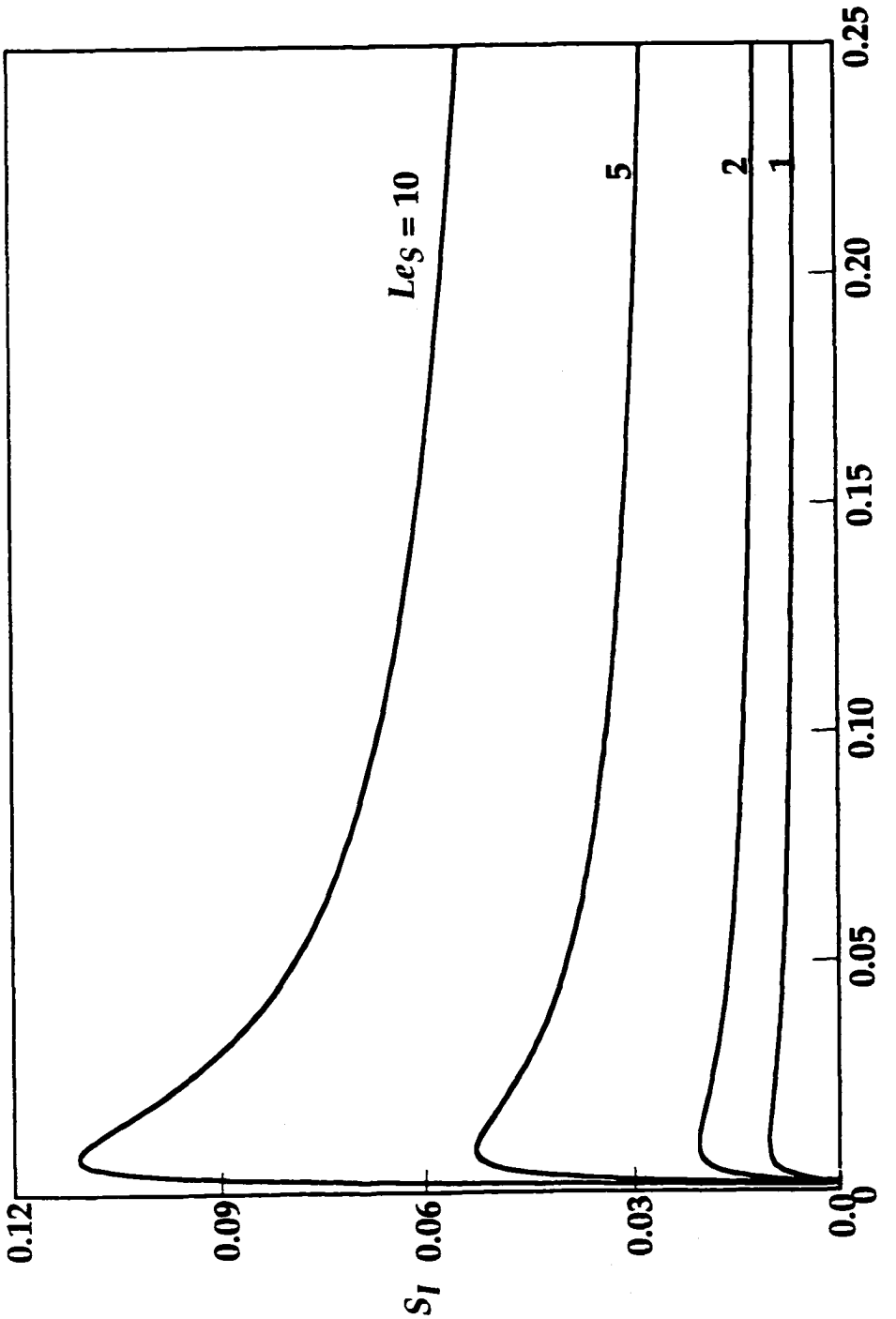

Figure 3.9 Variation of S_I with Da_2 for the fuel/air flame with $\alpha = Le_R = 1, \beta = O(\delta)$, and selected values of Le_S

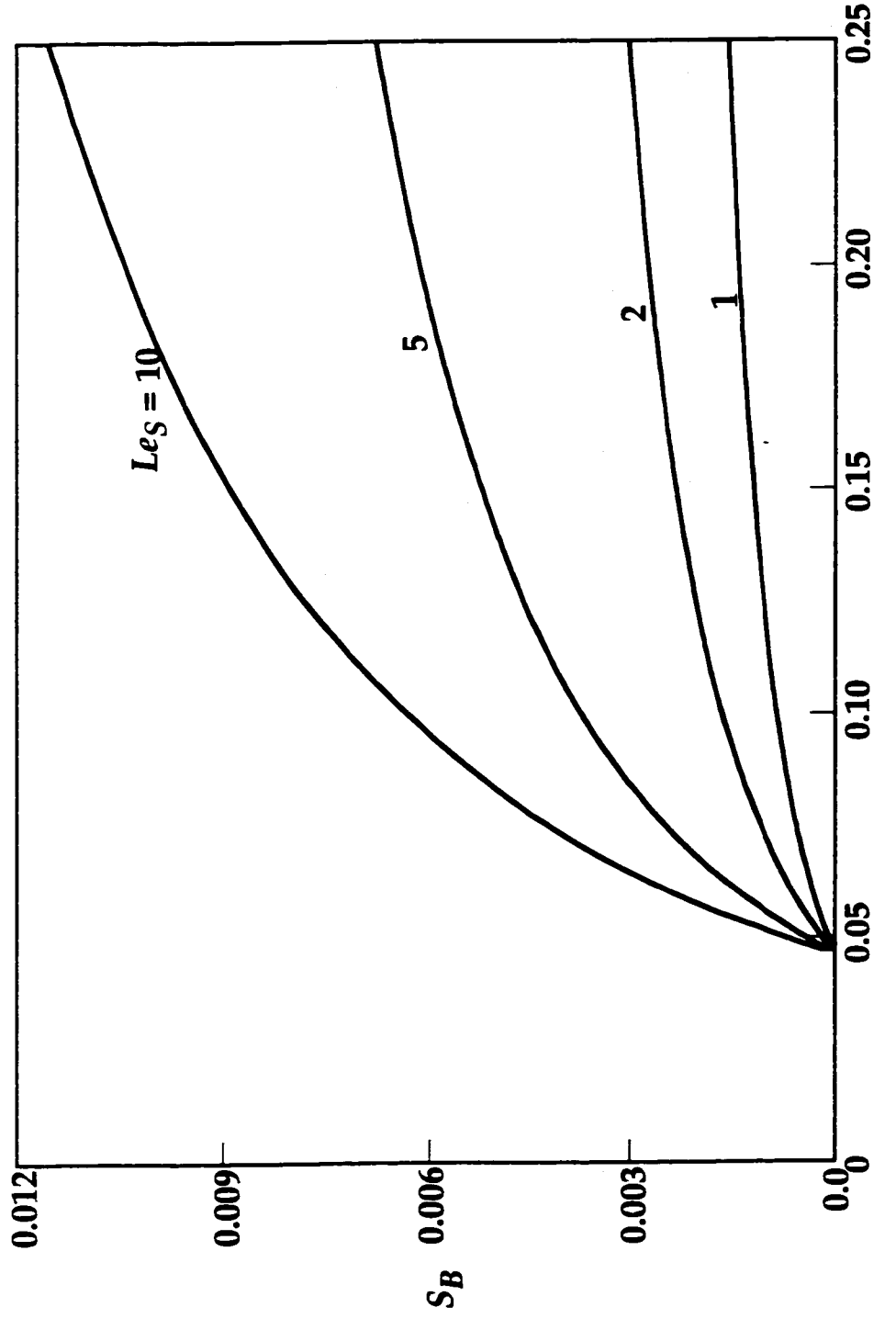

Figure 3.10 Variation of S_B corresponding to Fig. 3.9

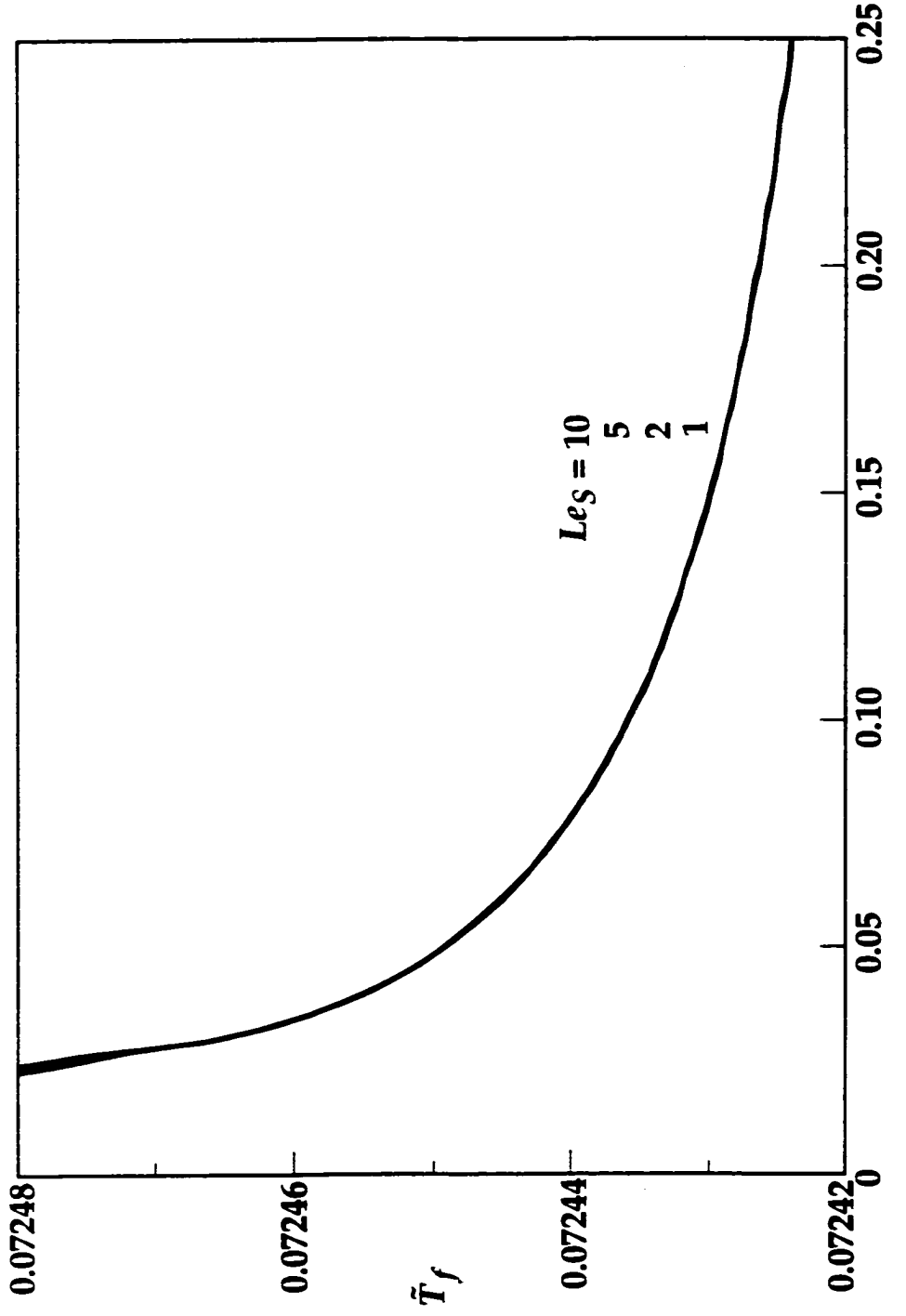

Figure 3.11 The flame temperature $\tilde{T}_f$ corresponding to Fig. 3.9

Figs. 3.6–3.8 with $\alpha = Le_R = 1$ and $\beta = O(\delta)$. The values of Le_S are selected to be larger than unity because the soot/precursor is heavier than the background gas and hence its diffusion velocity is slower. Similar to Chapter 2, one can conclude from Fig. 3.9 that the concentration of soot/precursor in the formation region increases with increasing Le_S because more soot/precursor is accumulated in this region due to its reduced diffusion rate. However, since the soot consumption reaction is negligible for $\beta = O(\delta)$ and the diffusion of soot/precursor does not affect the soot formation reaction, the total amount of soot/precursor produced is independent of Le_S. This is evidenced by the same flame temperature for all Le_S in Fig. 3.11. The higher soot/precursor concentration in the soot formation region for higher values of Le_S also leads to a higher S_B as shown in Fig. 3.10. Unlike the earlier discussion, the variation of S_B due to the change of Le_S does not represent the variation of total soot production. It only shows the redistribution of soot/precursor through the change of its diffusion rate.

The behavior is qualitatively different when the soot consumption reaction is not negligible. To study the difference, a representative example is presented in Fig. 3.12 which shows the flame temperature, $\tilde{T}_f$, versus Da_2 for $\beta = 0.025$ and $\alpha = Le_R = 1$. This figure exhibits a higher flame temperature for larger Le_S because the soot concentration in the soot consumption region is higher. In addition, the slower soot/precursor diffusion provides a longer residence time for the consumption reaction. These factors allow more soot/precursor to be consumed through the consumption reaction and consequently more heat is released. Thus the flame temperature is increased and the overall soot production is reduced.

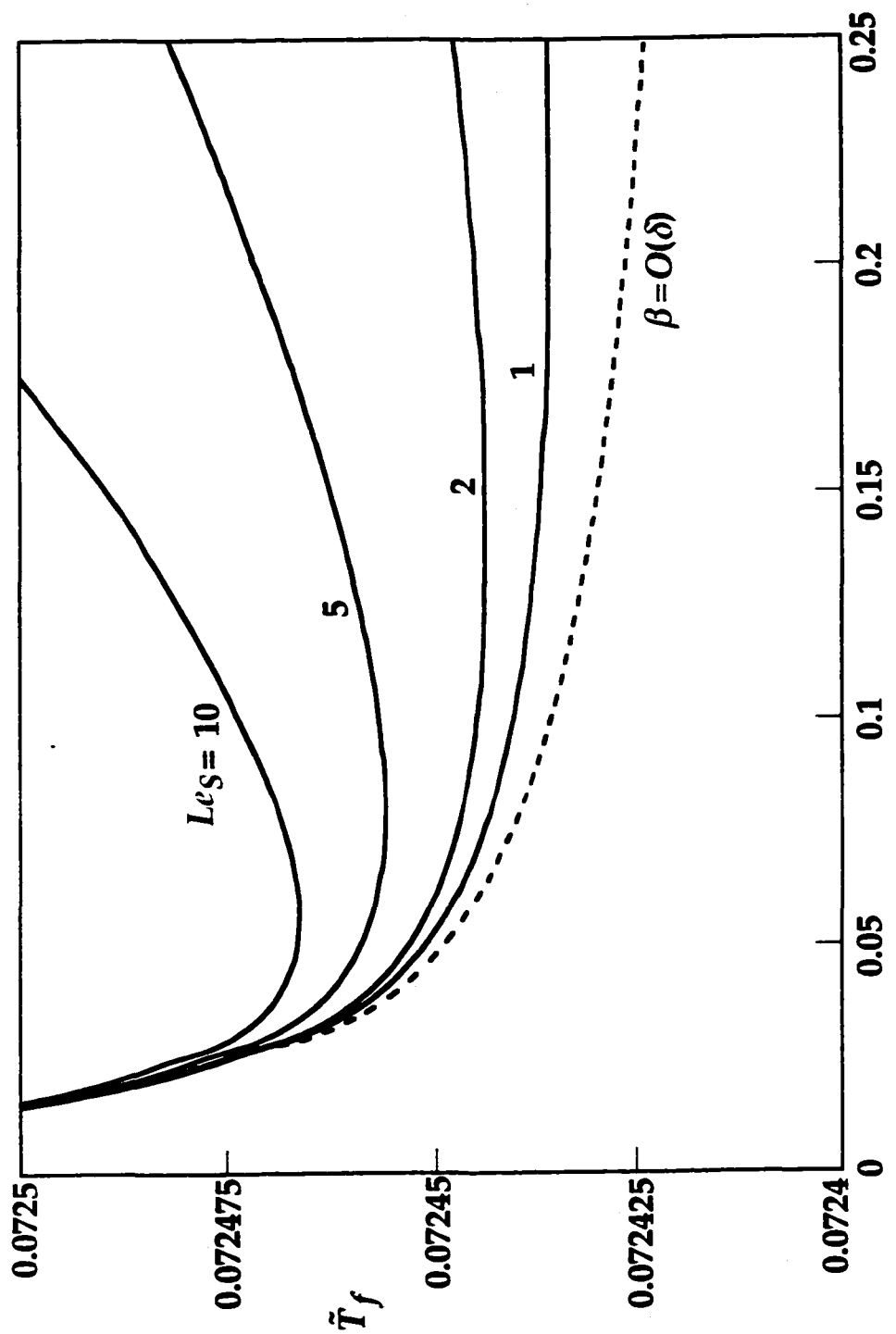

Figure 3.12 Variation of $\tilde{T}_f$ with Da_2 for the fuel/air flame with $\alpha = Le_R = 1$ and $\beta = 0.025$. The solution for $\beta = O(\delta)$ is also included in dotted curve for comparison.

Up to the present, all the discussions in this chapter were based on the variation of Da_2, which is the rate of the soot formation reaction. Physically, Da_2 is fixed when a specific fuel/oxidizer system is adopted in experiments. To better understand the sooting behavior, it is more instrumental to study the effect of mass flow rate from the burner. In this regard, a representative case is presented in Figs. 3.13–3.16. These figures show, respectively, the flame temperature, $\tilde{T}_f$, flame location, $\tilde{r}_f$, soot/precursor indicator, S_I, and soot/precursor breakthrough parameter, S_B, versus the burner flow rate, $\tilde{m}$, for $\alpha = Le_R = Le_S = 1$ and $Da_2 = 0.1$. In the inert region at the fuel side of the reaction regions, diffusion of heat, the radical and the soot/precursor from the reaction regions toward the burner must occur against convection. Thus when the burner flow rate $\tilde{m}$ is increased, the heat transfer from the flame to the burner is decreased due to a stronger outward flow. Such reduced heat transfer yields a lower heat loss to the coolant and a higher flame temperature as shown in Fig. 3.13. The increase of $\tilde{m}$ also forces the reaction regions to move out toward the ambient, as shown in Fig. 3.14, because there is more fuel to be consumed and a new stoichiometric location with higher oxidizer supply is necessary. For small values of $\tilde{m}$, an increase of $\tilde{m}$ yields a greater decrease in the heat loss such that $\tilde{T}_f$ increases more rapidly. The increase in $\tilde{T}_f$ slows down with continuous increase in $\tilde{m}$ for the reaction regions are farther away from the surface and the reduction in the heat loss to the burner is less significant.

Returning to the soot/precursor formation, Fig. 3.15 shows that by continuously increasing $\tilde{m}$ from a small value, S_I first increases, attains a maximum, and then decreases, similar to that of Fig. 3.2. This suggests that

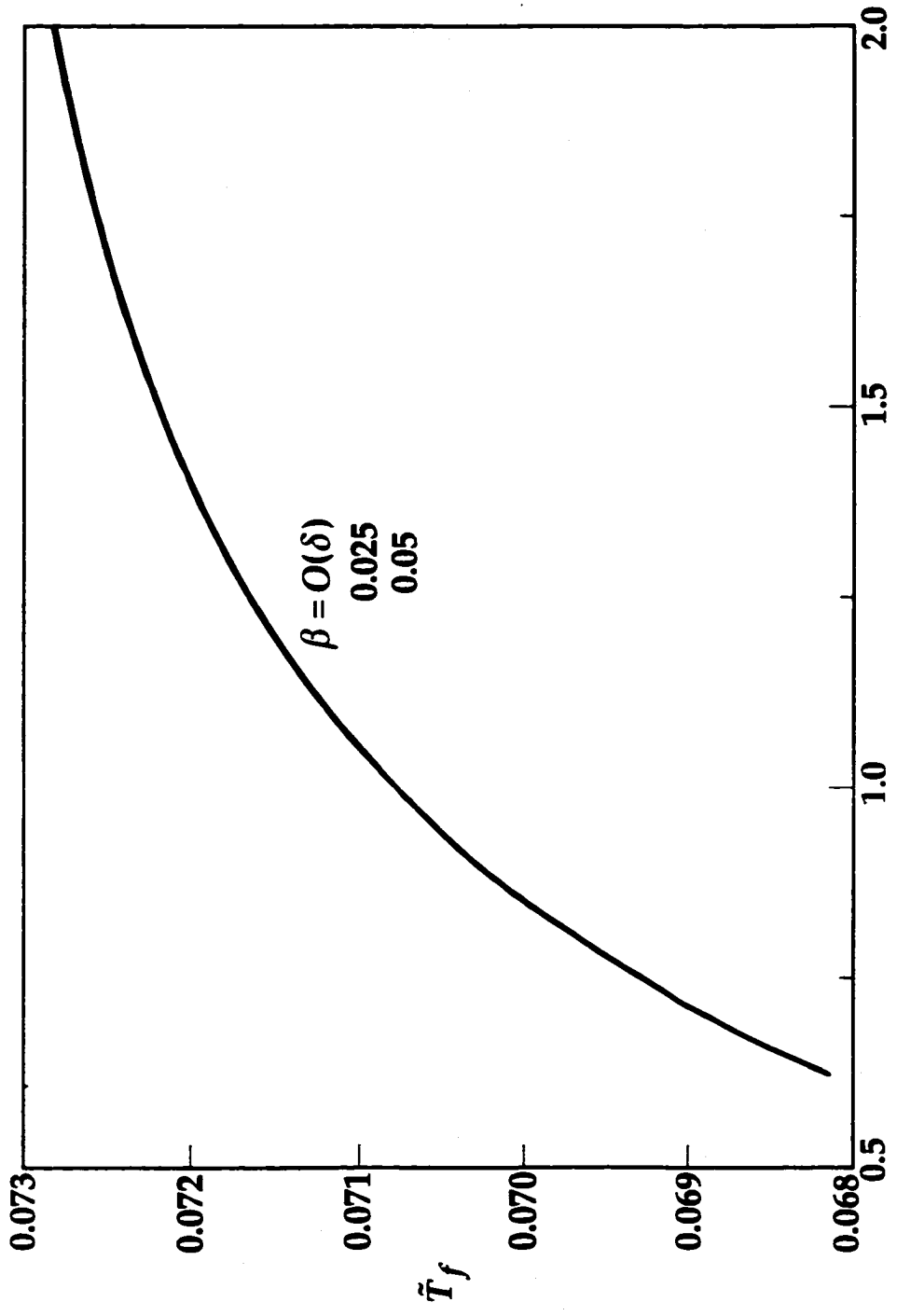

Figure 3.13 Variation of $\tilde{T}_f$ with $\tilde{m}$ for the fuel/air flame with $\alpha = Le_R = Le_S = 1$, $Da_2 = 0.1$, and selected values of β

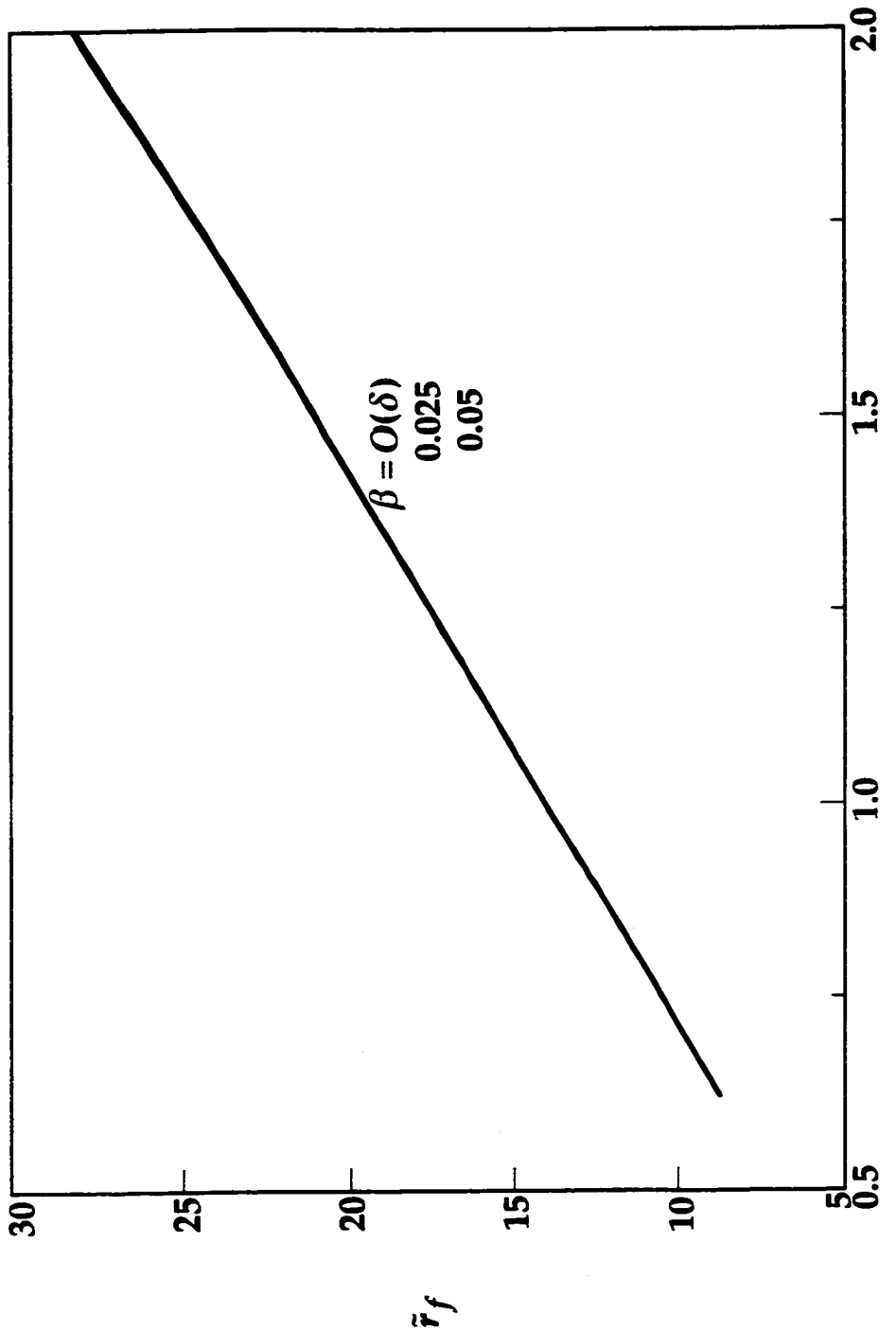

Figure 3.14 The flame sheet location $\tilde{r}_f$ corresponding to Fig. 3.13

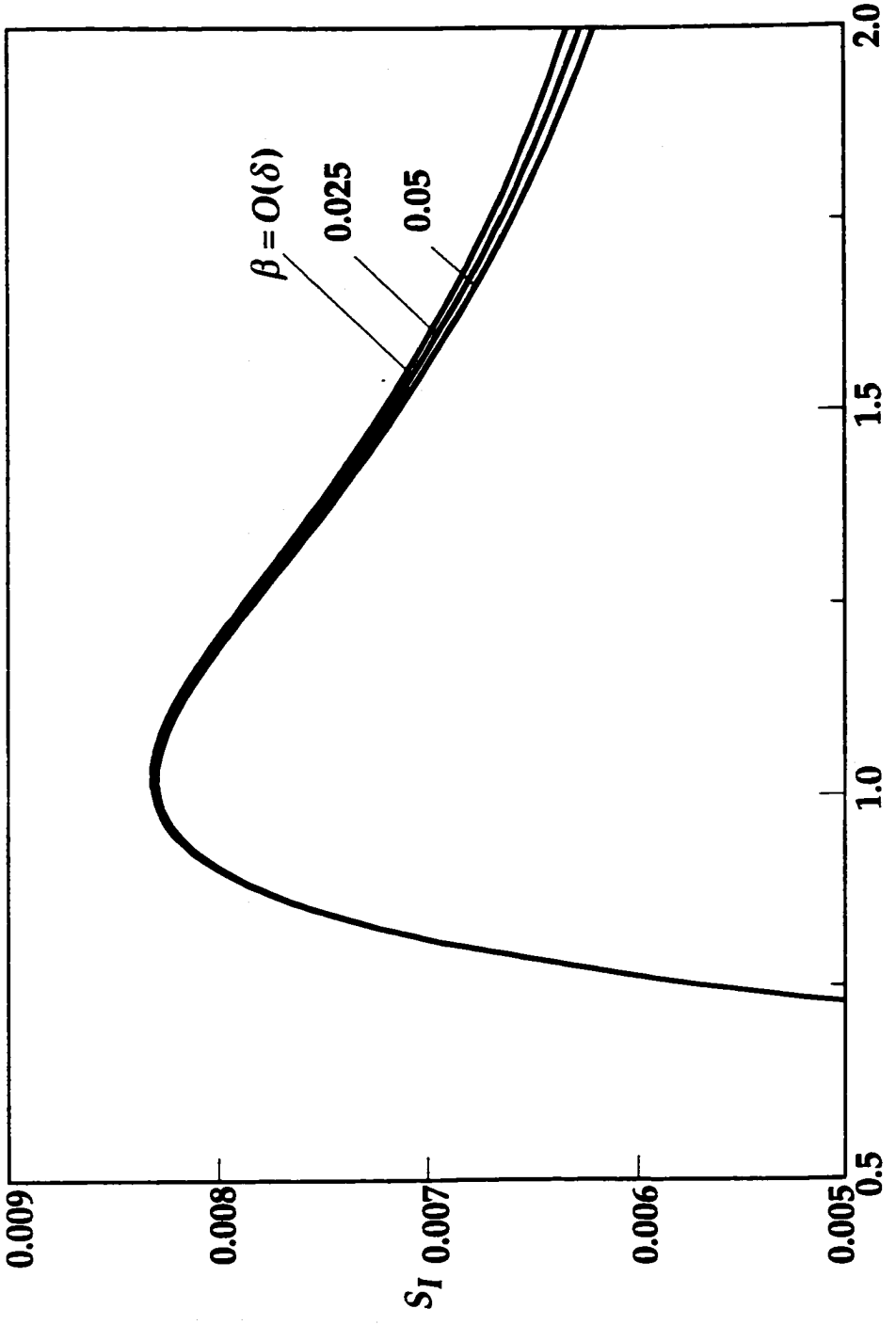

Figure 3.15 Variation of S_I corresponding to Fig. 3.13

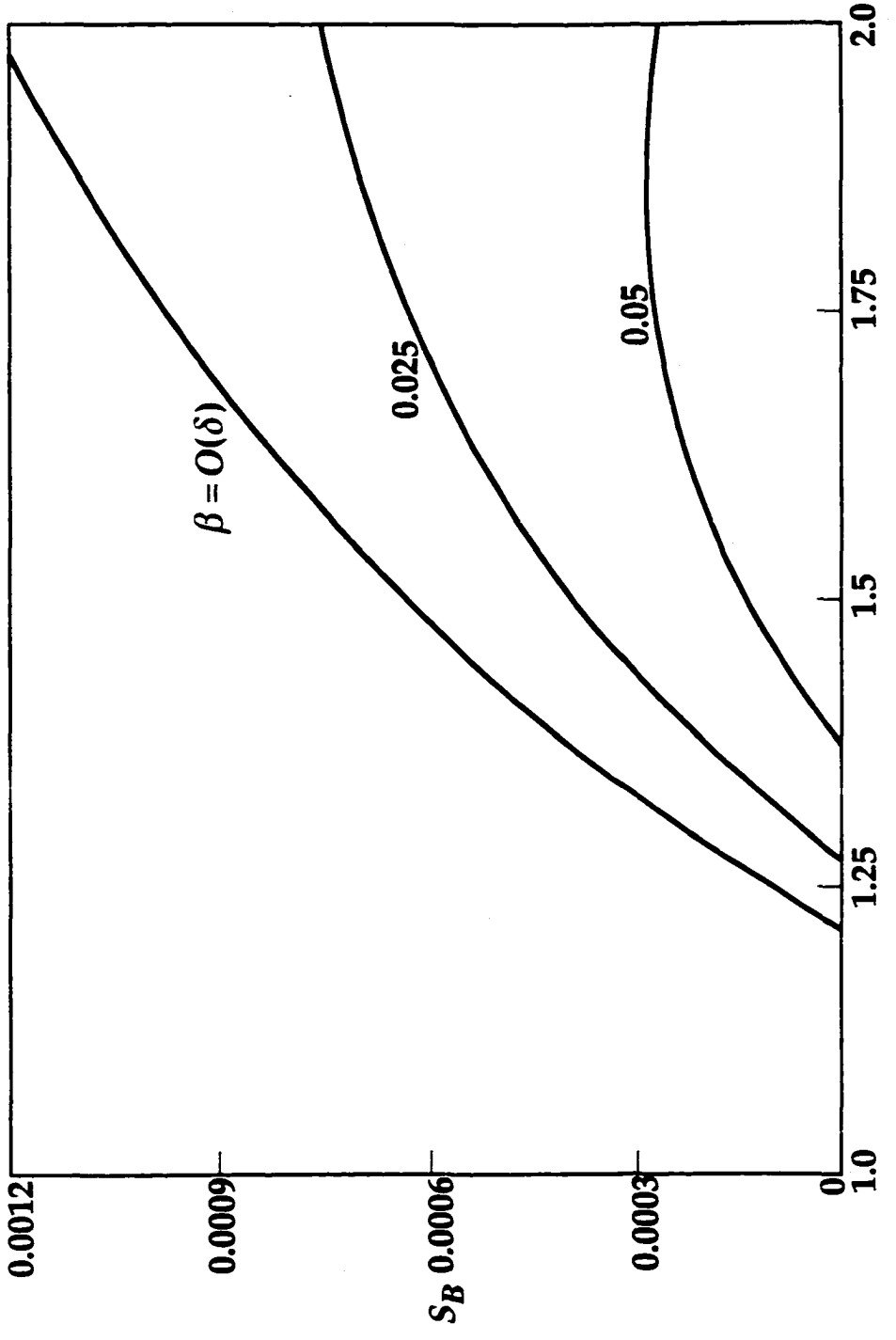

Figure 3.16 Variation of S_B corresponding to Fig. 3.13

the effect of $\tilde{m}$ on the sooting behavior may be qualitatively similar to that of Da_2. The behavior of S_B shown in Fig. 3.16 further supports the expectation. The cause of the sooting behavior, however, is different between these two cases. There are some competitive processes that arise by the variation of $\tilde{m}$. First, with the increase of $\tilde{m}$, the flame temperature increases so that the rate of the soot/precursor formation reaction is enhanced and more soot is produced. This yields a higher S_I and a higher total amount of soot/precursor production. As noted in Chapter 2, S_I does not represent the total soot/precursor production. Second, since the flame location, $\tilde{r}_f$, increases almost linearly with increasing $\tilde{m}$ and the surface area of the flame varies with $\tilde{r}_f^2$, the mass flux at the reaction regions, $(\rho u)_f = \tilde{m}/(4\pi\tilde{r}_f^2)$, decreases with increasing $\tilde{m}$ and the soot formation region is broadened while the soot consumption region is narrowed. Both the reduction of mass flux and the modification of reaction regions lead to the increase in the radical concentration and the residence time for the soot formation reaction such that both S_I and the total amount of soot/precursor production is further enhanced. Accompanying the increase of the residence time, however, is the reduction of fuel supply per unit area of the flame, which renders a lower fuel concentration in the soot formation region and a lower soot/precursor formation rate and a lower S_I. Finally, the reduction in the mass flux favors the diffusion of the radical through the soot formation region so that the total soot/precursor formation is decreased. This behavior is similar to the decrease in Le_R as discussed earlier.

For low burner flow rates, the increase of reaction rates corresponding to the increase of $\tilde{m}$ is more significant as evidenced by the large increase in the

flame temperature and a moderate increase in the flame location, as shown in Figs. 3.13 and 3.14. Consequently S_I increases with $\tilde{m}$. With continued increase in $\tilde{m}$, the impact of the reaction rates decays and the decrease in mass flux in the reaction regions dominates. As mentioned in the previous paragraph, although the decrease of mass flux increases residence time, which in turn enhances soot formation, the reduction of fuel supply per unit flame area is more significant such that S_I decreases. The total soot/precursor production for the $\beta = O(\delta)$ case, nonetheless, increases monotonically with $\tilde{m}$ as exhibited by S_B in Fig. 3.16. This is reasonable to expect since both the increase in the rate of soot formation reaction and the increase in the residence time favor the overall production of soot/precursor. The variation of β shown in Figs. 3.15 and 3.16 again exhibits a lower S_I and net soot production for a higher β as in Figs. 3.2 and 3.5, which has been discussed earlier. The dependence of the flame temperature and flame location on β, although consistent with those shown in Figs. 3.3 and 3.4, is not distinguishable in Figs. 3.13 and 3.14 because the changes are insignificant compared to those caused by the variation of $\tilde{m}$.

Extending from the above understanding, we may suspect that for sufficiently large values of $\tilde{m}$, when the heat transfer to the burner becomes negligible, the flame temperature for the $\beta = O(\delta)$ flame may decrease instead of increase with increasing $\tilde{m}$. The reason is that the overall soot production is higher for a greater $\tilde{m}$. For non-zero β flames, the flame temperature may increase again after it is dropped by continuously increasing $\tilde{m}$, or continue to increase without a drop if β is sufficiently large, until the adiabatic limit is reached because of the extra heat produced from the soot/precursor

consumption reaction. This will be confirmed later in the discussion on Fig. 3.21.

The variation of the activation energy ratio, α, is to yield a higher amount of soot/precursor and a lower flame temperature for a higher α and will not be elaborated as in Chapter 2.

The effect of stoichiometric mixture fraction on the production of soot/precursor is now examined by redistributing the inert gas from the oxidizer side to the fuel stream. In the extreme limit where all the inert gas in the air flow is diverted into the fuel stream, one has $Y_{O,\infty} = 1$ with $Y_{F,0}$ varying between 0.08143 and 0.08784 as in Chapter 2. This results in m varying between 18.53 and 17.19 mg/s, or $\tilde{m}$ varying between 20.19 and 18.73, when the fuel flow rate is maintained as 1.51 mg/s. Calculations were performed using the same quantities used in Chapter 2, $\alpha = Le_R = Le_S = 1$, and the results of S_I, $\tilde{T}_f$, $\tilde{r}_f$, and S_B were plotted versus Da_2 in Figs. 3.17–3.20. Similar to the behavior reported in Chapter 2, Figs. 3.17–3.20 and 3.2–3.5 show that the behavior of these two cases are qualitatively similar. However, Fig. 3.17 shows that the values of S_I are much smaller, while Da_2 for observable soot/precursor production are much larger for the diluted-fuel/oxygen flame. This indicates that it is much more difficult to produce soot/precursor when the inert gas is diverted to the fuel stream, which agrees with the conclusion drawn in Chapter 2 for counterflow diffusion flames. The difference between the two cases, nonetheless, is not as great as the two counterflow flame cases because there is no inversion of the flow direction. In addition, Figs. 3.18 and 3.19 show that the flame temperature is higher and the flame is much closer to the burner for the diluted-fuel/oxygen flame, in agreement with an earlier

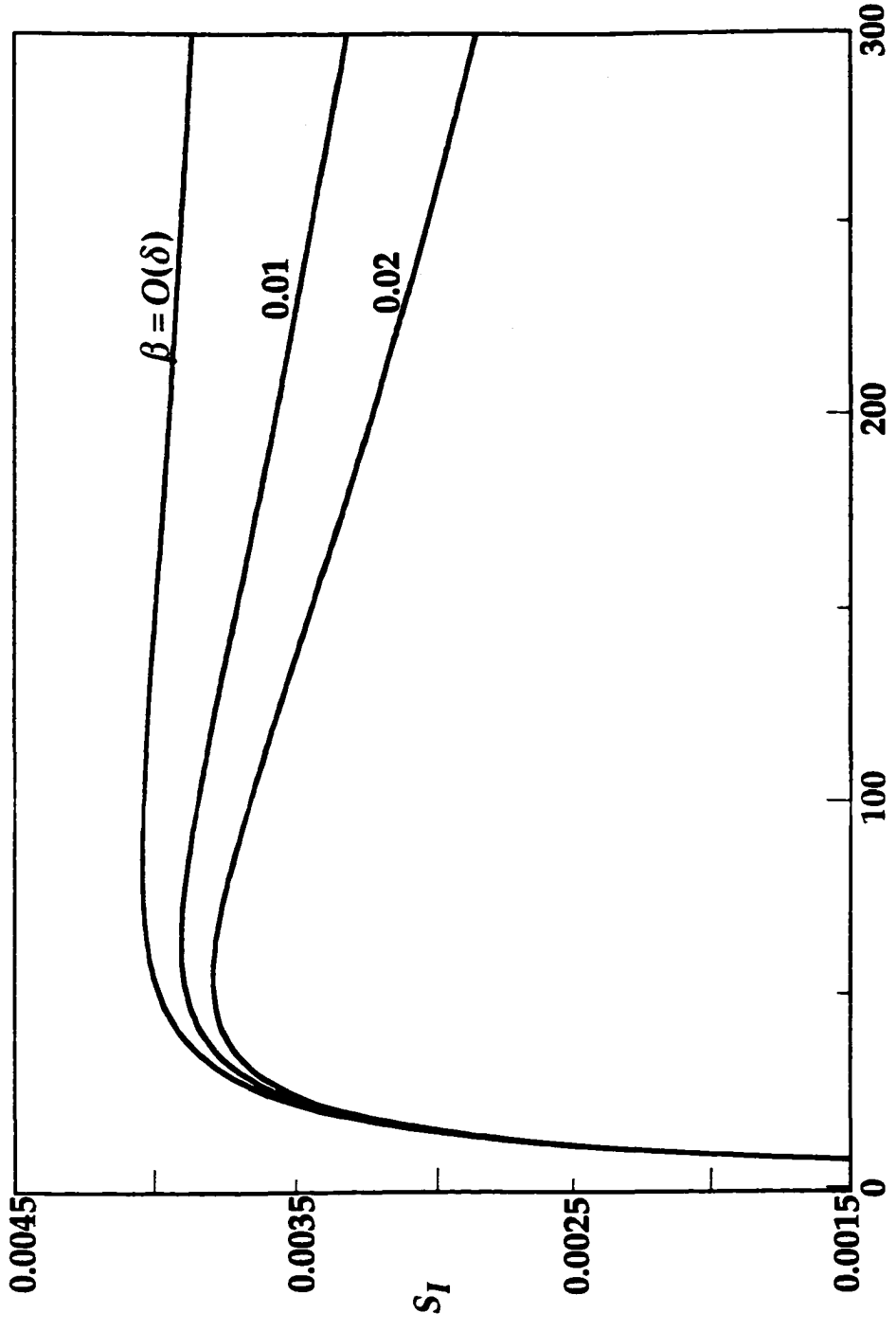

Figure 3.17 Variation of S_I with Da_2 for the diluted-fuel/oxygen flame with $\alpha = Le_R = Le_S = 1$ and selected values of β

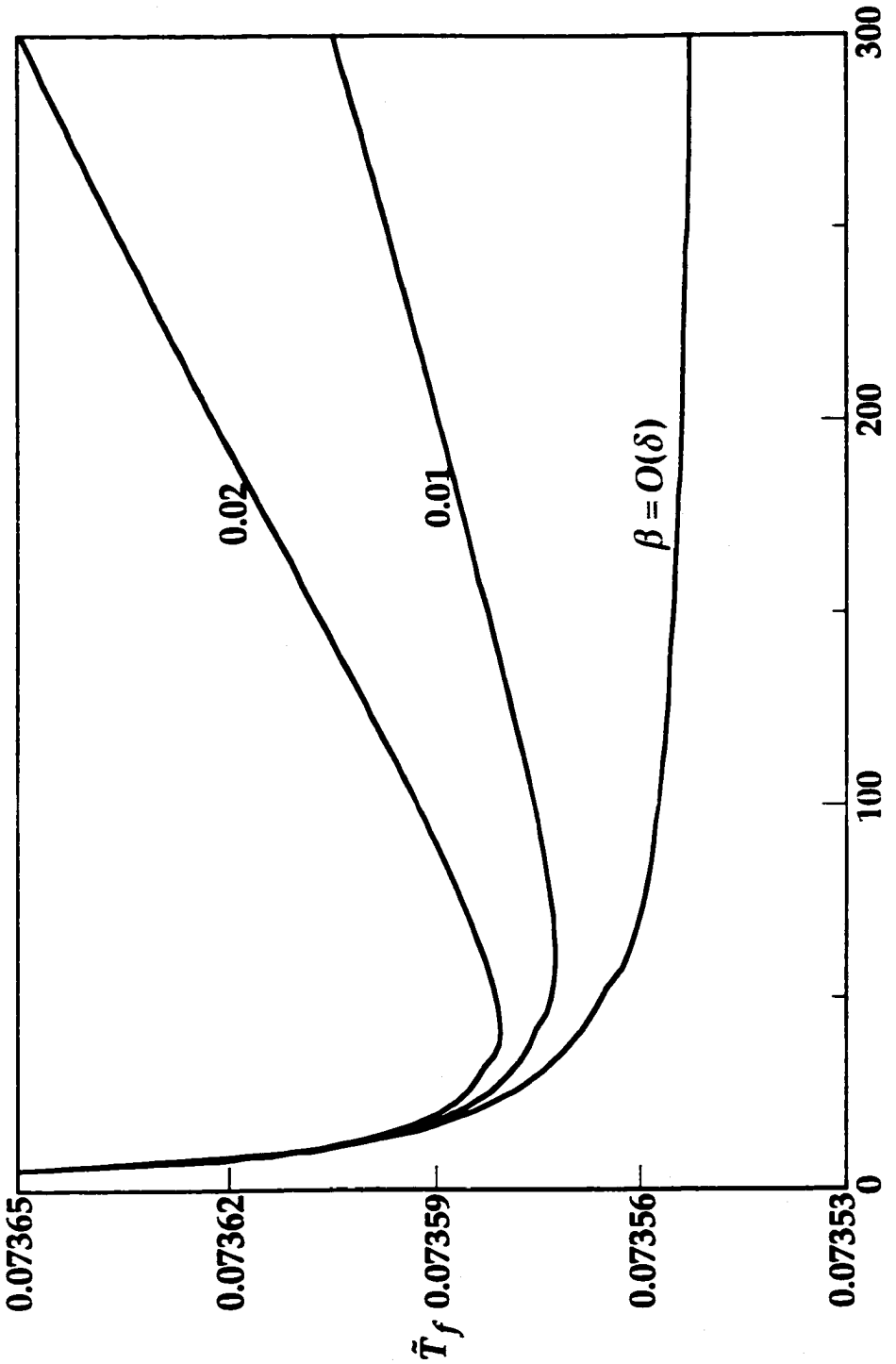

Figure 3.18 The flame temperature $\tilde{T}_f$ corresponding to Fig. 3.17

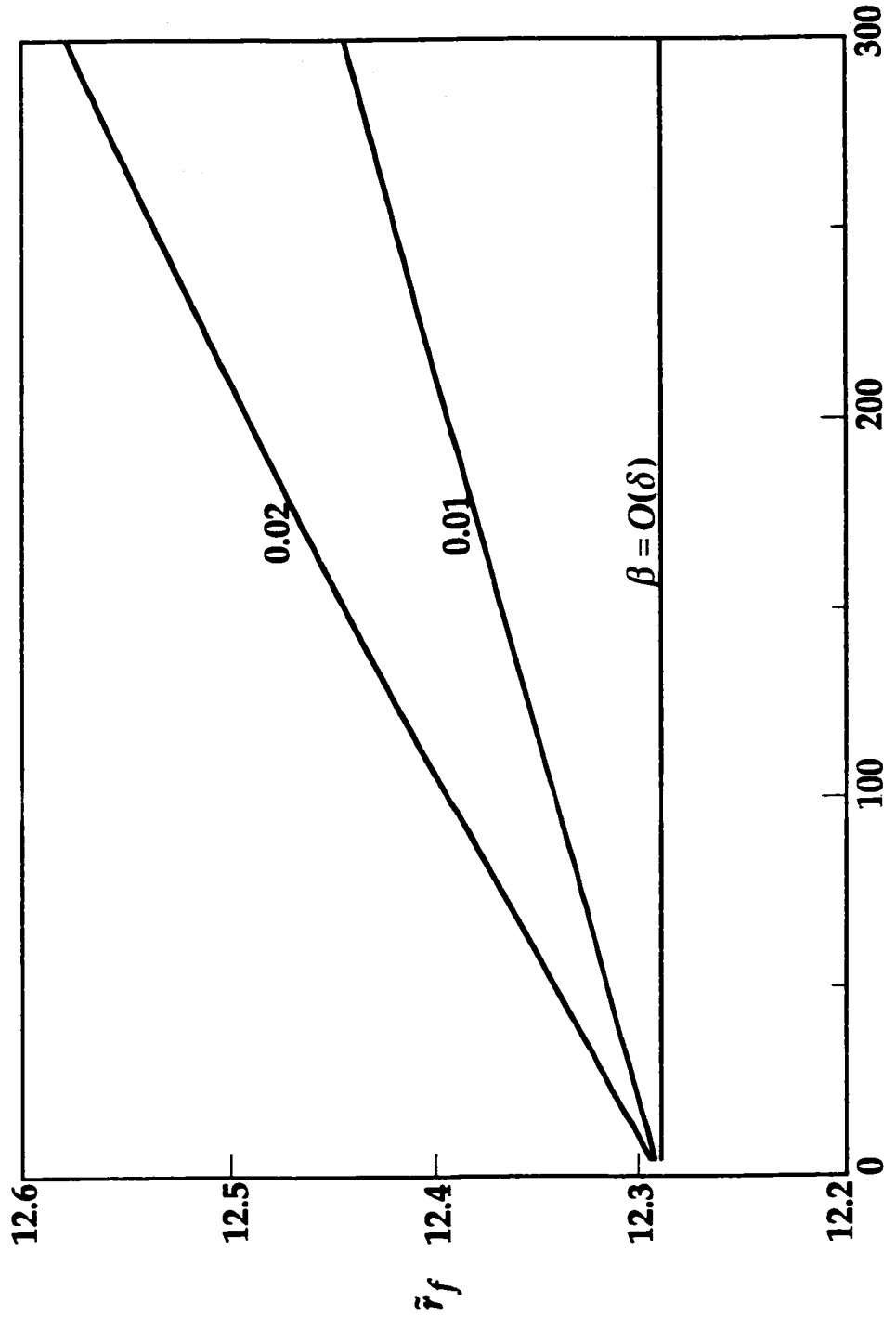

Figure 3.19 The flame sheet location $\tilde{r}_f$ corresponding to Fig. 3.17

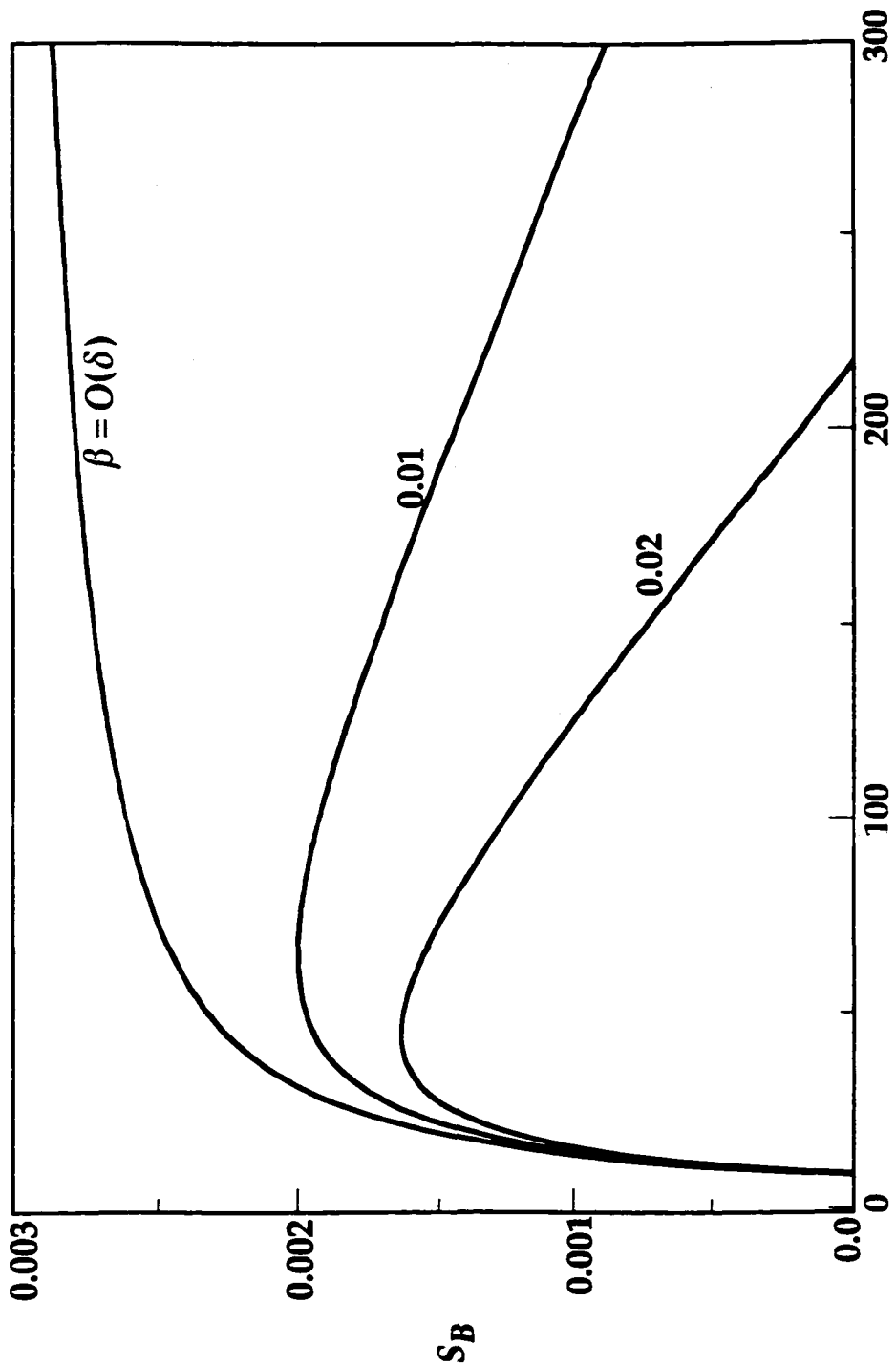

Figure 3.20 Variation of S_B corresponding to Fig. 3.17

discussion on Fig. 3.2. Although S_I is smaller, Fig. 3.20 shows higher maximum values of S_B for the diluted-fuel/oxygen flame compared to that of the fuel/air flame. This will be discussed in the next paragraph.

The differences in the flame behavior as a result of inert redistribution can be explained by the following. When the inert is supplied with the fuel, the initial fuel concentration is low and the initial oxidizer concentration is high so that the flame moves closer to the burner to seek a new stoichiometric location (Figs. 3.4 and 3.19). The inert redistribution also results in a large mass flow rate from the burner, which reduces the heat transfer from the flame to the burner and raises the flame temperature (Figs. 3.3 and 3.18). The higher burner flow rate and smaller flame standoff distance then yield a much higher mass flux near the flame so that the thickness of the soot/precursor formation region is reduced and the soot/precursor consumption region is broadened with respect to the fuel/air flame. The reduced residence time in the soot/precursor formation region inhibits the soot/precursor formation reaction so that much higher values of Da_2 are required to produce soot/precursor and the total amount of soot produced is lower. Although the higher flame temperature favors the production of soot/precursor, the effect of residence time dominates the process for the increase in the flame temperature is moderate as can be concluded from comparing Figs. 3.3 and 3.18. The approximately 12 time increase in the burner flow rate and 50 % decrease in the flame radius for the diluted-fuel/oxygen flame yield a mass flux approximately 40 times larger than that of the fuel/air flame and a significant reduction in the residence time. Although S_I is smaller, the stronger convection subsequently brings a large

fraction of soot/precursor to the consumption region to yield a high maximum value of S_B. It should be noted, however, that the values of S_B shown in Fig. 3.20 may not be obtainable since extremely high values of Da_2 are required. For the same range of Da_2 as that for the fuel/air flame, the diluted-fuel/oxygen flame is primarily soot free. As in Chapter 2, the reduced values of S_I and S_B indicate that inert redistribution (increase in the stoichiometric mixture fraction) is an effective approach to reduce soot production from non-premixed combustion systems.

Figures 3.17–3.20 also exhibit that the sooting behavior responding to the soot/precursor consumption reaction rate, β, is similar to that of the fuel/air flame. That is, a stronger soot/precursor consumption reaction yields a lower net soot/precursor production, a higher flame temperature and a larger flame standoff distance. This effect, however, is stronger for the diluted-fuel/oxygen flame in that a smaller increase of β results in a greater variation in the flame response. This behavior is attributed to the higher flame temperature and broadened soot/precursor consumption reaction region. The higher flame temperature strengthens the soot/precursor consumption reaction while the thicker consumption region provides a longer residence time for the consumption reaction to occur. Both are acting in favor of reducing the production of soot/precursor.

As in Figs. 3.13–3.16, the effect of burner flow rate on $\tilde{T}_f$, $\tilde{r}_f$, S_I, and S_B for the diluted-fuel/oxygen flame is presented in Figs. 3.21–3.24, with $\alpha = Le_R = Le_S = 1$ and $Da_2 = 100$. It is observed that the flame response corresponding to the variation of $\tilde{m}$ is qualitatively similar to that of the fuel/air flame. Moreover, Fig. 3.21 shows that the flame temperature for the

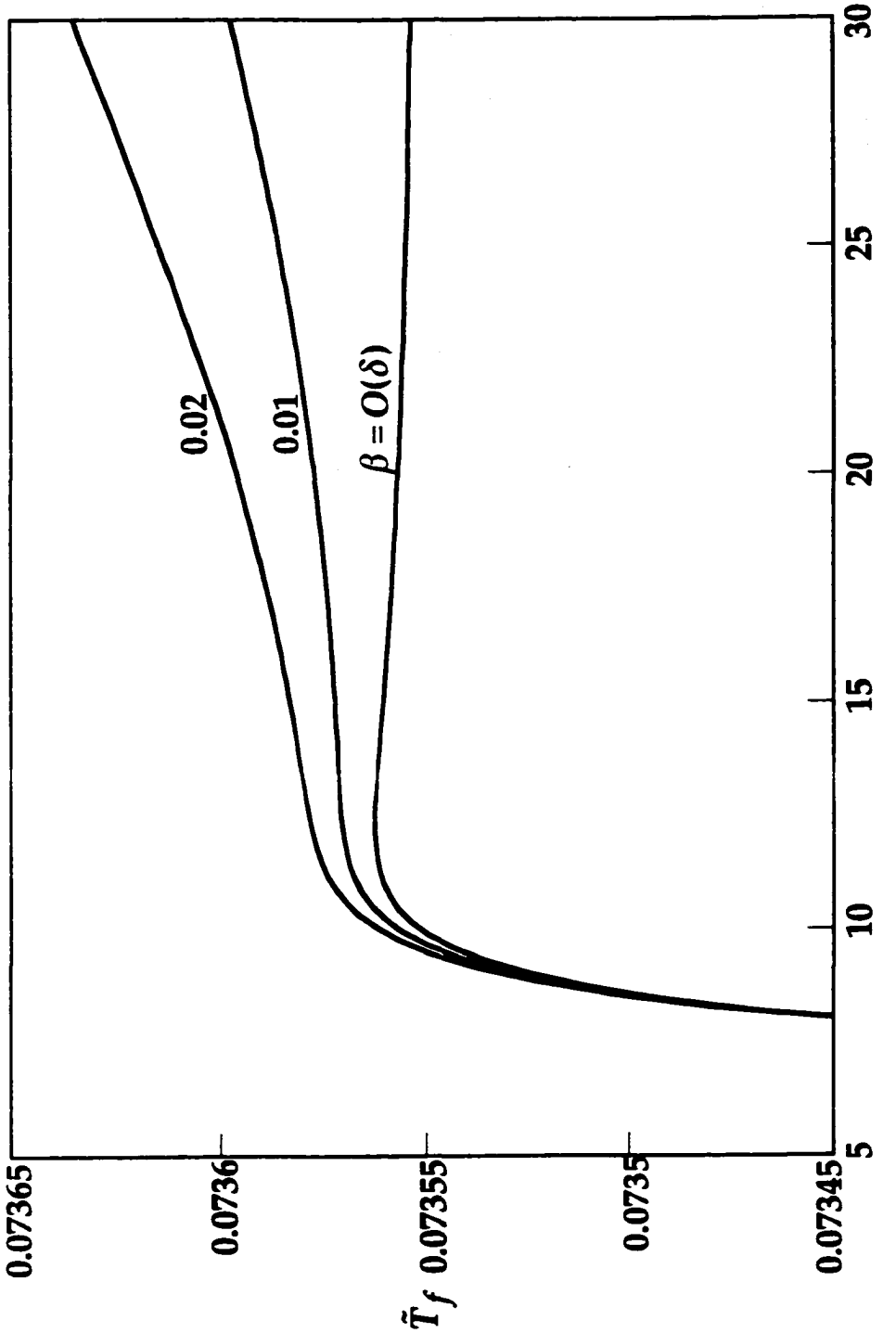

Figure 3.21 Variation of $\tilde{T}_f$ with $\tilde{m}$ for the diluted-fuel/oxygen flame with $\alpha = Le_R = Le_S = 1$, $Da_2 = 100$, and selected values of β

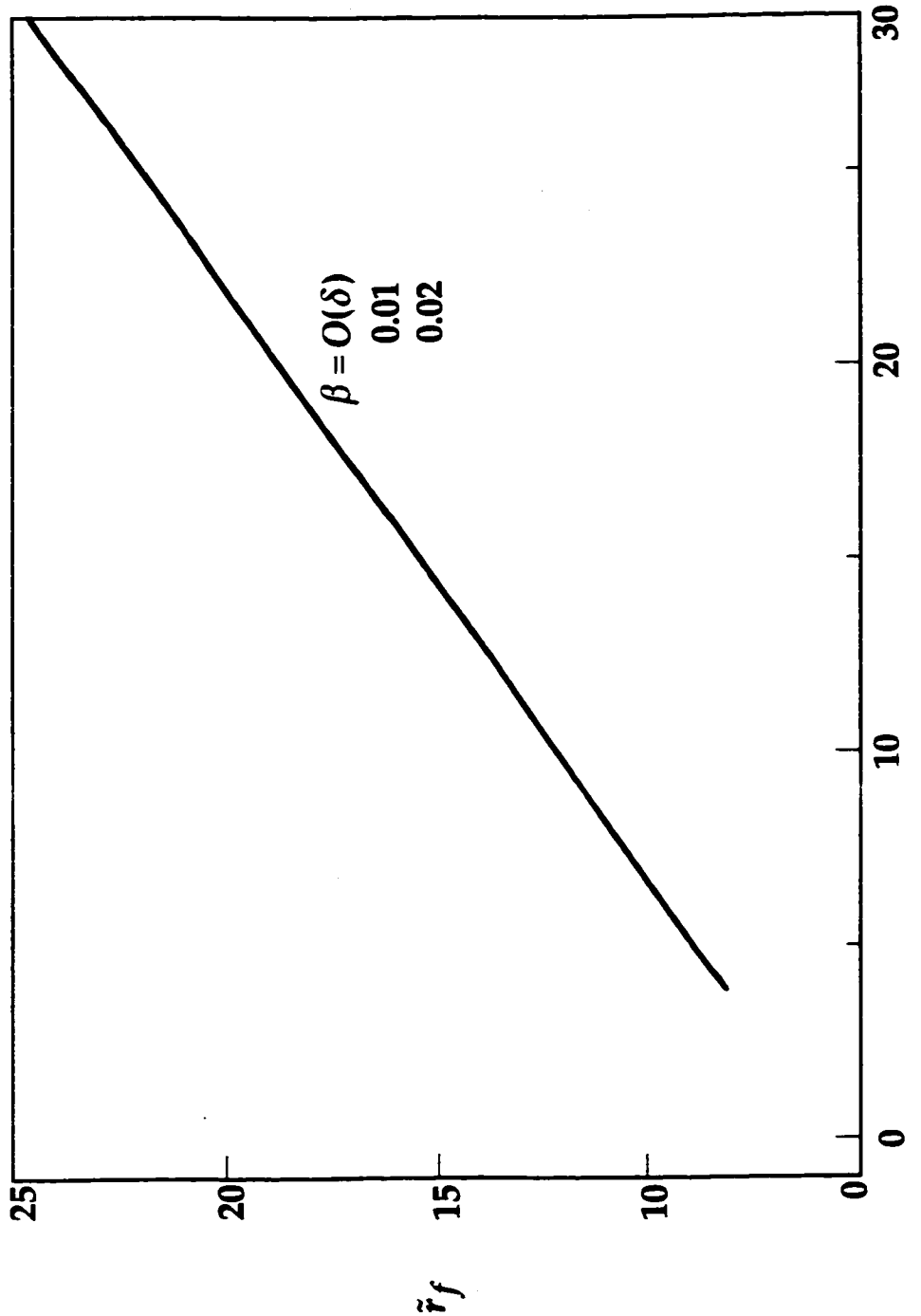

Figure 3.22 The flame sheet location $\tilde{r}_f$ corresponding to Fig. 3.21

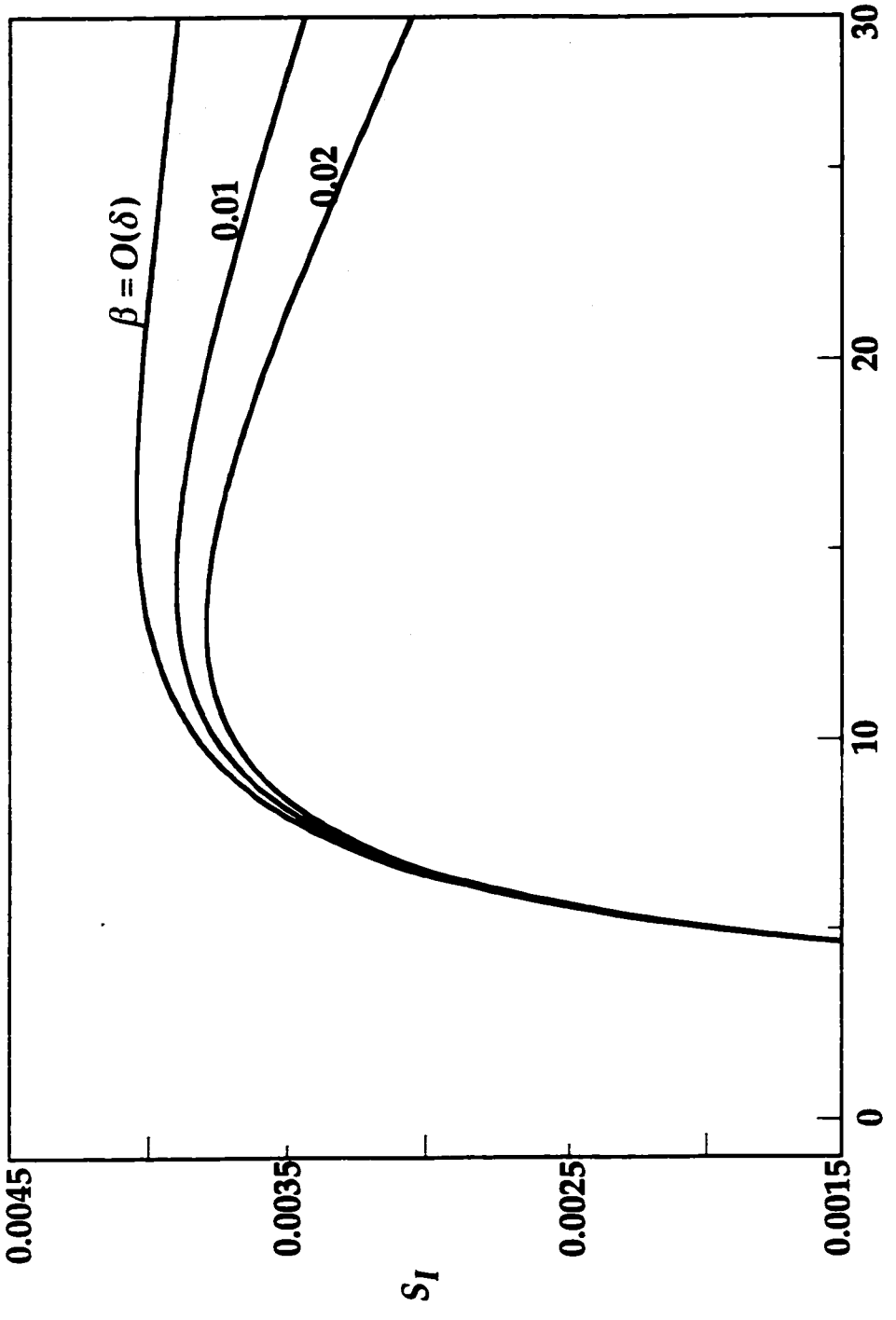

Figure 3.23 Variation of S_I corresponding to Fig. 3.21

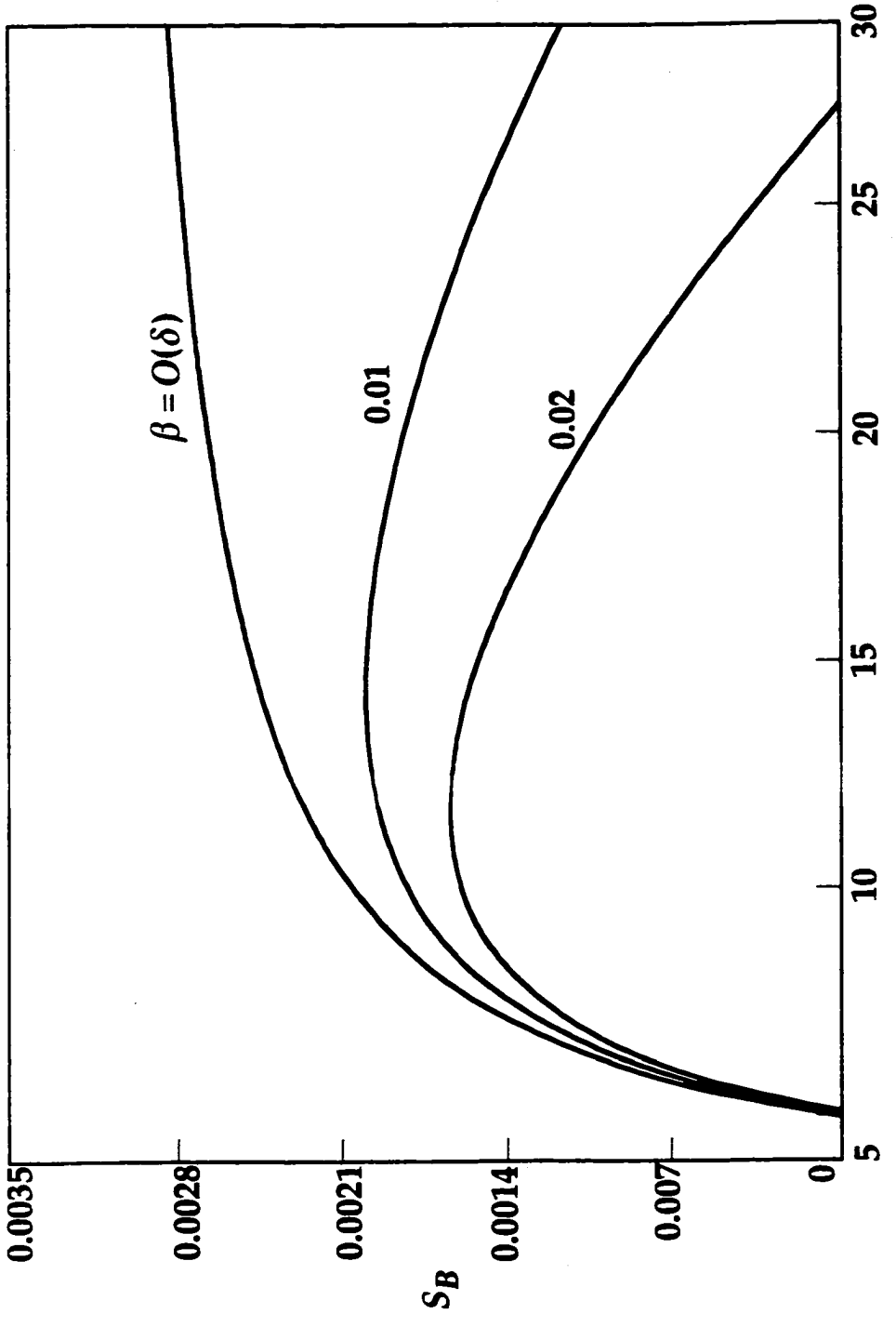

Figure 3.24 Variation of S_B corresponding to Fig. 3.21

$\beta = O(\delta)$ flame decreases with increasing $\bar{m}$ when $\bar{m}$ is sufficiently large. For non-zero β flames, the flame temperature increase again after it is dropped by continuously increasing $\bar{m}$. These confirm the earlier suspicion on the discussion of Figs. 3.13–3.16.

Finally, comparing the fuel/air and the diluted-fuel/oxygen flames with the same fuel consumption rate, it is found that the fuel/air flame has a lower flame temperature because of its low mass flow rate. More heat is transferred to the burner and carried away by the coolant as a result of its weak convective transport. Recognizing that both the soot formation and oxidation processes are highly temperature sensitive, and that the experiments to be performed by our collaborators in microgravity are without coolants, a comparison between these flames with the same adiabatic flame temperature is important to the success of this investigation. To achieve this goal, additional calculations that adopted $T_b = 802$ K were performed for the fuel/air flame such that both of the flames have the same flame temperature. Results of S_B versus Da_2 for this elevated T_b flame is shown in Fig. 3.25. Also shown in Fig. 3.25 is the solution for the original flame with $T_b = 300$ K for comparison. This figure exhibits that a higher amount of soot is produced when T_b, and hence the flame temperature is increased. Therefore the difference in soot production between the two limiting flames is further amplified when both have the same flame temperature. This result further supports the conclusion that significant reduction can be obtained by inert redistribution, which agrees with the experiments performed by our collaborators at Washington University, St. Louis and NASA Glenn Research Center.

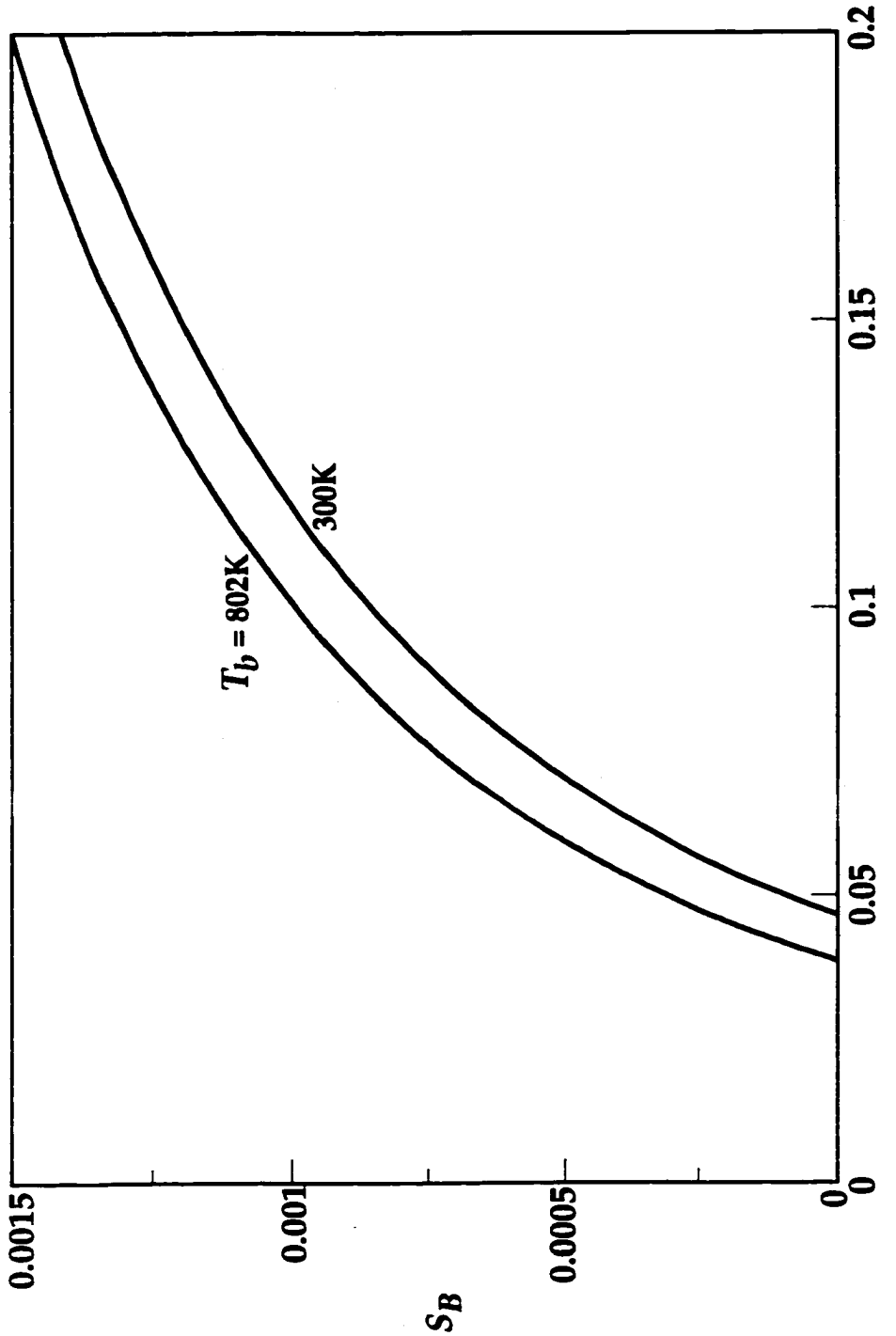

Figure 3.25 Variation of S_B with Da_2 for the fuel/air flame with $\alpha = Le_R = Le_S = 1$ and $\beta = O(\delta)$

CHAPTER 4

SPHERICAL DIFFUSION FLAMES SUPPORTED BY A POROUS BURNER WITH OXIDIZER SUPPLIED FROM THE BURNER

The study reported in Chapter 3 reveals that modification of the flame structure, represented by the variation of stoichiometric mixture fraction through inert redistribution, has a profound effect on the sooting behavior of a diffusion flame without the change in the flow direction. Formation of soot precursor, and consequently soot particles, is significantly reduced by the redistribution of inert gas from the oxidizer side to the fuel stream. One may criticize, however, that such an effort does not introduce a promising advantage because the soot/precursor produced in the soot formation region is convected to the soot consumption region and be largely consumed even for the fuel/air flame that produces the largest quantity of soot precursor. Only a tracing amount of soot breaks through the consumption region and appears in the final products. Recognizing that in practical combustion devices, the flow direction can be toward the fuel side, a flow field that favors soot formation, i.e., from the oxidizer to the fuel direction, needs to be considered. This task which fully characterizes the relevance of flame structure on the sooting behavior and exhibits the benefit of inert redistribution, can be achieved by issuing an oxidizer flow from the burner into a quiescent fuel environment.

4.1 Formulation

Following the above descriptions, the problem to be analyzed in this chapter is a diffusion flame burning at steady state and stabilized by a

spherical porous burner as in Chapter 3. A gaseous oxidizer flow of mass flow rate $m = 4\pi r^2 \rho u$ is issued from the burner at a temperature T_b. It is known from Chapter 3 that m is a constant at any r in the whole domain of interest. The quiescent ambient at a temperature of T_∞ is filled with fuel gas with an initial mass fraction $Y_{F,\infty}$. The flame is situated between the fuel and oxidizer at where the stoichiometric is located. Adopting the same assumptions taken in Chapter 3, we consider the porous burner to be perfect so that a uniform flow is supplied at its outer surface, and both the flow field and the flame are spherical symmetric. The same three-step reaction scheme given by Eqs. (R1)–(R3) is again used to describe the chemistry.

Following the above discussion, it is understood that both the flow geometry and the problem definition are the same as those of Chapter 3. Therefore, the equations governing the conservation of energy and species concentration are Eqs. (3.2)–(3.6). It is then expected that part of the expressions can be depicted from Chapter 3.

The boundary conditions, however, are different because of the inversion of the flow direction. The appropriate boundary conditions for this problem are

$$r = r_b \quad : \quad T = T_b \quad , \quad mY_O - 4\pi r_b^2 \rho D_O (dY_O / dr) = m_O \quad ,$$
$$mY_i - 4\pi r_b^2 \rho D_i (dY_i / dr) = 0 \quad , \quad i = F, R, S \quad ; \tag{4.1}$$

$$r \to \infty \quad : \quad T \to T_\infty \quad , \quad Y_F \to Y_{F,\infty} \quad , \quad Y_i \to 0 \quad , \quad i = O, R, S \quad , \tag{4.2}$$

where $m_O = m\, Y_{O,0}$ is the initial mass flow rate of the oxidizer issued from the burner. All other notations are the same as those adopted in Chapter 3 and will not be repeated.

Adopting the nondimensional quantities introduced in Chapters 2 and 3, then defining a nondimensional oxidizer flow rate parameter as

$$\overline{m}_O = \frac{m_O}{m}\frac{\nu_{F,1}W_F}{\nu_{O,1}W_O} \quad ,$$

we nondimensionalize Eqs. (3.2)–(3.6) to Eqs. (3.9)–(3.13), and Eqs. (4.1)–(4.2) to

$$\tilde{r}=1 \quad : \quad \tilde{T}=\tilde{T}_b \quad , \quad \tilde{m}\tilde{Y}_O - \frac{1}{Le_O}\frac{d\tilde{Y}_O}{d\tilde{r}} = \tilde{m}\overline{m}_O \quad ,$$

$$\tilde{m}\tilde{Y}_i - \frac{1}{Le_i}\frac{d\tilde{Y}_i}{d\tilde{r}} = 0 \quad , \quad i=F,R,S \quad ; \tag{4.3}$$

$$\tilde{r}\to\infty \quad : \quad \tilde{T}\to\tilde{T}_\infty \quad , \quad \tilde{Y}_F\to\tilde{Y}_{F,\infty} \quad , \quad \tilde{Y}_i\to 0 \quad , \quad i=O,R,S \quad . \tag{4.4}$$

4.2 Asymptotic Analysis

In the following analysis, the same high activation energy asymptotics adopted in Chapter 2 and 3 will be applied.

4.2.1 Outer Solutions

In the chemically inert outer regions, the process is controlled by the balance between the diffusion and convection transport. Designating the solutions in the oxidizer and fuel sides of the reaction regions by superscripts "–" and "+", respectively, and solving the source free expression of Eqs. (3.9)–(3.13) subject to the boundary conditions in Eqs. (4.3) and (4.4), we obtain the outer solutions:

$$\tilde{T}^- = \tilde{T}_b + \{[a^-_{\tilde{T},0} + \delta a^-_{\tilde{T},1} + O(\delta^2)] + O(\varepsilon)\}[\exp(-\tilde{m}/\tilde{r}) - \exp(-\tilde{m})] \quad , \tag{4.5a}$$

$$\tilde{T}^{+} = \tilde{T}_{\infty} + \{[a^{+}_{T,0} + \delta a^{+}_{T,1} + O(\delta^2)] + O(\varepsilon)\}[1 - \exp(-\tilde{m}/\tilde{r})] \quad , \tag{4.5b}$$

$$\tilde{Y}^{-}_{F} = \{[a^{-}_{F,0} + \delta a^{-}_{F,1} + O(\delta^2)] + O(\varepsilon)\}\exp(-Le_F \tilde{m}/\tilde{r}) \quad , \tag{4.6a}$$

$$\tilde{Y}^{+}_{F} = \tilde{Y}_{F,\infty} - \{[a^{+}_{F,0} + \delta a^{+}_{F,1} + O(\delta^2)] + O(\varepsilon)\}[1 - \exp(-Le_F \tilde{m}/\tilde{r})] \quad , \tag{4.6b}$$

$$\tilde{Y}^{-}_{O} = \overline{m}_{O} - \{[a^{-}_{O,0} + \delta a^{-}_{O,1} + O(\delta^2)] + O(\varepsilon)\}\exp(-Le_O \tilde{m}/\tilde{r}) \quad , \tag{4.7a}$$

$$\tilde{Y}^{+}_{O} = \{[a^{+}_{O,0} + \delta a^{+}_{O,1} + O(\delta^2)] + O(\varepsilon)\}[1 - \exp(-Le_O \tilde{m}/\tilde{r})] \quad , \tag{4.7b}$$

$$\tilde{Y}^{-}_{i} = \{[a^{-}_{i,0} + \delta a^{-}_{i,1} + O(\delta^2)] + O(\varepsilon)\}\exp(-Le_i \tilde{m}/\tilde{r}) \quad , \quad i = S, R \quad , \tag{4.8a}$$

$$\tilde{Y}^{+}_{i} = \{[a^{+}_{i,0} + \delta a^{+}_{i,1} + O(\delta^2)] + O(\varepsilon)\}[1 - \exp(-Le_i \tilde{m}/\tilde{r})] \quad , \quad i = S, R \quad , \tag{4.8b}$$

where $a^{\pm}_{i,j}$ are integration constants to be determined from the analysis.

4.2.2 Structure Equations in the Soot Formation Region

In the $O(\delta)$ soot/precursor formation region located in the fuel side of, and adjacent to, the oxidation region, only the soot/precursor formation reaction (R2) is significant and only $O(\delta)$ variations on all the quantities are possible. In this region, the stretched coordinate is defined as $\zeta = (\tilde{r} - \tilde{r}_f)/\delta$ with $\zeta > 0$, where the small parameter is given by $\delta = \tilde{T}^{2}_{f,0}/\tilde{E}_2$, and the expansion of the variables are Eqs. (3.54)–(3.56). As in Chapter 3, the soot/precursor concentration is considered an $O(1)$ quantity because the soot/precursor formation and consumption reactions have different rates, and $\Phi^{+}_{O,1} \equiv 0$ because only an $O(\varepsilon)$ oxidizer leakage through the oxidation region into this region possible.

Substituting Eqs. (3.54)–(3.56) into Eqs. (3.9)–(3.13), expanding, then

collecting terms of the same order in δ, we obtain the following structure equations:

$$\frac{d^2\Phi_{F,1}^+}{d\zeta^2} = \Lambda_2 \Phi_{F,1}^+ \Phi_{R,1}^+ \exp(-\Theta_1^+) \quad , \tag{4.9}$$

$$\frac{d^2\Phi_{S,0}^+}{d\zeta^2} = \frac{d^2\Theta_1^+}{d\zeta^2} = \frac{1}{Le_F}\frac{d^2\Phi_{F,1}^+}{d\zeta^2} - \frac{\tilde{\nu}_F}{Le_R}\frac{d^2\Phi_{R,1}^+}{d\zeta^2}$$

$$= \left(\tilde{m} - \frac{2\tilde{r}_f}{Le_S}\right)\frac{d\Phi_{S,0}^+}{d\zeta} - \tilde{r}_f^2\left(\frac{\tilde{\nu}_F}{Le_R}\frac{d^2\Phi_{R,1}^+}{d\zeta^2} + \frac{1}{Le_S}\frac{d^2\Phi_{S,1}^+}{d\zeta^2}\right) = 0 \quad , \tag{4.10}$$

$$\tilde{r}_f^2\left(\frac{d^2\Theta_2^+}{d\zeta^2} - \frac{\tilde{q}_S\hat{\nu}}{Le_O}\frac{d^2\Phi_{O,2}^+}{d\zeta^2}\right) - \left(\tilde{m} - 2\tilde{r}_f\right)\frac{d\Theta_1^+}{d\zeta} = 0 \quad , \tag{4.11}$$

$$\tilde{m}\left(\frac{d\Phi_{F,1}^+}{d\zeta} - \tilde{\nu}_F\frac{d\Phi_{R,1}^+}{d\zeta}\right) - \tilde{r}_f^2\left(\frac{1}{Le_F}\frac{d^2\Phi_{F,2}^+}{d\zeta^2} - \frac{\tilde{\nu}_F}{Le_R}\frac{d^2\Phi_{R,2}^+}{d\zeta^2}\right)$$

$$-2\tilde{r}_f\left(\frac{1}{Le_F}\frac{d\Phi_{F,1}^+}{d\zeta} - \frac{\tilde{\nu}_F}{Le_R}\frac{d\Phi_{R,1}^+}{d\zeta}\right) = 0 \quad , \tag{4.12}$$

$$\tilde{m}\left[\frac{d\Phi_{F,1}^+}{d\zeta} + \frac{d\Phi_{S,1}^+}{d\zeta}\right] - \tilde{r}_f^2\left[\frac{1}{Le_F}\frac{d^2\Phi_{F,2}^+}{d\zeta^2} + \frac{1}{Le_S}\frac{d^2\Phi_{S,2}^+}{d\zeta^2} - \frac{\hat{\nu}}{Le_O}\frac{d^2\Phi_{O,2}^+}{d\zeta^2}\right]$$

$$-2\tilde{r}_f\left[\frac{1}{Le_F}\frac{d\Phi_{F,1}^+}{d\zeta} + \frac{1}{Le_S}\frac{d\Phi_{S,1}^+}{d\zeta}\right] - 2\zeta\left[\frac{\tilde{m}}{\tilde{r}_f} - \frac{1}{Le_S}\right]\frac{d\Phi_{S,0}^+}{d\zeta} = 0 \quad , \tag{4.13}$$

where the reduced Damköhler number of the soot/precursor formation reaction, Λ_2, is given by Eq. (3.28).

4.2.3 Matching of Solutions in the Outer and Soot Formation Regions

The boundary conditions to solve Eqs. (4.9)–(4.13) need to be derived from matching the solutions in this region with the outer solutions in the

fuel side. Matching can be performed by the same procedure described in Section 3.2.3 except that the matching conditions obtained are for the limit of $\zeta \to \infty$.

Taking the matching of the fuel concentration as an illustration, by substituting Eq. (3.30) into Eq. (4.6b), rearranging in terms of δ, and equating the resulting equation with Eq. (3.55) for $i = F$, we obtain

$$\begin{aligned}
\tilde{Y}_F^+ &= \tilde{Y}_{F,\infty} - \{[a_{F,0}^+ + \delta a_{F,1}^+ + O(\delta^2)] + O(\varepsilon)\}[1 - \exp(-Le_F \tilde{m}/\tilde{r})] \\
&= \tilde{Y}_{F,\infty} - \{[a_{F,0}^+ + \delta a_{F,1}^+ + O(\delta^2)] + O(\varepsilon)\} \\
&\quad \times \left\{1 - \exp\left(-\frac{Le\tilde{m}}{\tilde{r}_f}\right)\left[1 + \delta\frac{Le\tilde{m}\zeta}{\tilde{r}_f^2} - \delta^2\frac{Le\tilde{m}}{\tilde{r}_f^3}\left(2 - \frac{Le\tilde{m}}{\tilde{r}_f}\right)\frac{\zeta^2}{2} + O(\delta^3)\right]\right\} \\
&= \tilde{Y}_{F,\infty} - a_{F,0}^+\left[1 - \exp\left(-\frac{Le_F\tilde{m}}{\tilde{r}_f}\right)\right] \\
&\quad - \delta\left\{a_{F,1}^+\left[1 - \exp\left(-\frac{Le_F\tilde{m}}{\tilde{r}_f}\right)\right] - a_{F,0}^+\frac{Le_F\tilde{m}}{\tilde{r}_f^2}\exp\left(-\frac{Le_F\tilde{m}}{\tilde{r}_f}\right)\zeta\right\} \\
&\quad + \delta^2\left\{a_{F,1}^+\zeta - \frac{a_{F,0}^+}{\tilde{r}_f}\left(2 - \frac{Le_F\tilde{m}}{\tilde{r}_f}\right)\frac{\zeta^2}{2} + const\right\}\frac{Le_F\tilde{m}}{\tilde{r}_f^2}\exp\left(-\frac{Le_F\tilde{m}}{\tilde{r}_f}\right) \\
&\quad + O(\delta^3) + O(\varepsilon) \\
&= \{[\delta\Phi_{F,1}^+ + \delta^2\Phi_{F,2}^+ + O(\delta^3)] + O(\varepsilon)\}_{\zeta\to\infty} \quad . \qquad (4.14)
\end{aligned}$$

By comparing terms of the same order in δ, we have the following matching conditions:

$$\begin{aligned}
&\tilde{Y}_{F,\infty} - a_{F,0}^+[1 - \exp(-Le_F\tilde{m}/\tilde{r}_f)] = 0 \\
&\text{or} \quad a_{F,0}^+ = \tilde{Y}_{F,\infty}/[1 - \exp(Le_F\tilde{m}/\tilde{r}_f)] \quad , \qquad (4.15)
\end{aligned}$$

$$\Phi^{+}_{F,1}(\zeta \to \infty) = -a^{+}_{F,1}[1-\exp(-Le_F \tilde{m} / \tilde{r}_f)]$$
$$+ a^{+}_{F,0}(Le_F \tilde{m} / \tilde{r}_f^2)\exp(-Le_F \tilde{m} / \tilde{r}_f)\zeta \quad , \tag{4.16a}$$

$$(d\Phi^{+}_{F,2} / d\zeta)_{\zeta\to\infty} = \left\{a^{+}_{F,1} - \frac{a^{+}_{F,0}}{\tilde{r}_f}\left(2 - \frac{Le_F \tilde{m}}{\tilde{r}_f}\right)\zeta\right\}\frac{Le_F \tilde{m}}{\tilde{r}_f^2}\exp\left(-\frac{Le_F \tilde{m}}{\tilde{r}_f}\right) \quad . \tag{4.17}$$

Equation (4.16a) also implies

$$(d\Phi^{+}_{F,1} / d\zeta)_{\zeta\to\infty} = a^{+}_{F,0}(Le_F \tilde{m} / \tilde{r}_f^2)\exp(-Le_F \tilde{m} / \tilde{r}_f) \quad . \tag{4.16b}$$

Applying the same procedure, the matching conditions for other variables are given by

$$a^{+}_{T,0} = (\tilde{T}_{f,0} - \tilde{T}_\infty) / [1-\exp(-\tilde{m} / \tilde{r}_f)] \quad , \tag{4.18}$$

$$a^{+}_{O,0} = a^{+}_{O,1} = a^{+}_{R,0} = 0 \quad , \tag{4.19}$$

$$\Theta^{+}_1(\zeta \to \infty) = -a^{+}_{T,1}\left[1-\exp\left(-\frac{\tilde{m}}{\tilde{r}_f}\right)\right] + a^{+}_{T,0}\frac{\tilde{m}}{\tilde{r}_f^2}\exp\left(-\frac{\tilde{m}}{\tilde{r}_f}\right)\zeta \quad , \tag{4.20}$$

$$\left(\frac{d\Theta^{+}_2}{d\zeta}\right)_{\zeta\to\infty} = -\left\{a^{+}_{T,1} - \frac{a^{+}_{T,0}}{\tilde{r}_f}\left(2 - \frac{\tilde{m}}{\tilde{r}_f}\right)\zeta\right\}\frac{\tilde{m}}{\tilde{r}_f^2}\exp\left(-\frac{\tilde{m}}{\tilde{r}_f}\right) \quad , \tag{4.21}$$

$$(d\Phi^{+}_{O,2} / d\zeta)_{\zeta\to\infty} = 0 \quad , \tag{4.22}$$

$$\Phi^{+}_{R,1}(\zeta \to \infty) = a^{+}_{R,1}[1-\exp(-Le_R \tilde{m} / \tilde{r}_f)] \quad , \tag{4.23}$$

$$(d\Phi^{+}_{R,2} / d\zeta)_{\zeta\to\infty} = a^{+}_{R,1}(Le_R \tilde{m} / \tilde{r}_f^2)\exp(-Le_R \tilde{m} / \tilde{r}_f) \quad , \tag{4.24}$$

$$\Phi^{+}_{S,0}(\zeta \to \infty) = a^{+}_{S,0}[1-\exp(-Le_S \tilde{m} / \tilde{r}_f)] \quad , \tag{4.25}$$

$$\Phi^{+}_{S,1}(\zeta \to \infty) = a^{+}_{S,1}[1-\exp(-Le_S \tilde{m} / \tilde{r}_f)]$$

$$-a_{S,0}^{+}(Le_S\tilde{m}/\tilde{r}_f^2)\zeta]\exp(-Le_S\tilde{m}/\tilde{r}_f) \quad , \tag{4.26}$$

$$\left(\frac{d\Phi_{S,2}^{+}}{d\zeta}\right)_{\zeta\to\infty}=\left\{a_{S,1}^{+}-\frac{a_{S,0}^{+}}{\tilde{r}_f}\left(2-\frac{Le_S\tilde{m}}{\tilde{r}_f}\right)\zeta\right\}\frac{Le_S\tilde{m}}{\tilde{r}_f^2}\exp\left(-\frac{Le_S\tilde{m}}{\tilde{r}_f}\right) \quad . \tag{4.27}$$

Integrating the four expressions in Eq. (4.10) twice and Eqs. (4.11)–(4.13) once subject to the above matching conditions, we obtain

$$\Phi_{S,0}^{+}=a_{S,0}^{+}[1-\exp(-Le_S\tilde{m}/\tilde{r}_f)] \quad , \tag{4.28}$$

$$\Theta_1^{+}=-a_{T,1}^{+}\left[1-\exp\left(-\frac{\tilde{m}}{\tilde{r}_f}\right)\right]+\left[\frac{(\tilde{T}_{f,0}-\tilde{T}_\infty)\tilde{m}/\tilde{r}_f^2}{\exp(\tilde{m}/\tilde{r}_f)-1}\right]\zeta \quad , \tag{4.29}$$

$$\frac{\Phi_{F,1}^{+}}{Le_F}-\tilde{\nu}_F\frac{\Phi_{R,1}^{+}}{Le_R}=-\frac{a_{F,1}^{+}}{Le_F}\left[1-\exp\left(-\frac{Le_F\tilde{m}}{\tilde{r}_f}\right)\right]$$
$$-\tilde{\nu}_F\frac{a_{R,1}^{+}}{Le_R}\left[1-\exp\left(-\frac{Le_R\tilde{m}}{\tilde{r}_f}\right)\right]+\frac{\tilde{Y}_{F,\infty}(\tilde{m}/\tilde{r}_f^2)}{\exp(Le_F\tilde{m}/\tilde{r}_f)}\zeta \quad , \tag{4.30}$$

$$\tilde{\nu}_F\frac{\Phi_{R,1}^{+}}{Le_R}+\frac{\Phi_{S,1}^{+}}{Le_S}=\tilde{\nu}_F\frac{a_{R,1}^{+}}{Le_R}\left[1-\exp\left(-\frac{Le_R\tilde{m}}{\tilde{r}_f}\right)\right]+\frac{a_{S,1}^{+}}{Le_S}\left[1-\exp\left(-\frac{Le_S\tilde{m}}{\tilde{r}_f}\right)\right]$$
$$-\frac{a_{S,0}^{+}\tilde{m}}{\tilde{r}_f^2}\exp\left(-\frac{Le_S\tilde{m}}{\tilde{r}_f}\right)\zeta \quad , \tag{4.31}$$

$$\left(\frac{d\Theta_2^{+}}{d\zeta}\right)-\frac{\tilde{q}_S\,\hat{\nu}}{Le_O}\left(\frac{d\Phi_{O,2}^{+}}{d\zeta}\right)=\frac{\tilde{m}}{\tilde{r}_f^2}\left[a_{T,1}^{+}+\frac{a_{T,0}^{+}}{\tilde{r}_f}\left(2-\frac{\tilde{m}}{\tilde{r}_f}\right)\zeta\right]\exp\left(-\frac{\tilde{m}}{\tilde{r}_f}\right) \quad , \tag{4.32}$$

$$\frac{1}{Le_F}\frac{d\Phi_{F,1}^{+}}{d\zeta}-\frac{\tilde{\nu}_F}{Le_R}\frac{d\Phi_{R,1}^{+}}{d\zeta}=\frac{\tilde{Y}_{F,\infty}(\tilde{m}/\tilde{r}_f^2)}{\exp(Le_F\tilde{m}/\tilde{r}_f)-1} \quad , \tag{4.33}$$

$$\frac{\tilde{\nu}_F}{Le_R}\frac{d\Phi_{R,1}^{+}}{d\zeta}+\frac{1}{Le_S}\frac{d\Phi_{S,1}^{+}}{d\zeta}=-\frac{a_{S,0}^{+}\tilde{m}}{\tilde{r}_f^2}\exp\left(-\frac{Le_S\tilde{m}}{\tilde{r}_f}\right) \quad , \tag{4.34}$$

$$\tilde{m}(\Phi^+_{F,1} - \tilde{\nu}_F \Phi^+_{R,1}) - \tilde{r}_f^2\left(\frac{1}{Le_F}\frac{d\Phi^+_{F,2}}{d\zeta} - \frac{\tilde{\nu}_F}{Le_R}\frac{d\Phi^+_{R,2}}{d\zeta}\right)$$

$$= -\tilde{m}(a^+_{F,1} + \tilde{\nu}_F a^+_{R,1}) + 2a^+_{F,0}(\tilde{m}/\tilde{r}_f)\exp(-Le_F\tilde{m}/\tilde{r}_f)\zeta \quad , \tag{4.35}$$

$$\tilde{m}(\tilde{\nu}_F\Phi^+_{R,1} + \Phi^+_{S,1}) - \tilde{r}_f^2\left(\frac{\tilde{\nu}_F}{Le_R}\frac{d\Phi^+_{R,2}}{d\zeta} + \frac{1}{Le_S}\frac{d\Phi^+_{S,2}}{d\zeta} - \frac{\hat{\nu}}{Le_O}\frac{d\Phi^+_{O,2}}{d\zeta}\right)$$

$$= \tilde{m}(\tilde{\nu}_F a^+_{R,1} + a^+_{S,1}) - a^+_{S,0}(2\tilde{m}/\tilde{r}_f)\exp(-Le_S\tilde{m}/\tilde{r}_f)\zeta \quad . \tag{4.36}$$

In the above, Eqs. (4.33) and (4.34) are obtained by differentiating Eqs. (4.30) and (4.31) with respect to ζ.

4.2.4 Structure Equations in the Soot Consumption Region

In the $O(\delta)$ soot/precursor consumption region located in the oxidizer side of, and adjacent to, the oxidation region, only the soot/precursor consumption reaction (R3) is important. In this region, the same stretched coordinate, $\zeta = (\tilde{r} - \tilde{r}_f)/\delta$, is used, but with $\zeta < 0$, and the expansion of the variables are Eqs. (3.20)–(3.22) with $\Phi^-_{F,1} \equiv 0$.

Substituting Eqs. (3.20)–(3.22) into Eqs. (3.9)–(3.13), expanding and collecting terms of the same order in δ, we obtain the following structure equations:

$$d^2\Phi^-_{O,1}/d\zeta^2 = \Lambda_3 \Phi^-_{S,0}\Phi^-_{O,1}\exp(-\alpha\Theta^-_1) \quad , \tag{4.37}$$

$$\frac{d^2\bar{\Phi}_{S,0}}{d\zeta^2}=\frac{d^2\bar{\Phi}_{R,1}}{d\zeta^2}=\frac{d^2\bar{\Theta}_1}{d\zeta^2}-\frac{\tilde{q}_S\,\hat{\nu}}{Le_O}\frac{d^2\bar{\Phi}_{O,1}}{d\zeta^2}$$

$$=\left(\frac{\hat{\nu}}{Le_O}\frac{d^2\bar{\Phi}_{O,1}}{d\zeta^2}-\frac{1}{Le_S}\frac{d^2\bar{\Phi}_{S,1}}{d\zeta^2}\right)+\left(\frac{\tilde{m}}{\tilde{r}_f^2}-\frac{2}{\tilde{r}_f Le_S}\right)\frac{d\bar{\Phi}_{S,0}}{d\zeta}=0 \quad , \tag{4.38}$$

$$\left(\frac{1}{Le_F}\frac{d^2\bar{\Phi}_{F,2}}{d\zeta^2}-\frac{\tilde{\nu}_F}{Le_R}\frac{d^2\bar{\Phi}_{R,2}}{d\zeta^2}\right)+\tilde{\nu}_F\left(\frac{\tilde{m}}{\tilde{r}_f^2}-\frac{2}{\tilde{r}_f Le_R}\right)\frac{d\bar{\Phi}_{R,1}}{d\zeta}=0 \quad , \tag{4.39}$$

$$\tilde{r}_f^2\left(\frac{d^2\bar{\Theta}_2}{d\zeta^2}-\frac{\tilde{q}_S\,\hat{\nu}}{Le_O}\frac{d^2\bar{\Phi}_{O,2}}{d\zeta^2}\right)-\tilde{m}\left(\frac{d\bar{\Theta}_1}{d\zeta}-\tilde{q}_S\,\hat{\nu}\frac{d\bar{\Phi}_{O,1}}{d\zeta}\right)$$

$$+2\tilde{r}_f\left(\frac{d\bar{\Theta}_1}{d\zeta}-\frac{\tilde{q}_S\,\hat{\nu}}{Le_O}\frac{d\bar{\Phi}_{O,1}}{d\zeta}\right)=0 \quad , \tag{4.40}$$

$$\tilde{r}_f^2\left[\frac{\hat{\nu}}{Le_O}\frac{d^2\bar{\Phi}_{O,2}}{d\zeta^2}-\frac{1}{Le_S}\frac{d^2\bar{\Phi}_{S,2}}{d\zeta^2}-\frac{1}{Le_F}\frac{d^2\bar{\Phi}_{F,2}}{d\zeta^2}\right]+\tilde{m}\left[\frac{d\bar{\Phi}_{S,1}}{d\zeta}-\hat{\nu}\frac{d\bar{\Phi}_{O,1}}{d\zeta}\right]$$

$$+2\tilde{r}_f\left[\frac{\hat{\nu}}{Le_O}\frac{d\bar{\Phi}_{O,1}}{d\zeta}-\frac{1}{Le_S}\frac{d\bar{\Phi}_{S,1}}{d\zeta}\right]-2\zeta\left[\frac{\tilde{m}}{\tilde{r}_f}-\frac{1}{Le_S}\right]\frac{d\bar{\Phi}_{S,0}}{d\zeta}=0 \quad , \tag{4.41}$$

where the reduced Damköhler number of the soot/precursor consumption reaction, Λ_3, is given by Eq. (3.62).

4.2.5 Matching of Solutions in the Outer and Soot Consumption Regions

Matching of the solutions in the soot consumption region with the outer solutions in the oxidizer side is performed by an approach similar to that described in Section 3.2.3 and illustrated in Eqs. (3.29), (3.30) and (4.14), with $\zeta\to-\infty$. The process yields the solutions of leading order constants,

$$a_{\bar{T},0}=(\tilde{T}_{f,0}-\tilde{T}_b)/[\exp(-\tilde{m}/\tilde{r}_f)-\exp(-\tilde{m})] \quad , \tag{4.42}$$

$$a_{O,0}^{-} = \overline{m}_O \exp(Le_O \tilde{m} / \tilde{r}_f)] \quad , \tag{4.43}$$

$$a_{F,0}^{-} = a_{F,1}^{-} = a_{R,0}^{-} = 0 \quad , \tag{4.44}$$

and the boundary conditions required to solve Eqs. (4.37)–(4.41), given by

$$\Phi_{O,1}^{-}(\zeta \to -\infty) = -a_{O,1}^{-} \exp(-Le_O \tilde{m} / \tilde{r}_f) - (Le_O \tilde{m} \overline{m}_O / \tilde{r}_f^2)\zeta \quad , \tag{4.45a}$$

$$\Theta_1^{-}(\zeta \to -\infty) = -a_{T,1}^{+}[\exp(-\tilde{m} / \tilde{r}_f) - \exp(-\tilde{m})]$$
$$-[a_{T,0}^{-}(\tilde{m} / \tilde{r}_f^2)\exp(-\tilde{m} / \tilde{r}_f)]\zeta \quad , \tag{4.46}$$

$$\left(\frac{d\Theta_2^{-}}{d\zeta}\right)_{\zeta \to -\infty} = -\frac{\tilde{m}}{\tilde{r}_f^2}\left[a_{T,1}^{-} - \frac{a_{T,0}^{-}}{\tilde{r}_f}\left(2 - \frac{\tilde{m}}{\tilde{r}_f}\right)\zeta\right]\exp\left(-\frac{\tilde{m}}{\tilde{r}_f}\right) \quad , \tag{4.47}$$

$$(d\Phi_{F,2}^{-} / d\zeta)_{\zeta \to -\infty} = 0 \quad , \tag{4.48}$$

$$\left(\frac{d\Phi_{O,2}^{-}}{d\zeta}\right)_{\zeta \to -\infty} = -\left[a_{O,1}^{-} - \frac{a_{O,0}^{-}}{\tilde{r}_f}\left(2 - \frac{Le_O \tilde{m}}{\tilde{r}_f}\right)\zeta\right]\frac{Le_O \tilde{m}}{\tilde{r}_f^2}\exp\left(-\frac{Le_O \tilde{m}}{\tilde{r}_f}\right) \quad , \tag{4.49}$$

$$\Phi_{R,1}^{-}(\zeta \to -\infty) = a_{R,1}^{-} \exp(-Le_R \tilde{m} / \tilde{r}_f) \quad , \tag{4.50}$$

$$(d\Phi_{R,2}^{-} / d\zeta)_{\zeta \to -\infty} = a_{R,1}^{-}(Le_R \tilde{m} / \tilde{r}_f^2)\exp(-Le_R \tilde{m} / \tilde{r}_f) \quad , \tag{4.51}$$

$$\Phi_{S,0}^{-}(\zeta \to -\infty) = a_{S,0}^{-}[1 - \exp(-Le_S \tilde{m} / \tilde{r}_f)] \quad , \tag{4.52}$$

$$\Phi_{S,1}^{-}(\zeta \to -\infty) = [a_{S,1}^{-} + a_{S,0}^{-}(Le_S \tilde{m} / \tilde{r}_f)\zeta]\exp(-Le_S \tilde{m} / \tilde{r}_f)] \tag{4.53}$$

$$\left(\frac{d\Phi_{S,2}^{-}}{d\zeta}\right)_{\zeta \to -\infty} = \left[a_{S,1}^{-} - \frac{a_{S,0}^{-}}{\tilde{r}_f}\left(2 - \frac{Le_S \tilde{m}}{\tilde{r}_f}\right)\zeta\right]\frac{Le_S \tilde{m}}{\tilde{r}_f^2}\exp\left(-\frac{Le_S \tilde{m}}{\tilde{r}_f}\right) \quad . \tag{4.54}$$

Equation (4.45a) also implies

$$(d\Phi_{O,1}^{-}/d\zeta)_{\zeta\to-\infty} = -(Le_O\,\tilde{m}\,\overline{m}_O/\tilde{r}_f^2) \quad . \tag{4.45b}$$

Integrating the four expressions in Eq. (4.38) twice and Eqs. (4.39)–(4.41) once subject to the above matching conditions, we have

$$\Phi_{S,0}^{-} = a_{S,0}^{-}\exp(-Le_S\,\tilde{m}/\tilde{r}_f) \quad , \tag{4.55}$$

$$\Phi_{R,1}^{-} = a_{R,1}^{-}\exp(-Le_R\,\tilde{m}/\tilde{r}_f) \quad , \tag{4.56}$$

$$\Theta_1^{-} - \tilde{q}_S\,\hat{\nu}\frac{\Phi_{O,1}^{-}}{Le_O} = a_{O,1}^{-}\frac{\tilde{q}_S\,\hat{\nu}}{Le_O}\exp\left(-\frac{Le_O\,\tilde{m}}{\tilde{r}_f}\right) - a_{T,1}^{-}\left[\exp\left(-\frac{\tilde{m}}{\tilde{r}_f}\right) - \exp(-\tilde{m})\right]$$
$$-\frac{\tilde{m}}{\tilde{r}_f^2}\left[\frac{\tilde{T}_{f,0}-\tilde{T}_b}{1-\exp[\tilde{m}(\tilde{r}_f^{-1}-1)]} - \tilde{q}_S\,\hat{\nu}\,\overline{m}_O\right]\zeta \quad , \tag{4.57}$$

$$\hat{\nu}\frac{\Phi_{O,1}^{-}}{Le_O} - \frac{\Phi_{S,1}^{-}}{Le_S} = -\frac{a_{O,1}^{-}\,\hat{\nu}}{Le_O}\exp\left(-\frac{Le_O\,\tilde{m}}{\tilde{r}_f}\right) - \frac{a_{S,1}^{-}}{Le_S}\exp\left(-\frac{Le_S\,\tilde{m}}{\tilde{r}_f}\right)$$
$$-\frac{\tilde{m}}{\tilde{r}_f^2}\left[\hat{\nu}\,\overline{m}_O + a_{S,0}^{-}\exp\left(-\frac{Le_S\,\tilde{m}}{\tilde{r}_f}\right)\right]\zeta \quad , \tag{4.58}$$

$$\frac{1}{Le_F}\frac{d\Phi_{F,2}^{-}}{d\zeta} - \frac{\tilde{\nu}_F}{Le_R}\frac{d\Phi_{R,2}^{-}}{d\zeta} = -a_{R,1}^{-}\,\tilde{\nu}_F\frac{\tilde{m}}{\tilde{r}_f^2}\exp\left(-\frac{Le_R\,\tilde{m}}{\tilde{r}_f}\right) \quad , \tag{4.59}$$

$$\frac{d\Theta_1^{-}}{d\zeta} - \frac{\tilde{q}_S\,\hat{\nu}}{Le_O}\frac{d\Phi_{O,1}^{-}}{d\zeta} = -\frac{\tilde{m}}{\tilde{r}_f^2}\left[\frac{\tilde{T}_{f,0}-\tilde{T}_b}{1-\exp[\tilde{m}(\tilde{r}_f^{-1}-1)]} - \tilde{q}_S\,\hat{\nu}\,\overline{m}_O\right] \quad , \tag{4.60}$$

$$\frac{\hat{\nu}}{Le_O}\frac{d\Phi_{O,1}^{-}}{d\zeta} - \frac{1}{Le_S}\frac{d\Phi_{S,1}^{-}}{d\zeta} = -\frac{\tilde{m}}{\tilde{r}_f^2}\left[\hat{\nu}\,\overline{m}_O + a_{S,0}^{-}\exp\left(-\frac{Le_S\,\tilde{m}}{\tilde{r}_f}\right)\right] \quad , \tag{4.61}$$

$$\tilde{r}_f^2[(d\Theta_2^{-}/d\zeta) - (\tilde{q}_S\,\hat{\nu}/Le_O)(d\Phi_{O,2}^{-}/d\zeta)] - \tilde{m}(\Theta_1^{-} - \tilde{q}_S\,\hat{\nu}\Phi_{O,1}^{-})$$
$$= (2\tilde{m}/\tilde{r}_f)[a_{T,0}^{-}\exp(\tilde{m}/\tilde{r}_f) - \tilde{q}_S\hat{\nu}\,\overline{m}_O]\zeta - \tilde{m}a_{T,1}^{-}\exp(-\tilde{m}) \quad , \tag{4.62}$$

$$\tilde{r}_f^2[(\hat{v}/Le_O)(d\bar{\Phi}_{O,2}/d\zeta)-(1/Le_S)(d\bar{\Phi}_{S,2}/d\zeta)-(1/Le_F)(d\bar{\Phi}_{F,2}/d\zeta)]$$
$$=(2\tilde{m}/\tilde{r}_f)[\bar{a}_{S,0}\exp(-Le_S\tilde{m}/\tilde{r}_f)+\hat{v}\bar{m}_O]\zeta-\tilde{m}(\bar{\Phi}_{S,1}-\hat{v}\bar{\Phi}_{O,1}) \quad . \tag{4.63}$$

In the above, Eqs. (4.60) and (4.61) are obtained by differentiating Eqs. (4.57) and (4.58) with respect to ζ. These equations will be used later in the analysis.

4.2.6 Expansions in the Oxidation Region

In the $O(\varepsilon)$ oxidation region, the dominating reaction is the oxidation reaction (R1). The proper stretched coordinate in this region is $\tilde{r}=\tilde{r}_f+\varepsilon\xi$, where $\varepsilon=\tilde{T}_f^2/\tilde{E}_1$. The expansions of the variables are Eqs. (3.85)–(3.89), and the conservation equations are Eqs. (3.90)–(3.92).

4.2.7 Matching of Solutions in the Oxidation, Soot Formation and Soot Consumption Regions

The boundary conditions required to integrate Eqs. (3.90)–(3.92) need to be determined from matching the solutions in the oxidation region with those in the soot/precursor formation and consumption regions as $\xi\to\pm\infty$ and $\zeta\to 0$. Matching is performed following the same procedure introduced in Section 2.2.7 and will not be repeated. Taking the matching of fuel concentration as an example, by substituting Eq. (2.91) into Eqs. (3.21) and (3.55) with $i = F$, we have:

$$\tilde{Y}_F=[\delta^2\bar{\Phi}_{F,2}+O(\delta^3)]+O(\varepsilon)$$
$$=O(\delta^2)+\varepsilon[const+\delta(d\bar{\Phi}_{F,2}/d\zeta)_{\zeta=0}\xi+O(\delta^2)+O(\varepsilon/\delta)]+O(\varepsilon^2)$$
$$=\varepsilon\{[\phi_{F,1}+\delta\phi_{F,2}+O(\delta^2)]+O(\varepsilon/\delta)\}+O(\varepsilon^2)\Big|_{\xi\to-\infty} \quad . \tag{4.64}$$

$$\tilde{Y}_F^+ = [\delta \Phi_{F,1}^+ + \delta^2 \Phi_{F,2}^+ + O(\delta^3)] + O(\varepsilon)$$

$$= [\delta \Phi_{F,1}^+(\zeta = 0) + O(\delta^2)]$$

$$+ \varepsilon\{const + [(d\Phi_{F,1}^+ / d\zeta)_{\zeta=0} + \delta(d\Phi_{F,2}^+ / d\zeta)_{\zeta=0} + O(\delta^2)]\xi\}$$

$$+ O(\varepsilon^2) + O(\varepsilon / \delta)$$

$$= \varepsilon\{[\phi_{F,1} + \delta\phi_{F,2} + O(\delta^2)] + O(\varepsilon / \delta)\} + O(\varepsilon^2)\Big|_{\xi\to\infty} \quad , \tag{4.65}$$

Comparing terms of the same order in ε between Eqs. (4.64) and (4.65), we obtain

$$\Phi_{F,1}^+(\zeta = 0) = 0 \quad , \tag{4.66}$$

$$(d\phi_{F,j} / d\xi)_{\xi\to\pm\infty} = (d\Phi_{F,j}^{\pm} / d\zeta)_{\zeta=0} \quad , \quad j = 1, 2 \quad . \tag{4.67}$$

Application of the same matching procedure to other variables then gives:

$$\Phi_{O,1}^-(\zeta = 0) = 0 \quad , \tag{4.68}$$

$$\tilde{T}_{f,1} = \Theta_1^-(\zeta = 0) = \Theta_1^+(\zeta = 0) = -a_{T,1}^+[1 - \exp(-\tilde{m} / \tilde{r}_f)] \quad , \tag{4.69}$$

$$a_{T,1}^-\left[\exp\left(-\frac{\tilde{m}}{\tilde{r}_f}\right) - \exp(-\tilde{m})\right] - a_{O,1}^- \frac{\tilde{q}_S \hat{v}}{Le_O}\exp\left(-\frac{Le_O\tilde{m}}{\tilde{r}_f}\right)$$

$$= a_{T,1}^+[1 - \exp(-\tilde{m} / \tilde{r}_f)] \quad , \tag{4.70}$$

$$\tilde{Y}_{S,0}(\xi \to -\infty) = a_{S,0}^- \exp(-Le_S\tilde{m} / \tilde{r}_f) \quad , \tag{4.71a}$$

$$\tilde{Y}_{S,0}(\xi \to \infty) = a_{S,0}^+\left[1 - \exp(-Le_S\tilde{m} / \tilde{r}_f)\right] \quad , \tag{4.71b}$$

$$\phi_{R,0}(\xi \to -\infty) = a_{R,1}^- \exp(-Le_R\tilde{m} / \tilde{r}_f) \quad , \tag{4.72a}$$

$$\phi_{R,0}(\xi\to\infty)=a_{R,1}^{+}\left[1-\exp\left(-\frac{Le_R\tilde{m}}{\tilde{r}_f}\right)\right]+\frac{a_{F,1}^{+}Le_R}{\tilde{\nu}_F Le_F}\left[1-\exp\left(-\frac{Le_F\tilde{m}}{\tilde{r}_f}\right)\right] \quad , \tag{4.72b}$$

$$\phi_{S,0}(\xi\to-\infty)=a_{S,1}^{-}\exp\left(-\frac{Le_S\tilde{m}}{\tilde{r}_f}\right)+a_{O,1}^{-}\frac{\hat{\nu}Le_S}{Le_O}\exp\left(-\frac{Le_O\tilde{m}}{\tilde{r}_f}\right) \quad , \tag{4.73a}$$

$$\phi_{S,0}(\xi\to\infty)=a_{S,1}^{+}\left[1-\exp\left(-\frac{Le_S\tilde{m}}{\tilde{r}_f}\right)\right]-\frac{a_{F,1}^{+}Le_S}{Le_F}\left[1-\exp\left(-\frac{Le_F\tilde{m}}{\tilde{r}_f}\right)\right] \quad , \tag{4.73b}$$

$$(d\theta_j/d\xi)_{\xi\to\pm\infty}=(d\Theta_j^{\pm}/d\zeta)_{\zeta=0} \quad , \quad j=1,2 \quad , \tag{4.74}$$

$$(d\phi_{i,j}/d\xi)_{\xi\to\pm\infty}=(d\Phi_{i,j}^{\pm}/d\zeta)_{\zeta=0} \quad , \quad i=O,R,S \quad , \quad j=1,2 \quad . \tag{4.75}$$

Equations (4.28)–(4.31) and (4.55)–(4.58) were applied in the derivation of Eqs. (4.69)–(4.73).

Integrating the three expressions in Eq. (3.90) twice and the four expressions in each of Eqs. (3.91) and (3.92) once subject to Eqs. (4.67) and (4.71)–(4.75) results in

$$\tilde{Y}_{S,0}=\Phi_{S,0}^{-}=\Phi_{S,0}^{+} \quad , \tag{4.76}$$

$$\frac{a_{F,1}^{+}Le_R}{\tilde{\nu}_F Le_F}\left[1-\exp\left(-\frac{Le_F\tilde{m}}{\tilde{r}_f}\right)\right]=a_{R,1}^{-}\exp\left(-\frac{Le_R\tilde{m}}{\tilde{r}_f}\right)-a_{R,1}^{+}\left[1-\exp\left(-\frac{Le_R\tilde{m}}{\tilde{r}_f}\right)\right] \quad , \tag{4.77}$$

$$\frac{a_{F,1}^{+}Le_S}{Le_F}\left[1-\exp\left(-\frac{Le_F\tilde{m}}{\tilde{r}_f}\right)\right]+\frac{a_{O,1}^{-}\hat{\nu}Le_S}{Le_O}\exp\left(-\frac{Le_O\tilde{m}}{\tilde{r}_f}\right)$$
$$=a_{S,1}^{+}\left[1-\exp\left(-\frac{Le_S\tilde{m}}{\tilde{r}_f}\right)\right]-a_{S,1}^{-}\exp\left(-\frac{Le_S\tilde{m}}{\tilde{r}_f}\right) \quad , \tag{4.78}$$

$$(d\Phi_{S,1}^{-}/d\zeta)_{\zeta=0}=(d\Phi_{S,1}^{+}/d\zeta)_{\zeta=0} \quad , \tag{4.79}$$

$$(d\Theta_{1}^{-}/d\zeta)_{\zeta=0}+Le_F^{-1}(d\Phi_{F,1}^{+}/d\zeta)_{\zeta=0}=-a_{T,0}^{+}(\tilde{m}/\tilde{r}_f^{2})\exp(-\tilde{m}/\tilde{r}_f) \quad , \tag{4.80}$$

$$Le_F^{-1}(d\Phi_{F,1}^{+}/d\zeta)_{\zeta=0}+Le_O^{-1}(d\Phi_{O,1}^{-}/d\zeta)_{\zeta=0}=0 \quad , \tag{4.81}$$

$$Le_F^{-1}(d\Phi_{F,1}^{+}/d\zeta)_{\zeta=0}+Le_R^{-1}(d\Phi_{R,1}^{+}/d\zeta)_{\zeta=0}=0 \quad , \tag{4.82}$$

$$(d\Theta_{2}^{-}/d\zeta)_{\zeta=0}-(d\Theta_{2}^{+}/d\zeta)_{\zeta=0}$$
$$=Le_F^{-1}[(d\Phi_{F,2}^{-}/d\zeta)_{\zeta=0}-(d\Phi_{F,2}^{+}/d\zeta)_{\zeta=0}] \quad , \tag{4.83}$$

$$Le_F^{-1}[(d\Phi_{F,2}^{-}/d\zeta)_{\zeta=0}-(d\Phi_{F,2}^{+}/d\zeta)_{\zeta=0}]$$
$$=Le_O^{-1}[(d\Phi_{O,2}^{-}/d\zeta)_{\zeta=0}-(d\Phi_{O,2}^{+}/d\zeta)_{\zeta=0}] \quad , \tag{4.84}$$

$$Le_F^{-1}[(d\Phi_{F,2}^{-}/d\zeta)_{\zeta=0}-(d\Phi_{F,2}^{+}/d\zeta)_{\zeta=0}]$$
$$=-Le_R^{-1}[(d\Phi_{R,2}^{-}/d\zeta)_{\zeta=0}-(d\Phi_{R,2}^{+}/d\zeta)_{\zeta=0}] \quad , \tag{4.85}$$

$$(d\Phi_{S,2}^{-}/d\zeta)_{\zeta=0}=(d\Phi_{S,2}^{+}/d\zeta)_{\zeta=0} \quad . \tag{4.86}$$

4.2.8 Completion of the Analysis

The analysis will be finalized by substituting Eqs. (4.18), (4.33), (4.34), (4.60) and (4.61) into Eqs. (4.79)–(4.82) and rearranging, we obtain

$$\frac{\tilde{T}_{f,0}-\tilde{T}_b}{1-\exp[\tilde{m}(\tilde{r}_f^{-1}-1)]}+\frac{\tilde{T}_{f,0}-\tilde{T}_\infty}{\exp(\tilde{m}/\tilde{r}_f)-1}$$
$$=\frac{(1-\tilde{q}_S\,\hat{v})}{1+\tilde{v}_F}\frac{\tilde{Y}_{F,\infty}}{\exp(Le_F\,\tilde{m}/\tilde{r}_f)-1}+\tilde{q}_S\,\hat{v}\,\overline{m}_O \quad , \tag{4.87}$$

$$\tilde{Y}_{S,0} = \hat{\nu}\left[\frac{\nu^* \tilde{Y}_{F,\infty}}{\exp(Le_F \tilde{m}/\tilde{r}_f)-1} - \overline{m}_O\right]\left[1-\exp\left(-\frac{Le_S \tilde{m}}{\tilde{r}_f}\right)\right] \quad , \tag{4.88}$$

$$Le_F^{-1}(d\Phi^+_{F,1}/d\zeta)_{\zeta=0} = [\tilde{Y}_{F,\infty}(\tilde{m}/\tilde{r}_f^2)/(1+\tilde{\nu}_F)]/[\exp(Le_F\tilde{m}/\tilde{r}_f)-1] \quad , \tag{4.89}$$

$$Le_O^{-1}(d\Phi^-_{O,1}/d\zeta)_{\zeta=0} = -[\tilde{Y}_{F,\infty}(\tilde{m}/\tilde{r}_f^2)/(1+\tilde{\nu}_F)]/[\exp(Le_F\tilde{m}/\tilde{r}_f)-1] \quad . \tag{4.90}$$

Equations (4.87) and (4.88) are the ones that determine the leading order flame temperature, $\tilde{T}_{f,0}$, and soot/precursor concentration in the oxidation region, $\tilde{Y}_{S,0}$, in terms of flame sheet location, $\tilde{r}_f$. The solution of $\tilde{Y}_{S,0}$ can then be applied to determine $a^{\pm}_{S,0}$ through Eqs. (4.28), (4.55) and (4.76). In addition, substitution of Eqs. (4.32), (4.35)–(4.36) and (4.59), (4.62)–(4.63) into Eqs. (4.83)–(4.86) and rearranging results in

$$(1+\tilde{\nu}_F)[a^-_{T,1}\exp(-\tilde{m})+a^+_{T,1}] = (1-\tilde{q}_S\,\hat{\nu})(a^+_{F,1}+\tilde{\nu}_F\,a^+_{R,1}) \quad , \tag{4.91}$$

$$\hat{\nu}[a^+_{F,1}\nu^* - a^+_{R,1}(\nu^*-1)] - a^+_{S,1} = 0 \quad . \tag{4.92}$$

4.2.9 Rescale of the Structure Equations for Numerical Computations

The two remaining differential equations, Eq. (4.9) in the soot formation region and Eq. (4.37) in the soot consumption region, need to be solved numerically. Equation (4.9) with Θ^+_1 and $\Phi^+_{R,1}$ respectively given by Eqs. (4.29) and (4.30) is to be numerically integrated subject to the boundary conditions given by Eqs. (4.16a, b), (4.66) and (4.89). Similarly, Eq. (4.37) with Θ^-_1 given by Eq. (4.57), and $\Phi^-_{S,0}$ given by Eqs. (4.76) and (4.88) can be numerically solved subject to the boundary conditions described by Eqs. (4.45a, b), (4.68) and (4.90).

The numerical procedure can be facilitated by a transformation of variables. The transformation of Eq. (4.9) is performed by defining the rescaled variable and parameter

$$\eta = \{\tilde{Y}_{F,\infty}(Le_F \tilde{m} / \tilde{r}_f^2) / [\exp(Le_F \tilde{m} / \tilde{r}_f) - 1]\}\zeta \quad , \tag{4.93}$$

$$\tilde{\Lambda}_2 = (Da_2 Le_R / \tilde{\nu}_F)(\tilde{T}_{f,0}^2 / \tilde{E}_2)^3 \{[\exp(Le_F \tilde{m} / \tilde{r}_f) - 1] / [\tilde{Y}_{F,\infty}(Le_F \tilde{m} / \tilde{r}_f^2)]\}^2$$
$$\times \exp\{a_{T,1}^+ [1 - \exp(-\tilde{m} / \tilde{r}_f)] - \tilde{E}_2 / \tilde{T}_{f,0}\} \quad . \tag{4.94}$$

Substituting these transformations into Eqs. (4.29) and (4.30), we obtain

$$\Theta_1^+ = -a_{T,1}^+ [1 - \exp(-\tilde{m} / \tilde{r}_f)]$$
$$+ \left[\frac{\tilde{T}_{f,0} - \tilde{T}_\infty}{Le_F \tilde{Y}_{F,\infty}} \frac{\exp(-Le_F \tilde{m} / \tilde{r}_f) - 1}{\exp(\tilde{m} / \tilde{r}_f) - 1} \right] \eta \quad , \tag{4.95}$$

$$\Phi_{R,1}^+ = a_{R,1}^- \exp(-Le_R \tilde{m} / \tilde{r}_f) + [Le_R / (\tilde{\nu}_F Le_F)](\Phi_{F,1}^+ - \eta) \quad . \tag{4.96}$$

Subsequent substitution of Eqs. (4.93)–(4.96) into Eqs. (4.9), (4.16a, b), (4.66) and (4.89) then yields the transformed equation and boundary conditions, given by

$$\frac{d^2 \Phi_{F,1}^+}{d\eta^2} = \tilde{\Lambda}_2 \Phi_{F,1}^+ \left\{ \frac{\tilde{\nu}_F Le_F}{Le_R} a_{R,1}^- \exp\left(-\frac{Le_R \tilde{m}}{\tilde{r}_f} \right) + \Phi_{F,1}^+ - \eta \right\}$$
$$\times \exp\left\{ \frac{\tilde{T}_{f,0} - \tilde{T}_\infty}{Le_F \tilde{Y}_{F,\infty}} \frac{\exp(-Le_F \tilde{m} / \tilde{r}_f) - 1}{\exp(\tilde{m} / \tilde{r}_f) - 1} \eta \right\} \quad , \tag{4.97}$$

$$\Phi_{F,1}^+(\eta = 0) = 0 \quad , \tag{4.98a}$$

$$(d\Phi_{F,1}^+ / d\eta)_{\eta=0} = 1 / (1 + \tilde{\nu}_F) \quad , \tag{4.98b}$$

$$\Phi_{F,1}^{+}(\eta\to\infty)=\frac{\tilde{\nu}_F Le_F}{Le_R}\left\{a_{R,1}^{+}\left[1-\exp\left(-\frac{Le_R\tilde{m}}{\tilde{r}_f}\right)\right]-a_{R,1}^{-}\exp\left(-\frac{Le_R\tilde{m}}{\tilde{r}_f}\right)\right\}+\eta \quad , \tag{4.99a}$$

$$(d\Phi_{F,1}^{+}/d\eta)_{\eta\to\infty}=1 \quad . \tag{4.99b}$$

Similarly, the system described by Eqs. (4.37), (4.45a, b), (4.68) and (4.90) can be transformed by defining

$$\eta=(Le_O\tilde{m}\overline{m}_O/\tilde{r}_f^2)\zeta \quad , \tag{4.100}$$

$$\tilde{\Lambda}_3=\frac{\beta Da_2}{Le_O\hat{\nu}}a_{S,0}^{-}\exp\left(-\frac{Le_S\tilde{m}}{\tilde{r}_f}\right)\left[\frac{\tilde{r}_f^2}{\tilde{m}\overline{m}_O}\frac{\tilde{T}_{f,0}^{\,2}}{\tilde{E}_2}\right]^2\exp\left(-\frac{\alpha\tilde{E}_2}{\tilde{T}_{f,0}}\right)$$

$$\times\exp\left\{\alpha\left\langle a_{T,1}^{-}\left[\exp\left(-\frac{\tilde{m}}{\tilde{r}_f}\right)-\exp(-\tilde{m})\right]-\frac{\tilde{q}_S\hat{\nu}}{Le_O}a_{O,1}^{-}\exp\left(-\frac{Le_O\tilde{m}}{\tilde{r}_f}\right)\right\rangle\right\} \quad , \tag{4.101}$$

substituting into Eqs. (4.57) and (4.70) to give

$$\Theta_1^{-}=-a_{T,1}^{-}\left[\exp\left(-\frac{\tilde{m}}{\tilde{r}_f}\right)-\exp(-\tilde{m})\right]+\frac{\tilde{q}_S\hat{\nu}}{Le_O}\left[\Phi_{O,1}^{-}+a_{O,1}^{-}\exp\left(-\frac{Le_O\tilde{m}}{\tilde{r}_f}\right)\right]$$

$$-\frac{1}{Le_O}\left[\frac{(\tilde{T}_{f,0}-\tilde{T}_b)/\overline{m}_O}{1-\exp[\tilde{m}(\tilde{r}_f^{-1}-1)]}-\tilde{q}_S\hat{\nu}\right]\eta \quad , \tag{4.102}$$

and applying these expressions to the equation system to yield

$$(d^2\Phi_{O,1}^{-}/d\eta^2)=\tilde{\Lambda}_3\Phi_{O,1}^{-}$$

$$\times\exp\left\{\frac{\alpha}{Le_O}\left[\frac{(\tilde{T}_{f,0}-\tilde{T}_b)/\overline{m}_O}{1-\exp[\tilde{m}(\tilde{r}_f^{-1}-1)]}-\tilde{q}_S\hat{\nu}\right]\eta-\frac{\alpha\tilde{q}_S\hat{\nu}}{Le_O}\Phi_{O,1}^{-}\right\} \quad , \tag{4.103}$$

$$\Phi_{O,1}^{-}(\eta=0)=0 \quad , \tag{4.104a}$$

$$(d\Phi_{O,1}^{-}/d\eta)_{\eta=0} = -\{\tilde{Y}_{F,\infty}/[\bar{m}_O(1+\tilde{\nu}_F)]\}/[\exp(Le_F\tilde{m}/\tilde{r}_f)-1] \quad ,(4.104b)$$

$$\Phi_{O,1}^{-}(\eta\to-\infty) = -a_{O,1}^{-}\exp(-Le_O\tilde{m}/\tilde{r}_f)-\eta \quad , \qquad (4.105a)$$

$$(d\Phi_{O,1}^{-}/d\eta)_{\eta\to-\infty} = -1 \quad . \qquad (4.105b)$$

4.2.10 Summary of the Analytical Results

The analysis is completed at this stage and the result is summarized as follows. For any specified conditions, Eq. (4.103) can first be integrated numerically subject to the four boundary conditions given by (4.104a, b) and (4.105a, b). The procedure is followed by the numerical integration of Eq. (4.97) subject to the four boundary conditions given by Eqs. (4.98a, b) and (4.99a, b). Because only two boundary conditions are required to solve each of these two second order differential equations, there are four additional conditions. These four extra conditions are then applied to determine the flame sheet location, $\tilde{r}_f$, and the eight undetermined constants, $a_{T,1}^{\pm}$, $a_{F,1}^{+}$, $a_{O,1}^{-}$, $a_{R,1}^{\pm}$ and $a_{S,1}^{\pm}$ when coupled with Eqs. (4.70), (4.77), (4.78), (4.91) and (4.92). By applying these results, $a_{S,0}^{\pm}$ can finally be determined from Eqs. (4.28), (4.55), (4.76) and (4.88) while the flame temperature, $\tilde{T}_f$, can be determined from Eqs. (3.89), (4.69) and (4.87).

The soot/precursor concentration at the boundary between the soot/precursor consumption region and the inert region at the oxidizer side of the reaction regions can be obtained from Eq. (4.8a) as

$$\tilde{Y}_S^{-}(\tilde{r}_f) = (a_{S,0}^{-}+\delta a_{S,1}^{-})\exp(-Le_S\tilde{m}/\tilde{r}_f)+\ldots \quad . \qquad (4.106)$$

This quantity is represented by a soot/precursor indicator, S_I. Accordingly, the soot/precursor concentration at the boundary between the soot/precursor formation region and the inert region at the fuel side of the reaction regions, which represents the amount of soot/precursor that exists in the combustion products, is given by Eq. (4.8b) as

$$\tilde{Y}_S^+(\tilde{r}_f) = (a_{S,0}^+ + \delta a_{S,1}^+)[1 - \exp(-Le_S \tilde{m} / \tilde{r}_f)] + \ldots \quad . \tag{4.107}$$

This quantity is expressed by a soot index parameter S_B to have the notation consistent with that of Chapter 3.

In the limiting case of extremely slow soot/precursor consumption reaction, the consumption reaction is considered an order of magnitude slower than the soot/precursor formation reaction so that $\beta = O(\delta)$. For this case, Eq. (4.103) can be integrated subject to Eqs. (4.104a, b) to yield

$$\Phi_{O,1}^- = -\{(\tilde{Y}_{F,\infty} / \overline{m}_O) / (1 + \tilde{\nu}_F) / [\exp(Le_F \tilde{m} / \tilde{r}_f) - 1]\}\eta \quad . \tag{4.108}$$

Subsequent application of Eqs. (4.105a, b) into Eq. (4.108) then results in $a_{O,1}^- = 0$ and

$$\tilde{r}_f = Le_F \tilde{m} / \ln\left[1 + (\tilde{Y}_{F,\infty} / \overline{m}_O) / (1 + \tilde{\nu}_F)\right] \tag{4.109}$$

such that the flame location is analytically determined. Equation (4.109) in turn can be substituted into Eq. (4.87) to yield the solution of $\tilde{T}_{f,0}$. Equation (4.97) still need to be solved numerically subject to the four boundary conditions in Eqs. (4.98a, b) and (4.99a, b), with two of which applied to determine $a_{T,1}^{\pm}$, $a_{F,1}^+$, $a_{R,1}^{\pm}$ and $a_{S,1}^{\pm}$ together with Eqs. (4.70), (4.77), (4.78), (4.91) and (4.92).

As mentioned in Chapters 2 and 3, the analysis is applicable only for a diffusion flame in Liñán's (1974) diffusion flame regime and sufficiently far away from the extinction limit.

4.3 Results and Discussions

The numerical calculations to complete the study are performed by adopting the same thermo-chemical data adopted in Chapter 3. As in Chapters 2 and 3, the study will cover two limiting cases, namely the air/fuel flame and the oxygen/diluted-fuel flame. The differences in the flame structure between the two limiting cases are shown schematically in Fig. 4.1.

For the air/fuel flame shown in Fig. 4.1 (a), air is supplied from the burner and flows into the quiescent ambient filled with fuel gas. The reaction regions, including the oxidation region, the soot formation region and the soot consumption region, are relatively close to the burner because of the low initial oxidizer concentration as compared to that of the fuel. In the other limit, namely the oxygen/diluted-fuel flame shown in Fig. 4.1 (b), the inert gas is separated from the air and supplied with the fuel so that only the pure oxygen is issued from the burner. The fuel consumption rate and the overall stoichiometry are maintained for both of these cases to ensure that the total enthalpy is unchanged. As in Chapter 3, the fuel consumption rate is kept at 1.51 mg/s, except when the effect of mass flow rate is addressed, such that the mass flow rate for the oxygen/diluted-fuel flame is lower. The redistribution of inert gas yields a reduction in the initial fuel concentration and an increase in the initial oxidizer concentration such that the reaction regions are much farther away from the burner. It also renders a lower/higher temperature gradient near the boundary between the reaction regions and the inert region at the oxidizer/fuel side. Moreover, the temperature gradient at the burner exit is increased as a result of reduced mass flow rate, and consequently the heat loss to the burner is enhanced and the flame temperature is reduced.

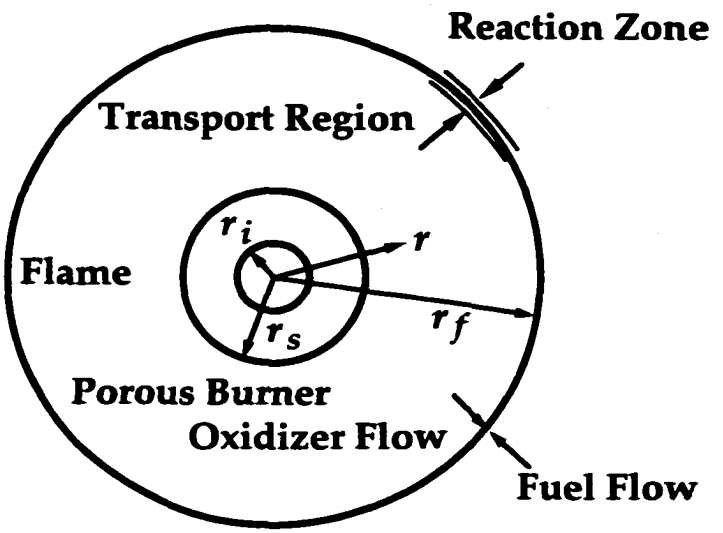

Transport Region

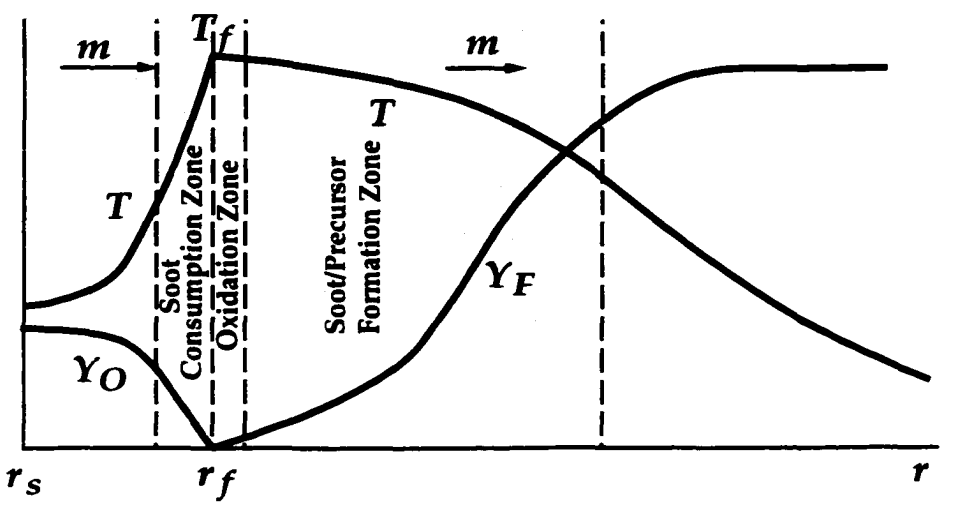

Figure 4.1(a) Schematic diagram of the flame structure for air/fuel flame in the spherical diffusion flame stabilized by a spherical porous burner with the oxidizer supplied from the burner

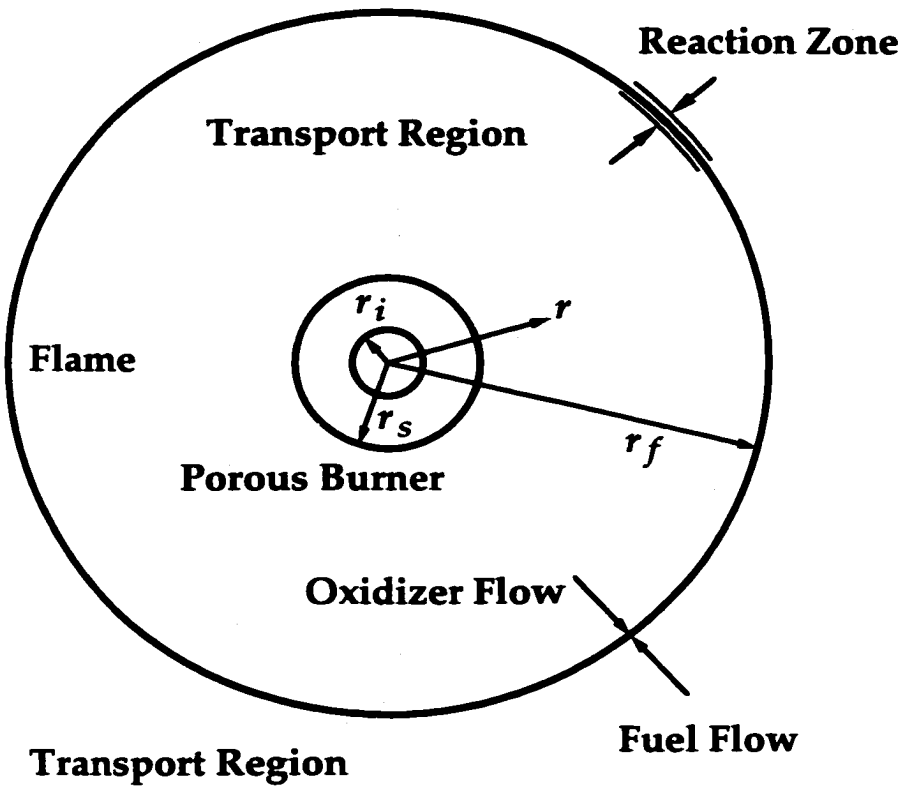

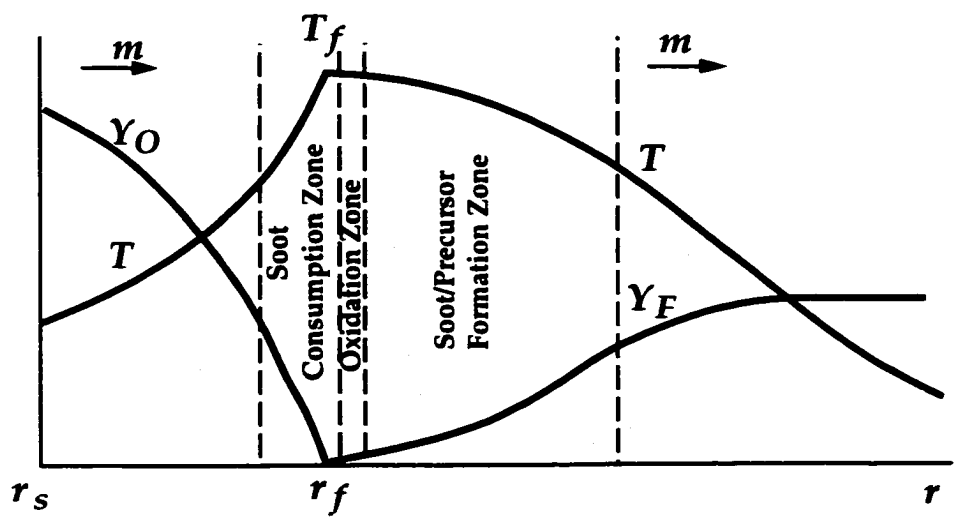

Figure 4.1(b) Schematic diagram of the flame structure for oxygen/diluted-fuel flame in the spherical diffusion flame stabilized by a spherical porous burner with the oxidizer supplied from the burner

As is known, both the soot formation and consumption reactions occur only at high temperatures because of their high activation energies. According to the temperature distribution discussed in the previous paragraph, formation of soot/precursor is favored for the air/fuel flame because of its thicker formation region and thinner consumption region. Its higher flame temperature further enhances the soot/precursor production rate. Both the residence time (thickness of the reaction regions) and the reaction rate (flame temperature) promote the overall soot production. It is then expected that inert redistribution has a profound effect on the reduction of soot precursors and particles produced from a diffusion flame with the flow direction towards the fuel side.

For the air/fuel flame, we have $Y_{F,\infty} = 1$, $Y_{O,0} = 0.233$ and m varying between 20.46 and 22.22 mg/s ($22.33 < \bar{m} < 24.26$). Because the flow direction is from the burner to the ambient, that is, from the oxidizer to the fuel side for the problem studied in this chapter, the soot/precursor produced in the formation region can only be transferred to the consumption region through diffusion against convection. It is then expected that the soot consumption reaction is less important and the soot indicator parameter S_I is very small. For this problem, the soot index parameter, S_B, which represents the concentration of soot precursor at the boundary between the soot formation region and the fuel side inert region, is more relevant in quantifying the overall soot production. Results of calculations on the values of S_I and S_B versus the Damköhler number of the soot/precursor formation reaction, Da_2, for selected values of β and $\alpha = Le_R = Le_S = 1$ are shown in Figs. 4.2 and 4.3.

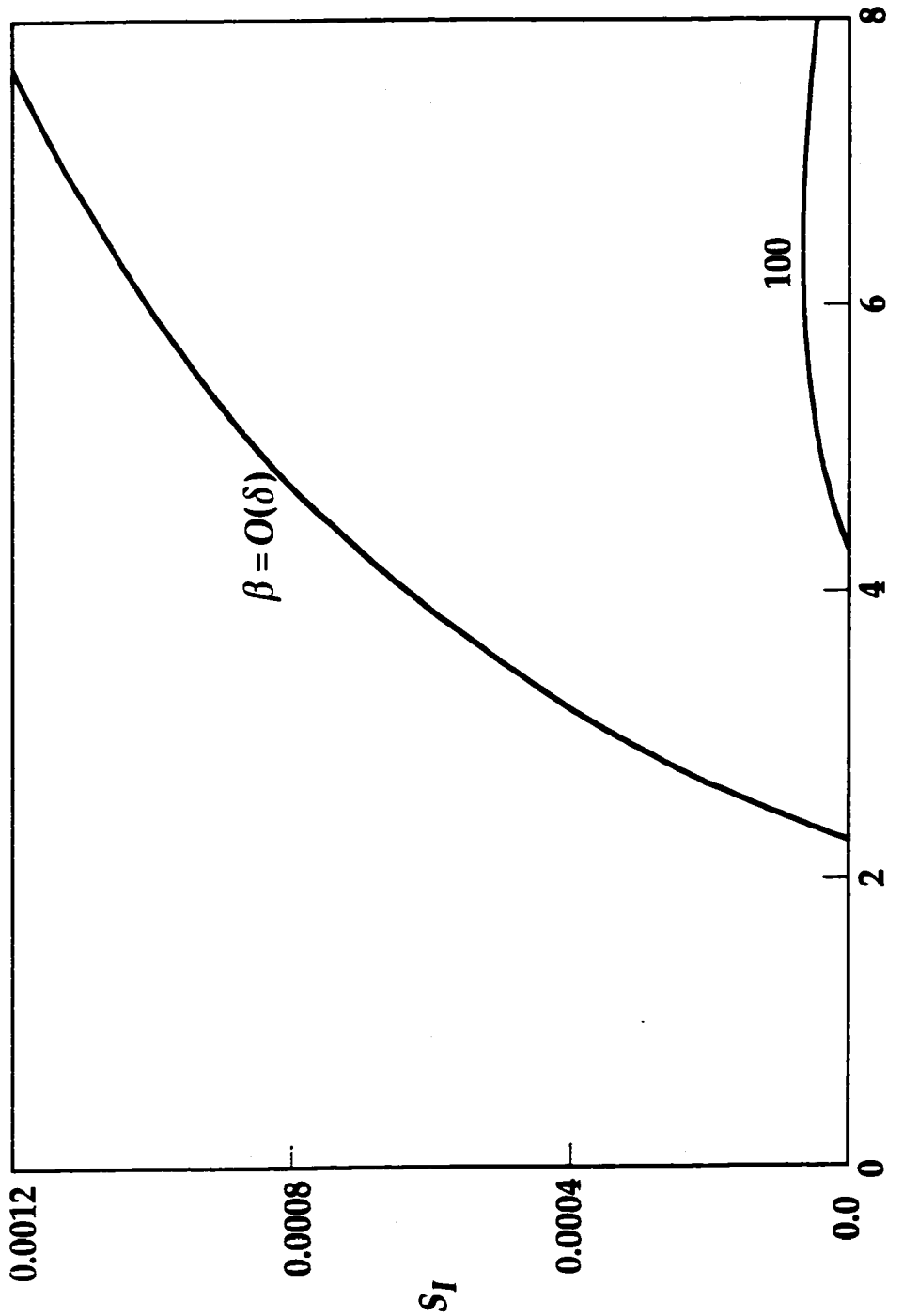

Figure 4.2 Variation of S_I with Da_2 for the air/fuel flame with $\alpha = Le_R = Le_S = 1$ and selected values of β

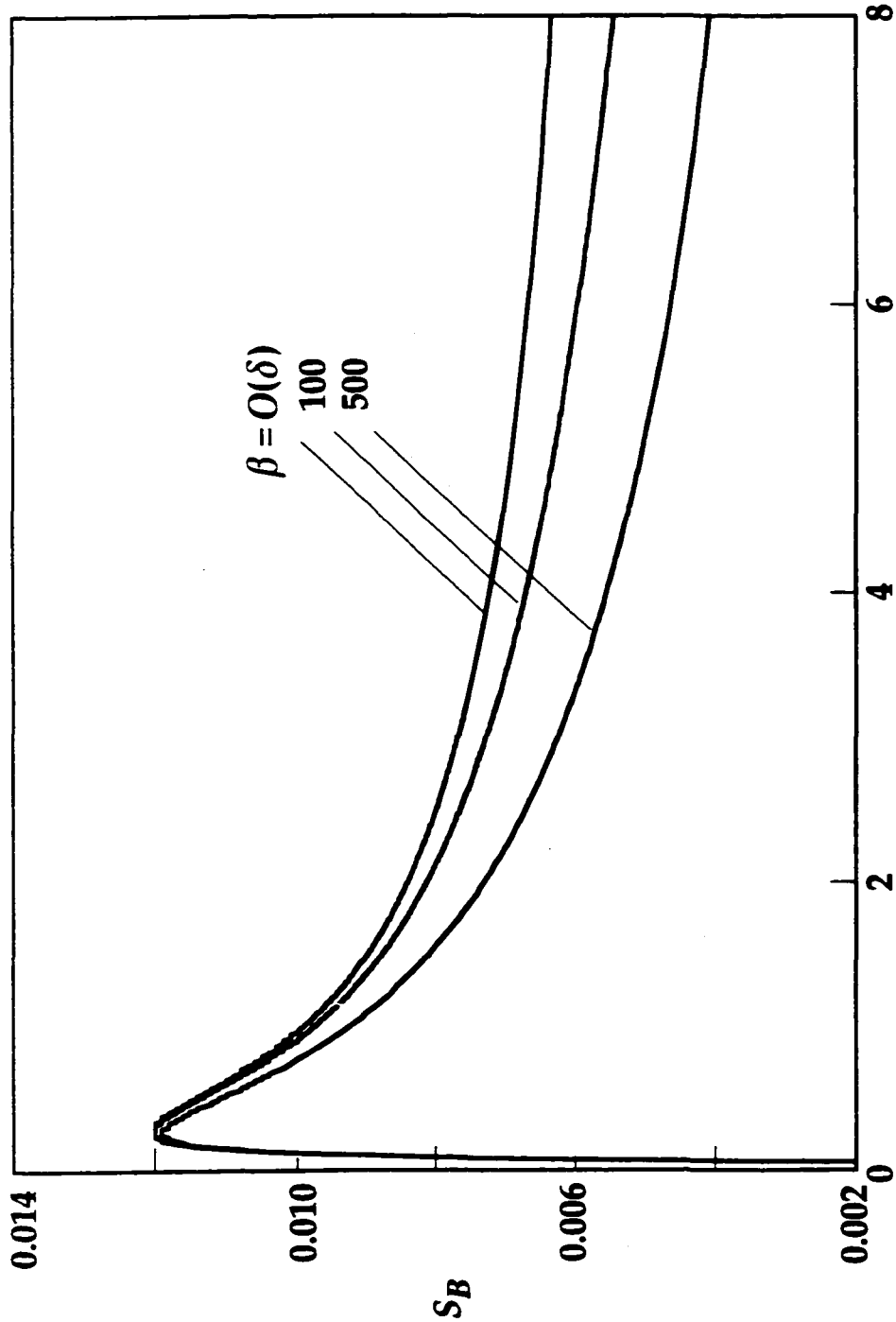

Figure 4.3 Variation of S_B with Da_2 for the air/fuel flame with $\alpha = Le_R = Le_S = 1$ and selected values of β

As in previous chapters, unity Lewis numbers are used as reference values to facilitate the discussion. The curve for $\beta = O(\delta)$ in the figures represents the limiting case of an extremely slow soot/precursor oxidation reaction. For this system, the variation of Da_2 is caused solely by the variation of the pre-exponential factor B, or the reaction rate. As expected, Fig. 4.2 shows that S_I is negligibly small comparing to S_B and will not be presented for the rest of this chapter.

It is shown in Fig. 4.3 that by increasing Da_2 from a small value, S_B first increases, attains a maximum, and then decreases, similar to the behavior of S_I presented in Fig. 3.2. This behavior does not agree with the expectation that S_B should increase monotonically with Da_2 because more soot/precursor is produced by increasing the rate of soot formation reaction and the direction of convection is toward the fuel side. The reason for the disagreement is again that S_B only represents the concentration at the boundary between the soot formation region and the fuel side transport region. The net soot production is known to increase monotonically with soot formation reaction rate until Da_2 is sufficiently large and all the radicals are consumed in a thin region next to the downstream boundary of the oxidation region. At this reaction sheet limit, the overall soot production reaches its maximum value asymptotically. With the increase of β, the soot consumption reaction occurs and S_B decreases. In addition to the above understanding, Fig. 4.3 also shows that the soot consumption reaction is distinguishable only for extremely large values of β, which further supports our expectation that the soot consumption reaction is less important.

To better understand the non-monotonic behavior shown in Fig. 4.3, the

composite solution of the soot concentration in the soot formation region and the fuel side inert region, $\tilde{Y}_S^+$, is plotted versus the spatial coordinate along the radial direction in Fig. 4.4 with $\alpha = Le_R = Le_S = 1$ and $\beta = O(\delta)$. The plot is presented by using the inner coordinate ξ such that the variation can be observed more clearly. Four values of Da_2, $Da_2 = 0.068$, 0.109, 0.275, and 2.49 are selected to include both the ascending and descending branches of S_B in Fig. 4.3. It is very clearly shown in Fig. 4.4 that for a low Da_2, *e.g.* $Da_2 = 0.068$, the soot formation reaction is weak and the value of $\tilde{Y}_S^+$ is relatively small. For this case, the consumption of the radical produced in the oxidation region is slow and a larger amount of radical enters the inert region in the fuel side without being converted to soot precursor. The soot formation reaction occurs in the whole formation region and the peak of $\tilde{Y}_S^+$ is located relatively away from the oxidation region (larger ξ). With an increase in Da_2, soot precursor is produced and the radical is consumed at a higher rate such that the amount of soot/precursor and $\tilde{Y}_S^+$ are increased. The peak of $\tilde{Y}_S^+$ also assumes a higher value and shifts toward the oxidation region because of the faster radical depletion rate. When the soot formation reaction is sufficiently strong, as represented by the $Da_2 = 2.49$ curve, most of the radical is reacted in a narrow region near the oxidation region such that the peak of $\tilde{Y}_S^+$ is high and at a low ξ. The soot formation reaction ceases in the rest of the formation region although the temperature is still high. The value of $\tilde{Y}_S^+$ then drops faster due to the higher diffusion rate caused by the higher concentration gradient, and results in a lower $\tilde{Y}_S^+$ at sufficiently large values of ξ. The curves shown in Fig. 4.3 represents a snap shot of $\tilde{Y}_S^+$ at a ξ large enough to be considered as the outer boundary of the soot formation region.

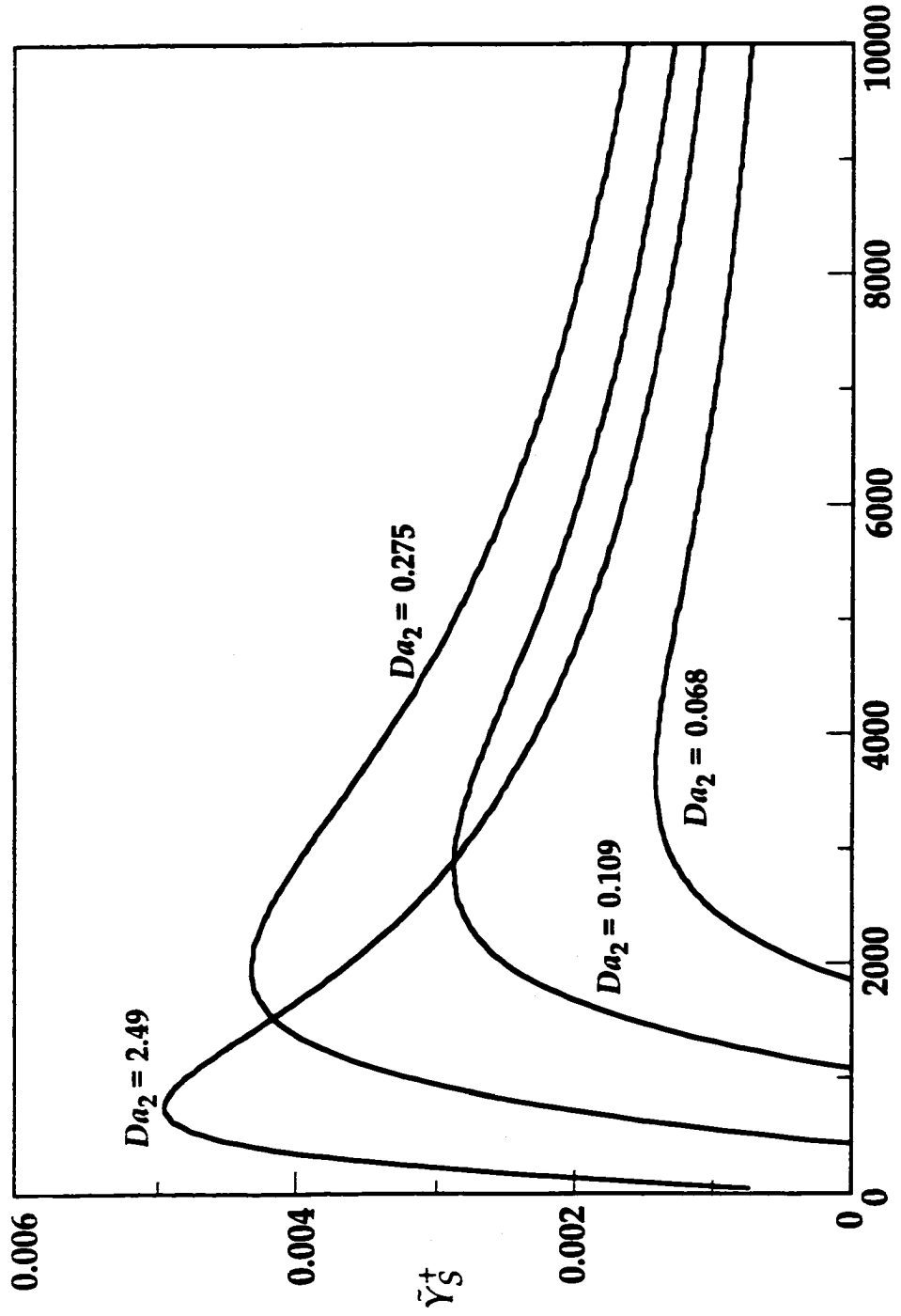

Figure 4.4 Concentration profile in spatial coordinate for the air/fuel flame with $\alpha = Le_R = Le_S = 1$ and $\beta = O(\delta)$

As is realized, the more instrumental parameter to represent the overall soot/precursor production is the flame temperature, $\tilde{T}_f$. As shown in Fig. 4.5, for the limiting case of $\beta = O(\delta)$, $\tilde{T}_f$ decreases monotonically with increasing Da_2, and reaches an asymptotic value for large values of Da_2. This shows that the net soot/precursor production increases monotonically with increasing Da_2, and reaches a maximum value when all the radical is consumed, as discussed earlier in this chapter and the previous two chapters. For non-zero values of β, there is a critical Da_2 at which $\tilde{T}_f$ attains its minimum value. $\tilde{T}_f$ increases with increasing Da_2 from this critical value because of the additional heat release through the soot consumption reaction. Moreover, the critical Da_2 decreases with increasing β. This is consistent with the observation in Chapter 3. It should be reminded, however, that for the flames studied in this chapter, the soot consumption reaction is not important. The unreasonably large values of β adopted in Figs. 4.3 and 4.5 is for scientific discussion only.

To complete the study, the flame sheet location $\tilde{r}_f$ is presented in Fig. 4.6 as a function of Da_2. Although the qualitative behavior exhibited in Fig. 4.6 is the same as that of Fig. 3.4, the reason for such behavior is different for non-zero β flames. From Chapter 3, it is understood that for the fuel/air flame, the soot/precursor consumption reaction yields an O(1) oxidation of soot/precursor and consumes an O(1) of the oxidizer when β is not zero. The reduction of the oxidizer supply then forces the flame to move towards the oxidizer side (ambient). For the air/fuel flame, the loss of oxidizer supply caused by the soot/precursor consumption reaction requires extra supply of oxidizer to maintain the specified fuel consumption rate. Consequently a higher mass flow rate must be issued from the burner, which results in a

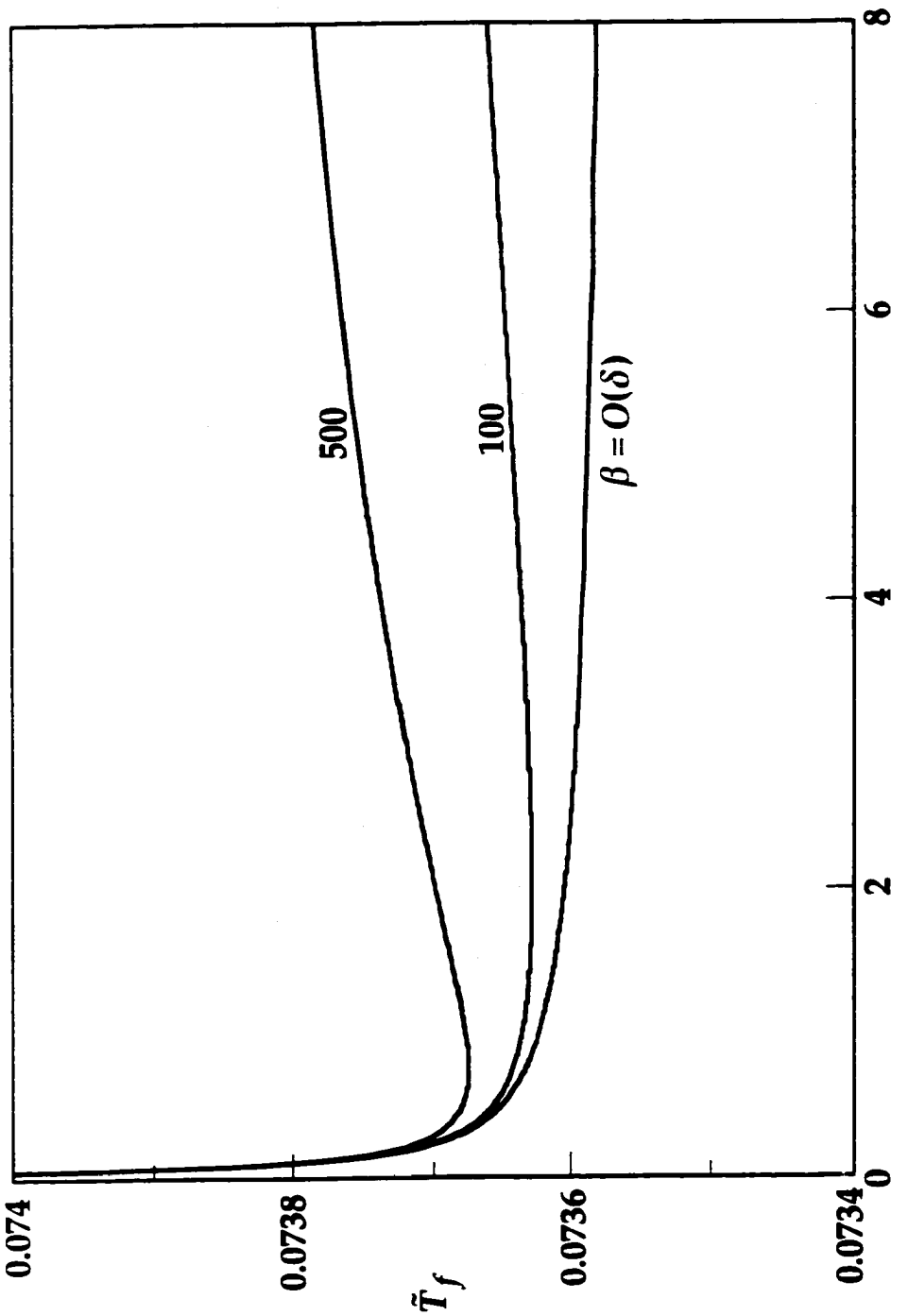

Figure 4.5 The flame temperature $\tilde{T}_f$ corresponding to Fig. 4.3

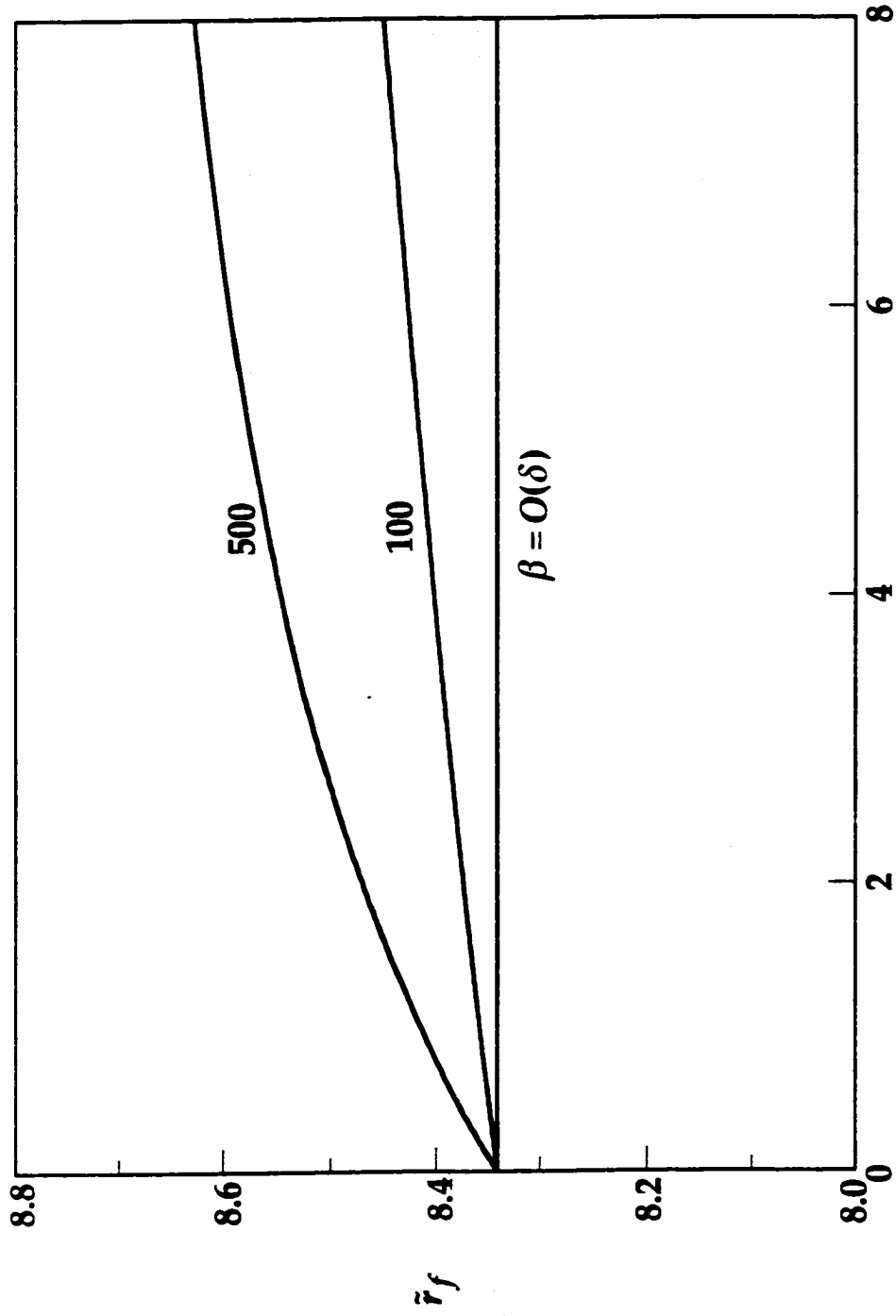

Figure 4.6 The flame sheet location $\tilde{r}_f$ corresponding to Fig. 4.3

larger $\tilde{r}_f$. The effect of mass flow rate, and the outward shift of $\tilde{r}_f$, is stronger with increasing β, which is expected.

As in Chapters 2 and 3, the effects of diffusion transport of the radical and soot/precursor will be addressed by varying one Lewis number at a time and the results are presented in Figs. 4.7 and 4.8 by plotting $\tilde{T}_f$ versus Da_2. Comparing Fig. 4.7 and 4.8 with Figs. 3.8 and 3.11, it is found that the effects of Le_R and Le_S for the air/fuel flame are qualitatively similar to those of the fuel/air flame. It is, however, noted from Fig. 4.8 that Le_S has only a secondary impact on the flame response. A magnified scale showing a narrow region of $\tilde{T}_f$ is necessary to exhibit the difference in the solution introduced by Le_S. As is known from Chapter 3, the solution of the $\beta = O(\delta)$ flames is independent of Le_S because of the negligible soot consumption reaction. For the air/fuel flame, the soot consumption reaction is weak even for non-zero values of β, which is a consequence of the unfavorable convection direction discussed earlier, such that the effect of β is insignificant.

Following the same sequence as in Chapter 3, the flame response to the variation of the burner flow rate also needs be discussed for it is the more realistic controllable variable in experimental studies. An example showing the physical behavior is shown in Figs. 4.9–4.11 by plotting the flame temperature, $\tilde{T}_f$, flame location, $\tilde{r}_f$, and soot/precursor index, S_B, versus the burner flow rate, $\tilde{m}$, respectively, for $\alpha = Le_R = Le_S = 1$ and $Da_2 = 2.0$. These figures show that the behavior of $\tilde{T}_f$ is similar to that presented in Figs. 3.13 (if the range of $\tilde{m}$ is extended) and 3.21, and the behavior of $\tilde{r}_f$ is qualitatively similar to that presented in Figs. 3.13 and 3.22. In addition, the behavior of S_B corresponding to the variation in $\tilde{m}$ is qualitatively similar to that of Da_2. All

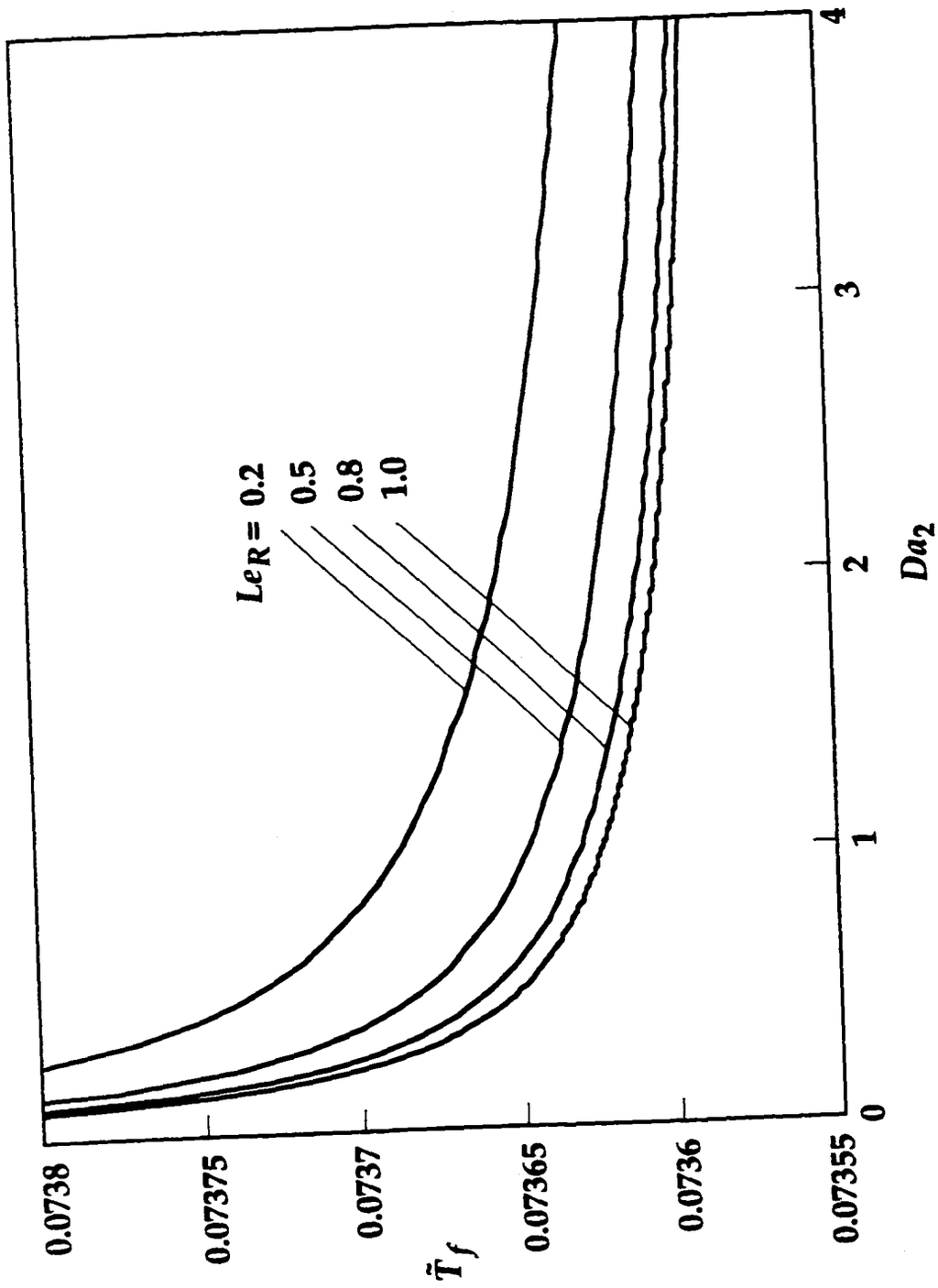

Figure 4.7 Variation of $\tilde{T}_f$ with Da_2 for the air/fuel flame with $\alpha = Le_S = 1, \beta = O(\delta)$, and selected values of Le_R

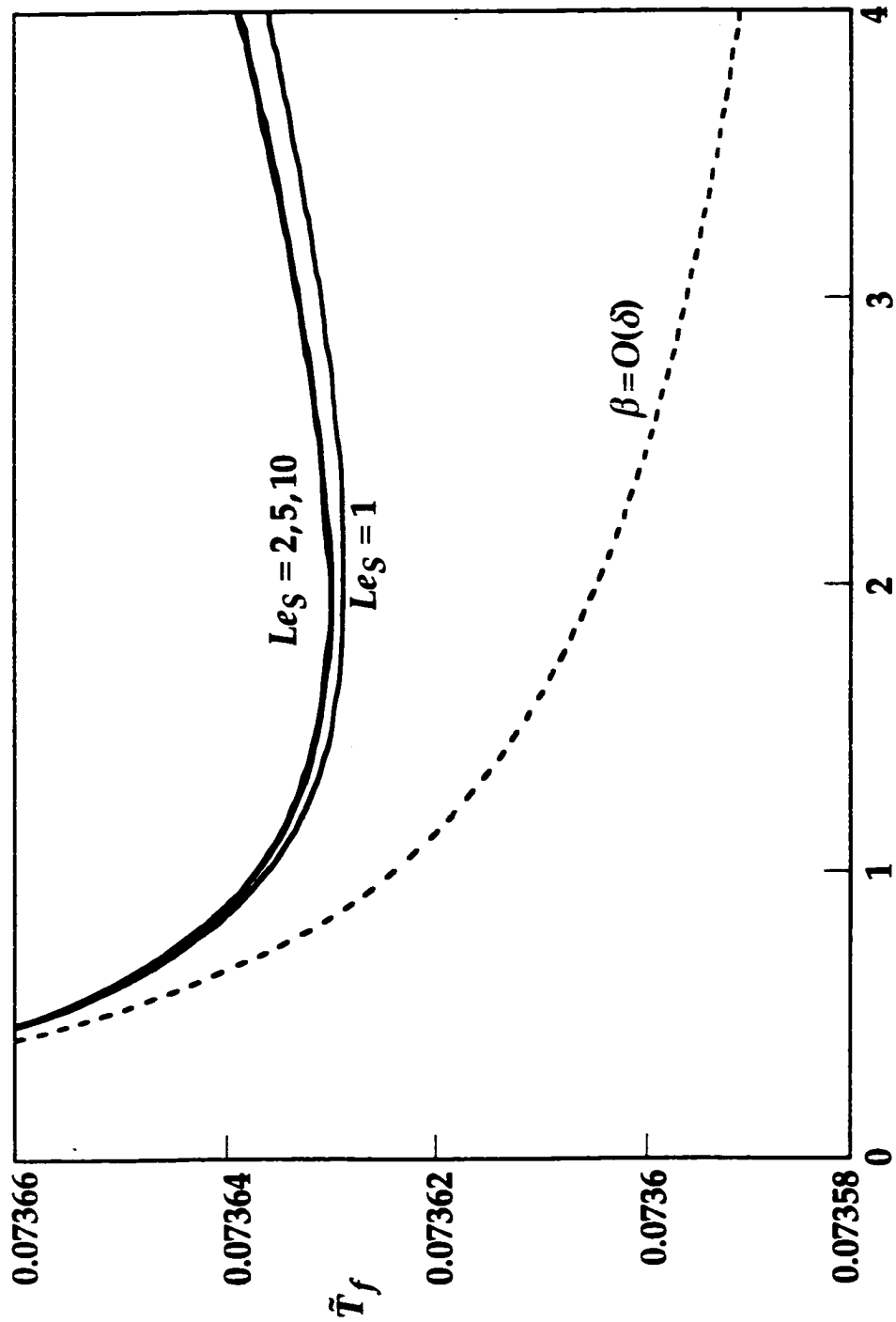

Figure 4.8 Variation of $\tilde{T}_f$ with Da_2 for the air/fuel flame with $\alpha = Le_R = 1$, $\beta = 100$ and selected values of Le_S. The solution for $\beta = O(\delta)$ is also included in dotted curve for comparison.

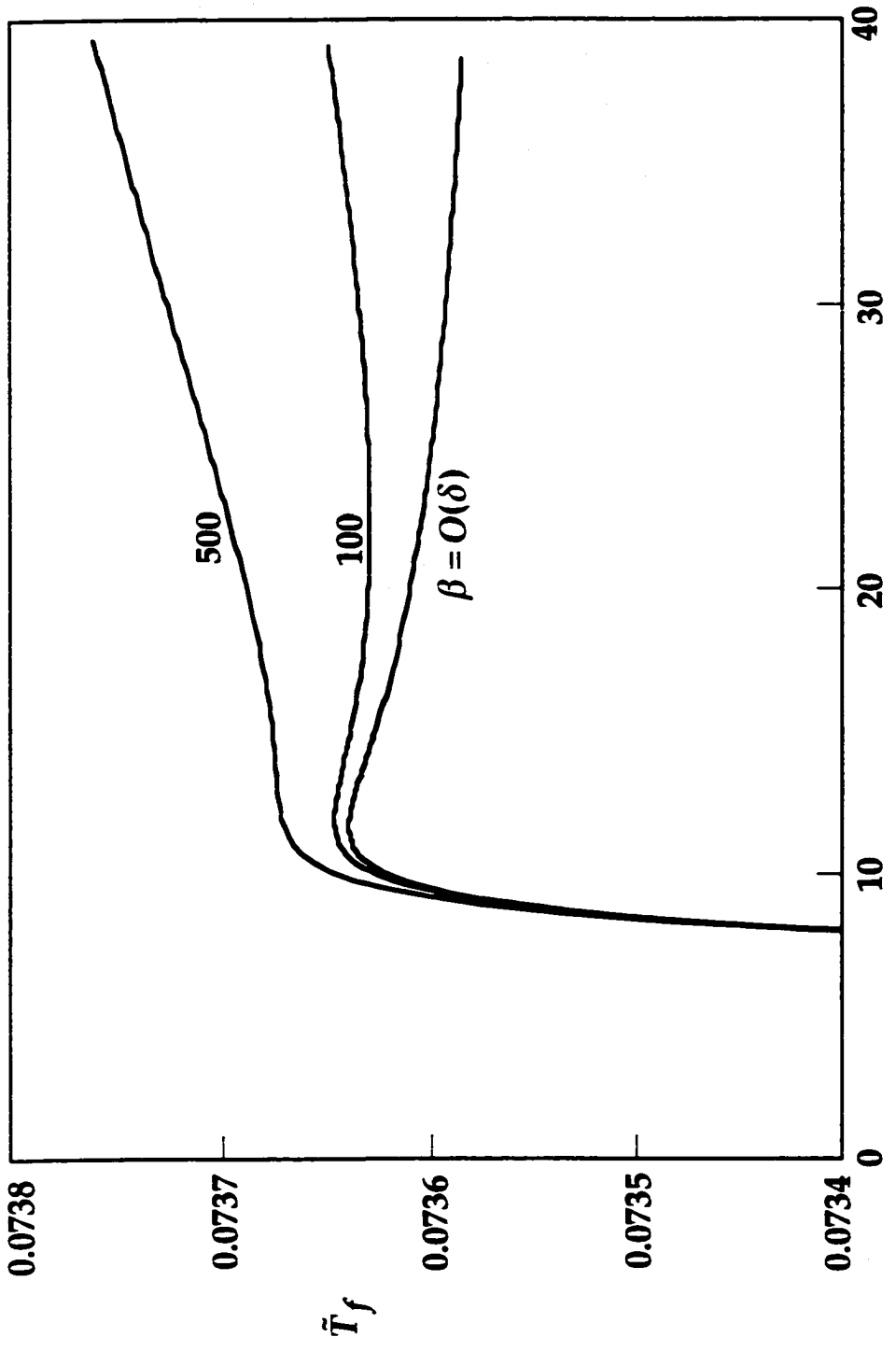

Figure 4.9 Variation of $\tilde{T}_f$ with $\tilde{m}$ for the air/fuel flame with $\alpha = Le_R = Le_S = 1$, $Da_2 = 2.0$ and selected values of β

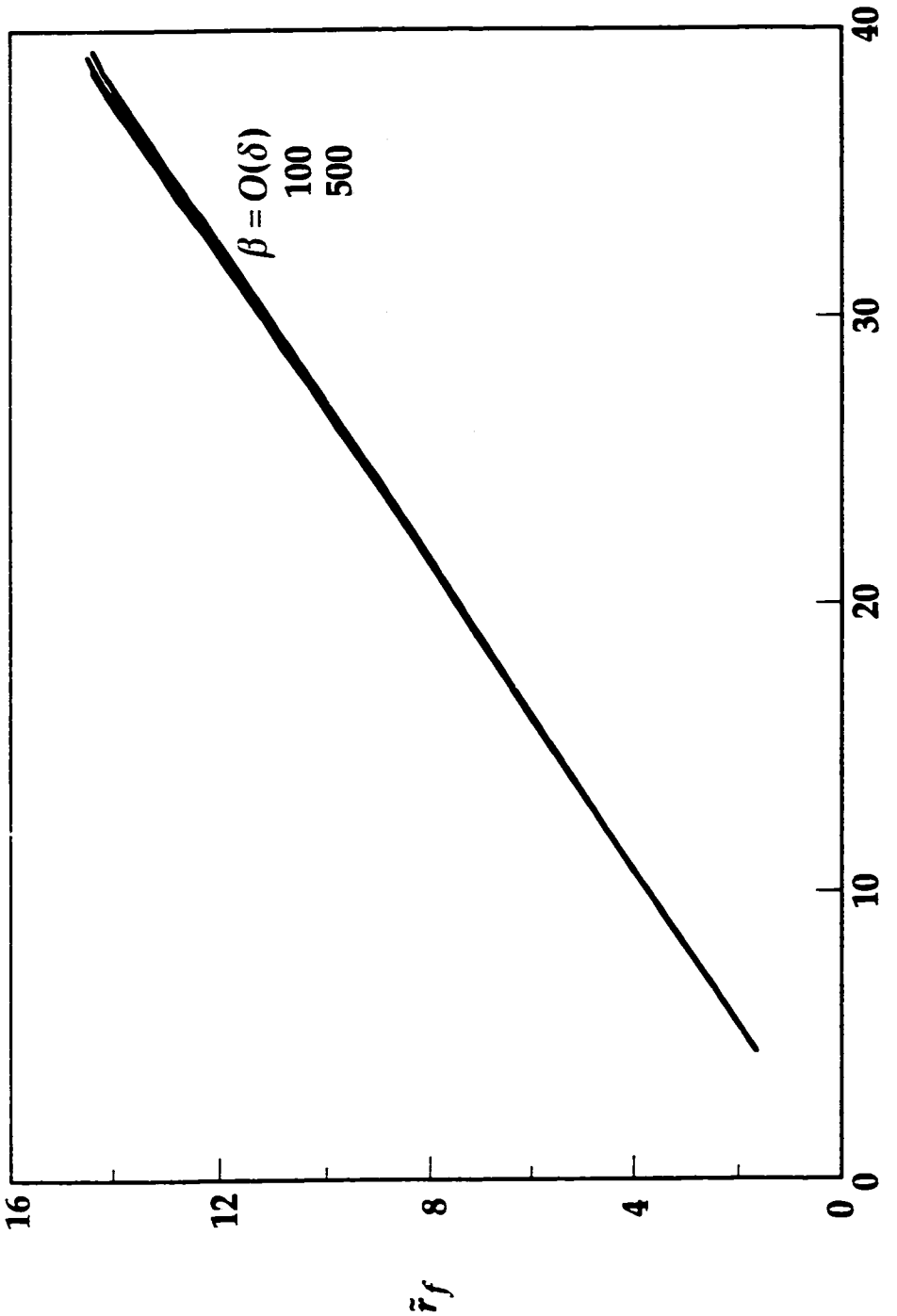

Figure 4.10 The flame sheet location $\tilde{r}_f$ corresponding to Fig. 4.9

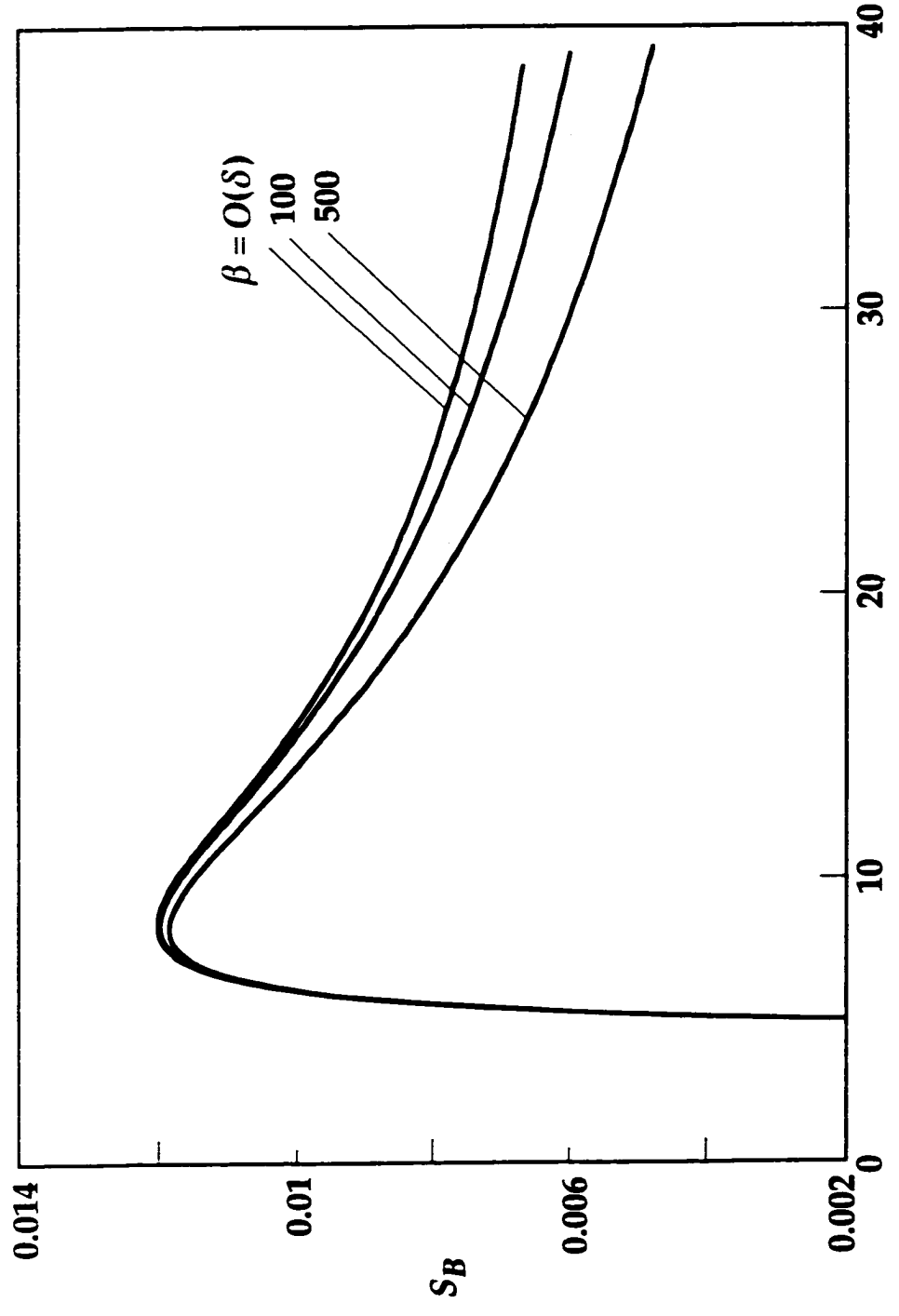

Figure 4.11 Variation of S_B corresponding to Fig. 4.9

of these agree with those in Chapter 3. Although Fig. 4.10 exhibits a weak dependence of $\tilde{r}_f$ on β when $\tilde{m}$ is large, in that $\tilde{r}_f$ decreases with increasing β because more oxygen is consumed from the soot/precursor consumption reaction, such variation is indistinguishable for reasonable values of β. The similar dependence, meaning that $\tilde{r}_f$ increases with increasing β, can be observed in Figs. 3.14 and 3.22 if the values of β are sufficiently large.

The study is continued with the flame response and sooting behavior corresponding to the variation of stoichiometric mixture fraction. As in the previous chapters, this task is performed by examining the limiting case that all the inert is supplied with the fuel gas in the ambient and the pure oxygen is from the burner while maintaining the same stoichiometric relation. In this limit, we again have $Y_{O,0} = 1$ and $Y_{F,\infty}$ varying between 0.08143 and 0.08784. Moreover, by maintaining the fuel consumption rate of 1.51 mg/s, m varies between 4.77 and 5.18 mg/s ($5.20 \le \tilde{m} \le 5.65$). Sample calculations were performed using $\alpha = Le_R = Le_S = 1$, and the results are presented by plotting S_B, $\tilde{T}_f$, and $\tilde{r}_f$ versus Da_2 in Figs. 4.12–4.14. Based on the experience gained from previous chapters, it is expected that the qualitative behavior of the oxygen/diluted-fuel flame is similar to that of the air/fuel flame. The comparison between Figs. 4.12–4.14 and 4.3, 4.5–4.6 supports this expectation. Although the peak of S_B for the $\beta = O(\delta)$ flame is not shown on Fig. 4.12, it exists at a higher Da_2.

Quantitatively, Figs. 4.12 and 4.3 show that for the oxygen/diluted-fuel flame, the value of S_B is much smaller and the value of Da_2 to yield the peak value of S_B is much higher. This implies that it is more difficult to produce soot/precursor and the amount of soot/precursor production is much lower.

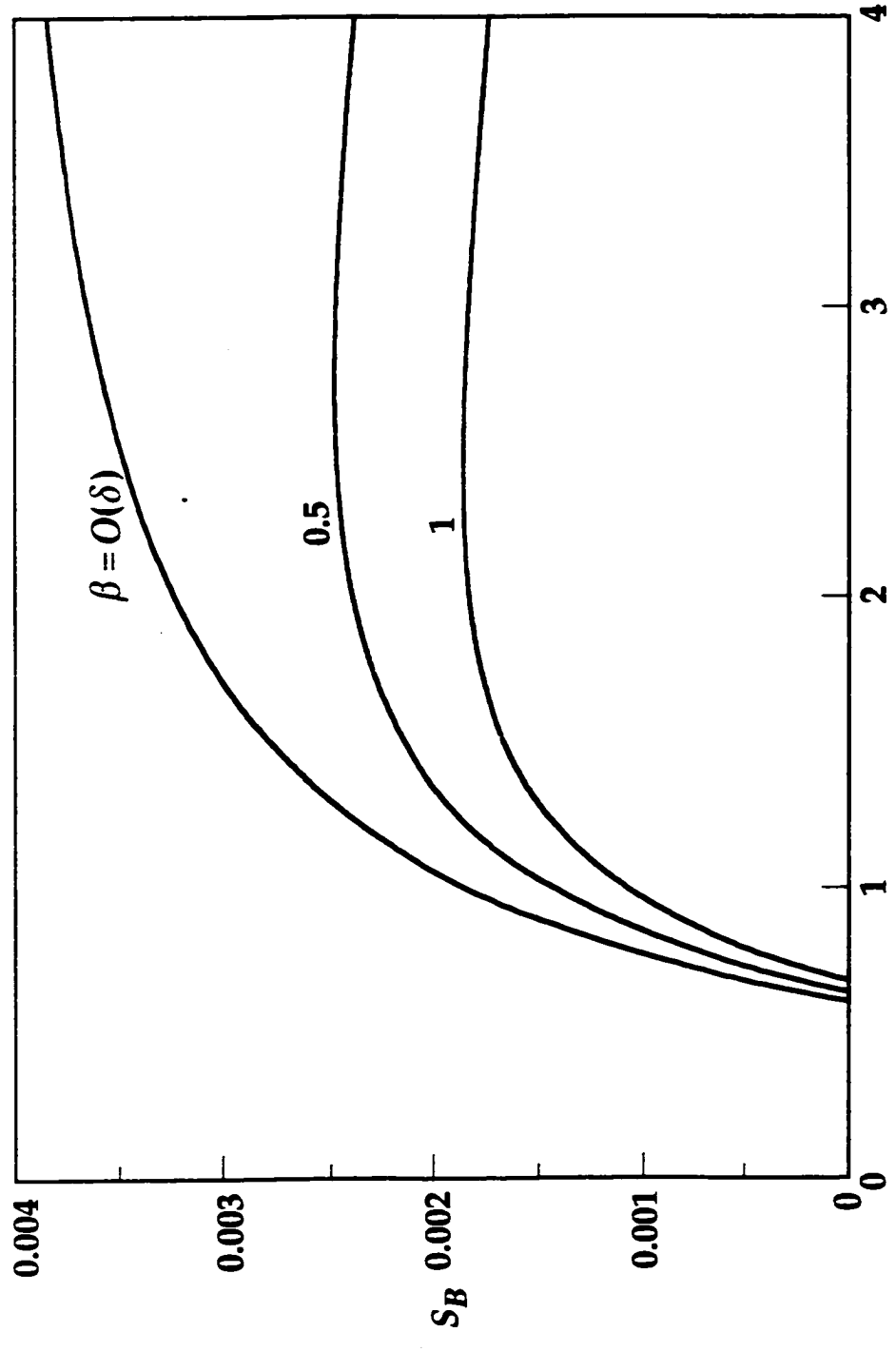

Figure 4.12 Variation of S_B with Da_2 for the oxygen/diluted-fuel flame with $\alpha = Le_R = Le_S = 1$ and selected values of β

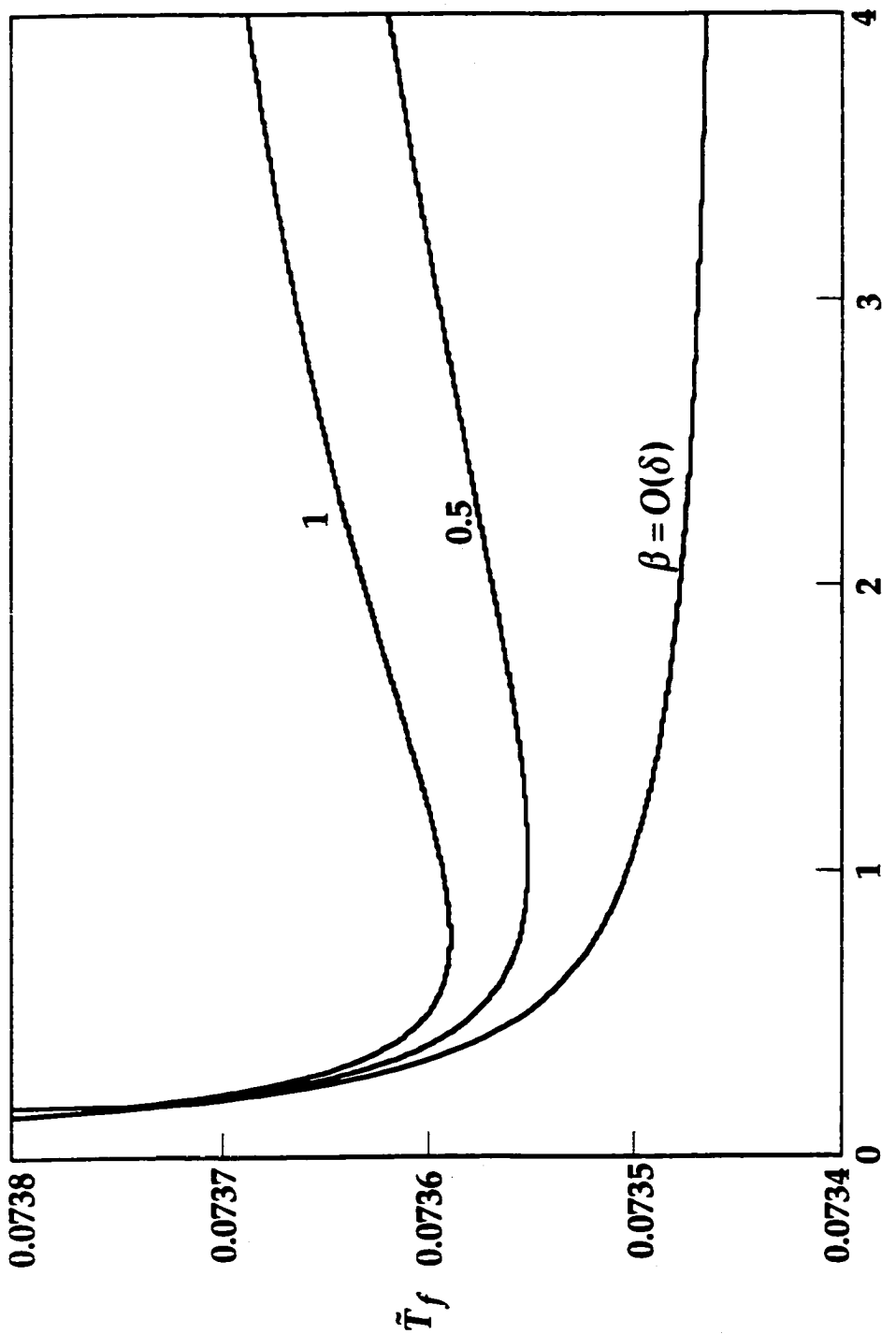

Figure 4.13 Variation of $\tilde{T}_f$ with Da_2 for the oxygen/diluted-fuel flame with $\alpha = Le_R = Le_S = 1$ and selected values of β

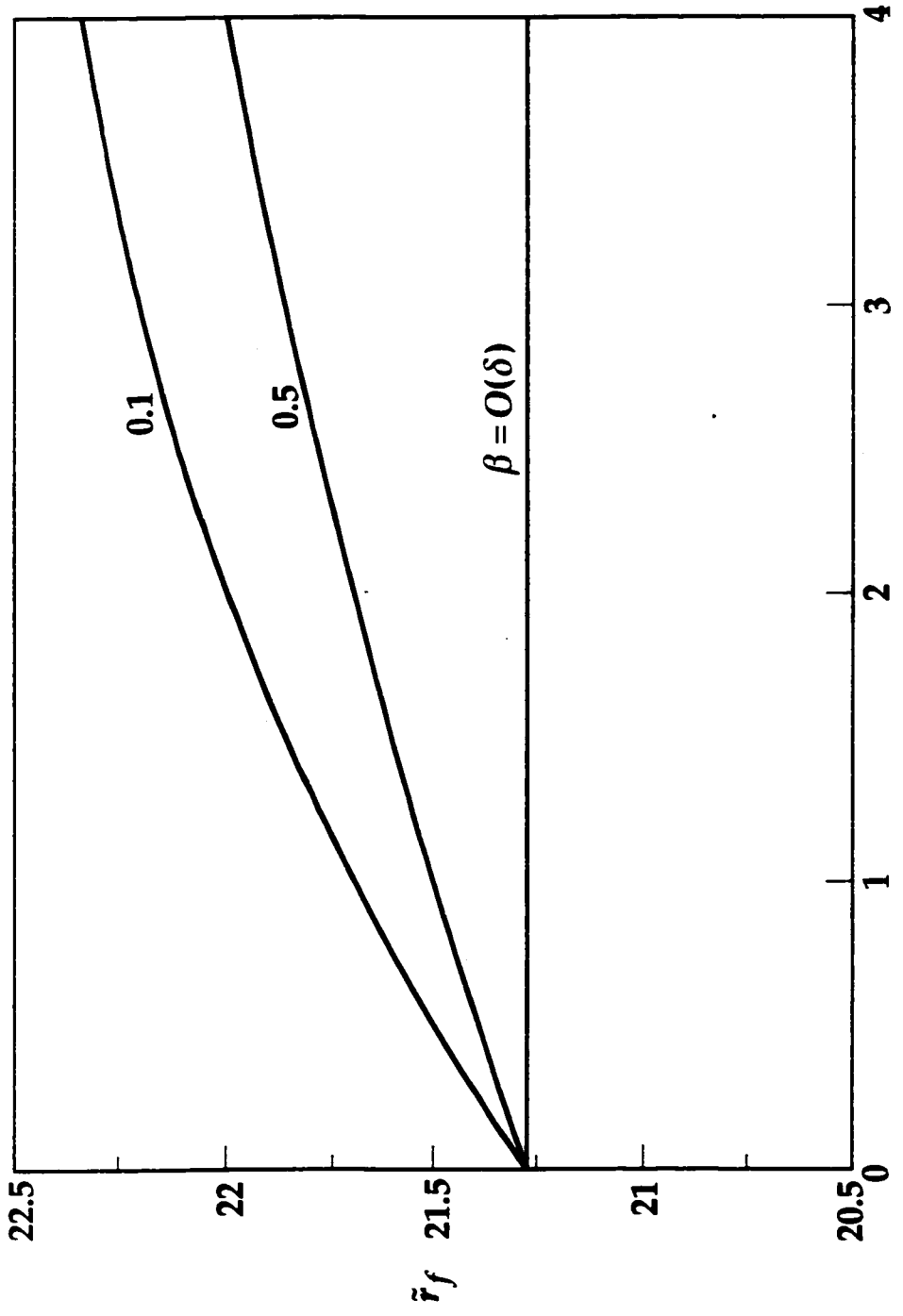

Figure 4.14 The flame sheet location $\tilde{r}_f$ corresponding to Fig. 4.12

Figures 4.5–4.6 and 4.13–4.14 then show that the oxygen/diluted-fuel flame is located further away from the burner and has a lower flame temperature. The differences in the flame location and flame temperature between the two limiting flames is relatively easy to understand. When the inert gas appears with the fuel, pure oxygen is issued from the burner and the mass flow rate is significantly reduced. This raises the heat loss from the gas to the burner such that the flame temperature is lower. The low initial fuel concentration and high oxygen concentration as a result of inert redistribution is responsible for the outward shift of the flame.

As to the reduction of soot production for the oxygen/diluted-fuel flame, it is understood that the decrease of the mass flow rate (reduced to 23.3 % of the air/fuel flame) and the increase of the flame standoff distance (increased to 256 % of air/fuel flame) results in a much lower mass flux (3.55 % of the air/fuel flame) near the reaction regions. Consequently, the thickness of the soot/precursor formation region is reduced and the soot/precursor consumption region is broadened. The reduction in the mass flux also promotes the diffusion of soot/precursor into the soot consumption region so that the soot consumption reaction is much more effective. This is supported by the larger difference produced by smaller values of β shown in Figs. 4.12–4.14. The reduced residence time in the soot/precursor formation region suppresses the soot/precursor formation reaction, while the enhanced soot consumption reaction consumes more soot/precursor, so that the total amount of soot produced is lower. In addition, the reduced flame temperature further retards the production of soot/precursor and lower the amount of soot formation.

Unlike the case in Chapter 3 for which the inert redistribution causes a large difference in the flame temperature, the inert redistribution for the air/fuel flame introduces only a slight difference in the flame temperature. For the burning of ethylene, each mole of ethylene reacts with three moles of oxygen. By keeping the ethylene consumption rate at 1.51 mg/s, the mass flow rate from the burner is much higher compared to that of the fuel/air flame studied in Chapter 3 even for the oxygen/diluted-fuel flame. Because a higher burner flow rate means a lower heat transfer rate to the burner, there is only an insignificant increase in the heat loss to the burner through the inert redistribution. The numerical calculation shows that the burner needs to be raised only to 317.15 K for the oxygen/diluted-fuel flame to keep the same flame temperature as the air/fuel flame with the burner temperature of 300 K. The negligible change in the flame temperature caused by the inert redistribution makes the separate comparison of sooting behavior between the two limiting flames with the same flame temperature unnecessary.

Finally, the effect of burner flow rate on the response of the oxygen/diluted-fuel flame is presented in Figs. 4.15–4.17 by plotting $\tilde{T}_f$, $\tilde{r}_f$, and S_B versus $\tilde{m}$ with $\alpha = Le_R = Le_S = 1$ and $Da_2 = 2.0$. These figures show that the flame response is qualitatively similar to that of the fuel/air flame presented in Figs. 4.9–4.11, consistent with the discussion in Chapter 3, and will not be further elaborated. The non-monotonic behavior observed in Fig. 4.9 can be seen in Fig. 4.15 when the range of $\tilde{m}$ is extended.

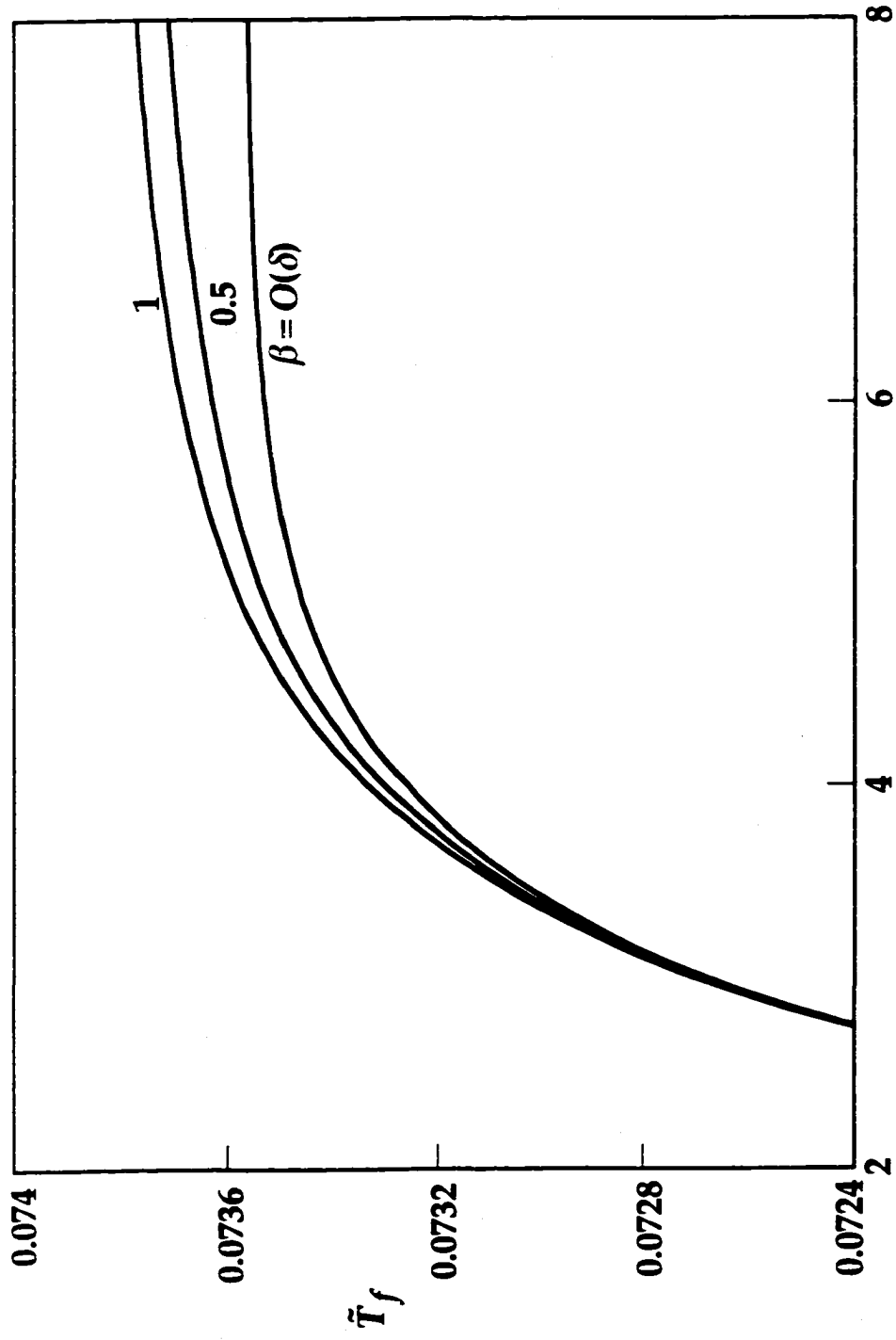

Figure 4.15 Variation of $\tilde{T}_f$ with $\tilde{m}$ for the oxygen/diluted-fuel flame with $\alpha = Le_R = Le_S = 1$, $Da_2 = 2.0$ and selected values of β

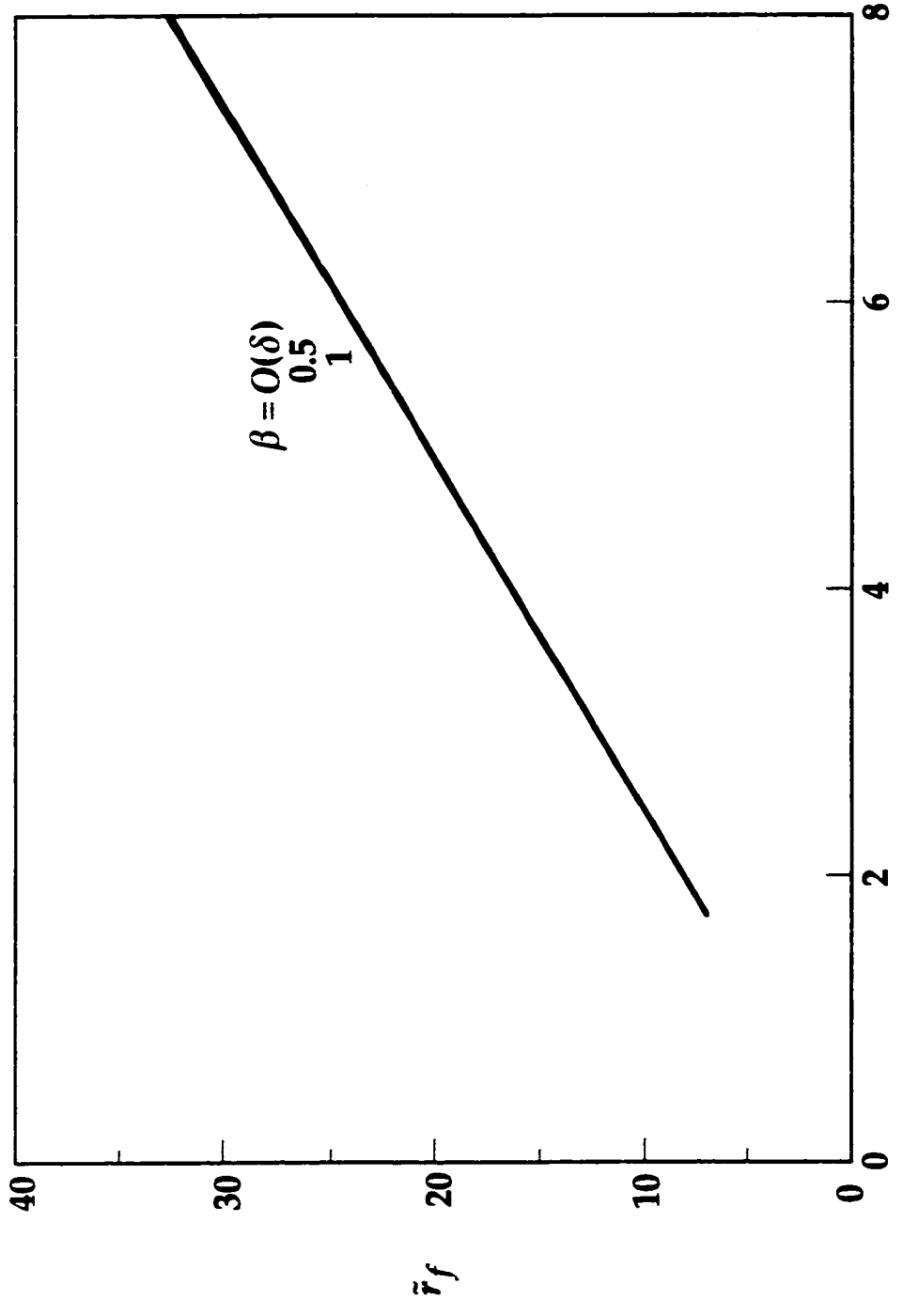

Figure 4.16 The flame sheet location $\tilde{r}_f$ corresponding to Fig. 4.15

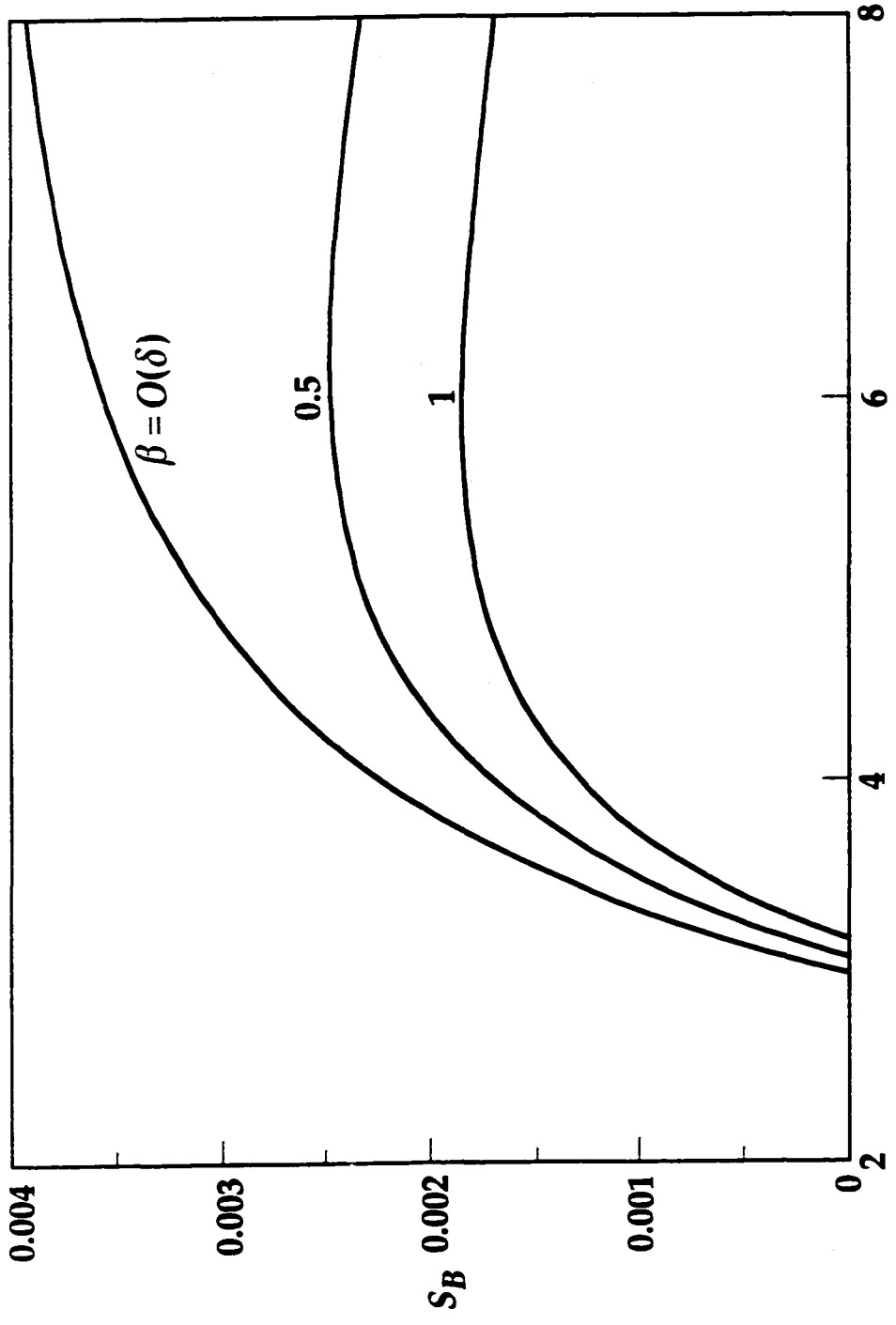

Figure 4.17 Variation of S_B corresponding to Fig. 4.15

CHAPTER 5

CONCLUDING REMARKS

In this study, the formation and consumption of soot/precursor in a diffusion flame is analyzed by activation energy asymptotics. Two model flames, namely, the counterflow flame and the spherical flame stabilized by a spherical porous burner, are investigated. Simplified three-step chemical kinetics is adopted to describe the oxidation, soot/precursor formation and soot/precursor consumption reactions. Flame responses to the reaction rates and transport processes are obtained. Two limiting cases, the fuel/air flame and the diluted-fuel/oxygen flame, are considered for both of the flame geometries to understand the effects of hydrodynamics and flame structure on soot inception in diffusion flames. Although the evolution of soot precursors to soot particles is not included in this study, the results are applicable based on the understanding that the production of soot particles is dependent on the availability of soot precursors.

The results show that in the limit of negligible soot consumption reaction, the amount of soot/precursor production increases, but the rate of increase slows down, with the soot formation reaction rate, Da_2. When the soot formation and consumption reactions are comparable, there exists a critical Da_2 at which the soot production is the highest. For values of Da_2 higher than this critical value, soot/precursor production decreases because of the enhanced soot consumption reaction. The critical Da_2 decreases with stronger soot consumption reaction. As to the molecular diffusion, the soot/precursor production reduces with faster radical diffusion. The

diffusion rate of soot/precursor does not affect the soot production if the soot consumption reaction is negligible. Otherwise, slower soot/precursor diffusion yields less soot generation because the residence time allowed for the soot consumption reaction is longer.

The effect of stoichiometric mixture fraction, Z_{st}, is studied by extracting the inert gas from the oxidizer mixture to the fuel. The inert redistribution shifts the flame location closer to the oxidizer side when the inert is supplied with the oxidizer (a smaller Z_{st}). For the representative calculations performed in this study, $Z_{st} = 0.064$ for the ethylene/air flame and 0.78 for the diluted-ethylene/oxygen flame. It is found that the soot consumption reaction is much more dominant for the diluted-fuel/oxygen flame than the fuel/air flame. As a result, the soot production is reduced and, in certain cases, completely suppressed by redistribution of inert from the air to the fuel.

The inert redistribution varies the two primary mechanisms that control the formation of soot precursors: the flame structure and the flow velocity (hydrodynamics) in the reaction regions. Among all the flames studied in this investigation, the inert redistribution introduces the strongest reduction in the production of soot/precursor for the counterflow flame. In the fuel/air counterflow flame, the direction of convection is from the oxidizer side to the fuel side and the soot formation region is much broader than the soot consumption region. Both of these favor the production of soot/precursor. These conditions are reversed for the diluted-fuel/oxygen flame, *i.e.*, the flow is from the fuel side to the oxidizer side and the soot formation region is much thinner than the soot consumption region, which retards the soot formation reaction and promotes the soot consumption reaction so that the

production of soot is suppressed.

Because the effects of flame structure and convection are inseparable for the counterflow flame, the spherical flame stabilized by a porous burner is studied. For the spherical flame, the convection is allowed to vary either from the fuel to the oxidizer side by issuing a fuel flow from the burner into a quiescent oxidizing mixture or from the oxidizer to the fuel side by supplying an oxidizer flow from the burner into a fuel ambient. The flame structure also can be independently controlled by supplying inert either with oxygen or fuel. The flexibility in varying the flow direction and the flame structure independently allows for the investigation of the four limiting cases as reported in Chapters 3 and 4.

For the fuel/air flame and the dilute-fuel/oxygen flame presented in Chapter 3, the flow direction is from the fuel side to the oxidizer. The soot/precursor produced from the soot formation region needs to pass through the soot consumption region before entering the inert region. The flow direction is reversed for the air/fuel flame and the oxygen/diluted-fuel flame presented in Chapter 4. For these flames, the soot/precursor produced in the soot formation region is convected away from the soot consumption region and directly into the inert region. Therefore, the hydrodynamics favors production of soot/precursor for the air/fuel and oxygen/diluted-fuel flames, and consumption of soot/precursor for the fuel/air and diluted-fuel/oxygen flames. Soot consumption reaction is not effective for soot production in the air/fuel and the oxygen/diluted-fuel flames because of their unfavorable flow direction.

The flame structure that varies with the inert redistribution then shows that the diluted-fuel/oxygen flame and the oxygen/diluted-fuel flame possess a much thinner soot formation region and thicker soot consumption region compared to the fuel/air flame and the air/fuel flame. This indicates that soot production is favored for the fuel/air and the air/fuel flames.

Taking the spherical fuel/air flame as the reference flame, which is sooty as indicated by the value of soot index S_B, the sooting behavior of the other three limiting spherical flames can be assessed by comparing them to it. For the range of Da_2 that yields a sooty fuel/air flame, S_B is practically zero for the diluted-fuel/oxygen flame. Non-zero S_B can be observed only when Da_2 is extremely large. This implies that the diluted-fuel/oxygen flame is primarily soot free. Moreover, the value of S_B for the air/fuel flame is much larger than that of fuel/air flame, indicating that the air/fuel flame is sootier than the fuel/air flame. Finally, similar to the diluted-fuel/oxygen flame, the oxygen/diluted-fuel flame shows negligibly small S_B and is another soot free flame.

According to the above discussions, the sooting behavior of the four limiting flames and their relationships to the flame structure and flow direction are shown in Table 5.1. It is clear from Table 5.1 that the air/fuel flame is sooty because the flame structure favors soot formation and the flow direction suppresses soot consumption. On the contrary, the diluted-fuel/oxygen flame is soot free for the flame structure suppresses soot formation and the flow direction promotes soot consumption. The sooting behavior of the fuel/air flame and the oxygen/diluted-fuel flame is not as clear because the effects of flame structure and flow direction oppose each

other. For the fuel/air flame, the flame structure favors soot formation while the flow direction favors soot consumption. As to the oxygen/diluted-fuel flame, the flame structure suppresses soot formation while the flow direction restrains soot consumption.

Table 5.1 Effects of flame structure and flow direction on the sooting behavior of the spherical flames

Flames	Flame Structure	Flow Direction	Sooting Behavior
Fuel/air	Favors soot formation	Promotes soot consumption	Sooty
Diluted-Fuel/ Oxygen	Retards soot formation	Promotes soot consumption	Soot Free
Air/Fuel	Favors soot formation	Restrains soot consumption	Sooty
Oxygen/ Diluted-Fuel	Retards soot formation	Restrains soot consumption	Soot Free

The results of this study, showing that the fuel/air flame is sooty and the oxygen/diluted-fuel flame is not, suggest that the soot inception process is primarily controlled by the flame structure, in agreement with the experimental study of Du and Axelbaum (1995). Recent experiments performed by our collaborators at NASA Glenn Research Center (Sunderland *et al.*, 2001) using the 2.2 sec drop tower show that the fuel/air and air/fuel flames are indeed sooty while the diluted-fuel/oxygen and oxygen/diluted-fuel flames are soot free. This further supports the finding of the present study. The flow direction (hydrodynamics), although important in the oxidation of soot precursors or particles, is secondary in soot inception.

Finally, because the soot formation reaction is retarded while the soot consumption reaction is promoted when the inert gas is supplied with the fuel, inert redistribution is an effective technique to reduce or completely suppress soot production in nonpremixed combustion systems.

REFERENCE

Abramson, M. (1991). Air Pollution Health Effects and Air Quality Objectives. *Medical Journal of Australia*, Vol. **154**, pp. 716.

Abramson, M. and Voigt T. (1991). Ambient Air Pollution and Respiratory Diseasy. *Medical Journal of Australia*, Vol. **154**, pp. 543.

Axelbaum, R.L. and Law, C.K. (1988). Preferential Diffusion and Concentration Modification in Sooting Counterflow Diffusion Flames. *Twenty-second Symposium (International) on Combustion*, pp. 379-386, The Combustion Institute.

Axelbaum, R.L. and Law, C.K. (1990). Soot Formation and Inert Addition in Diffusion Flames. *Twenty-third Symposium (International) on Combustion*, pp. 1517-1523, The Combustion Institute.

Balthasar, M., Heyl, A., Mauβ, F., Schmitt, F. and Bockhorn, H. (1996). Flamelet Modeling of Soot Formation in Laminar Ethyne/Air Diffusion Flames. *Twenty-sixth Symposium (International) on Combustion*, pp. 2369-2378, The Combustion Institute.

Barnes, P.J. (1994). Airpollution and Asthma. *Postgraduate Medical Journal*, Vol. **70**, No. 823, pp. 319.

Calcote, H.F. and Keil, D.G. (1990). The Role of Ions in Soot Formation. *Pure and Appl. Chem.*, **62**, 815-824.

Calcote, H.F. and Manos, D.M. (1983). Effect of Molecular Structure on Incipient Soot Formation. *Combust. Flame*, **49**, 289-304.

Chan-Yeung, M.N. (2000). Air Pollution and Health. *Hong Kong Medical Journal*, Vol. **6**, No. 4, pp.390-398.

Colket, M.B. (1995). Rapid Naphthalene Production from Allene and Toluene. *Fall Technical Meeting, The Eastern States Section of the Combustion Institute*, Oct. 16-18, Worcester, MA.

Cunningham, J., Dockery, D.W., Gold, D.R. and Speizer, F.E. (1995). Racial Differences in the Association Between Maternal Smoking During Pregnancy and Lung Function in Children. *American Journal of Respiratory and Critical Care Medicine*, Vol. **152**, No. 2, pp. 565-569.

Delichatsios, M.A. (1994). A phenomenological Model for Smoke-Point and Soot Formation in Laminar Flames. *Combust. Sci. Tech.*, **100**, 283-298.

Du, D.X., Axelbaum, R.L. and Law, C.K. (1988). Experiments on the Sooting Limits of Aerodynamically-Strained Diffusion Flames. *Twenty-second Symposium (International) on Combustion*, pp. 387-394, The Combustion Institute.

Du, D.X., Axelbaum, R.L. and Law, C.K. (1990). The Influence of Carbon Dioxide and Oxygen as Additives on Soot Formation in Diffusion Flames. *Twenty-third Symposium (International) on Combustion*, pp. 1501-1507, The Combustion Institute.

Du, D.X., Wang, H. and Law, C.K. (1998). Soot Formation in Counterflow Ethylene Diffusion Flames from 1 to 2.5 Atmospheres. *Combust. Flame*, **113**, 264-270.

Du, J. and Axelbaum, R.L. (1995). The Effect of Flame Structure on Soot-Particle Inception in Diffusion Flames. *Combust. Flame*, **100**, 367-375.

Fairweather, M., Jones, W.P. and Lindstedt, R.P. (1992). Predications of Radiative Transfer from a Turbulent Reacting Jet in a Cross-Wind. *Combust. Flame*, **89**, 45-64.

Frenklach, M. (1988). On the Driving Force of PAH Production. *Twenty-second Symposium (International) on Combustion*, pp. 1075-1082, The Combustion Institute.

Frenklach, M., Clary, D.W., Gardiner, Jr. and Stein, S.E. (1984). Detailed Kinetic Modeling of Soot Formation in Shock-Tube Pyrolysis of Acetylene. *Twentieth Symposium (International) on Combustion*, pp. 887-901, The Combustion Institute.

Frenklach, M. and Wang, H. (1990). Detailed Modeling of Soot Particle Nucleation and Growth. *Twenty-third Symposium (International) on Combustion*, pp. 1559-1566, The Combustion Institute.

Frenklach, M. and Wang, H. (1994). Detailed Mechanism and Modeling of Soot Particle Formation. *Soot Formation in Combustion*, H. Bockhorn (Ed.) pp. 162-190, Springer-Verlag, Berlin.

Gill, R.J. and Olson, D.B. (1984). Estimation of Soot Thresholds for Fuel Mixtures. *Combust. Sci. Tech.*, **40**, 307-315.

Glassman, I. (1996). Combustion. Third Edition. Academic Press, Inc. p399.

Green, M. (1995). Air Pollution and Health. *British Medical Journal*, Vol. **311**, No. 7002, pp. 401.

Gomez, A. and Glassman, I. (1986). Quantitative Comparison of Fuel Soot Formation Rates in Laminar Diffusion Flames. *Twenty-first Symposium (International) on Combustion*, pp. 1087-1095, The Combustion Institute.

Gomez, A., Sidebotham, G. and Glassman, I. (1984). Sooting Behavior in Temperature-Controlled Laminar Diffusion Flames. *Combust. Flame*, **58**, 45-57.

Harris, M.M., King, G.B. and Laurendau, N.M. (1986). Influence of Temperature and Hydroxyl Concentration on Incipient Soot Formation in Premixed Flames. *Combust. Flame*, **64**, 99-112.

Hiroyasu, H., Kadota, T. and Arai, M. (1983). Development and Use of a Spray Combustion Modeling to Predict Diesel Engine Efficiency and Pollutant Emissions. *Bull. JSME*, **26**, 569-575.

Holt, G.R. (1996). Effects of Air Pollution on the Upper Aerodigestive Tract. *Otolaryngology: Head and Neck Surgery*, Vol. **114**, No. 2, pp. 201-204.

Hura, H.S. and Glassman, I. (1988). Soot Formation in Diffusion Flames of Fuel/Oxygen Mixtures. *Twenty-second Symposium (International) on Combustion*, pp. 371-378, The Combustion Institute.

Kaplan, C.R., Baek, S.W., Oran, E.S. and Ellzey, J.L. (1994). Dynamics of a Strongly Radiating Unsteady Ethylene Jet Diffusion Flame. *Combust. Flame*, **96**, 1-22.

Kazakov, A., Wang, H. and Frenklach, M. (1995). Detailed Modeling of soot Formation in Laminar Premixed Ethylene Flames at a Pressure of 10 Bar, *Combust. Flame*, **100**, 111-120.

Kennedy, I.M. (1997). Models of Soot Formation and Oxidation. *Prog. Energy Combust. Sci.*, **23**, 95-132.

Kennedy, I.M., Kollmann, W. and Chen, J.-Y. (1990). A Model for Soot Formation in A Laminar Diffusion Flame. *Combust. Flame*, **81**, 73-85.

Kennedy, I.M., Rapp, D.R., Santoro, R.J. and Yam, C. (1996). Modeling and Measurements of Soot and Species in A Laminar Diffusion Flame. *Combust. Flame*, **107**, 368-383.

Lahiri, T., Roy, S., Basu, C., Ganguly, S. Ray, M.R. and Lahiri, P. (2000). Air Pollution in Calcutta Elicits Adverse Pulmonary Reaction in Children. *Indian Journal of Medical Research*, Vol. 112, No. JUL, pp. 21-26.

Lewis, P.R., Hensley, M.J., and Calvert, D. (1998). Outdoor Air Pollution and Children's Respiratory Symptoms in the Steel of New South Wales. *Medical Journal of Australia*, Vol. **169**, No. 9, pp. 459.

Lin, K.C. and Faeth, G.M. (1996). Hydrodynamic Suppression of Soot Emissions in Laminar diffusion Flames. *J. Propul. Power*, Vol. **12**, No. 1, 10-17.

Liñán, A. (1974). The Asymptotic Structure of Counterflow Diffusion Flames for Large Activation Energies. *Acta Astronautica*, Vol. **1**, No. 1, pp. 1007-1039.

Lindstedt, P.R. (1994). Simplified soot nucleation and surface growth steps for non-premixed flames. *Soot Formation in Combustion*, H. Bockhorn (Ed.), pp. 417-439, Springer-Verlag, Berlin.

Meyer, P., Mannion, D. and Redd, S. (1999). Air Pollution and Health: What Georgia Physicians Should Know. *Journal of the Medical Association of Georgia*, Vol. **88**, No. 4, 18.

Moss, J.B., Stewart, C.D. and Syed, K.J. (1988). Flowfield Modeling of Soot Formation at Elevated Pressure. Twenty-*second Symposium (International) on Combustion*, pp. 413-423, The Combustion Institute.

Olson, D.B., Pickens, J.C. and Gill, R.J. (1985). The Effects of Molecular Structure on Soot Formation II: Diffusion Flames. *Combust. Flame*, **62**, 43-60.

Palmer, H.B. and Cullis, H.F. (1965). *The Chemistry and Physics of Carbon*, Vol. **1** p. 205. Dekker, New York, 1965.

Said, R., Garo, A. and Borghi, R. (1997). Soot Formation Modeling for Turbulent Flames. *Combust. Flame*, **108**, 71-86.

Sunderland, P.B., Axelbaum, R.L., Urban, D.L., Chao, B.H. and Liu, S (2001). Effects of Structure and Hydrodynamics on the Sooting Behavior of Spherical Microgravity Diffusion Flames. Submitted to *Combust. Flame.*

Takahashi, F. and Glassman, I. (1984). Sooting Correlations for Premixed Flames. *Combust. Sci. Tech.*, **37**, 1-19.

Talbot, L., Cheng, R.K., Schefer, R.W. and Willis, D.R. (1980). Thermophoresis of Particles in A Heated Boundary Layer. *J. Fluid Mech.*, **101**, 737-758.

Tesner, P.A. Snegiriova, T.D. and Knorre, V.G. (1971). Kinetics of Dispersed Carbon Formation. *Combust. Flame*, **17**, 253-260.

Vandsburger, U., Kennedy, I. and Glassman, I. (1984). Sooting Counterflow Diffusion Flames with Varying Oxygen Index. *Combust. Sci. Tech.*, **39**, 263-285.

Williams, F. A. (1985). *Combustion Throry.* Benjamin/Cummings, Menlo Park, CA.

Williams, F. A. (1991). *Reduced Kinetic Mechanisms and Asymptotics Approximations for Methane-Air Flames* (M.D.Smooke, ED.), Springer-Verlag.

Yoshihara, Y., Kazakov, A., Wang, H. and Frenklach, M. (1994). Reduced Mechanism of Soot Formation -- Application to Natural Gas-Fueled Diesel Combustion. *Twenty-fifth Symposium (International) on Combustion*, pp. 941-948, The Combustion Institute.